

Stony Brook University



OFFICIAL COPY

The official electronic file of this thesis or dissertation is maintained by the University Libraries on behalf of The Graduate School at Stony Brook University.

© All Rights Reserved by Author.

Modification of Adenoviral Tropism to Cancer Cells via Metabolic Labeling of Unnatural Sugars and/or Unnatural Amino acids and Subsequent Bioorthogonal Conjugations

A Dissertation Presented

by

Yoon Hyeun Oum

to

The Graduate School

in Partial Fulfillment of the

Requirements

for the Degree of

Doctor of Philosophy

in

Chemistry

Stony Brook University

December 2012

Stony Brook University

The Graduate School

Yoon Hyeun Oum

We, the dissertation committee for the above candidate for the
Doctor of Philosophy degree, hereby recommend
acceptance of this dissertation.

**Isaac S. Carrico, Ph. D., – Dissertation Advisor
Associate Professor, Department of Chemistry**

**Daniel Raleigh, Ph. D., - Chairperson of Defense
Professor, Department of Chemistry**

**Iwao Ojima, Ph. D., - Third Member
Professor, Department of Chemistry**

**Patrick Hearing, Ph. D., - Outside Member
Professor, Department of Molecular Genetics and Microbiology**

This dissertation is accepted by the Graduate School

Charles Taber
Interim Dean of the Graduate School

Abstract of the Dissertation

Modification of Adenoviral Tropism to Cancer Cells via Metabolic Labeling of Unnatural Sugars and/or Unnatural Amino acids and Subsequent Bioorthogonal Conjugations
by

Yoon Hyeun Oum

Doctor of Philosophy

in

Chemistry

Stony Brook University

2012

Adenoviral (Ad) vectors have significant potential as gene delivery agents, oncolytic agents and vaccine scaffolds. Despite extensive effort, adenoviruses have not yet realized this potential. Primarily, this is a result of immune responses to the introduced vectors and our inability to efficiently target therapeutically relevant tissues. Considerable resources have been directed at addressing these limitations; however progress is still hampered by the drawbacks of current virus engineering approaches. In this context, our group reported a novel chemoselective method for modification of Ad vectors using bioorthogonal unnatural sugars and/or unnatural amino acids.

With the aim of expanding Ad tropism to diverse cancer cells, we developed various effective cancer-targeting Ad vectors *via* metabolic labeling and bioorthogonal “click” chemistry. That is, in order to prepare “clickable” targeting ligands, the alkyne moiety was covalently linked with different synthetic peptides or affibody proteins which have specific affinities to the corresponding receptors overexpressed on an array of cancer cells. Then, the “click” reaction was performed between alkyne-peptides (or alkyne-proteins) and azide-enabled Ad vectors

containing a reporter transgene. Targeting studies indicate substantial (~1000 fold) to modest (~3 fold) increases in infectivity dependent of both the nature of the cell line and the method of virus modification. To wit, significantly increased gene deliveries were observed in the cells expressing target receptors with higher density and with the Ad vectors modified *via* copper-catalyzed “click” reaction, compared with the cases of lower-receptor density and strain-promoted “click” reaction. Interestingly, cyclic-RGD-peptide-conjugated Ad showed unexpected lower transduction efficiencies in mouse melanoma cells than linear-RGD-Ad whose ligand has lower affinity to the target receptor ($\alpha_v\beta_3$ integrin) than cyclic RGD peptide. Focusing on the selective role of homologous $\alpha_v\beta_5$ integrin which promotes Ad-mediated membrane permeabilization and subsequent endosome rupture, we hypothesized that this unexpected low transductions was due to “ $\alpha_v\beta_5$ -excluded endocytosis” caused by the higher binding specificity of cyclic RGD peptide to $\alpha_v\beta_3$ integrin than $\alpha_v\beta_5$ particularly in the cells expressing $\alpha_v\beta_3$ integrin predominantly over $\alpha_v\beta_5$, which was supported by our thin-sectioning TEM study.

Lastly, for the purpose of extending our approach to *in vivo* studies, we attempted to conjugate a panel of ligands to label positron emitters such as ^{18}F , ^{64}Cu , ^{68}Ga , and ^{89}Zr onto viral capsid *via* “click” chemistry. In this context, cancer-targeting-folate- and ^{89}Zr -labeling-DFO-moieties were conjugated onto Ad capsid *via* Staudinger ligation and subsequent copper-catalyzed [3+2] azide-alkyne cycloaddition, which demonstrated promising 100% radiolabeling yield.

This dissertation is dedicated to my parents.

Table of Contents

Chapter 1. Adenoviral Vectors for Virotherapy.....	1
1.1 Gene Therapy.....	1
1.2 Adenovirus for Virotherapy.....	1
1.3 The Biology of Adenovirus.....	3
1.3.1 Ad Structure.....	3
1.3.2 Ad Serotype.....	6
1.3.3 Ad Cell Entry.....	7
1.4 Engineering Ad Vector for Virotherapy.....	11
Chapter 2. Engineering Adenovirus <i>via</i> Bioorthogonal “Click Chemistry”.....	20
2.1 Introduction.....	20
2.2 Chemoselective Ligation and Bioorthogonal Reagent Pairs.....	20
2.3 Introducing Clickable Tags into Biomolecules.....	25
2.3.1 Bioorthogonal Noncanonical Amino acid Tagging (BONCAT).....	26
2.3.2 Metabolic Labeling of Unnatural Sugars.....	28
2.3.3 Unnatural Substrate Labeling onto Adenoviral Capsids.....	31
2.3.3.1 Recycling of Azidohomoalanine.....	33
Chapter 3. Retargeting Adenoviral Vectors via Peptide “Click” Conjugations.....	40
3.1 Introduction.....	40
3.2 Targeting to the $\alpha_v\beta_3$ Integrin.....	41
3.3 RGD Peptide.....	43

3.4	Results and Discussion	45
3.4.1	Synthesis of Alkyne-PEG- <i>c</i> (RGDfK).....	46
3.4.2	Production of Azidosugar (<i>O</i> -GlcNAz)-labeled Ad	50
3.4.3	Conjugation of Azide-enabled Ad with Alkyne-PEG-RGD Peptide via CuAAC..	52
3.4.4	Infection Assays with $\alpha_v\beta_3$ -Integrin-targeting Ad <i>in vitro</i>	53
3.4.4.1	Targeting to the Mouse Melanoma with RGD-Ad.....	54
3.4.4.2	Comparison between Linear- vs. Cyclic-Peptide Targeting to B16BL6.....	55
3.4.4.2.1	Infection Assay with Linear- and Cyclic-RGD-Peptide-conjugated Ad.....	58
3.4.4.2.2	Endosome Rupture Assay using FITC/Cy5-dextran	61
3.4.4.2.3	Subcellular Localization of Ad particles by Thin-sectioning Electron Microscopy	63
3.4.4.3	Expression of Ad knob for CAR Inhibition.....	67
3.4.4.4	Targeting to the Human Glioma with RGD-Ad	70
3.4.5	Targeting to Angiogenesis	73
3.4.5.1	Synthesis of VEGFR2 and Tie2-Targeting Peptides-PEG-alkyne	73
3.4.5.2	Infection Assays with Angiogenesis-targeting Ad to HUVEC <i>in vitro</i>	76
3.4.6	Conclusion	78
3.4.7	Materials and methods	79
Chapter 4.	Retargeting Adenoviral Vectors via Affibody “Click” Conjugation.....	100
4.1	Introduction.....	101
4.2	Targeting to the Epidermal Growth Factor Receptors (EGFR or ErbB)	102

4.3	Affibody	103
4.4	Results and Discussion	106
4.4.1	Preparation of Affibody-conjugated Ad <i>via</i> CuAAC or SPAAC	106
4.4.1.1	Quantifying “click” efficiency for Ad Fiber Modification via SPAAC	107
4.4.2	Infection Assays with Affibody-Clicked Ads.....	116
4.5	Conclusion	124
4.6	Materials and methods	125
Chapter 5.	Labeling Ad with Positron Emitters for <i>In Vivo</i> Tracking	138
5.1	Introduction.....	138
5.2	Labeling Ad with ¹⁸ F	139
5.3	Labeling Ad with Longer-Lived Positron Emitters.....	142
5.4	Results and Discussion	147
5.4.1	¹⁸ F Labeling	147
5.4.1.1	Synthesis of BCN-[¹⁸ F]fluorobenzamide	147
5.4.1.2	SPAAC between AHA-Ad and BCN-[¹⁸ F]fluorobenzamide	151
5.4.2	⁶⁴ Cu/ ⁶⁸ Ga Labeling.....	152
5.4.2.1	Synthesis of NOTA-BCN	152
5.4.2.2	“Click” Test of ⁶⁹ Ga-NOTA-BCN with TAMRA-azide	154
5.4.2.3	<i>In vitro</i> Infection Assay Using ⁶³ Cu/ ⁶⁹ Ga-Labeled Ad without HPLC	156
5.4.3	Labeling Folate-Targeting Ad with ⁸⁹ Zr.....	158
5.4.3.1	Usage of Azide/Alkyne-enabled Ad for Labeling Retargeted Ad.....	160

5.4.3.2	Synthesis of Folate-Staudinger Phosphine and DFO-azide.....	160
5.4.3.3	“Click”reaction of HPG/GlcNAz-Ad with folate-phosphine and DFO-azide.....	162
5.4.3.4	Labeling DFO/Folate-Ad with ⁸⁹ Zr.....	163
5.5	Conclusion	163
5.6	Materials and methods	165
	General Conclusion and Future Direction	178
	Bibliography	180
	Appendix.....	201

List of Figures

Figure 1-1. Vectors Used in Gene Therapy Clinical Trials (until June, 2012).....	2
Figure 1-2. Reconstructed Cryo-EM image of Ad5 with Ad35 fiber	4
Figure 1-3. Anatomical Structure of Ad Virion.....	5
Figure 1-4. Schematic Diagram of Ad Receptor-Mediated Cell Entry	8
Figure 1-5. Different Cellular Receptors for Ad Entry.....	9
Figure 1-6. Ad fiber knob structure and cocrystal structure with CAR D1 domain.....	10
Figure 1-7. Structure of Ad Penton and Interaction Model of RGD Motif with Integrin on Cell Surface	11
Figure 1-8. Different Strategies for Ad Retargeting	13
Figure 2-1. Conceptual Representation of Orthogonal Reactivity.....	21
Figure 2-2. The BONCAT strategy for labeling newly synthesized proteins.....	26
Figure 2-3. Incorporation of unnatural sugars on cell surface glycans.....	28
Figure 2-4. Incorporation of unnatural sugars into nucleocytoplasmic proteins	29
Figure 2-5. The GlcNAc and GalNAc salvage and O-GlcNAc signaling pathways	30
Figure 2-6. Biosynthetic Incorporation of Unnatural Amino acids and Sugars into Viral Protein	31
Figure 2-7. Alkyne Substrate HPG, AC ₄ GalPen	32
Figure 2-8. Anti-FLAG Western-blot for Recycled AHA Labeled Ad.....	35
Figure 3-1. Genetic Methods for Generating Diverse Viral Libraries.....	41
Figure 3-2. a Diagram of Integrin Receptor Heterocomplex and Signal Transduction.....	42
Figure 3-3. Induction of Selectivity to the RGD Peptide by Cyclization	45
Figure 3-4. Qualitative Analysis of Azido Sugar Incorporation into Ad5 Fiber	51

Figure 3-5. Infection Assay with cRGD-Ad to B16BL6	55
Figure 3-6. Infection Assays with IRGD-Ad and cRGD-Ad to B16BL6	58
Figure 3-7. The hypothesis of $\alpha_v\beta_5$ integrin-dependent endosome escape with IRGD-Ad vs. cRGD-Ad	59
Figure 3-8. Superposition of the $\alpha_v\beta_3$ Receptor (grey) and the Homology Model of the $\alpha_v\beta_5$ (white) both represented as Connolly surface.....	60
Figure 3-9. Assay for Ad-induced Endosome Rupture Using Flow Cytometry.....	62
Figure 3-10. TEM Image of the Late Stages of IRGD-Ad Entry in B16BL6 Cell	64
Figure 3-11. TEM Image of the Late Stages of cRGD-Ad Entry in B16BL6 Cell	65
Figure 3-12. Morphometric Analysis of Ad entry into B16BL6 Cells	66
Figure 3-13. CAR Inhibition with Ad knob.....	67
Figure 3-14. Expression of Ad12 knob in <i>E. coli</i>	68
Figure 3-15. Sequence Alignment between Ad5 knob and Ad12 knob	69
Figure 3-16. Infection Assay with cRGD-Ad to Human Glioma	71
Figure 3-17. Infection Assays with cRGD-Ad and IRGD-Ad to Human Glioma	72
Figure 3-18. Infection Assays with Angiogenesis Targeting Ad.....	77
Figure 4-1. ErbB Receptors and Signalling Downstream.....	103
Figure 4-2. The Structure of Affibody	104
Figure 4-3. Illustration of Affibody Modification	108
Figure 4-4. Quantitation of Viral Fibers Labeled <i>via</i> SPAAC Using Gel Fluorescence Assay with TAMRA-BCN.....	109
Figure 4-5. Standard calibration curve for determination of [TAMRA-BCN] conjugated on viral fibers	110
Figure 4-6. MALDI-TOF Spectra of Affibody-PEG-Alkyne.....	113
Figure 4-7. TEM Images of Ad Particles.....	114

Figure 4-8. Western Blot against Ad Fiber.....	115
Figure 4-9. Thermal Stability Assays of Modified Ad Particles	115
Figure 4-10. Zeta Potential and Particle Size of Virions Measured by Dynamic Light Scattering	116
Figure 4-11. Comparison of Gene Delivery Capabilities of AffiEGFR-PEG-CCH Modified and Unmodified Ad	118
Figure 4-12. Effects of Cu(I) on Gene Delivery with AffiEGFR-PEG-CCH Modified Particles	119
Figure 4-13. Infection Assays with affiEGFR-PEG-BCN “Clicked” Ad via SPAAC	120
Figure 4-14. Gene Delivery with AffiHER2-PEG-CCH Modified and Unmodified Ad to Cells Expressing High Levels of Her2.....	121
Figure 4-15. Comparison of Her2 Mediated Gene Delivery in Cells with High (SK-BR-3) and Low (RD) Her2 Levels	122
Figure 4-16. Comparison of Her2 Mediated Gene Delivery with Intact Ad (-Cu) and AffiHer2 “Clicked” Ad (+Cu)	123
Figure 5-1. Prosthetic Groups Frequently Used for ¹⁸ F-Labeling	140
Figure 5-2. Examples of ¹⁸ F-Labeling Prosthetic Groups for "Click" Reaction.....	141
Figure 5-3. Different Copper Chelators for PET	144
Figure 5-4. Reaction Monitoring by Radio TLC Scanning	148
Figure 5-5. HPLC Traces of BCN-fluorobenzamide.....	149
Figure 5-6. ESI-Mass Spectrum of Decayed Compound 4.....	149
Figure 5-7. SPAAC Reaction between BCN-[¹⁸ F]fluorobenzamide and AHA-Ad Monitored by Radio TLC	151
Figure 5-8. MALDI-TOF Spectrum of ⁶⁹ Ga-NOTA-TAMRA (8).....	155
Figure 5-9. Infection Assays with "Clicked" Metal-Chelated Ad	157
Figure 5-10. Structure of DFO.....	158

Figure 5-11. ^{89}Zr Labeling Monitored by radio TLC 163

List of Tables

Table 1-1. Pros and Cons of Ad Vector as a Gene Delivery Vehicle	2
Table 1-2. Ad Structural Proteins	5
Table 1-3. Human Ad Serotypes.....	6
Table 2-1. Bioorthogonal Reagent Pairs Used in Living Systems.....	23
Table 3-1. Integrins in Cancer Progression.....	43
Table 4-1. The Number of Dye Molecules Conjugated on a Virion via SPAAC.....	110
Table 5-1. Characteristics of Selected Longer-Lived Positron-Emitting Radionuclides.....	143

List of Schemes

Scheme 3-1. Synthesis of <i>c</i> (RGDfK).....	48
Scheme 3-2. Synthesis of Alkyne-PEG-maleimide	49
Scheme 3-3. Synthesis of Alkyne-PEG- <i>c</i> (RGDfK).....	49
Scheme 3-4. Synthesis of Alkyne- <i>c</i> (RGDfK) without PEG linker.....	50
Scheme 3-5. Synthesis of Ac ₄ GalNAz.....	50
Scheme 3-6. Overall Scheme for $\alpha_v\beta_3$ Integrin Targeting with Ad-PEG- <i>c</i> (RGDfK).....	53
Scheme 3-7. Synthesis of Linear RGD-PEG-alkyne	57
Scheme 3-8. Synthesis of VEGFR2 Targeting Peptide-PEG-alkyne	74
Scheme 3-9. Synthesis of Tie2 Receptor Targeting Peptide-PEG-alkyne.....	75
Scheme 4-1. Overall Scheme of Cancer Targeting with Affibody-Clicked Ad	105
Scheme 4-2. Synthesis of Maleimide-PEG-BCN	107
Scheme 5-1. ¹⁸ F Labeling of Ad Particle via SPAAC	142
Scheme 5-2. ⁶⁴ Cu and ⁶⁸ Ga Labeling of Ad via SPAAC.....	146
Scheme 5-3. Synthesis of BCN-[¹⁸ F]fluorobenzamide.....	147
Scheme 5-4. Synthesis of NOTA-PEG-BCN	152
Scheme 5-5. ⁶³ Cu-Complexation of NOTA-BCN	153
Scheme 5-6. ⁶⁹ Ga-Complexation of NOTA-BCN	153
Scheme 5-7. "Click" Test of ⁶⁹ Ga-NOTA-BCN (7) with TAMRA-azide	154
Scheme 5-8. ⁸⁹ Zr-Labeling of Folate-Receptor-Targeting Ad Using DFO Chelator.....	159
Scheme 5-9. Synthesis of Folate-Staudinger Phosphine.....	161
Scheme 5-10. Synthesis of DFO-PEG-N ₃	162

List of Abbreviations

AAAS	american association for the advancement of science
Ac ₄ GalNAz	peracetylated <i>N</i> -acetylgalactosamine
Ac ₄ GalPen	peracetylated <i>N</i> -4-pentynylacetylgalactosamine
Ac ₄ GlcNAz	peracetylated <i>N</i> -acetylglucosamine
Ac ₄ GlcPen	peracetylated <i>N</i> -4-pentynylacetylglucosamine
Ad	adenovirus
Ad12	adenovirus serotype 12
Ad2	adenovirus serotype 2
Ad5	adenovirus serotype 5
ADIBO	azadibenzocyclooctyne
affiEGFR	anti-epidermal growth factor receptor affibody
affiHer2	anti-human epidermal growth factor receptor 2 affibody
AHA	azidohomoalanine
AIDS	acquired immune deficiency syndrome
AIDS	acquired immunodeficiency syndrome
ASM	american society for microbiology
BBN	borabicyclononane
BCA	bicinchoninic acid
BCN	bicyclononyne
BCS	bovine calf serum
BONCAT	bio-orthogonal non-canonical amino acid tagging
C4BP	component C4 binding protein
CAR	coxsackie adenovirus receptor
CB-TE2A	Cross-bridged 1,4,8,11-tetraazacyclotetradecane-1,8-diacetic acid
CMV	cytomegalovirus
cryo-EM	cryo-electron microscopy
CuAAC	copper-catalyzed azide–alkyne cycloaddition
DCC	1,3-dicyclohexylcarbodiimide
DFO	deferoxamine
DIC	1,3-diisopropylcarbodiimide
DIEA	<i>N,N</i> -diisopropylethylamine
DIGE	difference gel electrophoresis
DLS	dynamic light scattering
DMF	<i>N,N</i> -Dimethylformamide
DMSO	dimethylsulphoxide
DNA	deoxyribonucleic acid
DOTA	1,4,7,10-tetraazacyclododecane-1,4,7,10-tetraacetic acid
DTPA	Diethylenetriamine pentaacetate
<i>E. coli</i>	escherichia coli
EDC	1-ethyl-3-(3-dimethylaminopropyl)carbodiimide)

EDTA	ethylene diamino tetra acetic acid
EGF	epidermal growth factor
EGFR	epidermal growth factor receptor
ER	endoplasmic reticulum
ErbB	epidermal growth factor receptor (the gene symbol)
FDA	food and drug administration
FDG	2-deoxy-2-[¹⁸ F]-fluoro- <i>D</i> -glucose
FIX	coagulation factor IX
Fmoc	9-fluorenylmethoxycarbonyl
FX	vitamin K-dependent coagulation factor X
GALE	UDP-galactose 4'-epimerase
GalNAz	<i>N</i> -azidoacetylglucosamine
GFP	green fluorescent protein
Her2	Human Epidermal Growth Factor Receptor 2
HOBt	1-hydroxybenzotriazole
HPG	homopropargylglycine
HSPG	heparin sulfate proteoglycan
HSV1-tk	herpes simplex virus serotype 1 thymidine kinase
IPTG	isopropyl β- <i>D</i> -thiogalactopyranoside
mAb	monoclonal antibody
MC	methylene chloride
Met	methionine
MW	molecular weight
MWCO	molecular weight cut off
NHS	<i>N</i> -Hydroxysuccinimide
NOTA	1,4,7-triazacyclononane-1,4,7-triacetic acid
NPFP	4-nitrophenyl 2-[¹⁸ F]fluoropropionate
NPG	nature publishing group
NTA	Ni-nitrilotriacetic acid
OGA	<i>O</i> -GlcNAc hydrolase
<i>O</i> -GlcNAc	<i>O</i> -linked <i>N</i> -acetylglucosamine
<i>O</i> -GlcNAz	<i>O</i> -linked <i>N</i> -azidoacetylglucosamine
OGT	<i>O</i> -GlcNAc transferase
pI	isoelectric point
RGD	arginine-glycine-aspartate
RT	room temperature
SarAr	1- <i>N</i> -(4-aminobenzyl)-3,6,10,13,16,19-hexaazabicyclo[6.6.6]icosane-1,8-diamine
scFv	single-chain antibody
SDS-PAGE	sodium dodecyl sulfate polyacrylamide gel electrophoresis
SFB	<i>N</i> -succinimidyl 4-[¹⁸ F]fluorobenzoate
SPAAC	strain-promoted alkyne-azide cycloaddition

SR-A	scavenger receptors type A
TAMRA	tetramethylrhodamine
TCO	<i>trans</i> -cyclooctene
TEA	triethylamine
TEM	transmission electron microscope
TETA	1,4,8,11-tetraazacyclotetradecane-1,4,8,11-tetraacetic acid
TGF	transforming growth factor
UV/VIS	ultraviolet and visible

Acknowledgments

First, I would like to thank my advisor Prof. Isaac Carrico for his support, positive encouragement, and constant trust throughout my Ph.D. course. He welcomed a novice who had little clue on chemical biology into his lab and guided to the fields of virus engineering with cutting-edge technology. His academic enthusiasm with warm personality will be a paragon of virtue all through my scientific career. I would also like to thank Prof. Daniel Raleigh and Prof. Iwao Ojima for serving as my committee and their helpful suggestions in passing through the gates required for my Ph.D. Prof. Patrick Hearing, our lab's adenovirus mentor, gladly accepted my request for being an external committee member. I appreciate his time and work to do so.

I am grateful to our collaborators as well. Dr. Sung-Won Kim and Prof. Joanna Flower gave me the opportunity to work in BNL and learn about PET chemistry. I appreciate their support and hospitality sincerely. I also thank to members of Joanna Flower group (Lisa, So-Jung, and Dr. Do-Hyun Kim *et al.*) for their help with the “hot” lab work. I would also like to express my gratitude to Prof. Jason Lewis and Dr. Nerissa Viola-Villegas in Memorial Sloan-Kettering Cancer Center regarding Ad-⁸⁹Zr-labeling project for dynamic *in vivo* imaging.

I appreciate generous donations from Prof. Nakagawa (for B16BL6 cell), Prof. Darell Bigner (for D65-MG cell), Dr. Paul Freimuth (for Ad knob plasmid), and Dr. Kai Wu (for α -Ad fiber antibody), which were critical for my experiments. I would also like to thank Dr. Toni Kohler of the SBU proteomics facility for help with mass spectrometry, Prof. Martin Schoonen for Zeta potential / particle size measurement, and Dr. Susan Horn of the Central Microscopy Imaging Center for TEM imaging.

During the last 5 years, members of Carrico group have given me a hand both in and out of the lab. Dr. Partha Banerjee was my mentor for adenovirus. Without his excellent previous works, I would have started the adenovirus project from the beginning, which might necessitate tremendous time and efforts to get the results. Thank you Partha! Lakshmi and Yanjie have been great colleagues since I joined the group. They taught me basic biological experimental skills (electrophoresis, Western blot, etc.) in every detail repeatedly and spent day and night with me in the lab. I never forget so many Sunday nights when we were in suspense to prepare Monday morning meeting! You have been such good friends of mine through the life in a foreign country. Thank you Lakshmi and Yanjie! I also thank Lisa for helping me to revise my dissertation and Fred for many pleasant talks, help with many syntheses, and revising my third meeting proposal.

I cannot but thank members of other bio and organic groups in chemistry department for allowing me to use their instruments and reagents generously. Thank the members of Boon (especially Bernie, Dhruv, Niu, Saj, Tanaya, Yueming and Zhou), Ojima (especially Bora and Edison), Parker (especially Geunsoo, Heenam, and Jon), Raleigh (especially Humeyra, and Ping for peptide synthesis), Sampson (especially Younjoo and Siyoen), Schärer (especially Burak, Yan, Jerome and Jung-eun for oligonucleotide synthesis), and Tong group (especially Eduard, Li, Nina, and Pan).

I would also like to extend special gratitude to my Korean friends in Stony Brook. They help me when I needed a hand and cheer me up when I was exhausted and felt lonely. Bora, Doekkyu, Eunjung, Geunsoo, Gunwoo, Huck, Heejung, Heenam, Hyeyoung, Kyunghwan, Kun-eek, Jaeyoung, Jongsik, Junyong, Jungyong, Siyoen, Tae-jin, Yesle, Yoo-jin and Younjoo. Thank you all!

Finally, I would like to thank my family and beloved, especially my parents for their endless, unconditional love and support throughout my life. Without their support and sacrifice, I could not have done anything. My love and deepest thanks to my parents again! My beloved sons, Taeyun and Taesang, I will always remember my debt for the time I could not spend with you as a father. You are most wonderful gifts in my life.

Chapter 1. Adenoviral Vectors for Virotherapy

1.1 Gene Therapy

“Gene therapy (or genetic therapy) offers a promising strategy for treating genetic defects and other diseases at their molecular source by replacing damaged or abnormal genes with healthy ones or reprogramming cells to fight disease” [4]. These programmed genes are delivered by a vector, a “molecular vehicle”, into the patients’ cells. Gene therapy also provides alternative treatments for the diseases having no effective conventional therapy or poor prognoses, such as cancer or AIDS. However, despite considerable advances in the field of gene therapy since the first patient study in 1990, the drawbacks in most current vectors such as low *in vivo* efficacy and immunogenicity still hamper progress in clinical trials and the ultimate success of gene therapy [4-5].

1.2 Adenovirus for Virotherapy

Adenovirus (Ad) is one of the most promising gene therapy vectors (Figure 1-1) due to many advantages such as i) an efficient transduction ability to a wide variety of dividing and non-dividing cells [6], ii) a capability of accommodating large DNA [7], iii) easy generation of high titer recombinants [8], iv) zero integration into the host cell genome (i.e., least disruption of host genome), and v) stability for easy purification and a long term storage. Recently, the replication-competent oncolytic (i.e., conditionally replicating) adenoviruses are being evaluated as innovative anticancer agents with “relative success in preclinical and clinical trials” [9-10]. Nevertheless, promiscuous tropism, immunogenicity and inability to infect certain types of

medically relevant cell, are the major challenges in utilizing Ad vectors in the field of virotherapy and significant efforts have been focused on overcoming these limitations [2].

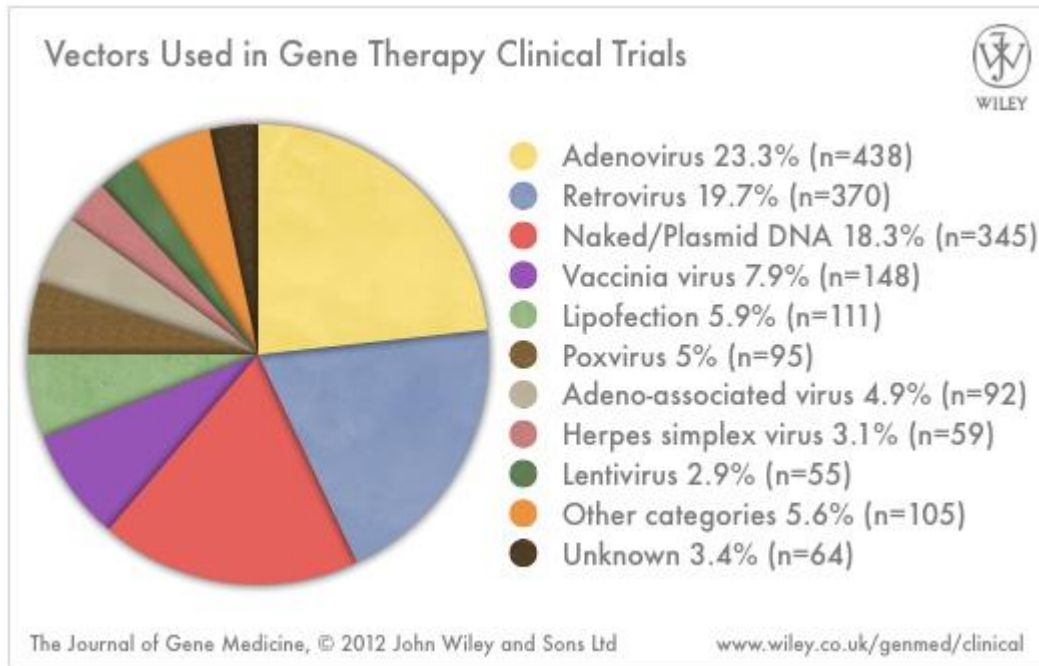


Figure 1-1. Vectors Used in Gene Therapy Clinical Trials (until June, 2012)

Table 1-1. Pros and Cons of Ad Vector as a Gene Delivery Vehicle

Advantages	Disadvantages
<ul style="list-style-type: none"> - High transduction efficiency - Accessibility of high titer - Stability - Large capacity or gene delivery - Safety (No integration to host genome) 	<ul style="list-style-type: none"> - Pre-existing immune response - Nonspecific tropism and liver uptake - Refractory cells to infect with Ad virus <ul style="list-style-type: none"> * Advanced cancer cells (squamous cell carcinoma, melanoma, bladder cancer) * Peripheral blood cell * Hematopoietic stem cell

1.3 The Biology of Adenovirus

1.3.1 Ad Structure

The knowledge of adenoviral structural components associated with cell entry and subsequent gene delivery is essential to developing novel gene therapy vectors having desired natures. Accordingly, extensive research has been focused on elucidating structural details related to Ad's internalizing mechanisms. Ad is medium-sized (70 ~100 nm), nonenveloped (without an outer lipid bilayer), icosahedral virus composed of multiple copies of 11 different structural proteins as shown in Figure 1-3, seven of which form the icosahedral capsid (II, III, IIIa, IV, VI, VIII, IX) and four of which are packaged with the linear double-stranded DNA (~ 35-36 kbp for human Ad) in the core of the particle (V, VII, mu, and terminal protein) [11]. In 1991, the first complete three-dimensional structure of the Ad2 virion at 35-Å resolution was determined by cryo-electron microscopy (cryo-EM) and image reconstruction method [12]. The reconstructed image demonstrated the trimeric shape of the hexon, the pentameric shape of the penton base, and a short portion (~88 Å) of fiber shaft (full length ≈ 300 Å including the knob domain) [11-13](Figure 1-2).

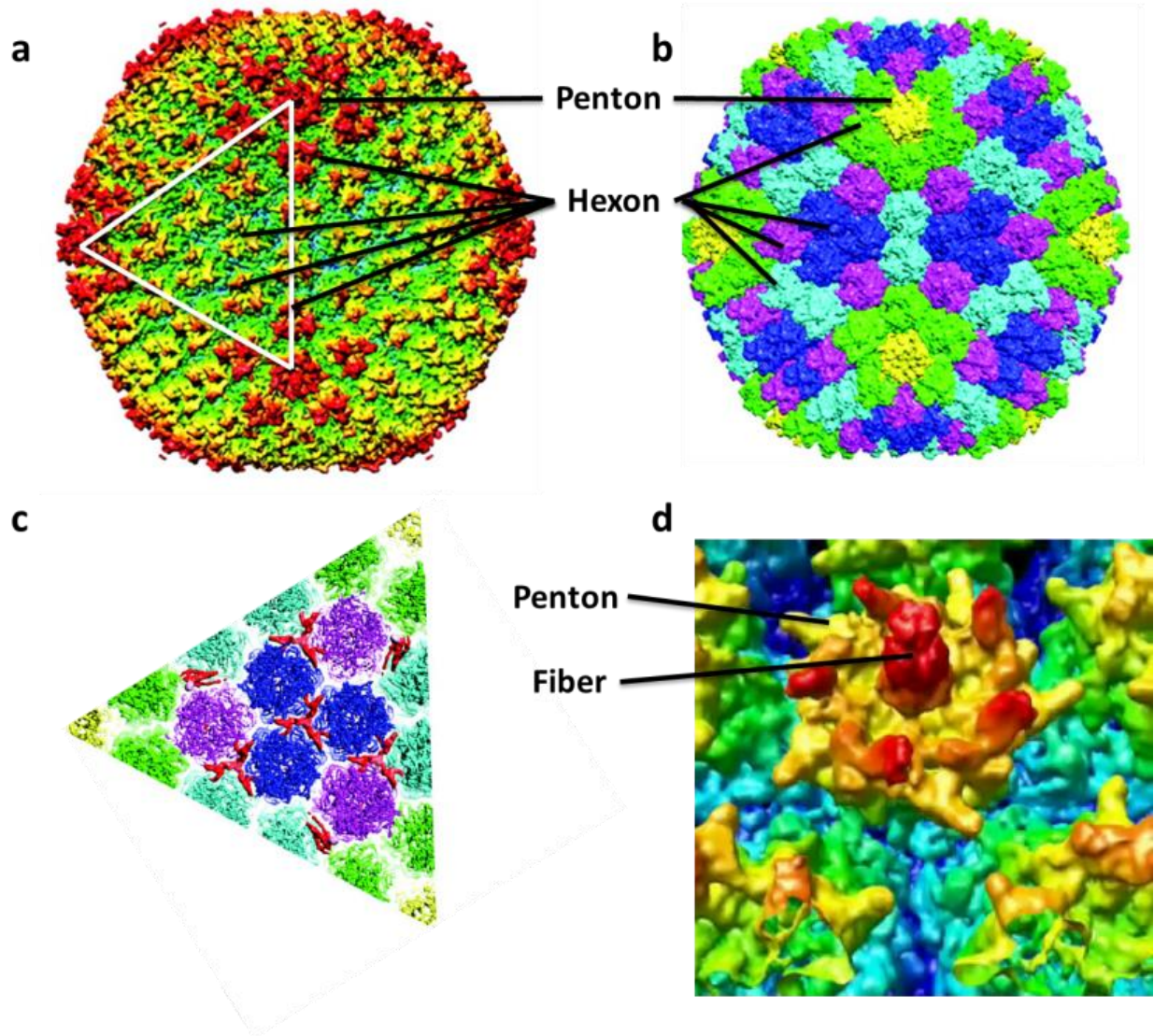


Figure 1-2. Reconstructed Cryo-EM image of Ad5 with Ad35 fiber

a) Surface view along a twofold symmetry axis (6 Å resolution); b) Pseudoatomic capsid calculated by applying icosahedral symmetry; c) One icosahedral face of the capsid including 12 hexon units (Ad5) and 1 penton unit (Ad2); d) One vertex region of the capsid illustrating penton base (Ad2) and fiber (Ad35F).
 *This figure was modified from reference [1] and [14] with the permission of publisher ("ASM Press").

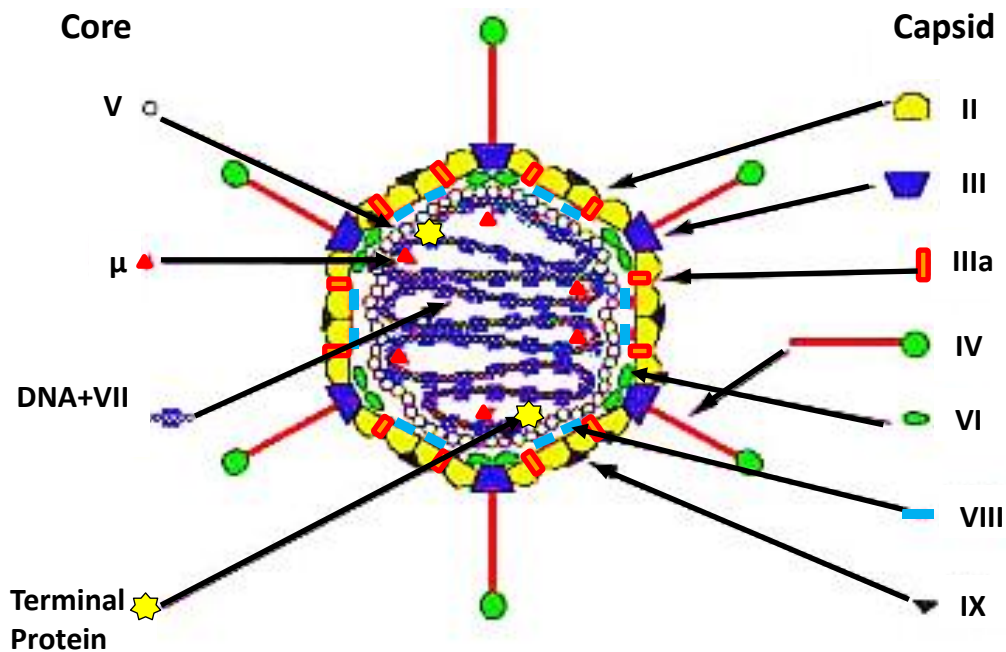


Figure 1-3. Anatomical Structure of Ad Virion

*This figure was reprinted from reference [2] with the permission of publisher (“nature publishing group”).

Table 1-2. Ad Structural Proteins

Protein	Mw (Da)	No. of copies	Location	Function
II	109,677	720	Hexon (trimer)	Formation of capsid shell
III	63,296	60	Penton base (pentamer)	Formation of capsid shell; entry
IV	61,960	36	Fiber (trimer)	Attachment to host cell; entry
IIIa	63,287	74 ± 1	Inner capsid surface below the penton base	Stabilization of capsid
VI	23,449	342 ± 4	Hexon-associated, inner capsid surface	Stabilization of capsid
VIII	14,539	211 ± 2	Hexon-associated, inner capsid surface	Stabilization of capsid
IX	14,339	247 ± 2	Outer surface of groups-of-nine hexons; edges of icosahedral faces	Stabilization of capsid
V	41,631	157 ± 1	Core, outer surface	Packaging of DNA genome
VII	19,412	835 ± 20	Core, bound to DNA	Packaging of DNA genome
μ	2,441	120 ± 1	Core	Packaging of DNA genome

*This table was based on Ad2 structure and reprinted from reference [1] with the permission of publisher (“ASM Press”).

1.3.2 Ad Serotype

To date, more than 50 human Ad serotypes are discovered and classified into six groups (A, B, C, D, E, F) based on percentages of guanine, cytosine in the DNA molecule and the ability to agglutinate red blood cells [15]. Members of the same group share a similar structure and pathogenicity (Table 1-3). Among different serotypes including non-human adenoviruses, human adenovirus serotype 2 (Ad2) and 5 (Ad5) have been most extensively studied and the majority of biological knowledge on the molecular basis was acquired from the studies of those two species. Accordingly, Ad2 and 5 have long been explored as “prototype vectors” [16] for virotherapy such as gene therapy, oncolytic therapy, and genetic immunization.

Table 1-3. Human Ad Serotypes

Subgroup	Serotype	Tropism
A	12 ^b , 18, 31 ^b	Cryptic
B1	3 ^{c,e} , 7, 16 ^c , 21 ^c , 50 ^c , 55	Respiratory
B2	11 ^c , 14 ^c , 34, 35 ^c	Renal
C	1, 2 ^{b,f} , 5 ^{b,f} , 6, 57	Respiratory
D	8 ^d , 9, 10, 13, 15b, 17, 19p ^b , 19a ^d , 20, 22-30, 32, 33, 36, 37 ^{c,d} , 38, 39, 42-49, 51, 53, 54, 56	Ocular & other
E	4 ^b	Respiratory
F	40, 41 ^b , 52	Intestinal

► Cell entry receptors found, **b**: CAR; **c**: CD46, **d**: SA (sialic acid), **e**: CD80/86, **f**: Heparan sulfate. *This table was modified from reference [17] with the permission of publisher ("ASM Press").

1.3.3 Ad Cell Entry

The majority of adenovirus serotypes (A, C, D, E and F with long fiber) employ fiber proteins to attach to the coxsackie and adenovirus receptor (CAR), which initiates cell entry. In addition to this high-affinity receptor interaction, secondary interaction of arginine-glycine-aspartate (RGD) motif in the virus penton protein with $\alpha_v\beta_3$ or $\alpha_v\beta_5$ integrin of host cell facilitates virus internalization. This integrin-mediated Ad internalization also requires the participation of several signaling molecules (Figure 1-4) [3]. Although CAR represents the major host cell receptor for Ad binding and infection, recently other host cell molecules are also reported to be involved in Ad's cell entry [18] (Figure 1-5). Notably, heparin sulfate proteoglycan (HSPG) *via* the bridge of coagulation factor IX (FIX) or vitamin K-dependent coagulation factor X (FX) or component C4 binding protein (C4BP) (Figure 1-5) [19-21] as well as SR-A (scavenger receptors type A) on Kupffer cells [22] were identified as the receptors for Ad2 and Ad5, explaining Ad's liver tropism. After endocytosis, mildly acidic conditions (~pH 6.0) trigger the escape of virions from endosomes into the cytoplasm prior to degradation by lysosomal proteases [23-24]. However, "the precise mechanisms involved in Ad-mediated endosome penetration remain poorly defined" [3]. Recently, Nemerow *et al.* provided the results suggesting that $\alpha_v\beta_5$ integrin selectively promote endosome penetration compared with $\alpha_v\beta_3$ integrin [25]. After released from endosome, viral capsids are rapidly transported in the cytoplasm along microtubules and dock onto the nuclear pore complex, then deliver the viral genome into the nucleus (Figure 1-4) [26].

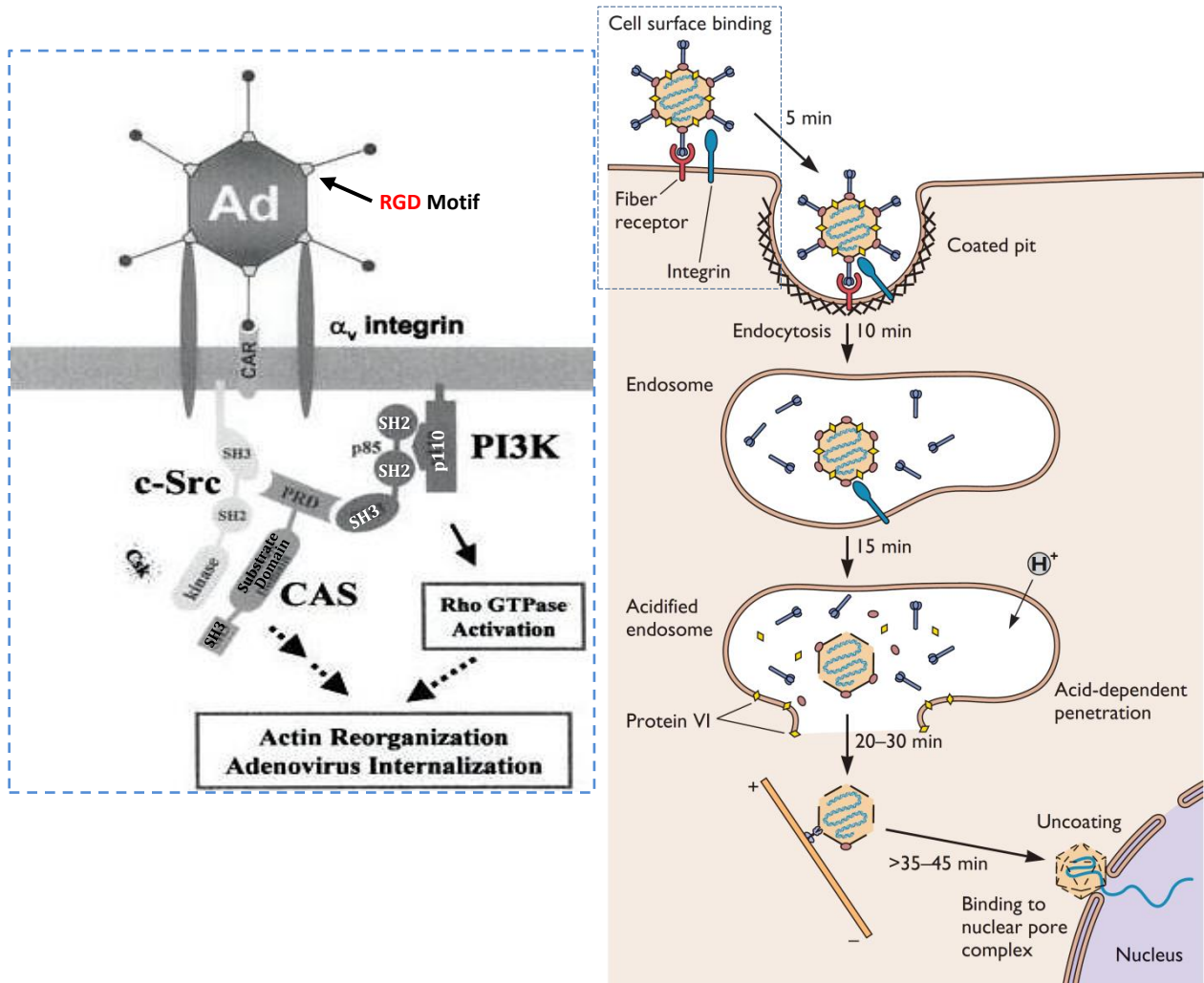


Figure 1-4. Schematic Diagram of Ad Receptor-Mediated Cell Entry

*This figure was modified from reference [1] and [3] with the permission of publisher ("ASM Press" and "Elsevier").

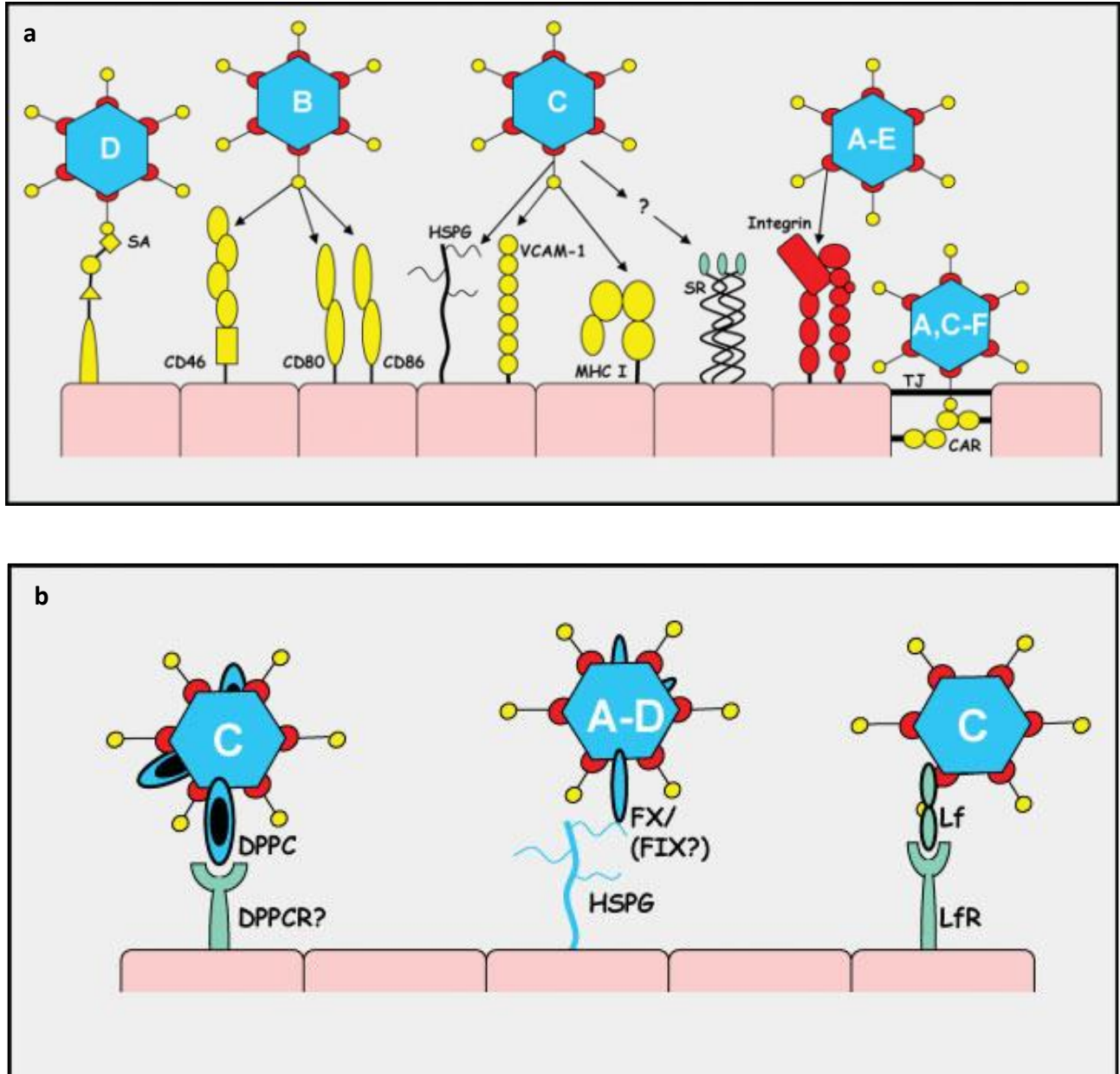


Figure 1-5. Different Cellular Receptors for Ad Entry

a) Direct bindings, SA: sialic acids, VCAM-1: vascular cell adhesion molecule 1, MHC-I: major histocompatibility complex class I, SR: scavenger receptors, TJ: tight junction **b) Indirect bindings**, DPPC(R): dipalmitoyl phosphatidylcholine (receptor), Fx: coagulation factor X, Lf(R): Lactoferrin (receptor). *This figure was reprinted from reference [2] with the permission of publisher ("John Wiley and Sons").

The molecular interactions of the fiber knob domain of adenovirus (Ad12) with the CAR extracellular domain was elucidated in detail *via* x-ray crystallography studies and mutagenesis experiments in 1999 [27-28]. That is, Bewley *et al.* reported the first crystal structure of the adenovirus fiber knob domain complexed with domain I of cellular CAR receptor [27]. The authors also claimed that the nature of the specificity of Ad12 knob for CAR is owing to the interactions of four loop regions of Ad12 with a single face of the CAR-D1 sandwich. Particularly, the AB loop in Ad12 knob contributes over 50% of interfacial protein-protein interactions, including the three hydrogen bonds and the conserved P418 residue [27]. As the authors demonstrated (Figure 1-6), the interaction of AB loop with CAR receptor is “lateral”, not the center of knob, which shed some light on understanding the Ad knob-CAR interactions at the molecular level and suggested a way to modify the tropism of Ad.

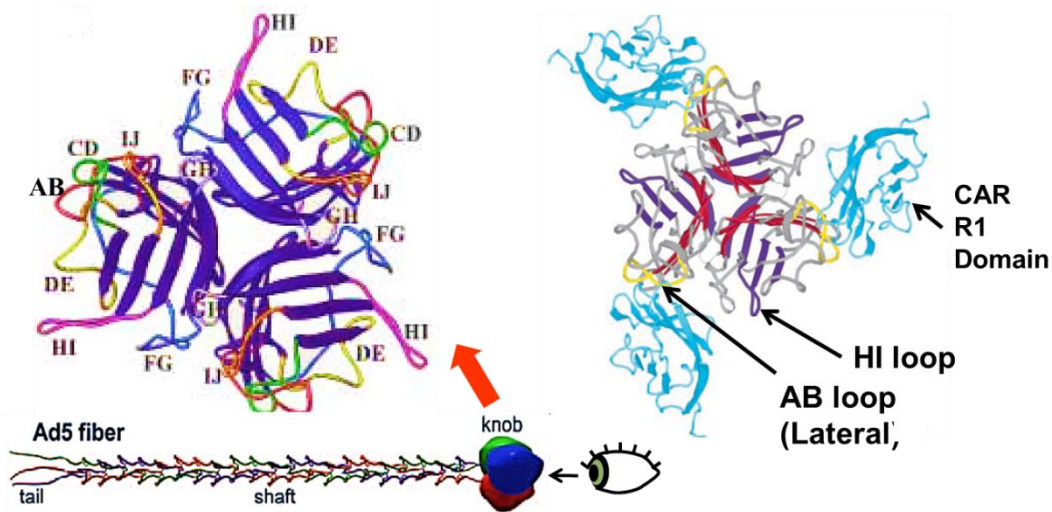


Figure 1-6. Ad fiber knob structure and cocrystal structure with CAR D1 domain

The CAR-binding site within the Ad5 knob domain involves the AB- and DE- loop, as well as β -strands B, E, and F. *This figure was modified from reference [2] and [27] with the permission of publisher ("NPG" and "AAAS").

Additionally, Chiu *et al.* proposed the interaction model between Ad-knob and cellular CAR, based on a crystal structure of penton protein and a pseudotyping experiment of knob protein, which can explain the cellular tropism of different serotypes. To wit, Chiu *et al.* claimed that Ad37 may not utilize CAR for cell entry due to the geometric constraints imposed by a rigid and short fiber [29]. The authors also demonstrated the hypothetical interaction model between RGD motifs and integrin coreceptors on cell membrane using cryo-EM image reconstruction (Figure 1-7).

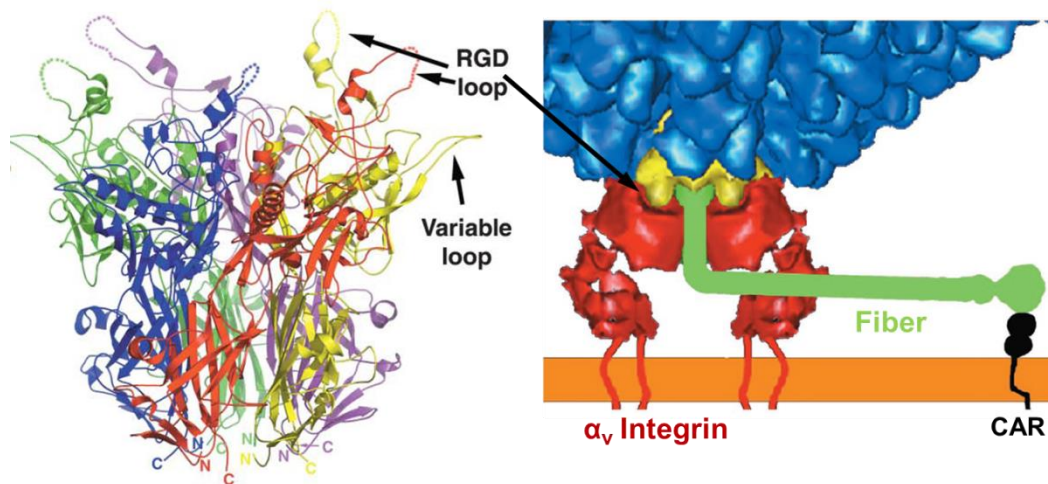


Figure 1-7. Structure of Ad Penton and Interaction Model of RGD Motif with Integrin on Cell Surface

The five RGD motifs on the penton base are indicated as dotted line in the left figure with different colors. The right cartoon illustrates the hypothetical model how RGD motif can interact with $\alpha_v\beta_3$ or $\alpha_v\beta_5$ integrin coreceptors for internalization. After the attachment of fiber knob to CAR on the cell surface (note that the interaction is lateral), then the flexible shaft is bent to allow the interaction between RGD motif and integrin. *This figure was modified from reference [30] and [31] with the permission of publisher ("Elsevier " and "ASM Press").

1.4 Engineering Ad Vector for Virotherapy

Despite encouraging early clinical advances, progress in therapeutic application of Ad has been hampered by a few limitations including promiscuous tropism, immunogenicity, and hepatic uptake. Ad's promiscuous tropism, the first hurdle to be overcome in Ad virotherapy, is

due to the non-specific expression of native receptors (e.g., CAR) among the different human tissues, which dictate the infectivity of Ad vectors. Unfortunately, CAR expression is not associated with any diseases. Further, “many types of tumor cells such as such as malignant glioma, ovarian, renal, bladder, prostate, colorectal cancers, express CAR at marginal or undetectable levels and are thus Ad-refractory” [3], which is the major obstacle in cancer gene therapy using Ad vectors. On the other hand, the normal human tissues expressing high level of CAR can be “random targets” by administered therapeutic vectors, causing the widespread dissemination of vehicles and subsequent uncontrolled transduction which may result in severe side effects such as direct toxicity and host immune responses as observed in the precedent [32]. Therefore, extensive studies have been performed to modify Ad’s CAR dependency. Ideally, novel Ad vectors should be capable of delivering therapeutic genes to addressed cells selectively through recognizing one distinct type of cell surface receptor uniquely expressed on the target cells (i.e., retargeting) in a CAR-independent manner (i.e., detargeting).

The strategies for Ad retargeting can be classified into three distinct approaches [2], i) direct conjugation of the ligand to the capsid using cross-linking chemical reaction [33], ii) genetic incorporation of the ligand into one of the proteins constituting the Ad capsid [34-37], iii) utilization of a “noncovalent protein bridge” (also known as an “adapter”, e.g., protein bearing CAR domain and avidin domain simultaneously), which has dual affinities to Ad surface structures (e.g., Ad knob domain) and a targeting ligand (e.g., biotin-ligand, Figure 1-8, c) [38]. All three strategies can allow a physical linkage between Ad particles and targeting molecules, but there are trade-offs between one approach and another. To wit, the chemical approach utilizes solvent accessible functional groups in capsid proteins such as ϵ -amino groups [33] of the lysines or sulfhydryl groups of cysteines [39] (Figure 1-8, a).

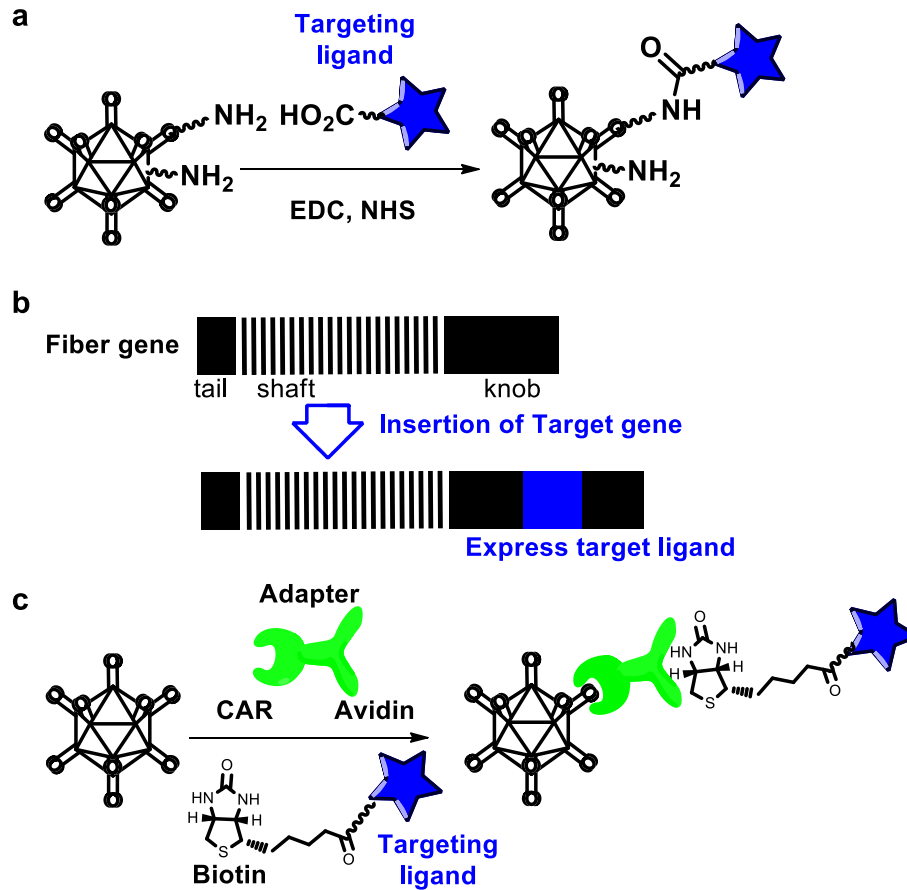


Figure 1-8. Different Strategies for Ad Retargeting

a) Chemical ligation of targeting molecules, b) Genetic insertion of targeting peptide into Ad fiber, c) Bispecific “adapter” approach.

The major advantage of chemical approach is the accessibility to a variety of ligands including synthetic small molecules, peptides, oligonucleotides, vitamins, growth factors, antibodies, which can be covalently linked to viral capsid and used to retarget Ad vectors. Additionally, this strategy does not require any modifications of Ad particles. However, chemical method has poor specificity for modifying viral proteins usually with low yield and can affect viral infectivity as well. Moreover, “a heterogeneous population of conjugated molecules complicates the issues in obtaining regulatory approval for a clinical trial” [3]. Genetic modification involves ablation of Ad’s natural tropism to CAR and concurrent generation of alternative receptor specificity to the

vector by well-developed genetic engineering techniques and has been a major targeting maneuver. Further, genetic approach provides a homogeneous single component vector. However, genetic ablation causes problems in viral production due to the abrogation of natural tropism and accompanies laborious cell culture works. More importantly, advantages of the genetic method are severely limited by the shortage of naturally existing molecules suitable for use as ligands. The variety of candidate protein ligands can be restrained not only by their steric disturbance with authentic viral proteins but also by incompatibility between the ligands and the Ad fiber regarding “biosynthesis and intracellular trafficking” [16], which results in the interference of viral assembly. Furthermore, the assembly of Ad virion takes place within infected cell nuclei, missing a window of opportunity for targeting proteins’ posttranslational modification which normally occurs in the endoplasmic reticulum (ER) or Golgi apparatus [40]. Thus, many attractive ligand candidates such as antibodies, growth factor have been limited by this genetic approach [35]. Finally, “Noncovalent bridge” approach can offer diverse functionality and little influence on viral physiology. Advantageously, this approach allows both retargeting and detargeting at once using the bispecific ligand having the dual affinity to a targeted receptor and Ad-knob domain, which abrogate the binding to its native primary receptor on the cell surface and induce a new affinity to the targeted receptor (Figure 1-8, c). However, the adaptor approach shows significant compositional variation between batches and standardization of the vector production is not trivial, rendering them less attractive for clinical use. Further, noncovalent interactions between the Ad virion and the ligand employed in a protein bridge may not be strong enough to confer high stability to the entire targeting complex *in vivo*, thereby compromise the efficiency of targeting. Recently, as an alternative, a bispecific recombinant fusion protein was employed as retargeting molecule, which can produce a single

stable component and permit the dual retargeting and detargeting functions simultaneously. For example, a single chain Fv antibody fragment (scFv) specific to Ad knob protein was genetically fused to cell receptor-specific ligands such as epidermal growth factor (EGF), which was termed as “adenobody” [41-42] and demonstrated a promising retargeting results *in vitro*. However, “the incorporation of exogenous targeting moieties can often have a remarkable impact on the solubility of resultant fusion protein” [3]. To overcome this drawback, the extracellular domain of CAR or monoclonal antibody (mAb) was fused with targeting moieties [43-44]. Nevertheless, the shortage of available targeting moieties and the reduced affinity upon fusion remain as issues in this fusion protein approach for the same reasons in the genetic approach. To resolve this conundrum, considerable efforts have been made, but more work is needed.

Ideal Ad retargeting strategy should allow access to any physiologically active molecules particularly having affinities to the receptors on the targeted cells without disturbing either viral physiology or effector functionality. In addition, the vector modification should be specific in order to produce a homogenous single component vector for a clinical trial and not hamper a facile Ad production. Lastly, all the requirements should be met without trade-off.

References

1. Flint, S. J.; Enquist, L. W.; Racaniello, V. R.; Skalka, A. M., *Principles of virology*. ASM Press: Washington, DC, **2009**.
2. Victor N. Krasnykh, J. T. D., Victor W. van Beusechem, Genetic Targeting of Adenoviral Vectors. *Mol. Ther.* **2000**, *1* (5), 391–405.
3. Curiel, D. T.; Douglas, J. T., Adenoviral vectors for gene therapy. 2002; p 165.
4. *Report and Recommendations of the Gene Therapy Working Group*; National Institutes of Health: Bethesda, Maryland, November 1, 2005.
5. Stuart H. Orkin, A. G. M. *Report and recommendations of the panel to assess the NIH investment in research gene therapy*; National Institutes of Health: December 7, 1995.
6. Hitt, M. M.; Addison, C. L.; Graham, F. L., Human adenovirus vectors for gene transfer into mammalian cells. *Adv Pharmacol* **1997**, *40*, 137-206.
7. Graham, F. L.; Prevec, L., Methods for construction of adenovirus vectors. *Mol. Biotechnol.* **1995**, *3* (3), 207-20.
8. Yeh, P.; Perricaudet, M., Advances in adenoviral vectors: from genetic engineering to their biology. *FASEB J.* **1997**, *11* (8), 615-623.
9. Toth, K.; Dhar, D.; Wold, W. S., Oncolytic (replication-competent) adenoviruses as anticancer agents. *Expert Opin. Biol. Ther.* **2010**, *10* (3), 353-368.
10. Cervantes-García, D.; Ortiz-López, R.; Mayek-Pérez, N.; Rojas-Martínez, A., Oncolytic virotherapy. *Ann. Hepatol* **2008**, *7*, 34-45.
11. Rux, J. J.; Burnett, R. M., Adenovirus Structure. *Hum. Gene Ther.* **2004**, *15* (12), 1167-1176.
12. Stewart, P. L.; Burnett, R. M.; Cyrklaff, M.; Fuller, S. D., Image reconstruction reveals the complex molecular organization of adenovirus. *Cell* **1991**, *67* (1), 145-154.
13. Reddy, V. S.; Natchiar, S. K.; Stewart, P. L.; Nemerow, G. R., Crystal Structure of Human Adenovirus at 3.5 Å Resolution. *Science* **2010**, *329* (5995), 1071-1075.
14. Saban, S.; Silvestry, M.; Nemerow, G.; Stewart, P., Visualization of α -helices in a 6 Å resolution cryoEM structure of adenovirus allows refinement of capsid protein assignments. *J. Virol.* **2006**, *80*, 12049-12059.
15. Norrby, E.; van der Veen, J.; Espmark, A., A new serological technique for identification of adenovirus infections. *Proc. Soc. Exp. Biol. Med.* **1970**, *134* (3), 889-95.

16. Belousova, N.; Mikheeva, G.; Gelovani, J.; Krasnykh, V., Modification of Adenovirus Capsid with a Designed Protein Ligand Yields a Gene Vector Targeted to a Major Molecular Marker of Cancer. *J. Virol.* **2008**, *82* (2), 630-637.
17. Zhang, Y.; Bergelson, J. M., Adenovirus receptors. *J. Virol.* **2005**, *79* (19), 12125-12131.
18. Arnberg, N., Adenovirus receptors: implications for tropism, treatment and targeting. *Rev. Med. Virol.* **2009**, *19* (3), 165-178.
19. Dehecchi, M. C.; Tamanini, A.; Bonizzato, A.; Cabrini, G., Heparan sulfate glycosaminoglycans are involved in adenovirus type 5 and 2-host cell interactions. *Virology* **2000**, *268* (2), 382-390.
20. Parker, A. L.; Waddington, S. N.; Nicol, C. G.; Shayakhmetov, D. M.; Buckley, S. M.; Denby, L.; Kembal-Cook, G.; Ni, S.; Lieber, A.; McVey, J. H., Multiple vitamin K-dependent coagulation zymogens promote adenovirus-mediated gene delivery to hepatocytes. *Blood* **2006**, *108* (8), 2554-2561.
21. Waddington, S. N.; McVey, J. H.; Bhella, D.; Parker, A. L.; Barker, K.; Atoda, H.; Pink, R.; Buckley, S. M. K.; Greig, J. A.; Denby, L.; Custers, J.; Morita, T.; Francischetti, I. M. B.; Monteiro, R. Q.; Barouch, D. H.; van Rooijen, N.; Napoli, C.; Havenga, M. J. E.; Nicklin, S. A.; Baker, A. H., Adenovirus Serotype 5 Hexon Mediates Liver Gene Transfer. *Cell* **2008**, *132* (3), 397-409.
22. Haisma, H. J.; Boesjes, M.; Beerens, A. M.; van der Strate, B. W. A.; Curiel, D. T.; Plüddemann, A.; Gordon, S.; Bellu, A. R., Scavenger Receptor A: A New Route for Adenovirus 5. *Mol. Pharm.* **2009**, *6* (2), 366-374.
23. Blumenthal, R.; Seth, P.; Willingham, M. C.; Pastan, I., pH-dependent lysis of liposomes by adenovirus. *Biochemistry* **1986**, *25* (8), 2231-2237.
24. Greber, U. F.; Willetts, M.; Webster, P.; Helenius, A., Stepwise dismantling of adenovirus 2 during entry into cells. *Cell* **1993**, *75* (3), 477-486.
25. Wickham, T. J.; Filardo, E. J.; Cheresch, D. A.; Nemerow, G. R., Integrin alpha v beta 5 selectively promotes adenovirus mediated cell membrane permeabilization. *J. Cell Biol.* **1994**, *127* (1), 257-264.
26. Strunze, S.; Trotman, L. C.; Boucke, K.; Greber, U. F., Nuclear Targeting of Adenovirus Type 2 Requires CRM1-mediated Nuclear Export. *Mol. Biol. Cell* **2005**, *16* (6), 2999-3009.
27. Bewley, M. C.; Springer, K.; Zhang, Y.-B.; Freimuth, P.; Flanagan, J. M., Structural Analysis of the Mechanism of Adenovirus Binding to Its Human Cellular Receptor, CAR. *Science* **1999**, *286* (5444), 1579-1583.

28. Howitt, J.; Bewley, M. C.; Graziano, V.; Flanagan, J. M.; Freimuth, P., Structural Basis for Variation in Adenovirus Affinity for the Cellular Coxsackievirus and Adenovirus Receptor. *J. Biol. Chem.* **2003**, *278* (28), 26208-26215.
29. Chiu, C. Y.; Wu, E.; Brown, S. L.; Von Seggern, D. J.; Nemerow, G. R.; Stewart, P. L., Structural Analysis of a Fiber-Pseudotyped Adenovirus with Ocular Tropism Suggests Differential Modes of Cell Receptor Interactions. *J. Virol.* **2001**, *75* (11), 5375-5380.
30. Zubieta, C.; Schoehn, G.; Chroboczek, J.; Cusack, S., The Structure of the Human Adenovirus 2 Penton. *Mol. Cell* **2005**, *17* (1), 121-135.
31. Chiu, C. Y.; Wu, E.; Brown, S. L.; Von Seggern, D. J.; Nemerow, G. R.; Stewart, P. L., Structural analysis of a fiber-pseudotyped adenovirus with ocular tropism suggests differential modes of cell receptor interactions. *J. Virol.* **2001**, *75* (11), 5375-5380.
32. Raper, S. E.; Chirmule, N.; Lee, F. S.; Wivel, N. A.; Bagg, A.; Gao, G.-p.; Wilson, J. M.; Batshaw, M. L., Fatal systemic inflammatory response syndrome in a ornithine transcarbamylase deficient patient following adenoviral gene transfer. *Mol. Genet. Metab.* **2003**, *80* (1-2), 148-158.
33. O'Riordan, C. R.; Lachapelle, A.; Delgado, C.; Parkes, V.; Wadsworth, S. C.; Smith, A. E.; Francis, G. E., PEGylation of adenovirus with retention of infectivity and protection from neutralizing antibody in vitro and in vivo. *Hum. Gene Ther.* **1999**, *10* (8), 1349-1358.
34. Magnusson, M. K.; Hong, S. S.; Boulanger, P.; Lindholm, L., Genetic Retargeting of Adenovirus: Novel Strategy Employing "Deknocking" of the Fiber. *J. Virol.* **2001**, *75* (16), 7280-7289.
35. Magnusson, M. K.; See Hong, S.; Henning, P.; Boulanger, P.; Lindholm, L., Genetic retargeting of adenovirus vectors: functionality of targeting ligands and their influence on virus viability. *J. Gene Med.* **2002**, *4* (4), 356-370.
36. Henning, P.; Lundgren, E.; Carlsson, M.; Frykholm, K.; Johannisson, J.; Magnusson, M. K.; Tång, E.; Franqueville, L.; Hong, S. S.; Lindholm, L.; Boulanger, P., Adenovirus type 5 fiber knob domain has a critical role in fiber protein synthesis and encapsidation. *J. Gen. Virol.* **2006**, *87* (11), 3151-3160.
37. Magnusson, M. K.; Henning, P.; Myhre, S.; Wikman, M.; Uil, T. G.; Friedman, M.; Andersson, K. M. E.; Hong, S. S.; Hoeben, R. C.; Habib, N. A.; Stahl, S.; Boulanger, P.; Lindholm, L., Adenovirus 5 vector genetically re-targeted by an Affibody molecule with specificity for tumor antigen HER2//neu. *Cancer Gene Ther.* **2007**, *14* (5), 468-479.
38. Douglas, J. T.; Rogers, B. E.; Rosenfeld, M. E.; Michael, S. I.; Feng, M. Z.; Curiel, D. T., Targeted gene delivery by tropism-modified adenoviral vectors. *Nat. Biotechnol.* **1996**, *14* (11), 1574-1578.

39. Kreppel, F.; Gackowski, J.; Schmidt, E.; Kochanek, S., Combined genetic and chemical capsid modifications enable flexible and efficient de- and retargeting of adenovirus vectors. *Mol. Ther.* **2005**, *12* (1), 107-17.
40. Belousova, N.; Mikheeva, G.; Gelovani, J.; Krasnykh, V., Modification of adenovirus capsid with a designed protein ligand yields a gene vector targeted to a major molecular marker of cancer. *J. Virol.* **2008**, *82* (2), 630-7.
41. Haismaa, H. J.; Kampsa, G. K.; Boumaa, A.; Geelb, T. M.; Rotsb, M. G.; Kariatha, A.; Bellua, A. R., Selective targeting of adenovirus to $\alpha_v\beta_3$ integrins, VEGFR2 and Tie2 endothelial receptors by angio-adenobodies. *Int. J. Pharm.* **2010**, *391*, 155–161.
42. Watkins, S.; Mesyanzhinov, V.; Kurochkina, L.; Hawkins, R., The 'adenobody' approach to viral targeting: specific and enhanced adenoviral gene delivery. *Gene Ther.* **1997**, *4* (10), 1004.
43. Dmitriev, I.; Kashentseva, E.; Rogers, B. E.; Krasnykh, V.; Curiel, D. T., Ectodomain of coxsackievirus and adenovirus receptor genetically fused to epidermal growth factor mediates adenovirus targeting to epidermal growth factor receptor-positive cells. *J. Virol.* **2000**, *74* (15), 6875-6884.
44. Li, E.; Brown, S.; Von Seggern, D.; Brown, G.; Nemerow, G., Signaling antibodies complexed with adenovirus circumvent CAR and integrin interactions and improve gene delivery. *Gene Ther.* **2000**, *7* (18), 1593.

Chapter 2. Engineering Adenovirus *via* Bioorthogonal “Click Chemistry”

2.1 Introduction

When Kolb, Finn, and Sharpless first coined a term “click chemistry”, it was conceptually intriguing, but its potential was not noticed to the full [3]. However, since Sharpless and Meldal reported Cu(I) can remarkably enhance the rate of the Huisgen 1,3-dipolar cycloaddition reaction of organic azides and terminal alkynes [4-5], it have been rapidly applied over a broad range of areas and now became one of the most important chemistries in the field of bioconjugation, drug discovery, material science, and radio chemistry. Especially in the bioconjugation field, the impact of “click chemistry” has been extensive because it is “bioorthogonal” and well suited for the physiological reaction conditions (i.e., aqueous, pH ~7, RT). That is, the copper-catalyzed azide-alkyne [3+2] cycloaddition (CuAAC) is robust enough to work extremely low concentration even in the presence of a wide variety of other functionalities and irreversible in physiological condition. Besides those advantages, azide and alkyne moieties are readily introducible into biomolecules due to their small size and biological inertness.

2.2 Chemoselective Ligation and Bioorthogonal Reagent Pairs

One of the major challenges in engineering biological molecule was the requirement for the exquisite chemical reactions having a level of selectivity comparable to that of antibody-antigen recognition within the complex biological environment, which motivated the development of chemoselective ligation, “the selective covalent coupling of mutually and uniquely reactive functional groups under mild, aqueous conditions” [6]. In this context, the non-native ketone and aldehyde groups were introduced site-specifically into peptide segments, glycopeptides, and cell-surface glycoconjugates *via* chemical or enzymatic or metabolic methods

and functional groups having orthogonal reactivity (Figure 2-1) with ketone and aldehyde such as hydrazide, aminoxy, and thiosemicarbazone were employed as chemoselective coupling partners (Table 2-1) [6]. However, the orthogonality of those carbonyl condensations are limited by optimum pH (5~6) values that cannot be achieved *in vivo*, and abundant Keto-metabolites within cells and in biological fluids [7].

U (set of functional groups in the system) = {A, B, C, D, ...}

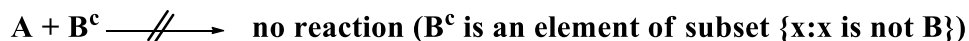
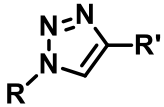
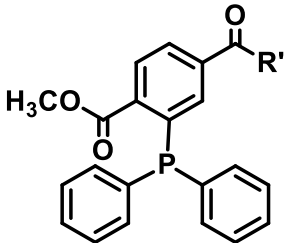
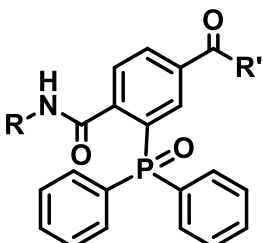
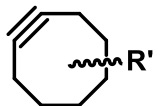
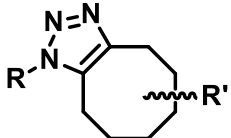
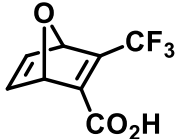
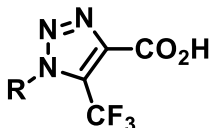


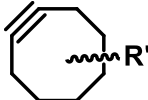
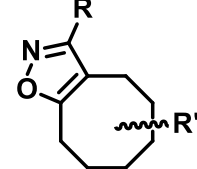
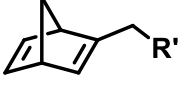
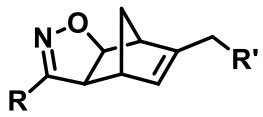
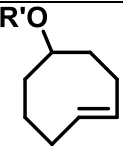
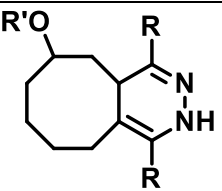
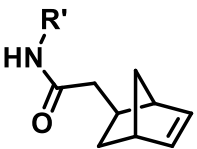
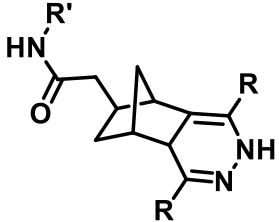
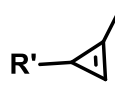
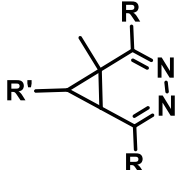
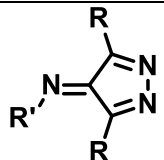
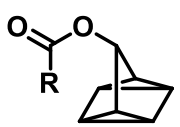
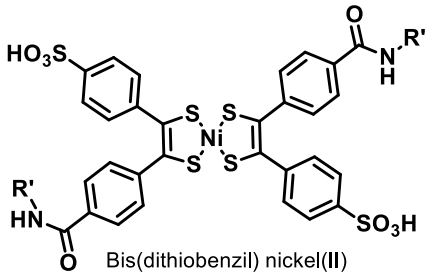
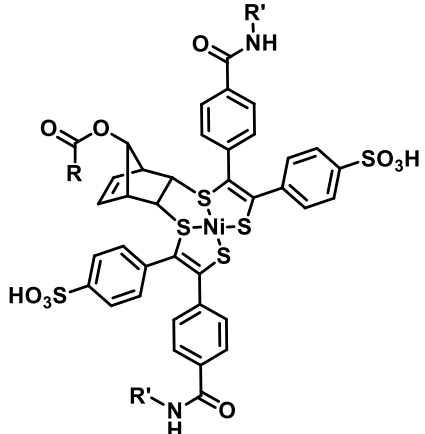
Figure 2-1. Conceptual Representation of Orthogonal Reactivity

After the advent of CuAAC, azide has been exploited as a bioorthogonal functional group owing to its advantages such as i) ideal orthogonality in biological milieu containing the abundance of nucleophiles, reducing agents, and other functionality (∵ azide and alkyne are unnatural moieties.), ii) reactivity in normal physiological conditions (optimal $k \approx 10^4 \sim 10^5 \text{ M}^{-1} \text{ s}^{-1}$ at RT, in aqueous solution [8-9]), and iii) stability of triazole (reaction product). However, the requirement for a cytotoxic cuprous catalyst restricts the utility of CuAAC *in vivo* application. Therefore, copper-free “click” reactions such as the Staudinger ligation of azides with functionalized phosphines, and strain-promoted alkyne-azide cycloaddition (SPAAC) were explored [10-12] as an alternative, despite slower reaction rates (e.g., Staudinger ligation $k \approx 0.002 \text{ M}^{-1} \text{ s}^{-1}$ in $\text{CD}_3\text{CN}/\text{H}_2\text{O} = 95/5$ at $20 \text{ }^\circ\text{C}$; azadibenzocyclooctyne, ADIBO, $k \approx 0.31 \text{ M}^{-1} \text{ s}^{-1}$ in CD_3OD at RT [13]) than CuAAC. Recently, inverse-electron-demand Diels–Alder cycloaddition

between *trans*-cyclooctene (TCO) and tetrazine, known to have an unrivaled kinetics ($k \approx 2,000 \text{ M}^{-1} \text{ s}^{-1}$ in MeOH/H₂O = 9/1 [14]) among metal-free bioorthogonal reactions, was also employed for the *in vivo* application, but the instability of TCO and tetrazine derivatives limits the wide application of this approach. Accordingly, other chemoselective reactions are actively being tested as novel bioorthogonal reagent pairs for *in vivo* application. (Table 2-1)

Table 2-1. Bioorthogonal Reagent Pairs Used in Living Systems

Bioorthogonal Pair A	Bioorthogonal Pair B	Product
$\text{R}-\overset{\text{O}}{\parallel}{\text{C}}-\text{R}''(\text{H})$ Aldehyde/Ketone [15-17]	$\text{H}_2\text{N}-\overset{\text{H}}{\parallel}{\text{N}}-\overset{\text{O}}{\parallel}{\text{C}}-\text{R}'$ Hydrazide	$\text{R}-\overset{\text{H}}{\parallel}{\text{N}}-\overset{\text{H}}{\parallel}{\text{N}}-\overset{\text{O}}{\parallel}{\text{C}}-\text{R}'$ Hydrazone
	$\text{H}_2\text{N}-\text{O}-\text{R}'$ Aminooxy	$\text{R}-\overset{\text{N}-\text{OR}'}{\parallel}{\text{C}}-\text{R}''$ Oxime
	$\text{H}_2\text{N}-\overset{\text{H}}{\parallel}{\text{N}}-\overset{\text{H}}{\parallel}{\text{C}}(\text{S})-\text{R}'$ Thiosemicarbazide	$\text{R}-\overset{\text{H}}{\parallel}{\text{N}}-\overset{\text{H}}{\parallel}{\text{N}}-\overset{\text{H}}{\parallel}{\text{C}}(\text{S})-\text{R}'$ Thiosemicarbazone
$\text{R}-\text{N}_3$ Azide	$\equiv\text{R}'$, Cu(I) Terminal alkyne w/ Copper(I)	
	 Staudinger-phosphine [18]	
	 Strained-alkyne [19-21]	
	 Oxanorbornadiene [22]	

$\text{R}-\text{N}^{\oplus}=\text{O}^{-}$ <p>Nitron</p>	 <p>Strained-alkyne [23]</p>	
	 <p>Norbornadiene [24]</p>	
$\begin{array}{c} \text{N}=\text{N} \\ \quad \\ \text{R} \quad \text{R} \\ \quad \\ \text{N}-\text{N} \end{array}$ <p>Tetrazine</p>	 <p><i>trans</i>-cyclooctene [25]</p>	
$\begin{array}{c} \text{N}=\text{N} \\ \quad \\ \text{R} \quad \text{R} \\ \quad \\ \text{N}-\text{N} \end{array}$ <p>Tetrazine</p>	 <p>Norbornene [26]</p>	
	 <p>Cyclopropene [27]</p>	
	$\text{R}'-\text{N}^{\oplus}=\text{C}^{-}$ <p>Isonitrile [28]</p>	
 <p>Quadricyclane [29]</p>	 <p>Bis(dithiobenzil) nickel(II)</p>	

2.3 Introducing Clickable Tags into Biomolecules

A variety of strategies have been attempted to incorporate azide tag as a “clickable” chemical handle, which include synthetic approach [30-31], *in vitro* enzymatic transfer [32-33], the use of covalent inhibitors [34], and metabolic labeling. Particularly, metabolic labeling techniques opened the door for *in vivo* incorporation of azide- or alkyne-labeled “biological building blocks” (amino acids, sugars, nucleotide, and lipids) into cellular structures [35-36]. In other words, the ability to utilize cellular machinery for the introduction of “clickable” bioorthogonal functionalities granted enormous benefits to elucidating biochemical mechanisms and engineering biomolecules with minimal perturbation.

2.3.1 Bioorthogonal Noncanonical Amino acid Tagging (BONCAT)

In 2006, Dieterich *et al.* reported a new technology which can identify newly synthesized proteins in mammalian cells with azide-bearing amino acid, azidohomoalanine (AHA) [35]. This metabolic labeling technique is based on the residue specific incorporation of AHA as a methionine (Met) surrogate through translational competition [37].

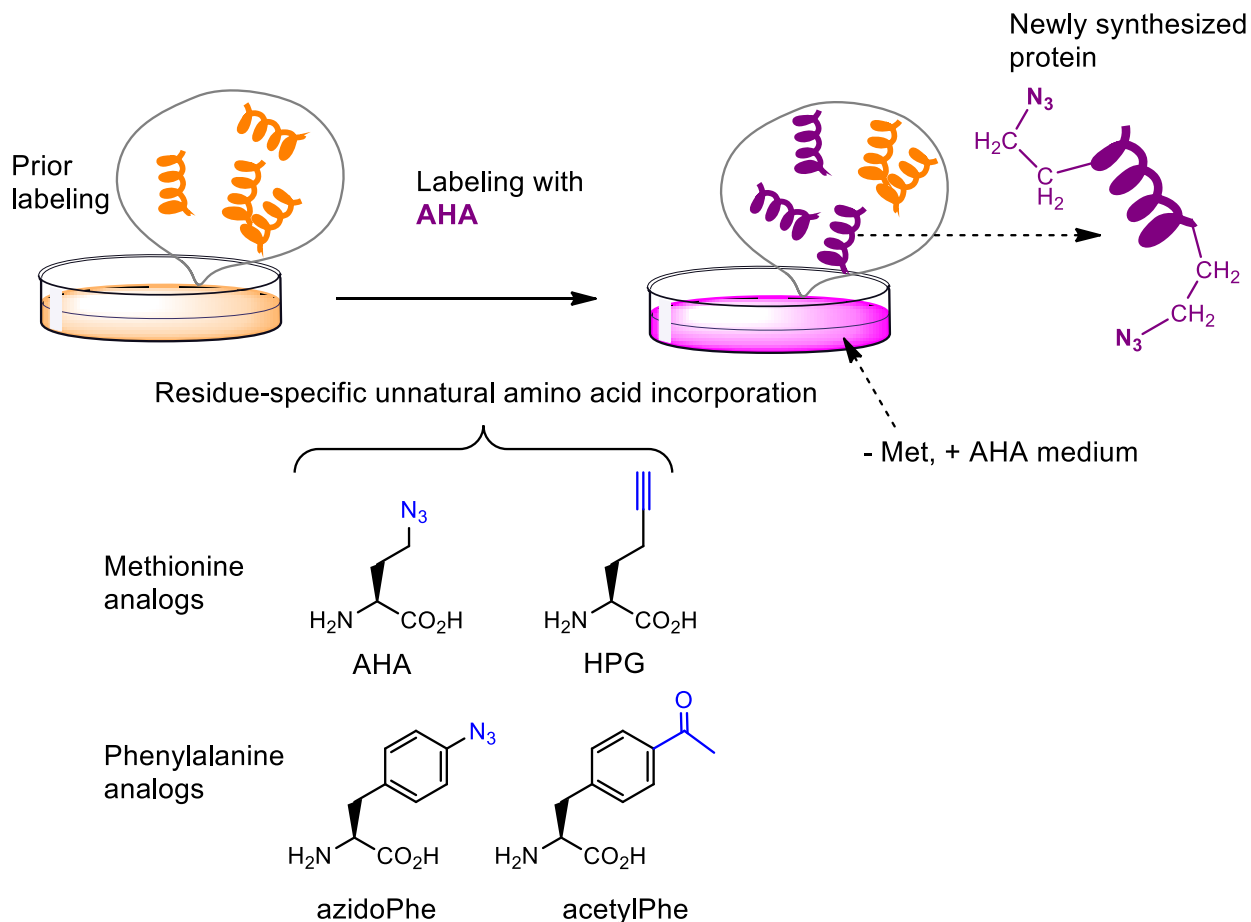


Figure 2-2. The BONCAT strategy for labeling newly synthesized proteins

*This picture was modified from reference [38] with the permission of publisher (“nature publishing group”).

The significance of this metabolic labeling technique lies on the fact that incorporation of AHA or homopropargylglycine (HPG) does not overtly perturb cellular physiology [35]. Hence, this

labeling technique could be employed to overcome the drawbacks of chemical modification for adenovirus with sustained accessibility to a wide variety of targeting molecules. In other words, incorporation of AHA or HPG into viral proteins is expected to have a minimal effect on virus physiology as demonstrated by BONCAT approach.

2.3.2 Metabolic Labeling of Unnatural Sugars

The Bertozzi group reported that unnatural azido sugars can be incorporated into glycoconjugates - carbohydrates covalently linked with other biological molecules such as proteins and lipids – *via* glycan biosynthetic pathways [1, 39]. That is, azido analogs of *N*-acetylmannosamine (ManNAz) [18] and sialic acid (SiaNAz) [40] are metabolized by cellular biosynthetic pathways and converted to cell surface azido sialosides (Figure 2-3). In addition, an azido analog of *N*-acetylglucosamine (GlcNAz) can be metabolically introduced at the core position of mucin-type *O*-linked glycoproteins [41] and also incorporated into cytoplasmic and nuclear glycoproteins [39] (Figure 2-4).

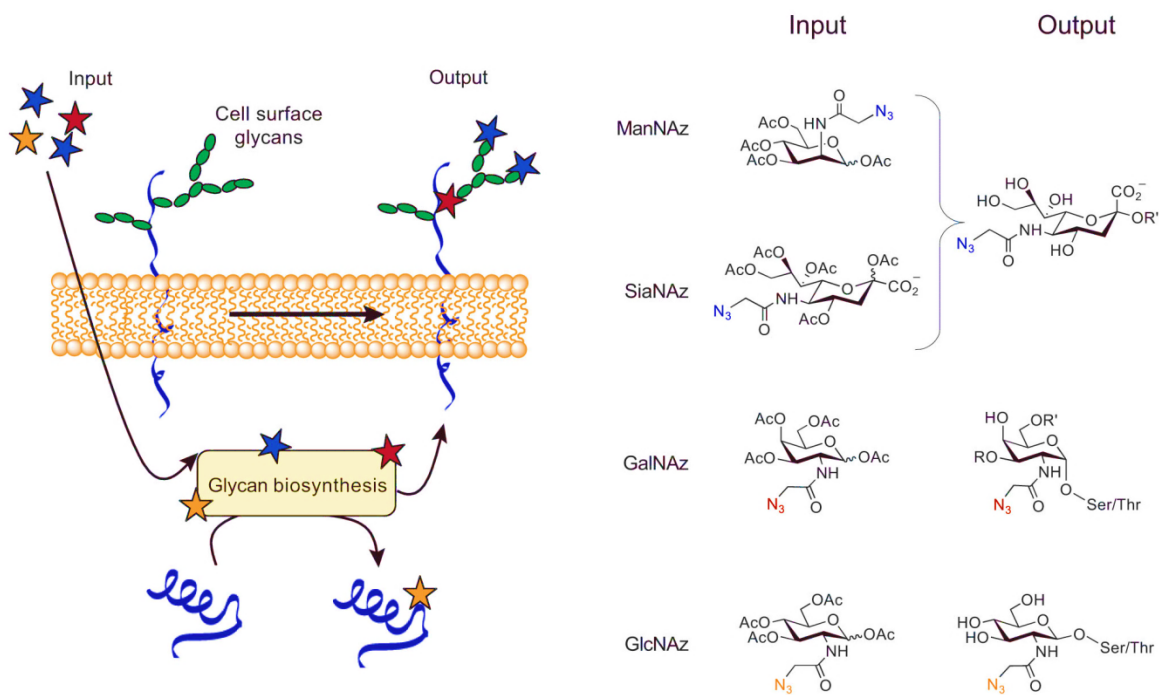


Figure 2-3. Incorporation of unnatural sugars on cell surface glycans

*This picture was reprinted from reference [39] with the permission of publisher (“nature publishing group”).

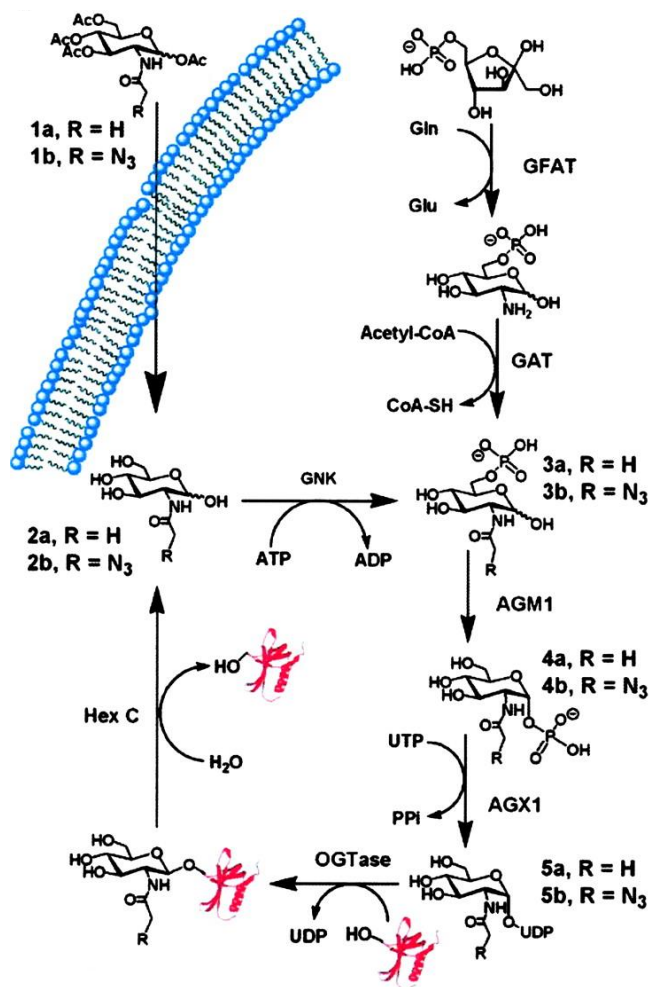


Figure 2-4. Incorporation of unnatural sugars into nucleocytoplasmic proteins

Exogenous unnatural sugar, Ac₄GlcNAz (1b), diffuses into the cell and is deacylated through the action of intracellular esterases, and then enters into the salvage pathway, resulting in labeling of nucleocytoplasmic glycoproteins with unnatural sugar (GlcNAz). *This figure was reprinted from the reference [1], © 2003 by National Academy of Sciences.

Notably, Boyce *et al.* reported that “*N*-azidoacetylgalactosamine (GalNAz) can be converted by endogenous mammalian biosynthetic enzymes (GALK2 and AGX1/2) to UDP-GalNAz through GalNAc salvage pathway and then epimerized to UDP-*N*-azidoacetylglucosamine (GlcNAz) by mammalian enzyme UDP-galactose 4'-epimerase (GALE). *O*-GlcNAc transferase accepts UDP-GlcNAz as a nucleotide-sugar donor, appending an azido sugar onto its native substrates” [2] (Figure 2-5).

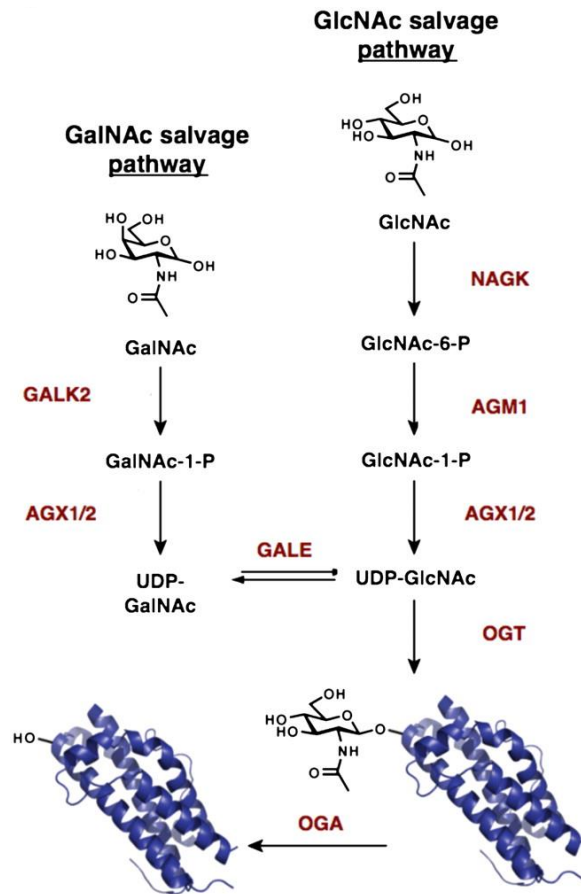


Figure 2-5. The GlcNAc and GalNAc salvage and O-GlcNAc signaling pathways

*This picture was reprinted from reference [2], © 2011 by National Academy of Sciences.

2.3.3 Unnatural Substrate Labeling onto Adenoviral Capsids

In the context of modifying Ad vectors without perturbing viral physiology and allowing the accessibility to a variety of targeting repertoire *via* “click” reaction. Carrico *et al.* introduced novel metabolic labeling strategies to engineering Ad particles using unnatural sugar analogs (GlcNAz or GalNAz) and unnatural amino acids (AHA or HPG) (Figure 2-6, Figure 2-7) [42-43].

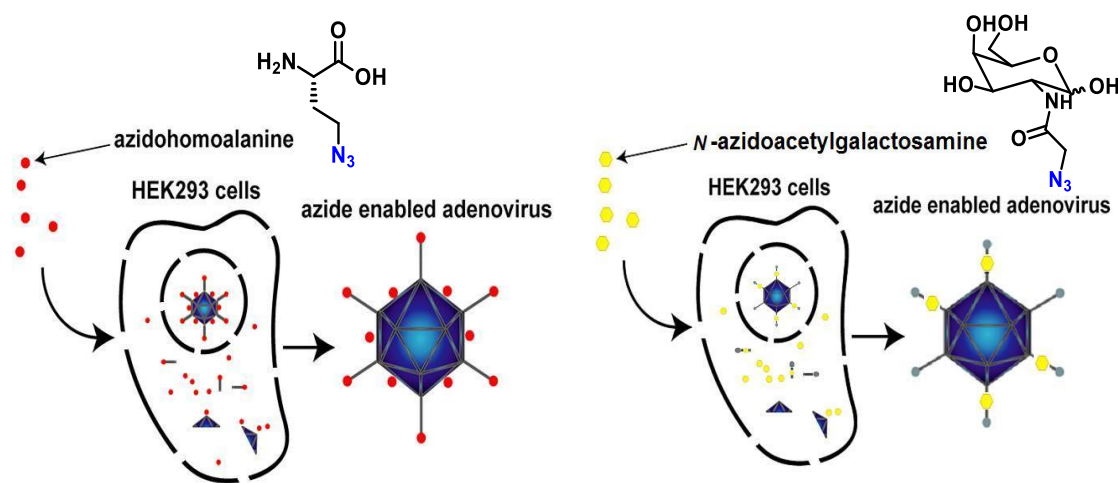


Figure 2-6. Biosynthetic Incorporation of Unnatural Amino acids and Sugars into Viral Protein

Ad5 was reported to have a single *O*-GlcNAc residue on Ser-109 of the fiber protein, a homotrimer protein extruded on 12 vertices of icosahedron viral capsid, and ~ 50% of fibers are known to be glycosylated [44]. Using cell growth media containing 50 μ M Ac₄GalNz, Carrico *et al.* could label Ad the same number of fibers (~50%) as intact Ad. The best labeling results was obtained by Ac₄GalNAz due to the peracetylated sugars' cell permeability and the absence of rate limiting phosphorylation step catalyzed by NAGK only existing in GlcNAc salvage pathway (*vid.* Figure 2-5).

The concentration of unnatural sugar was controlled at 50 μM level based on reported cytotoxicity of higher concentrated sugar analog. The *O*-GlcNAz enabled Ad was used as our major platform vector due to the well characterized specific modification sites and various clickable partner moieties such as a terminal alkyne, a Staudinger phosphine, and a strained alkyne.

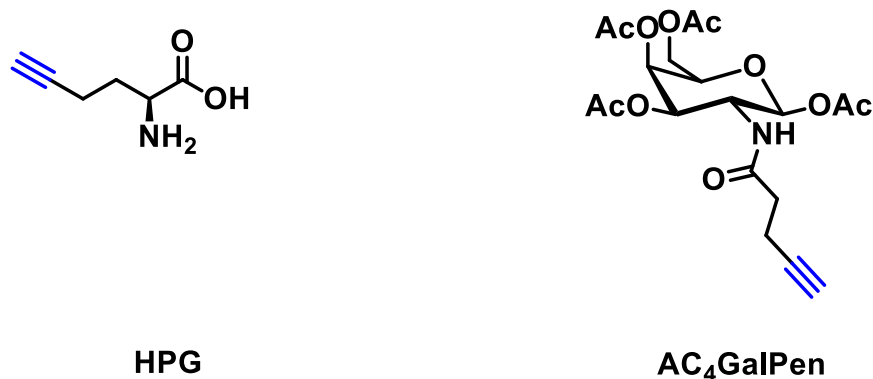


Figure 2-7. Alkyne Substrate HPG, AC₄GalPen

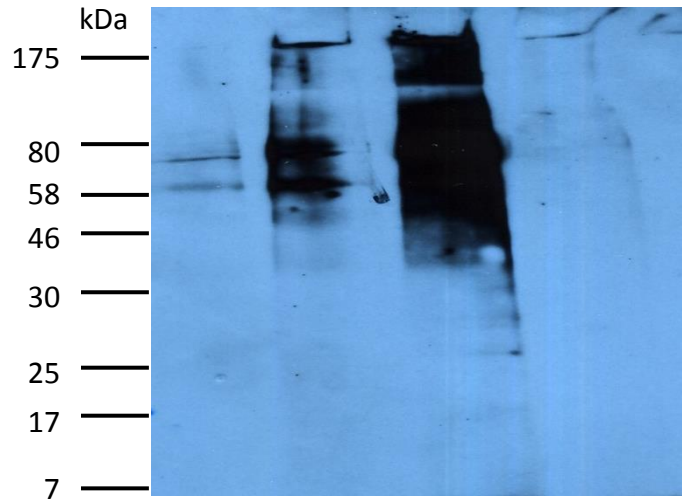
As reported by Carrico *et al.* [43, 45], AHA or HPG can be incorporated into Ad-proteins as a Met surrogate in the protein translational machinery. With 6 h pulse window (18 h ~ 24 h post infection based on Ad's protein expression profile) using a Met deficient growth media supplemented with 4 mM ~ 32 mM (saturation) unnatural amino acids during viral growth phase, Carrico *et al.* could successfully label viral proteins which was characterized by MALDI-TOF and Alkyne-FLAG western blot [45]. The use of mammalian producer cells (HEK 293) limits high level of azide incorporation due to a pre-existing Met pool within HEK 293. Additionally, Met is known to a 490-fold better substrate for the cognate amino acyl t-RNA synthetase compared with AHA in *E. coli*, which presumably lead to minimal perturbations on Ad's structural stability and infectivity. Minimal perturbations of viral physiology were assessed by particle production and infectivity assays using azide- or alkyne-enabled Ad [42-43, 45].

Moreover, the normal productions of penton viral proteins were also probed by fluorescent western blots using AHA-labeled Ad [46]. Finally, the number of labeled proteins were assessed by fluorescence gel scanning, representing ~360 hexons /720, ~60 pentons/60, ~36 fibers/36 with 32 mM AHA labeling; and ~130 hexons/720, ~36 pentons/60, ~20 fibers/36 with 4 mM HPG; and ~22 fibers/36 with Ac₄GalNAz. In an effort to develop dual functioning vectors (e.g. targeting + imaging), a dually labeled Ad vector was also generated using Ac₄GalNAz and HPG [43]. In other words, the dual modified Ads were prepared *via* the simultaneous metabolic labeling with azide-bearing unnatural sugar residue, peracetylated *N*-azidoacetylgalactosamine (Ac₄GalNAz) as a substrate for *O*-Glycosylation at viral fiber, and an alkyne-bearing unnatural amino acid, homopropargylglycine (HPG) as a methionine surrogate in protein biosynthesis. Introduction of these surrogates into Ad particles allows sequential Staudinger ligation of *O*-GlcNAz followed by copper assisted “click” modification of homopropargylglycine (HPG). Moreover, the two chemically orthogonal ligation reactions (Staudinger ligation and CuAAC) were envisioned to permit the specific conjugation of the targeting and imaging ligand with a viral capsid without mutual interference. (*vid.* chapter 5.4.3.1)

2.3.3.1 Recycling of Azidohomoalanine

Despite the recent improvement [47], the syntheses of unnatural substrates such as AHA, HPG, and azido sugars are still a cost-inefficient and time-consuming process. Particularly, if we consider the volume of cell culture media used in virus production, the amount of unnatural amino acid required for the metabolic labeling is massive even under 32 mM concentration, which may limit the large-scale production of modified viral vectors. To address this limitation, the feasibility of recycling culture medium containing excess AHA was assessed. 6 h AHA pulse window was considered to be short enough to retain all ingredients required for

maintaining host cells (HEK 293) without exhaustion. To wit, after a 6 h AHA pulse, the medium including AHA was collected and filtered with a 10 kDa-MWCO membrane to sterilize it and stored at 4 °C until recycling. To compensate the volume lost during the recycling process (i.e., incomplete aspiration and filtration), a new fresh medium (~10%) that contained the same ingredients except AHA was supplemented to the filtrate to meet the same final concentrations as the previous production and recycled for the next batch. After viral production using the recycled media, the incorporation of AHA into viral protein was assayed along with the previous batch by western-blot (Figure 2-8). The results presented successful incorporations of AHA in both fresh and recycled medium into viral proteins. (Note that additional AHA was not supplemented to the recycled medium, with the intention of only assessing the recycling feasibility of the “old” AHA reagent.)



AHA	4 mM	32 mM	32 mM Recycled	32 mM Recycled
Recycle	-	-	+	+
FLAG-phosphine	+	+	+	-
FLAG-phosphine-oxide	-	-	-	+

Figure 2-8. Anti-FLAG Western-blot for Recycled AHA Labeled Ad

First, the Staudinger reaction were performed with 50 μL of 1×10^{12} azide labeled viral particles/mL in a 100 mM tris buffer at pH 8.0 was treated with FLAG-Staudinger phosphine and FLAG- Staudinger phosphine oxide (as a negative control) at a final concentration of 400 μM at RT for 2 h and purified by size exclusion column (Centri-Sep CS-901; Princeton separations). The eluted samples were boiled at 95 $^{\circ}\text{C}$ for 10 min and run on a 10% polyacryamide electrophoresis gel and transferred onto nitrocellulose at 40 V over 2 h in a western transfer buffer (25 mM tris, 192 mM glycine, 0.5% SDS and 10% methanol). Blots were blocked by 5% milk in PBST and treated with anti-FLAG M2 HRP conjugate obtained from Sigma (St. Louis, MO) at a ratio of 1:12000 in 5% milk in PBST. Blots were washed with milk and PBST and developed by chemiluminescence (Millipore Immobilon Western kit).

References

1. Vocadlo, D. J.; Hang, H. C.; Kim, E. J.; Hanover, J. A.; Bertozzi, C. R., A chemical approach for identifying O-GlcNAc-modified proteins in cells. *Proc. Natl. Acad. Sci. U. S. A.* **2003**, *100* (16), 9116-9121.
2. Boyce, M.; Carrico, I. S.; Ganguli, A. S.; Yu, S.-H.; Hangauer, M. J.; Hubbard, S. C.; Kohler, J. J.; Bertozzi, C. R., Metabolic cross-talk allows labeling of O-linked β -N-acetylglucosamine-modified proteins via the N-acetylgalactosamine salvage pathway. *Proc. Natl. Acad. Sci. U. S. A.* **2011**, *108* (8), 3141-3146.
3. Kolb, H. C.; Finn, M. G.; Sharpless, K. B., Click Chemistry: Diverse Chemical Function from a Few Good Reactions. *Angew. Chem., Int. Ed. Engl.* **2001**, *40* (11), 2004-2021.
4. Rostovtsev, V. V.; Green, L. G.; Fokin, V. V.; Sharpless, K. B., A Stepwise Huisgen Cycloaddition Process: Copper(I)-Catalyzed Regioselective "Ligation" of Azides and Terminal Alkynes. *Angew. Chem., Int. Ed. Engl.* **2002**, *114* (14), 2708-2711.
5. Tornøe, C. W.; Christensen, C.; Meldal, M., Peptidotriazoles on Solid Phase: [1,2,3]-Triazoles by Regiospecific Copper(I)-Catalyzed 1,3-Dipolar Cycloadditions of Terminal Alkynes to Azides. *J. Org. Chem.* **2002**, *67* (9), 3057-3064.
6. Lemieux, G. A.; Bertozzi, C. R., Chemoselective ligation reactions with proteins, oligosaccharides and cells. *Trends Biotechnol.* **1998**, *16* (12), 506-513.
7. Prescher, J. A.; Bertozzi, C. R., Chemistry in living systems. *Nat. Chem. Biol.* **2005**, *1*, 13-21.
8. Chigrinova, M.; Blake, J. A.; Pezacki, J. P., Kinetics studies of rapid strain-promoted [3+2]-cycloadditions of nitrones with biaryl-aza-cyclooctynone. *Org. Biomol. Chem.* **2012**, *10* (15), 3066-3070.
9. Presolski, S. I.; Hong, V.; Cho, S.-H.; Finn, M. G., Tailored Ligand Acceleration of the Cu-Catalyzed Azide-Alkyne Cycloaddition Reaction: Practical and Mechanistic Implications. *J. Am. Chem. Soc.* **2010**, *132* (41), 14570-14576.
10. Arumugam, S.; Chin, J.; Schirmacher, R.; Popik, V. V.; Kostikov, A. P., [^{18}F]Azadibenzocyclooctyne ([^{18}F]ADIBO): A biocompatible radioactive labeling synthon for peptides using catalyst free [3+2] cycloaddition. *Bioorg. Med. Chem. Lett.* **2011**, *21* (23), 6987-6991.
11. Carpenter, R. D.; Hausner, S. H.; Sutcliffe, J. L., Copper-free click for PET: Rapid 1, 3-dipolar cycloadditions with a fluorine-18 cyclooctyne. *ACS Med. Chem. Lett.* **2011**, *2* (12), 885-889.

12. Sachin, K.; Jadhav, V. H.; Kim, E.-M.; Kim, H. L.; Lee, S. B.; Jeong, H.-J.; Lim, S. T.; Sohn, M.-H.; Kim, D. W., F-18 Labeling Protocol of Peptides Based on Chemically Orthogonal Strain-Promoted Cycloaddition under Physiologically Friendly Reaction Conditions. *Bioconjugate Chem.* **2012**, *23* (8), 1680-1686.
13. Debets, M. F.; van Berkel, S. S.; Schoffelen, S.; Rutjes, F. P. J. T.; van Hest, J. C. M.; van Delft, F. L., Aza-dibenzocyclooctynes for fast and efficient enzyme PEGylation via copper-free (3+2) cycloaddition. *Chem. Commun. (Cambridge, U. K.)* **2010**, *46* (1), 97.
14. Debets, M. F.; van Berkel, S. S.; Dommerholt, J.; Dirks, A. J.; Rutjes, F. P. J. T.; van Delft, F. L., Bioconjugation with Strained Alkenes and Alkynes. *Acc. Chem. Res.* **2011**, *44* (9), 805-815.
15. Chen, I.; Howarth, M.; Lin, W.; Ting, A. Y., Site-specific labeling of cell surface proteins with biophysical probes using biotin ligase. *Nat. Methods* **2005**, *2*, 99-104.
16. Zhang, Z.; Smith, B. A. C.; Wang, L.; Brock, A.; Cho, C.; Schultz, P. G., A new strategy for the site-specific modification of proteins in vivo. *Biochemistry* **2003**, *42* (22), 6735-6746.
17. Mahal, L. K.; Yarema, K. J.; Bertozzi, C. R., Engineering chemical reactivity on cell surfaces through oligosaccharide biosynthesis. *Science* **1997**, *276* (5315), 1125-1128.
18. Saxon, E.; Bertozzi, C. R., Cell Surface Engineering by a Modified Staudinger Reaction. *Science* **2000**, *287* (5460), 2007.
19. Jewett, J. C.; Sletten, E. M.; Bertozzi, C. R., Rapid Cu-Free Click Chemistry with Readily Synthesized Biarylazacyclooctynones. *J. Am. Chem. Soc.* **2010**, *132* (11), 3688-3690.
20. Sletten, E. M.; Nakamura, H.; Jewett, J. C.; Bertozzi, C. R., Difluorobenzocyclooctyne: Synthesis, Reactivity, and Stabilization by β -Cyclodextrin. *J. Am. Chem. Soc.* **2010**, *132* (33), 11799-11805.
21. Dommerholt, J.; Schmidt, S.; Temming, R.; Hendriks, L. J. A.; Rutjes, F. P. J. T.; van Hest, J. C. M.; Lefeber, D. J.; Friedl, P.; van Delft, F. L., Readily Accessible Bicyclononynes for Bioorthogonal Labeling and Three-Dimensional Imaging of Living Cells. *Angew. Chem., Int. Ed. Engl.* **2010**, *49* (49), 9422-9425.
22. van Berkel, S. S.; Dirks, A. J.; Debets, M. F.; van Delft, F. L.; Cornelissen, J. J. L. M.; Nolte, R. J. M.; Rutjes, F. P. J. T., Metal-Free Triazole Formation as a Tool for Bioconjugation. *ChemBioChem* **2007**, *8* (13), 1504-1508.
23. Ning, X.; Temming, R. P.; Dommerholt, J.; Guo, J.; Ania, D. B.; Debets, M. F.; Wolfert, M. A.; Boons, G.-J.; van Delft, F. L., Protein Modification by Strain-Promoted Alkyne-Nitrone Cycloaddition. *Angew. Chem., Int. Ed. Engl.* **2010**, *49* (17), 3065-3068.

24. Gutmiedl, K.; Wirges, C. T.; Ehmke, V.; Carell, T., Copper-Free “Click” Modification of DNA via Nitrile Oxide–Norbornene 1,3-Dipolar Cycloaddition. *Org. Lett.* **2009**, *11* (11), 2405-2408.
25. Blackman, M. L.; Royzen, M.; Fox, J. M., Tetrazine Ligation: Fast Bioconjugation Based on Inverse-Electron-Demand Diels–Alder Reactivity. *J. Am. Chem. Soc.* **2008**, *130* (41), 13518-13519.
26. Devaraj, N. K.; Weissleder, R.; Hilderbrand, S. A., Tetrazine-based cycloadditions: application to pretargeted live cell imaging. *Bioconjugate Chem.* **2008**, *19* (12), 2297.
27. Yang, J.; Šečkutè, J.; Cole, C. M.; Devaraj, N. K., Live-Cell Imaging of Cyclopropene Tags with Fluorogenic Tetrazine Cycloadditions. *Angew. Chem.* **2012**, *124* (30), 7594-7597.
28. Stockmann, H.; Neves, A. A.; Stairs, S.; Brindle, K. M.; Leeper, F. J., Exploring isonitrile-based click chemistry for ligation with biomolecules. *Org. Biomol. Chem.* **2011**, *9* (21), 7303-7305.
29. Sletten, E. M.; Bertozzi, C. R., A Bioorthogonal Quadricyclane Ligation. *J. Am. Chem. Soc.* **2011**, *133* (44), 17570-17573.
30. Weisbrod, S. H.; Marx, A., Novel strategies for the site-specific covalent labelling of nucleic acids. *Chem. Commun. (Cambridge, U. K.)* **2008**, (44), 5675-5685.
31. Sletten, E. M.; Bertozzi, C. R., Bioorthogonal chemistry: fishing for selectivity in a sea of functionality. *Angew. Chem., Int. Ed. Engl.* **2009**, *48* (38), 6974-6998.
32. Fernandez-Suarez, M.; Baruah, H.; Martinez-Hernandez, L.; Xie, K. T.; Baskin, J. M.; Bertozzi, C. R.; Ting, A. Y., Redirecting lipoic acid ligase for cell surface protein labeling with small-molecule probes. *Nat Biotech* **2007**, *25* (12), 1483-1487.
33. Ochiai, H.; Huang, W.; Wang, L.-X., Expeditious Chemoenzymatic Synthesis of Homogeneous N-Glycoproteins Carrying Defined Oligosaccharide Ligands. *J. Am. Chem. Soc.* **2008**, *130* (41), 13790-13803.
34. Lapinsky, D. J., Tandem photoaffinity labeling–bioorthogonal conjugation in medicinal chemistry. *Bioorg. Med. Chem.* **2012**, *20* (21), 6237-6247.
35. Dieterich, D. C.; Link, A. J.; Graumann, J.; Tirrell, D. A.; Schuman, E. M., Selective identification of newly synthesized proteins in mammalian cells using bioorthogonal noncanonical amino acid tagging (BONCAT). *Proc. Natl. Acad. Sci. U. S. A.* **2006**, *103* (25), 9482-9487.
36. Dube, D. H.; Bertozzi, C. R., Metabolic oligosaccharide engineering as a tool for glycobiology. *Curr. Opin. Chem. Biol.* **2003**, *7* (5), 616-625.

37. Johnson, J. A.; Lu, Y. Y.; Van Deventer, J. A.; Tirrell, D. A., Residue-specific incorporation of non-canonical amino acids into proteins: recent developments and applications. *Curr. Opin. Chem. Biol.* **2010**, *14* (6), 774-780.
38. Dieterich, D. C.; Lee, J. J.; Link, A. J.; Graumann, J.; Tirrell, D. A.; Schuman, E. M., Labeling, detection and identification of newly synthesized proteomes with bioorthogonal non-canonical amino-acid tagging. *Nat. Protoc.* **2007**, *2* (3), 532-540.
39. Prescher, J. A.; Bertozzi, C. R., Chemistry in living systems. *Nat. Chem. Biol.* **2005**, *1* (1), 13-21.
40. Mahal, L. K.; Yarema, K. J.; Bertozzi, C. R., Engineering Chemical Reactivity on Cell Surfaces Through Oligosaccharide Biosynthesis. *Science* **1997**, *276* (5315), 1125.
41. Hang, H. C.; Yu, C.; Kato, D. L.; Bertozzi, C. R., A metabolic labeling approach toward proteomic analysis of mucin-type O-linked glycosylation. *Proc. Natl. Acad. Sci. U. S. A.* **2003**, *100* (25), 14846-14851.
42. Banerjee, P. S.; Ostapchuk, P.; Hearing, P.; Carrico, I., Chemoselective Attachment of Small Molecule Effector Functionality to Human Adenoviruses Facilitates Gene Delivery to Cancer Cells. *J. Am. Chem. Soc.* **2010**, *132* (39), 13615-13617.
43. Banerjee, P. S.; Zuniga, E. S.; Ojima, I.; Carrico, I. S., Targeted and armed oncolytic adenovirus via chemoselective modification. *Bioorg. Med. Chem. Lett.* **2011**, *21* (17), 4985-4988.
44. Cauet, G.; Strub, J. M.; Leize, E.; Wagner, E.; Van Dorselaer, A.; Lusky, M., Identification of the glycosylation site of the adenovirus type 5 fiber protein. *Biochemistry* **2005**, *44* (14), 5453-5460.
45. Banerjee, P. S.; Ostapchuk, P.; Hearing, P.; Carrico, I. S., Unnatural Amino Acid Incorporation onto Adenoviral (Ad) Coat Proteins Facilitates Chemoselective Modification and Retargeting of Ad Type 5 Vectors. *J. Virol.* **2011**, *85* (15), 7546-7554.
46. Banerjee, P. S. Development of novel gene therapy vectors via metabolic labeling and chemoselective modification of adenovirus capsid. State University of New York at Stony Brook, 2011.
47. Roth, S.; Thomas, N. R., A concise route to L-azidoamino acids: L-azidoalanine, L-azidohomoalanine and L-azidonorvaline. *Synlett* **2010**, *2010* (4), 607.

Chapter 3. Retargeting Adenoviral Vectors via Peptide “Click” Conjugations

3.1 Introduction

In the context of engineering viral vectors with improved tropism for clinical applications, introduction of heterologous peptides that are selective for receptors on target cell surface has been attempted [2]. For example, “chimera viruses” were developed by inserting small peptides identified from other pathogens into the exposed protein loops of viral capsid *via* genetic engineering [3-7]. Furthermore, random peptide libraries were displayed on the viral surfaces to directly select mutants possessing desired tropisms [8-9]. However, in many instances, binding sites and other molecular determinants required for viral entry have not been easily mimicked by short peptides [2], mainly due to the low affinity of peptide and incompatibility of inserted exogenous peptides with authentic viral proteins and conformational changes of binding sites during biosynthesis. Consequently, directed evolution approaches including “error-prone PCR” and “DNA shuffling”, are employed to develop viral vectors with preferred tropisms (Figure 3-1) [10-12]. Nevertheless, those random screening strategies *per se* involve the drawbacks such as small biased libraries with limited complexity and accumulation of neutral mutations which may cause immunogenicity [13]. Alternative chemical covalent cross-linking and non-covalent bridge (adapter) approaches are also being applied to alter viral tropism using retargeting peptide motif as described in Chapter 1.

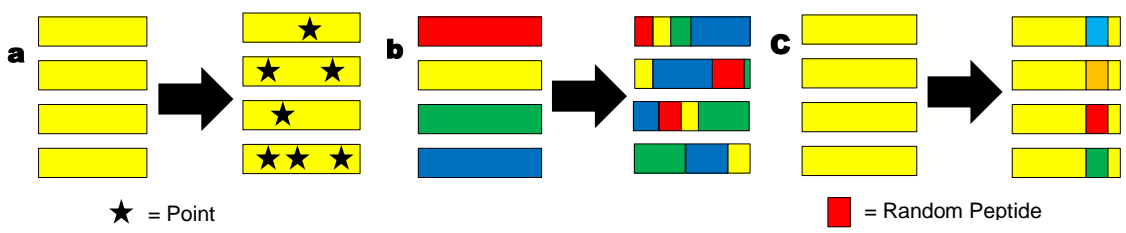


Figure 3-1. Genetic Methods for Generating Diverse Viral Libraries

a) random point mutagenesis (error-prone PCR), b) *in vitro* recombination (e.g., DNA shuffling) and c) insertion of random peptides. This figure was reproduced from reference [14] with the permission of publisher (“Nature Publishing Group”).

3.2 Targeting to the $\alpha_v\beta_3$ Integrin

Integrins are heterodimeric transmembrane glycoproteins that consist of two noncovalently associated alpha and beta subunits, and mediate cell-matrix and cell-cell adhesion. (Figure 3-2) [15-17]. Integrins function as bidirectional transducers of extra- and intracellular signals between cells and their surroundings, which regulates cell cycle, shape, and motility. Owing to the altered expressions of the various integrins occurred during tumor growth and progression, integrins and their associated proteins have been potential targets for cancer diagnosis and therapy [16]. Particularly, the $\alpha_v\beta_3$ integrin is highly expressed on activated endothelial cells and tumor cells, on the contrary, usually it is expressed at low or undetectable levels in most normal organ tissues, rendering $\alpha_v\beta_3$ integrin a prospective target for antiangiogenic cancer treatment [18-22]. Besides specific expression on the activated tumor vasculature, the expression of $\alpha_v\beta_3$ integrin correlates with increased cancer progression and decreased patient survival in various tumor types as shown in Table 3-1. Furthermore, $\alpha_v\beta_3$ integrin is not only a natural co-receptor for Ad cell entry, playing a pivotal role in endocytosis along with $\alpha_v\beta_5$ integrin as described in Chapter 1, but also can facilitate Ad endocytosis even in primary-receptor (CAR)-deficient cells through the interaction with arginine-glycine-aspartic acid (RGD) motif present in the viral penton base by itself [23].

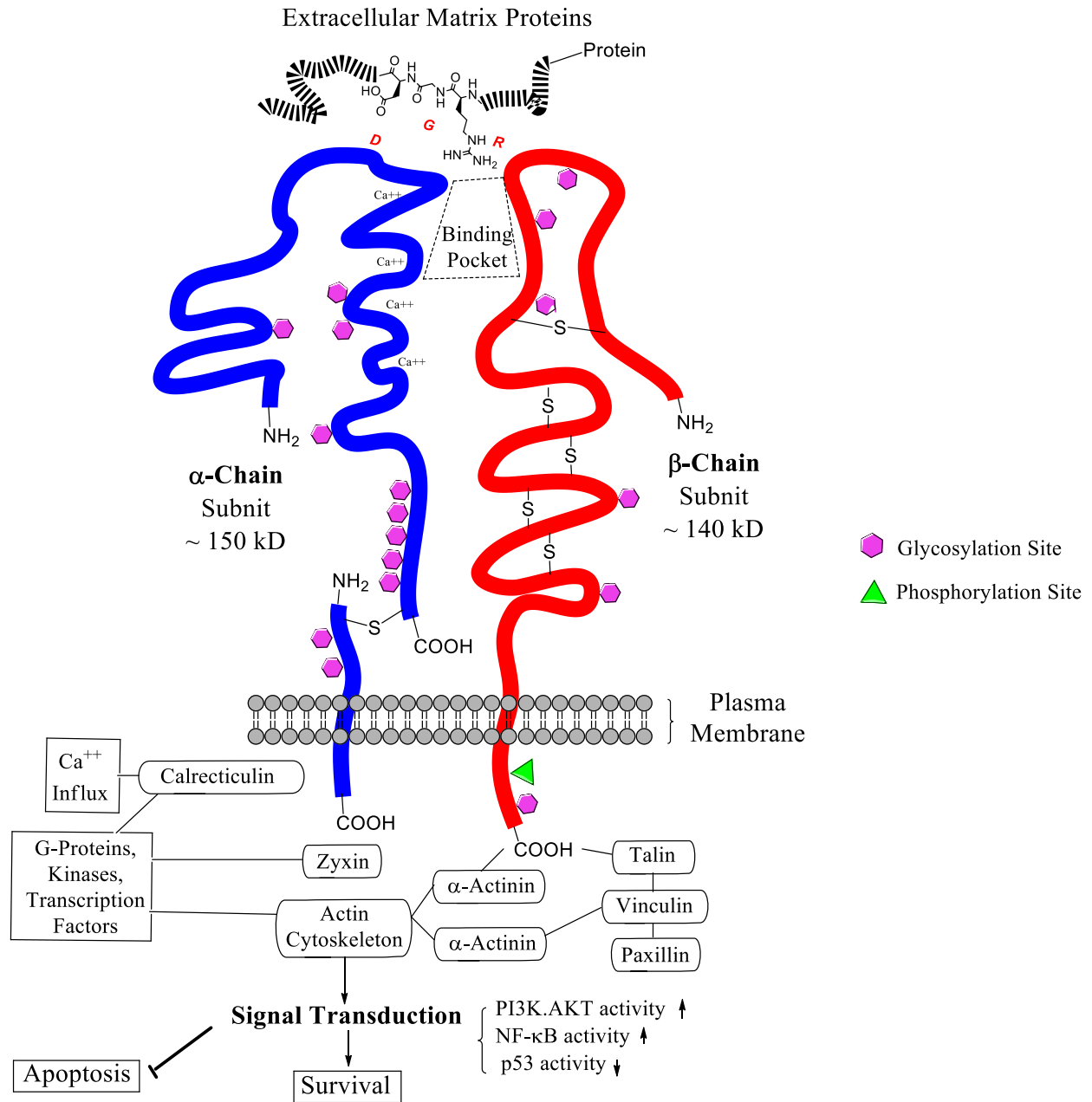


Figure 3-2. a Diagram of Integrin Receptor Heterocomplex and Signal Transduction

The recognition sites comprise amino acid code (e.g. RGD) from various ECM proteins are contained within the trapezoid box at the top of the diagram. Integrins can paradoxically initiate pro-survival as well as pro-apoptotic signals, which depends on the ligation status and type of expressed integrins [17].

*This figure was modified from reference [16] with the permission of publisher (“Royal Society of Medicine Press”).

Table 3-1. Integrins in Cancer Progression

Tumor type	Integrins expressed	Associated phenotypes
Melanoma	$\alpha_v\beta_3$ and $\alpha_5\beta_1$	Vertical growth phase and lymph node metastasis
Breast	$\alpha_6\beta_4$ and $\alpha_v\beta_3$	Increased tumor size and grade, and decreased survival ($\alpha_6\beta_4$). Increased bone metastasis ($\alpha_v\beta_3$)
Prostate	$\alpha_v\beta_3$	Increased bone metastasis
Pancreatic	$\alpha_v\beta_3$	Lymph node metastasis
Ovarian	$\alpha_4\beta_1$ and $\alpha_v\beta_3$	Increased peritoneal metastasis ($\alpha_4\beta_1$) and tumor proliferation($\alpha_v\beta_3$)
Cervical	$\alpha_v\beta_3$ and $\alpha_v\beta_6$	Decreased patient survival
Glioblastoma	$\alpha_v\beta_3$ and $\alpha_v\beta_5$	Both are expressed at the tumor–normal tissue margin and have a possible role in invasion
Non-small-cell -lung carcinoma	$\alpha_5\beta_1$	Decreased survival in patients with lymph node-negative tumors
Colon	$\alpha_v\beta_6$	Reduced patient survival

* This table was reprinted from the reference [17] with the permission of publisher (“Nature Publishing Group”).

3.3 RGD Peptide

Although many integrins recognize a common motif (e.g., RGD, RYD, LDV, etc.), they are able to distinguish among different natural ligands (e.g., fibronectin, vitronectin, laminin, etc.) containing the same recognition sequence, which leads to the assumption that integrin receptors also recognize a distinct conformation of binding motif (e.g., RGD) [24]. Kessler *et al.* demonstrated conformational restriction in cyclized peptide could make an impact on binding affinity and receptor specificity (Figure 3-3) [25], which is owed to “the decrease in conformational entropy that is lost upon binding” only in the case of receptor-matched conformation [24-25]. Moreover, in the cyclic penta- and hexa-peptide cases, the stabilizations of distinct conformations were also proved by NMR spectroscopy and MD simulations [25-27]. In succession, to induce the characteristic turn motifs within cyclic peptide synthetically, *D*-amino acid residue or proline was introduced. Diverse conformations of cyclic peptide were achieved by changing the chirality of selected amino acids (e.g., *c*(rGDFV) from *c*(GrdFV): a

minuscule stands for *D*-amino acid, italic *c* and parenthesis indicates cyclic peptide) or altering ring size or sequence inversion (e.g., *c*(VfdGr) from *c*(RGDfV)). A library of cyclic RGD peptide was screened by inhibitory capacity (IC₅₀) for $\alpha_v\beta_3$ -vitronectine binding, identifying the peptide *c*(RGDfV) which display a 100-fold improved IC₅₀ than the reference peptide GRGDS [26]. A number of structural modifications of the cyclic-peptide have been performed to find better $\alpha_v\beta_3$ antagonist [28-32], but mostly afforded less active peptides. One of the most important modifications turned out to be the incorporation of *N*-methylated amino acids into the peptide sequence [33], resulting in an increased proteolytic stability through lipophilicity change and steric hindrance [34-37]. For the peptide *c*(RGDfNMeVal) [38], which includes *N*-methylated valine, a Phase III clinical study is being conducted in patients with glioblastoma as $\alpha_v\beta_3$ integrin inhibitor by Merck KGaA under the name of “cilengitide”.

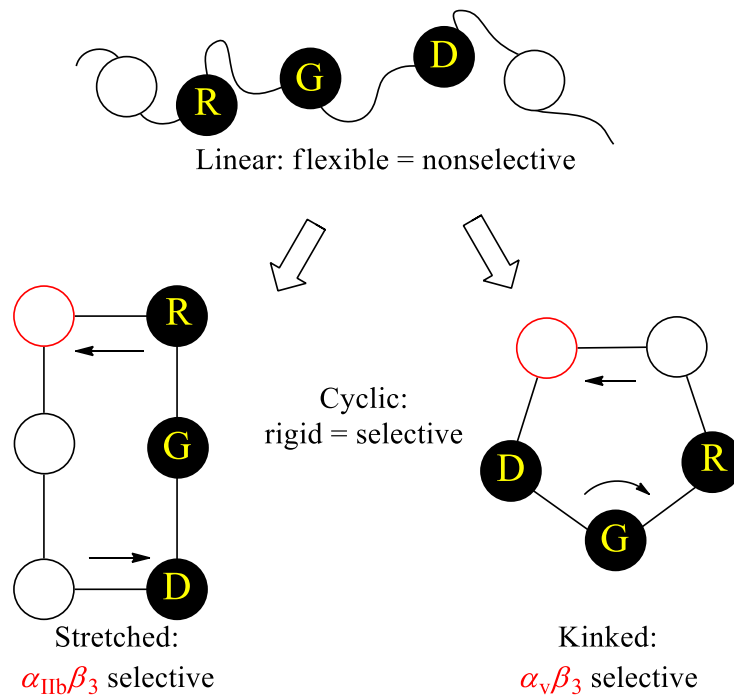


Figure 3-3. Induction of Selectivity to the RGD Peptide by Cyclization

The red circles indicate the position of *D*-amino acid or proline residue required for cyclization. *This figure was reproduced from reference [24] with the permission of publisher ("Elsevier").

3.4 Results and Discussion

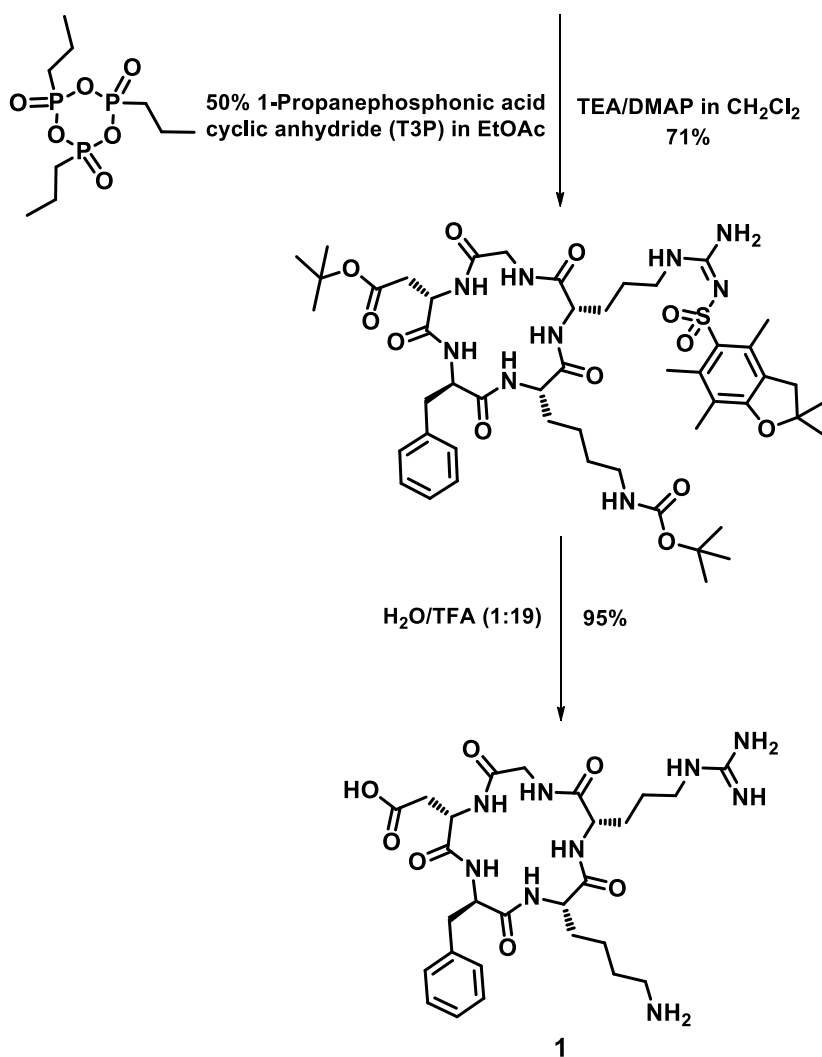
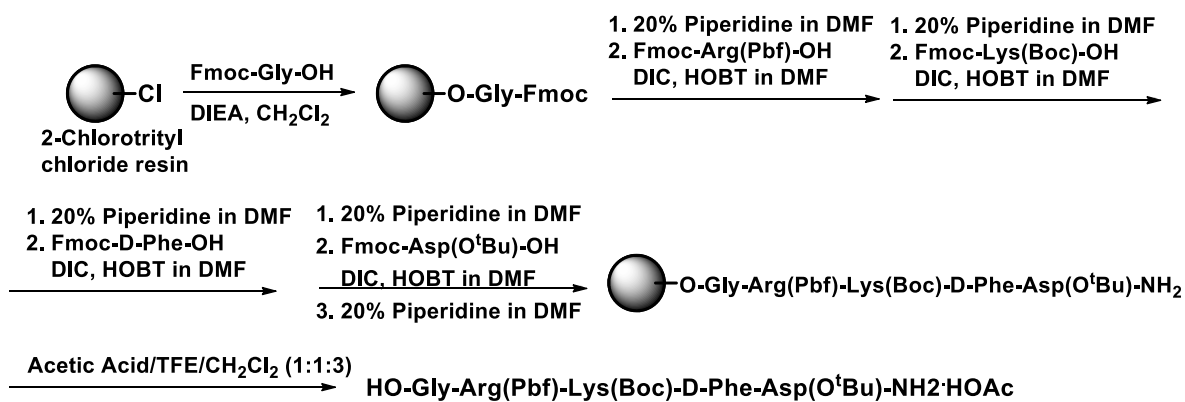
As an $\alpha_{\text{v}}\beta_3$ -integrin-targeting peptide, dicyclic CDCRGDCFC motif (known as RGD-4C), which was identified as $\alpha_{\text{v}}\beta_5$ integrin antagonist from phage-display libraries screening, was used to target angiogenic blood vessels of relevant tumors (*vide supra*) or tumor cells themselves [7, 39-40]. However, RGD-4C includes two reducible disulfide bridges that are prone to cleavage during synthesis or in biological media, but important to maintain the specific three-dimensional structure. In addition, RGD-4C moiety has less affinity to $\alpha_{\text{v}}\beta_3$ integrin than other optimized cyclic peptides [41], and poor water solubility is another drawback to synthetic approaches. As a consequence, synthetic cyclic RGD peptides (e.g., *c*(RGDfK), which has a comparable receptor-affinity to the reference standard cyclic peptide *c*(RGDfV) [42] and can be covalently linked *via*

side chain ϵ -amino group of the lysine have been broadly used to target $\alpha_v\beta_3$ integrin in chemical conjugation or non-covalent adapter approaches [22, 43-47].

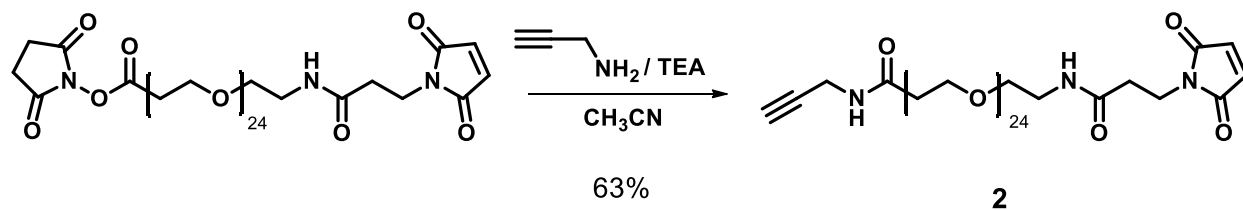
3.4.1 Synthesis of Alkyne-PEG-*c*(RGDfK)

In order to conjugate targeting cyclic peptide, *c*(RGDfK), onto the azide-labeled Ad surface by CuAAC, alkyne moiety was cross-linked with cyclic peptide using heterobifunctional polyethylene glycol (PEG) reagents (maleimide-PEG₂₄-NHS ester, where NHS = *N*-hydroxysuccinimide) as shown in reaction Scheme 3-3. Briefly, cyclic peptide *c*(RGDfK) was prepared by 9-fluorenylmethoxycarbonyl (Fmoc) solid phase peptide synthesis [48] and cyclized using a highly effective coupling reagent, 1-propane-phosphonic acid cyclic anhydride (T3P) as described by Dai *et al.* (Scheme 3-1) [49]. After cyclization, the peptide was further modified for the subsequent coupling, using *N*-succinimidyl-*S*-acetylthioacetate (SATA) and hydroxylamine to generate sulfhydryl group as demonstrated by Chen *et al.* (Scheme 3-3) [50]. Alkyne-PEG₂₄-maleimide was synthesized separately through the reaction of propargylamine and maleimide-PEG₂₄-NHS ester, *scilicet*, the NHS ester group reacted with amino group of propargylamine to form amide linkage with loss of NHS (Scheme 3-2). Notably, this NHS-PEG₂₄-maleimide reagent provides a 95.2 Å spacer [51] that compares to the distance from glycosylation site of Ad5 fiber to natural primary binding motif on the viral fiber knob [52], expecting to permit RGD ligands an appropriate length to contact target receptors on cell surface. Finally, sulfhydryl group introduced to cyclic peptide, was reacted to remaining maleimide group of PEG linker (maleimide-PEG₂₄-alkyne), *videlicet*, one of the carbons adjacent to the maleimide double bond underwent nucleophilic attack by the thiolate anion included in cyclic peptide, to afford alkyne-PEG₂₄-*c*(RGDfK) *via* thioether bond (Scheme 3-3). Further, in order to evaluate

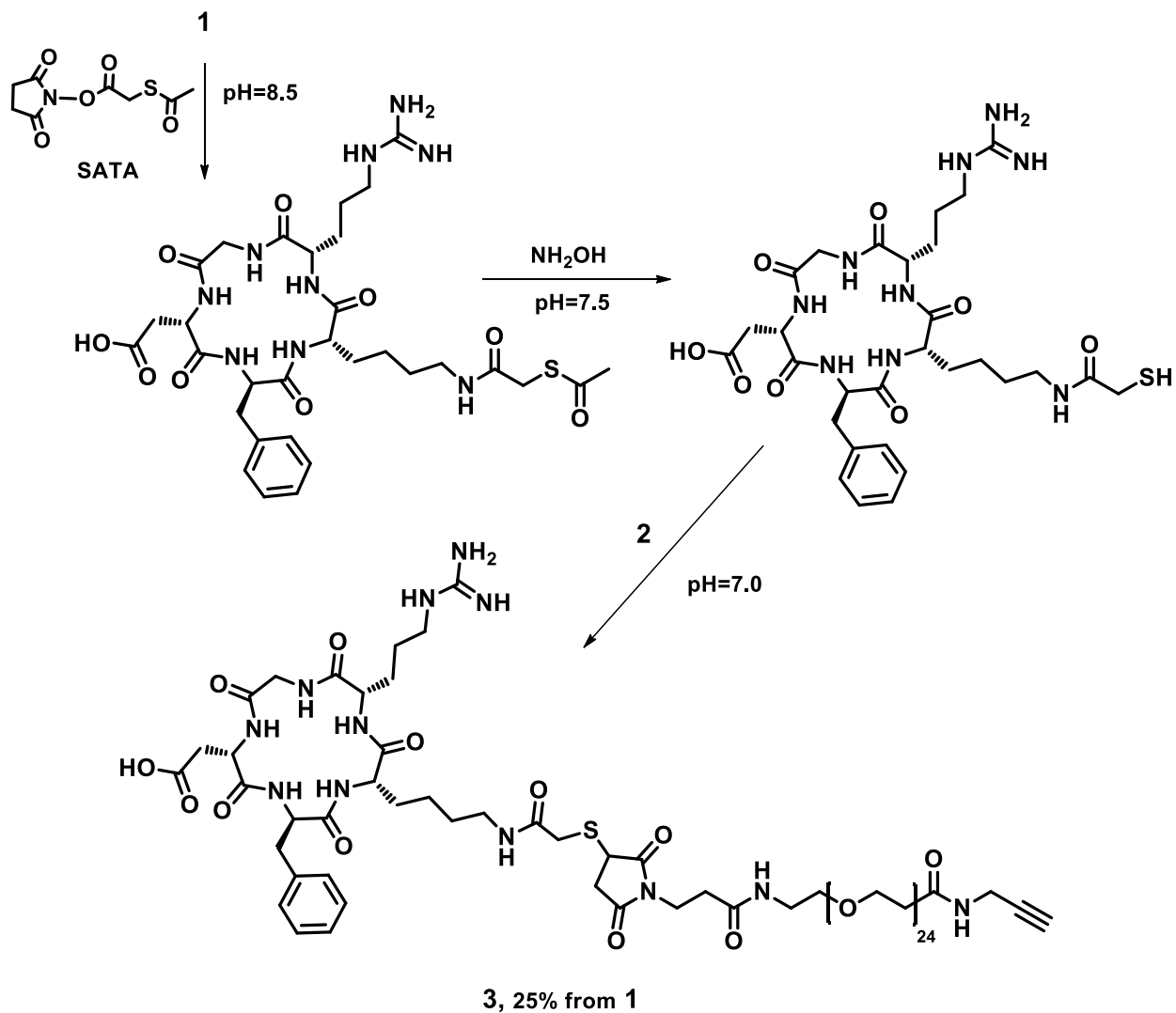
the linker effect on transduction efficiency of $\alpha_v\beta_3$ integrin-targeting Ad, alkyne-*c*(RGDfK), the molecule in which *c*(RGDfK) was directly coupled to alkyne moiety without PEG linker, was also synthesized as shown in Scheme 3-4.



Scheme 3-1. Synthesis of *c*(RGDFK)



Scheme 3-2. Synthesis of Alkyne-PEG-maleimide



Scheme 3-3. Synthesis of Alkyne-PEG-*c*(RGDfK)

Then, HEK 293 cells were infected with intact adenovirus particles with an MOI of 5 PFU/cell. The complete media was supplemented with 50 μ M peracetyl-*N*-azidoacetyl galactosamine (Note that UDP-GalNAz can be converted to UDP-GlcNAz by mammalian 4'-empimerase (GALE) and GalNAz is a more effective surrogate for *O*-GlcNAc residue than GlcNAz as described in Chapter 2) and the cells were incubated at 37 °C. The infected cells were harvested 42-46 h post infection and lysed by three repeated freeze-thaw cycles to release viral particles which were purified by ultracentrifugation over the CsCl density gradient. The virus band at the boundary interface between the two CsCl layers (1.25 mL / 1.40 mL) was collected and repurified by 2nd ultracentrifugation over CsCl solution (1.34 mL) overnight. The incorporation of GlcNAz was confirmed by bioorthogonal “click” reaction using alkyne-TAMRA fluorescent dye as described by our group before [53].

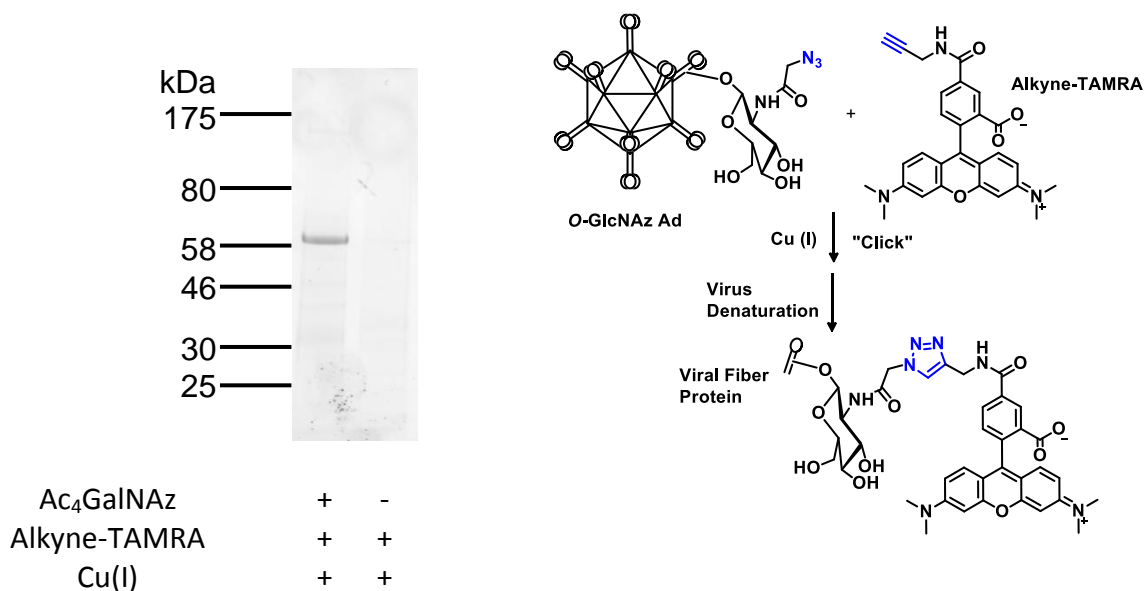
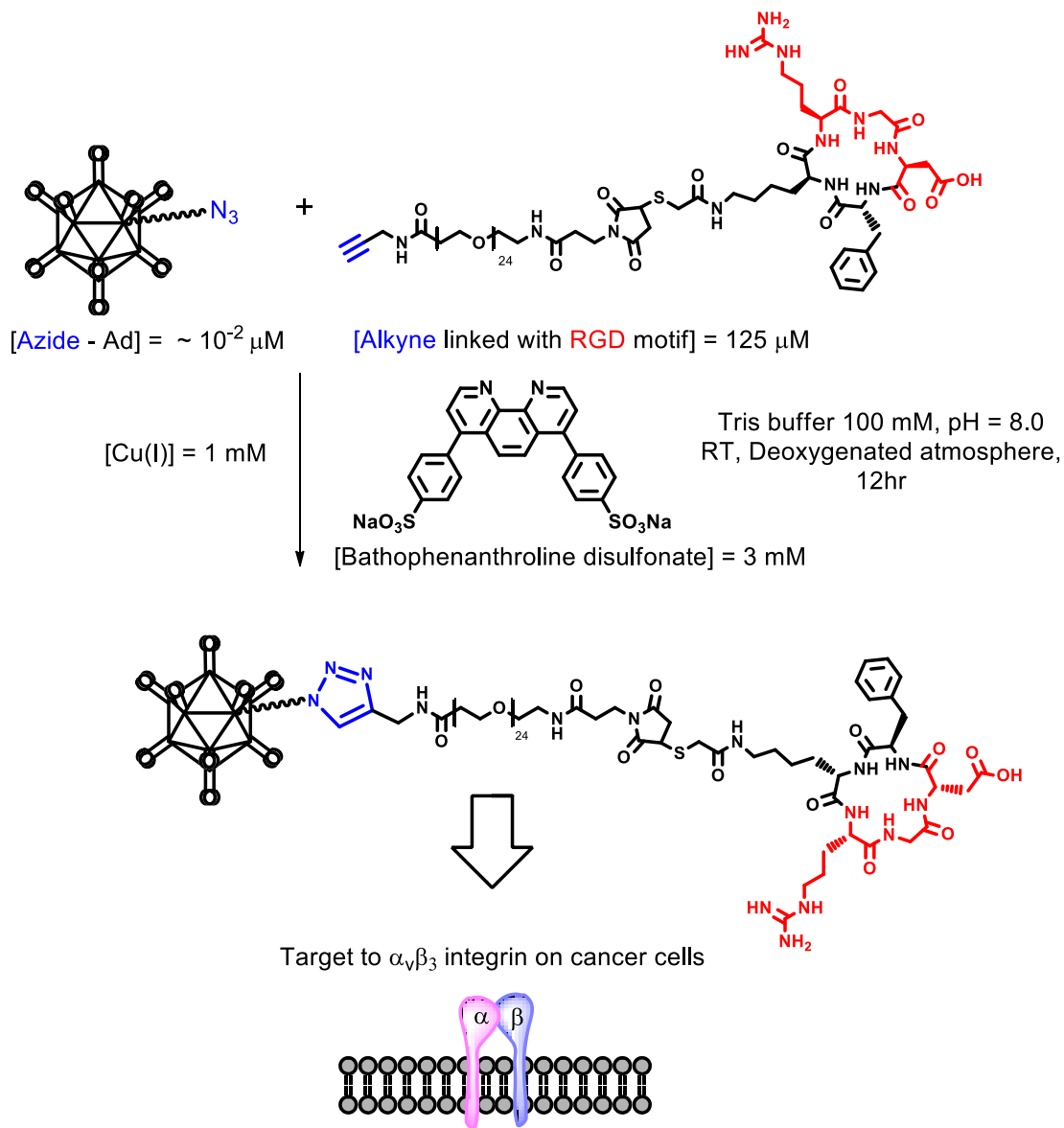


Figure 3-4. Qualitative Analysis of Azido Sugar Incorporation into Ad5 Fiber

In-gel fluorescent image of denatured *O*-GlcNAz-enabled virions and intact virions both treated with alkyne-TAMRA reagent under CuAAC condition. Only Ac₄GalNAz-treated Ad showed a fluorescent signal corresponding to viral fiber's Mw (62 KDa), which confirmed azido sugar was specifically incorporated into viral fiber protein via an *O*-glycosidic bond.

3.4.3 Conjugation of Azide-enabled Ad with Alkyne-PEG-RGD Peptide via CuAAC

Since Sharpless and Meldal discovered Cu(I) can remarkably enhance the rate of the Huisgen 1,3-dipolar cycloaddition reaction of organic azides and terminal alkynes [55-56], a wide variety of conditions and sources of Cu(I), which should be maintained at a high concentration level at all times during reaction, have been introduced [57]. Finn *et al.* first employed CuAAC to engineer cowpea mosaic viral particles [58] and improved a ligand and reaction conditions for CuAAC which enabled more effective and robust chemoselective bioconjugations [59]. Our previous studies also demonstrated that azide-labeled Ad can be successfully conjugated with other molecules including alkyne moiety without losing transduction efficiency *via* the same CuAAC conditions as described by Finn *et al.*, using CuBr and a water-soluble sulfonated bathophenanthroline ligand in Tris buffer (pH 8) under deoxygenated atmosphere [53, 60-61]. Therefore, we adopted the same CuAAC reaction conditions to conjugate cyclic RGD peptide onto azide-labeled Ad surface as shown in Scheme 3-6.



Scheme 3-6. Overall Scheme for $\alpha_v\beta_3$ Integrin Targeting with Ad-PEG-*c*(RGDfK)

3.4.4 Infection Assays with $\alpha_v\beta_3$ -Integrin-targeting Ad *in vitro*

To assess adenoviral infection on targeted cells, a recombinant E1-deleted Ad expressing the luciferase reporter gene under the CMV promoter (Ad-CMV-LUC) were conjugated with alkyne-PEG-*c*(RGDfK) and linker-absent alkyne-*c*(RGDfK) *via* CuAAC respectively. After

“click” reaction, the excess of chemical reagents including peptide ligands were purified by spin-gel filtration and the viral titer was quantitated by a Picogreen assay as shown in ‘Materials and methods’.

3.4.4.1 Targeting to the Mouse Melanoma with RGD-Ad

We desired to evaluate only $\alpha_v\beta_3$ integrin-dependent transduction without background ascribed to the infection mediated by natural primary receptors (CAR). Therefore, B16BL6 (mouse melanoma cell), known to express high level of $\alpha_v\beta_3$ integrins on cell surface, while refractory to Ad infection due to deficient CAR expression [62], was chosen first and infected with *c*(RGDfK) conjugated Ad (*c*RGD-Ad) at a multiplicity of infection (MOI) of 1000. 24 h post infection, the expression levels of luciferase transgene were determined by a photometer with the luciferase assay kit (Figure 3-5). For this experiment, virus produced in the absence of azido sugar was used as a control. Apart from omission of the azido sugar, all other processing was identical, including purification, exposure to click reagents, and removal of these reagents. As a result, a ~5-fold increase in gene delivery was observed with *c*(RGDfK)-PEG-Ad and ~4-fold with *c*(RGDfK)-Ad (without PEG linker) in comparison with unmodified Ad. Notably, a moderate increase was observed for *c*(RGDfK)-PEG-Ad, compared to linker-absent *c*(RGDfK)-Ad, which can support our previous hypothesis that *O*-GlcNAz glycosylation site (Ser-109) provides exposure enough to interact with receptors even a lack of linker by virtue of the flexibility of Ad5 fiber shaft [53, 63].

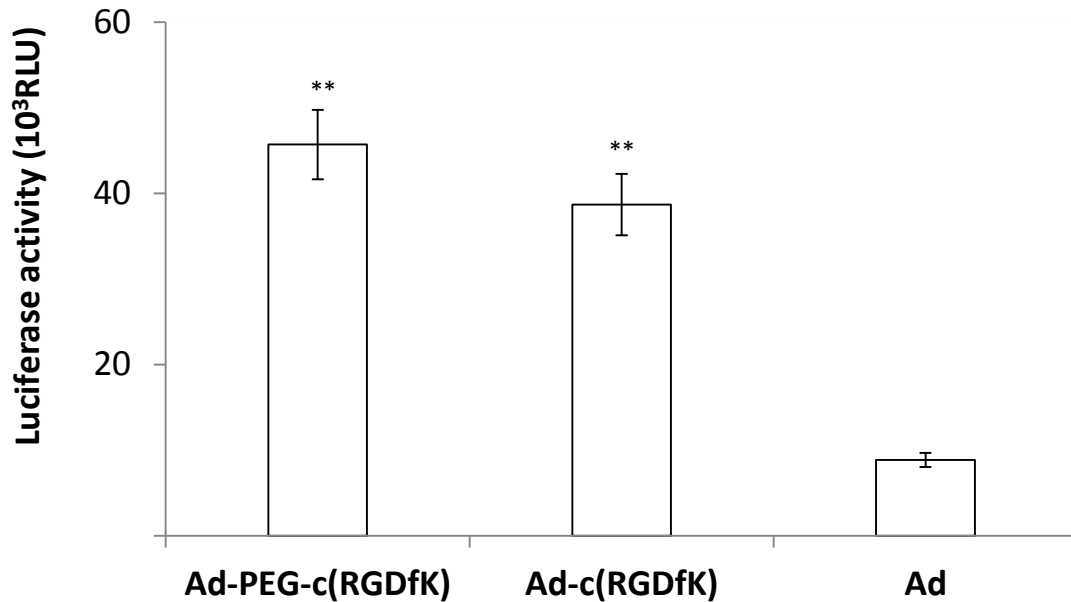


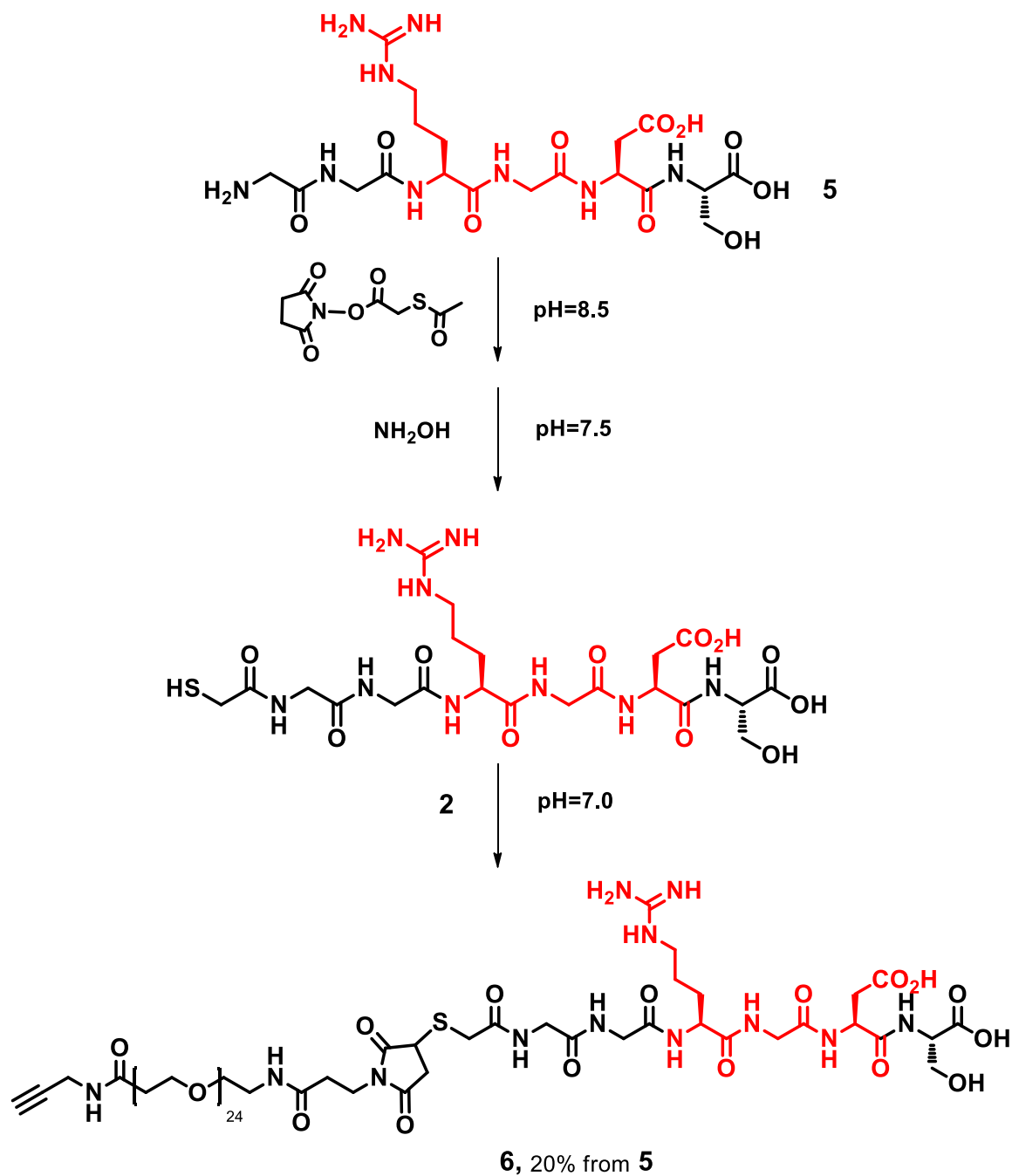
Figure 3-5. Infection Assay with cRGD-Ad to B16BL6

Mouse melanoma cells (B16BL6) were seeded in 96-well black and clear bottom plates at a density of 1×10^4 cells/well, 1 day before infection. Monolayer cells were washed with PBS. Virus stock was added to the infection buffer (PBS, TC, 2% serum) at a multiplicity of infection (MOI) of 1000 and cells were incubated in infection buffer at 37 °C. After 1 h, cell growth media were added and cells were incubated at 37°C. 24 h post infection, the expression levels of luciferase transgene were determined by a photometer with the luciferase assay kit (Bright-Glo, Promega). (Experiments were performed in triplicate and presented as mean \pm standard deviation. *p*-values were calculated by a two-tailed unpaired Student's *t*-test. **: *p* < 0.01)

3.4.4.2 Comparison between Linear- vs. Cyclic-Peptide Targeting to B16BL6

In order to assess the effect of receptor-binding affinity on adenoviral transduction efficiency, linear RGD peptide (GGRGDS, a glycine was included as a spacer) which has less binding affinity to $\alpha_v\beta_3$ integrin than cyclic RGD (*vide supra*, Chapter 3.3), was prepared by Fmoc solid phase peptide synthesis and *N*-terminus of the peptide was modified / conjugated to

maleimide-PEG₂₄-alkyne *via* the same chemistry as the case of cyclic RGD peptide as shown in Scheme 3-7.



Scheme 3-7. Synthesis of Linear RGD-PEG-alkyne

3.4.4.2.1 Infection Assay with Linear- and Cyclic-RGD-Peptide-conjugated Ad

Infection assays were performed with linear (lRGD-Ad) and cyclic-RGD-peptide-conjugated Ad (cRGD-Ad), under the same condition as described in Chapter 3.4.4.1 simultaneously. Surprisingly, depending on MOI, unexpected 8 ~ 50-fold increases in gene delivery were observed with lRGD-Ad in comparison with cRGD-Ad (50 ~ 120-fold increases with lRGD-Ad, compared with unmodified Ad) as shown in Figure 3-6, which was contrary to what we expected in terms of binding affinity.

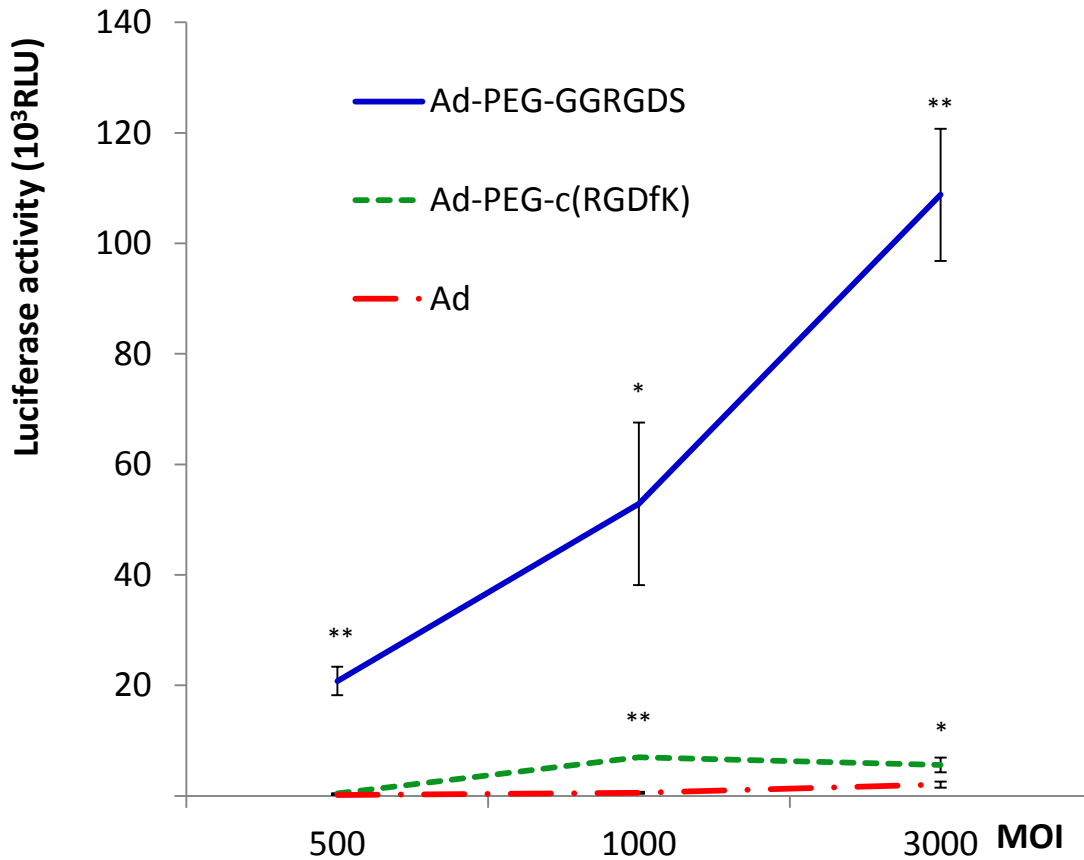


Figure 3-6. Infection Assays with lRGD-Ad and cRGD-Ad to B16BL6

Mouse melanoma cells (B16BL6) were seeded in 96-well black and clear bottom plates at a density of 1×10^4 cells/well, 1 day before infection. Monolayer cells were washed with PBS. Virus stock was added to the infection buffer (PBS, TC, 2% serum) at a multiplicity of infection (MOI) of 500, 1000, and 3000 and cell were incubated in infection buffer at 37 °C. After 1 h, cell growth media were added and cells were incubated at 37°C. 24 h post infection, the expression levels of luciferase transgene were determined by a photometer with the luciferase assay kit (Bright-Glo, Promega). (Experiments were performed in triplicate and presented as mean \pm standard deviation. *p*-values were calculated by a two-tailed unpaired Student's *t*-test. *: *p* < 0.05, **: *p* < 0.01)

In order to account for this unexpected opposite trend of transduction efficiency, we sought a reasonable interpretation and focused on the role of $\alpha_v\beta_5$ integrin which selectively promotes Ad-mediated membrane permeabilization and subsequent endosome rupture as described by Nemerow *et al.* [64]. While both $\alpha_v\beta_3$ and $\alpha_v\beta_5$ integrins mediate viral endocytosis as described in Chapter 1, Nemerow *et al.* claimed that $\alpha_v\beta_5$ integrin facilitates viral escape from cytoplasmic vesicles significantly more than $\alpha_v\beta_3$ integrin [64-65]. In addition, recently, Lyle *et al.* also asserted that $\alpha_v\beta_5$ integrin can play a role as an alternate primary receptor for Ad infection in CAR-deficient cells, *scilicet*, authors found high correlation between the expression level of $\alpha_v\beta_5$ integrin and Ad transduction efficiency in CAR-negative cells, but low correlation in the case of the other integrins [66]. From those claims and predominant expression of $\alpha_v\beta_3$ over $\alpha_v\beta_5$ integrin in B16BL6 [62], we framed a hypothesis that cyclic RGD peptide has such a high binding specificity to $\alpha_v\beta_3$ integrin that could exclude the interaction with $\alpha_v\beta_5$ integrin, that is critical to escape of virions into the cytoplasm prior to lysosomal degradation, which results in low transductional efficiency.

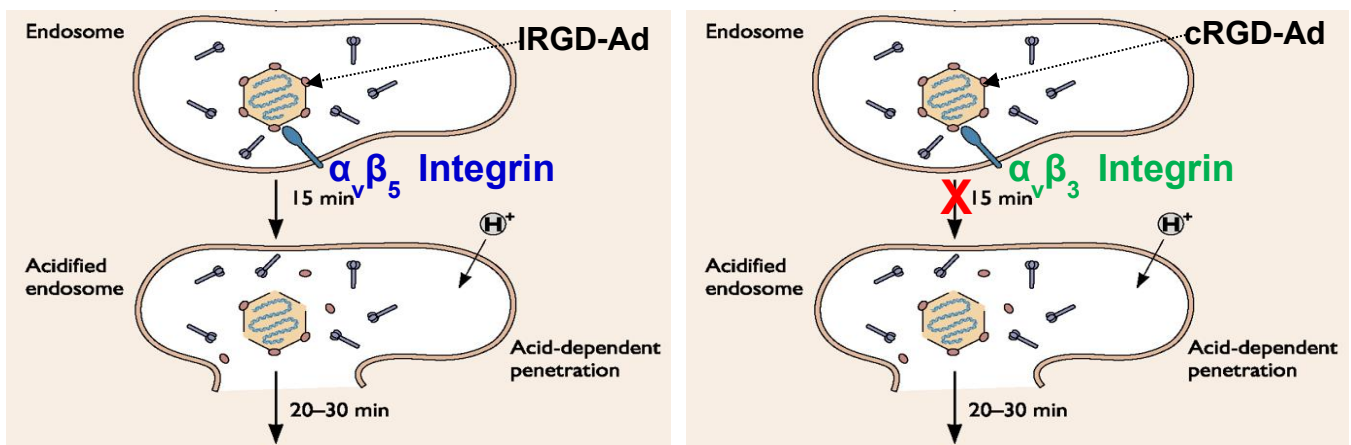


Figure 3-7. The hypothesis of $\alpha_v\beta_5$ integrin-dependent endosome escape with IRGD-Ad vs. cRGD-Ad
 The interaction of cyclic RGD peptide with $\alpha_v\beta_3$ integrin facilitates virus internalization, but might not trigger the disruption of the early endosome allowing escape of viral particles into the cytoplasm, which is indispensable to trafficking of viral capsids and transporting of viral DNA into the nucleus. This figure was modified from reference [1] with the permission of publisher ("ASM Press").

Cyclic RGD peptide also has an affinity to $\alpha_v\beta_5$ integrin, but 10 ~ 100-fold less than $\alpha_v\beta_3$, depending on cells and peptide structures [67-69] (Figure 3-8). Moreover, if the cell expresses much higher level of $\alpha_v\beta_3$ integrins than $\alpha_v\beta_5$, the binding with cyclic RGD would be more severely biased to $\alpha_v\beta_3$ integrins.

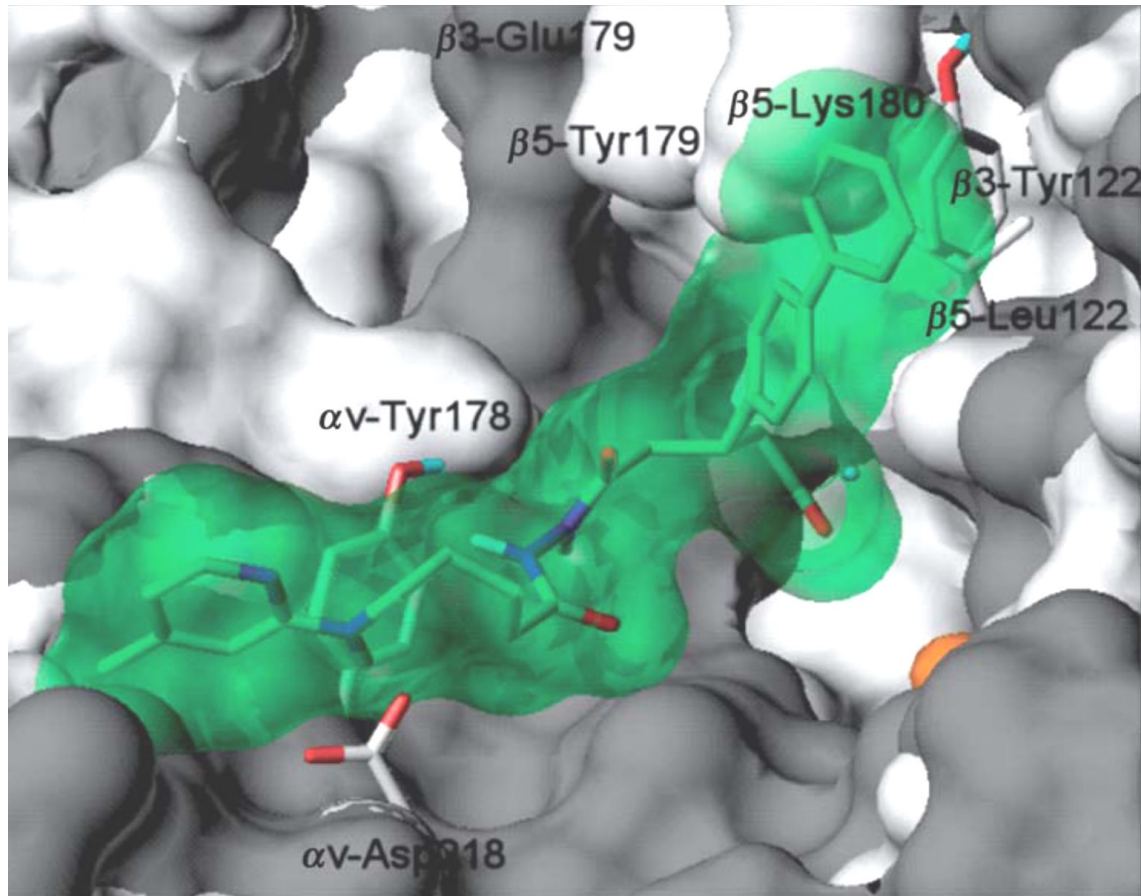


Figure 3-8. Superposition of the $\alpha_v\beta_3$ Receptor (grey) and the Homology Model of the $\alpha_v\beta_5$ (white) both represented as Connolly surface

The $\alpha_v\beta_3$ -selective ligand is docked into the $\alpha_v\beta_3$ receptor (green transparent), the metal ion-dependent adhesion site (MIDAS) cation is shown as orange sphere. This figure was reprinted from reference [24] with the permission of publisher ("Elsevier").

3.4.4.2.2 Endosome Rupture Assay using FITC/Cy5-dextran

In order to test our hypothesis, Ad-induced endosome rupture assay was employed using flow cytometry and “the dual fluorescence ratio method” as described by Schober *et al.* [70]. Briefly, pH sensitive fluid-phase marker (FITC-dextran), and pH insensitive fluid-phase marker (Cy5-dextran) were co-internalized into HeLa cells with and without Ad, and then the ratio of fluorescent intensity (FITC/Cy5) was measured by flow cytometry. Concurrently, the same measurements were performed on the HeLa cells incubated in different pH buffers to obtain a calibration curve. Finally, the higher pH of labeled compartments in the presence of Ad, owing to virus-induced acidic endosome rupture and release of fluorescent makers into the pH neutral cytoplasm, was compared to lower pH in the absence of Ad, demonstrating the capability of this method to monitor viral endosomolytic activities (Figure 3-9). Therefore, we expected to quantitate the degree of endosomolysis in the case of IRGD-Ad and cRGD-Ad using the same technique.

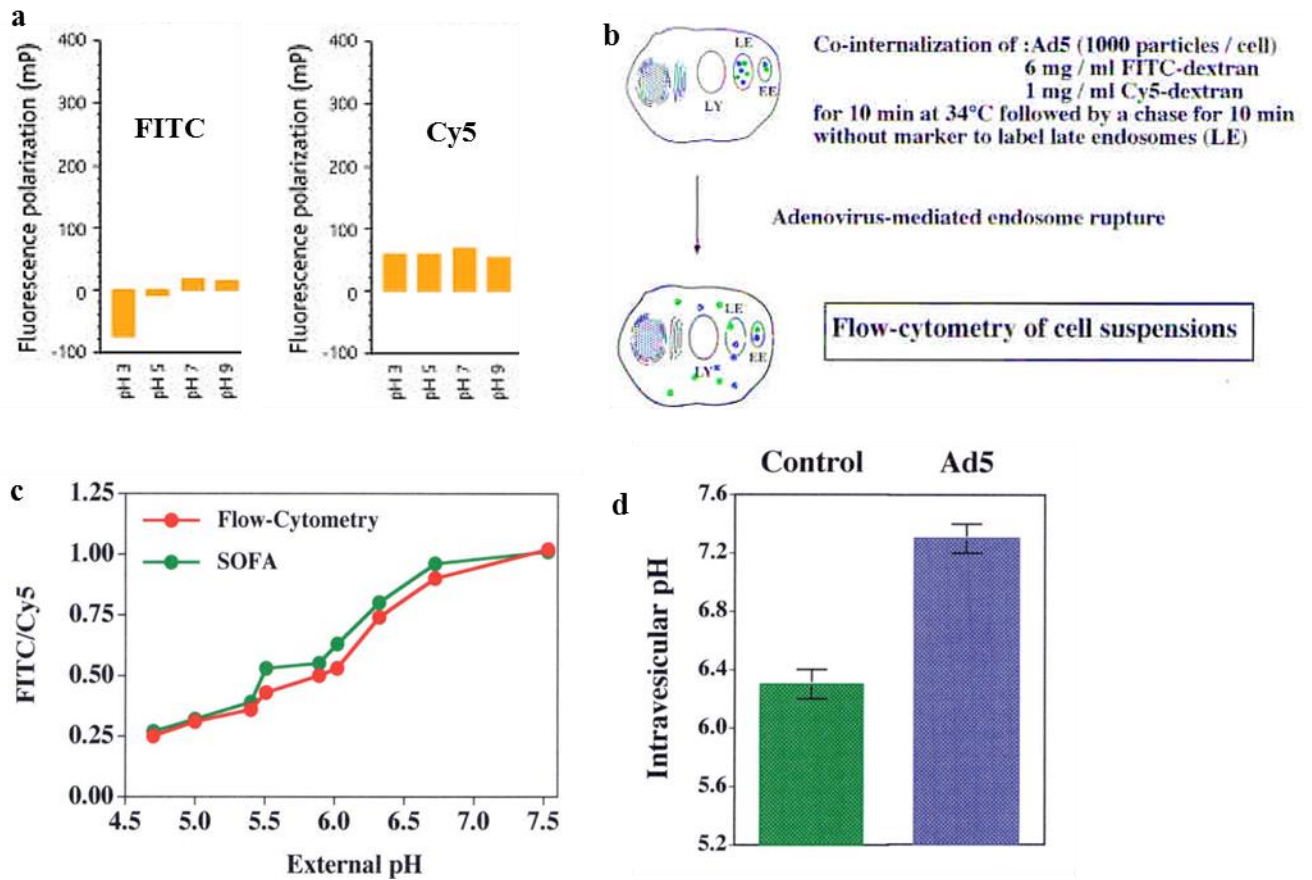


Figure 3-9. Assay for Ad-induced Endosome Rupture Using Flow Cytometry

a) pH dependence of FITC and Cy5, b) Experimental set-up, HeLa cells infected with Ad5 in the presence of FITC- and Cy5-dextran, c) Normalized pH calibration curves of FITC/Cy5-dextran labeled endosomes obtained by flow cytometry, d) Influence of Ad on the pH of labeled compartment, suggesting Ad-induced endosome rupture and release of internalized marker into the pH neutral cytoplasm. This figure was modified from the reference [70].

Hence, the Ad-induced endosome rupture assay was performed using the same fluid-markers (FITC/Cy5-dextran) with both IRGD-Ad and cRGD-Ad. However, only moderate increase on the pH of labeled compartment was observed with IRGD-Ad in comparison to cRGD-Ad and the pHs (~ 5.0) determined by the calibration curve were much lower than the expected value (~7.0), which may stem from a substantial portion of late endosome vesicles (pH < 5.6) *via* non-specific internalization of fluid-phase markers. Due to the difference in cellular susceptibility (HeLa vs.

B16BL6) of viruses compared to fluid-phase markers and the demanding requirement of fast processing time in this endosome rupture assay, we sought more straightforward and facile method to examine our hypothesis, therefore, alternatively, subcellular-Ad-particle localization assays were performed using thin-sectioning electron microscopy as described by Nemerow *et al.* [65].

3.4.4.2.3 Subcellular Localization of Ad particles by Thin-sectioning Electron Microscopy

B16BL6 cells were incubated separately with IRGD-Ad and cRGD-Ad at 4 °C for 1h to allow virus attachment and warmed to 37 °C for 20 min. Then, the cells were washed, fixed, processed, and examined by transmission electron microscopy as described in ‘Materials and methods’ section. As shown in Figure 3-10, stained Ad capsids were frequently discovered in the cytoplasm in close proximity to the nucleus in IRGD-Ad-infected B16BL6 cells, indicating that Ad particles had successfully induced endosome disruption and escaped from it. In stark contrast, virions inside cRGD-Ad-infected B16BL6 cells, were observed rarely free in the cytoplasm, but instead were found mostly inside vacuoles (Figure 3-11). To statistically confirm these results, morphometric analysis of Ad entry into B16BL6 cells infected by cRGD-Ad and IRGD-Ad respectively as shown in Figure 3-12, the location of Ad particles, 100 per time point in randomly selected 10 different cells, was determined directly from electron micrographs. Virus particles were identified and counted as being free in the cytoplasm or inside vesicles, showing an accumulation of virions inside vesicles (83 %) with fewer free particles (17%) in the cytoplasm of cells infected by cRGD-Ad, whereas the opposite trend was observed in IRGD-Ad infected cells. In summary, this thin-sectioning TEM experiment strongly supports our

hypothesis of $\alpha_v\beta_5$ integrin-dependent transduction efficiencies in the cases of RGD peptide conjugated Ads.

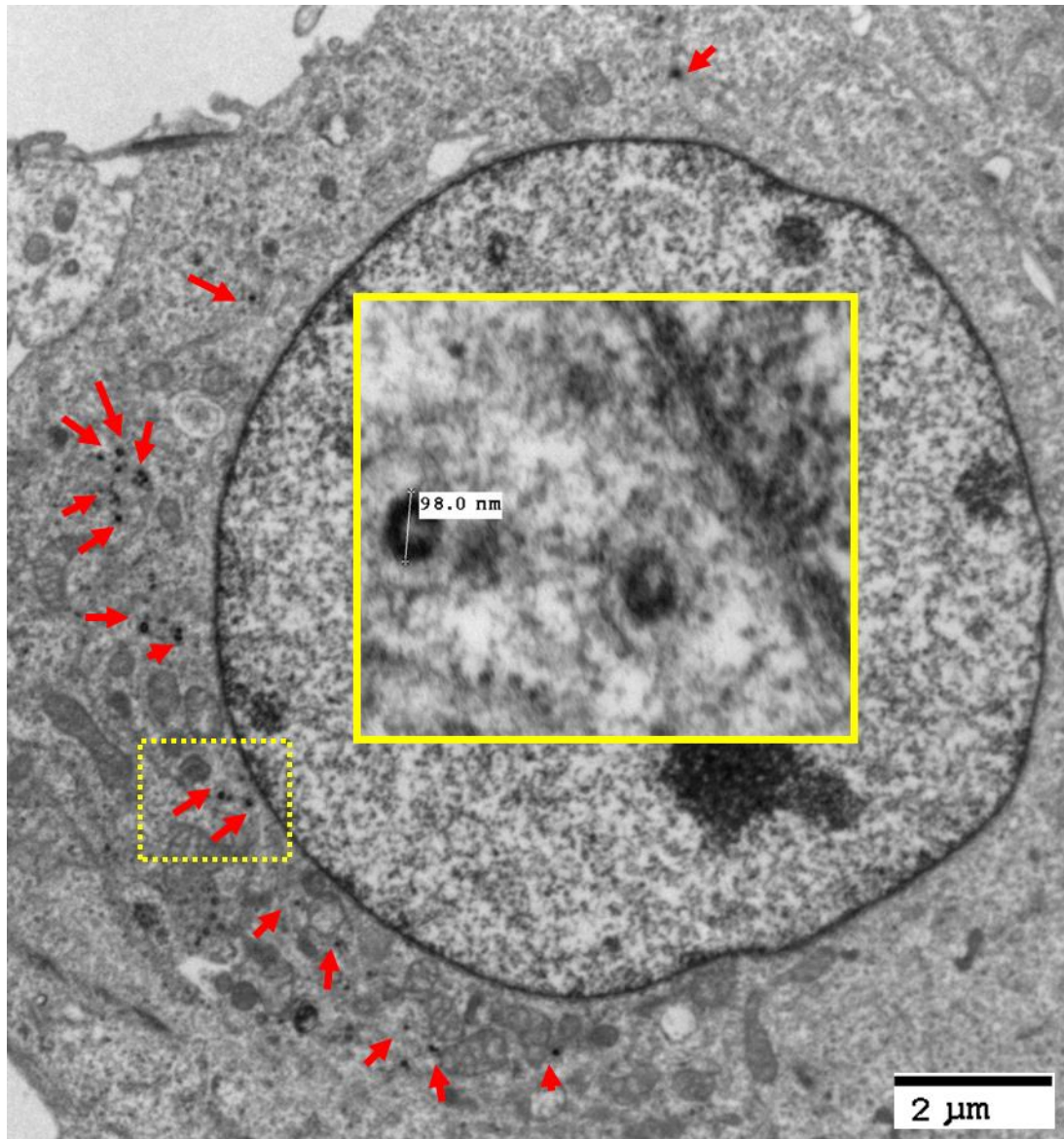


Figure 3-10. TEM Image of the Late Stages of IRGD-Ad Entry in B16BL6 Cell

Ad particles (indicated by the arrows) were observed free in the cytoplasm in close proximity to the nucleus in B16BL6 cells infected by linear RGD peptide conjugated Ad at 20 min after warming to 37 °C. The yellow rectangular region was magnified to verify the size of Ad particles.

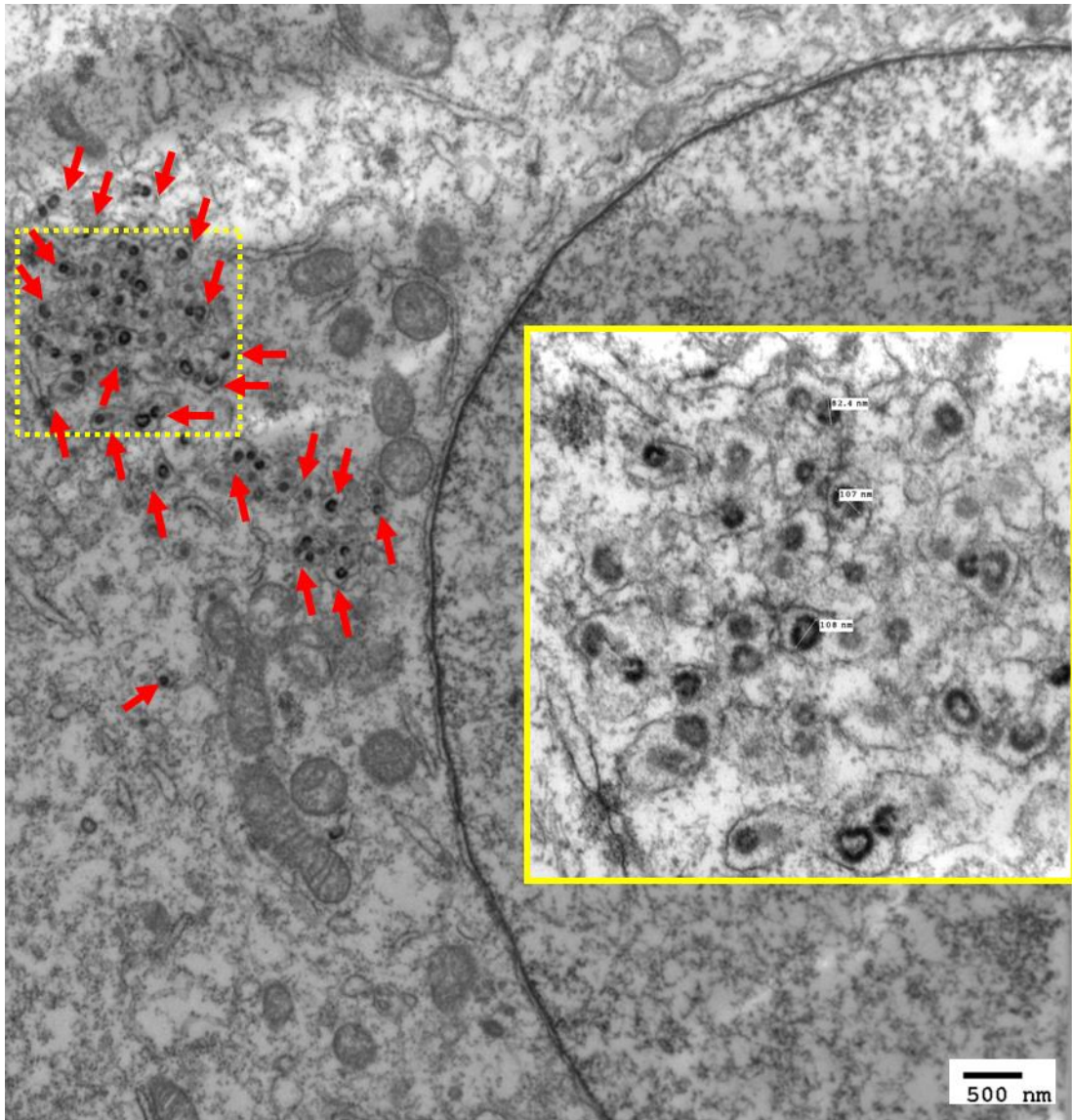


Figure 3-11. TEM Image of the Late Stages of cRGD-Ad Entry in B16BL6 Cell

In contrast to Figure 3-10, most Ad particles (indicated by the arrows) were confined in vacuoles in B16BL6 cells infected by cyclic RGD peptide conjugated Ad at 20 min after warming to 37 °C. The yellow rectangular region was magnified to verify the size of Ad particles and clearly present vacuoles.

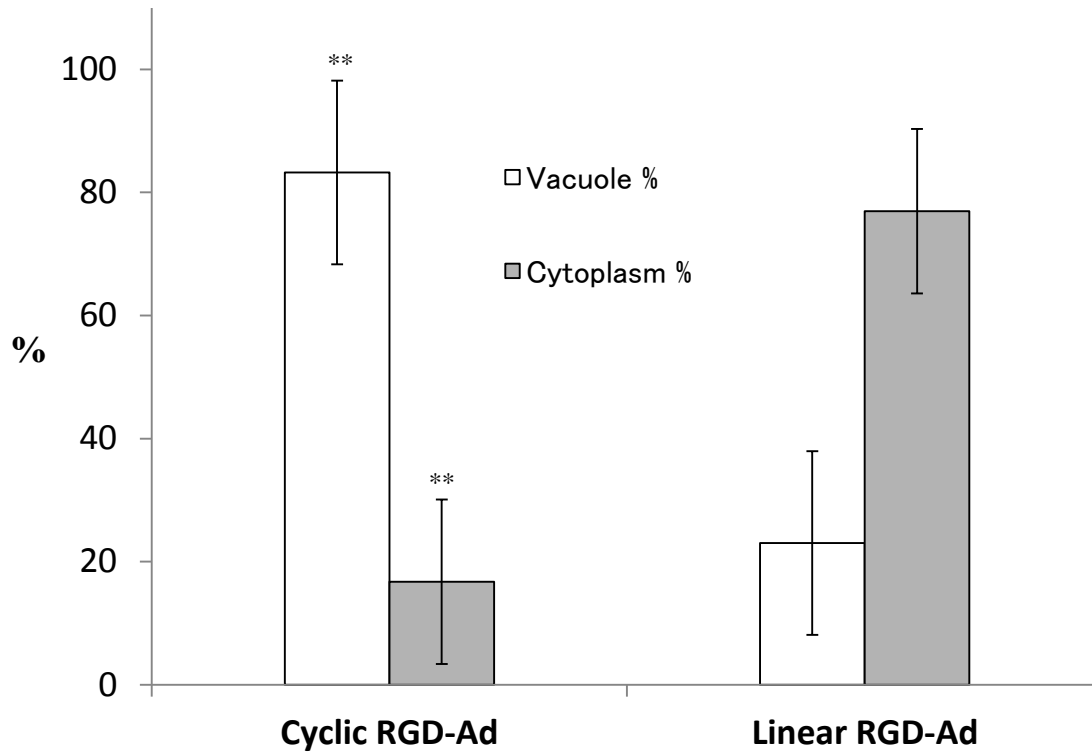


Figure 3-12. Morphometric Analysis of Ad entry into B16BL6 Cells

The location of Ad particles, 100 per time point in randomly selected 10 different cells, was determined directly from thin-sectioning electron micrographs in B16BL6 cells infected by cRGD-Ad and lRGD-Ad, respectively. Virus particles were identified and counted as being free in the cytoplasm or inside vesicles. (Experimental data were presented as mean \pm standard deviation. p -values were calculated by a two-tailed unpaired Student's t -test. **: $p < 0.01$)

3.4.4.3 Expression of Ad knob for CAR Inhibition

Different from B16BL6, many therapeutically relevant cells have different basal levels of the primary receptor for adenovirus (CAR), which leads to the unwanted variable background infections. To mitigate this background, a truncated soluble form of the fiber protein, which serves as the ligand for the primary adenovirus receptor (CAR), was added to the medium prior to infection with modified Ad particles (Figure 3-13). This soluble knob domain is readily overexpressed in *E. coli* (Figure 3-14) and derived from a different serotype adenovirus, Ad12 [71-72]. However, the Ad12 knob has high sequence homology to the Ad5 knob (45% identity, Figure 3-15) and can inhibit other serotype's (e.g., Ad2) infections mediated by CAR receptor as reported by Freimuth *et al.* [73].

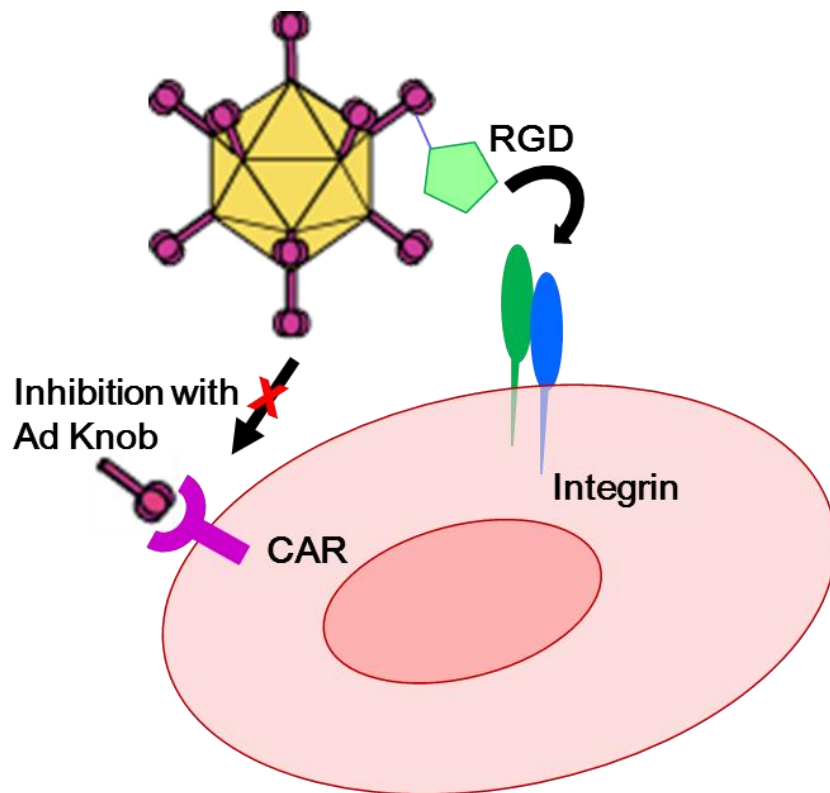


Figure 3-13. CAR Inhibition with Ad knob

To inhibit background infection mediated by natural primary receptor (CAR) of Ad5, soluble Ad knob was added prior to the infection by RGD peptide conjugated Ad.

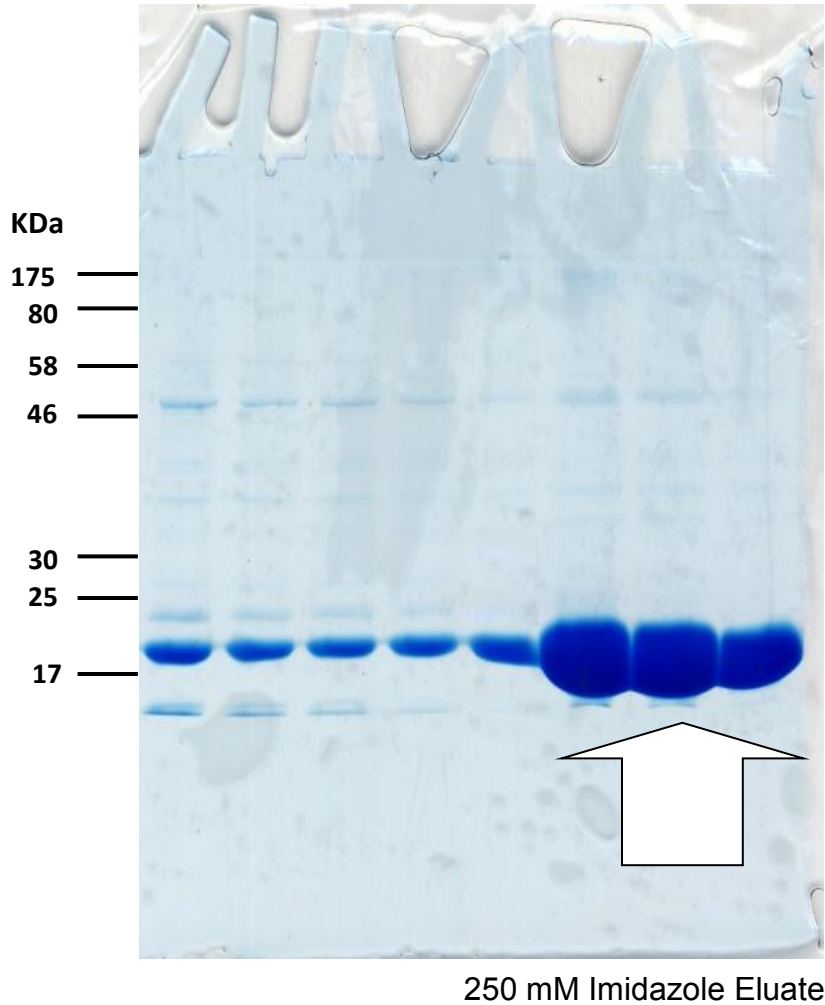


Figure 3-14. Expression of Ad12 knob in *E. coli*

pET15b-Ad12 knob plasmid (kindly donate by Dr. Freimuth) including codes for His₆ tag at *N*-terminus, was transformed into *E. coli* (BL21-DE3) and cultured in LB broth containing penicillin G. Knob expression was induced by adding IPTG. Then cells were lysed and centrifuged (25,000 × g). Knob was purified from supernatant of cell lysate by NTA affinity chromatography. The purified Knob was characterized by SDS-PAGE and Coomassie blue staining which clearly indicated the expression of Knob protein (Mw. 22.4 KDa)

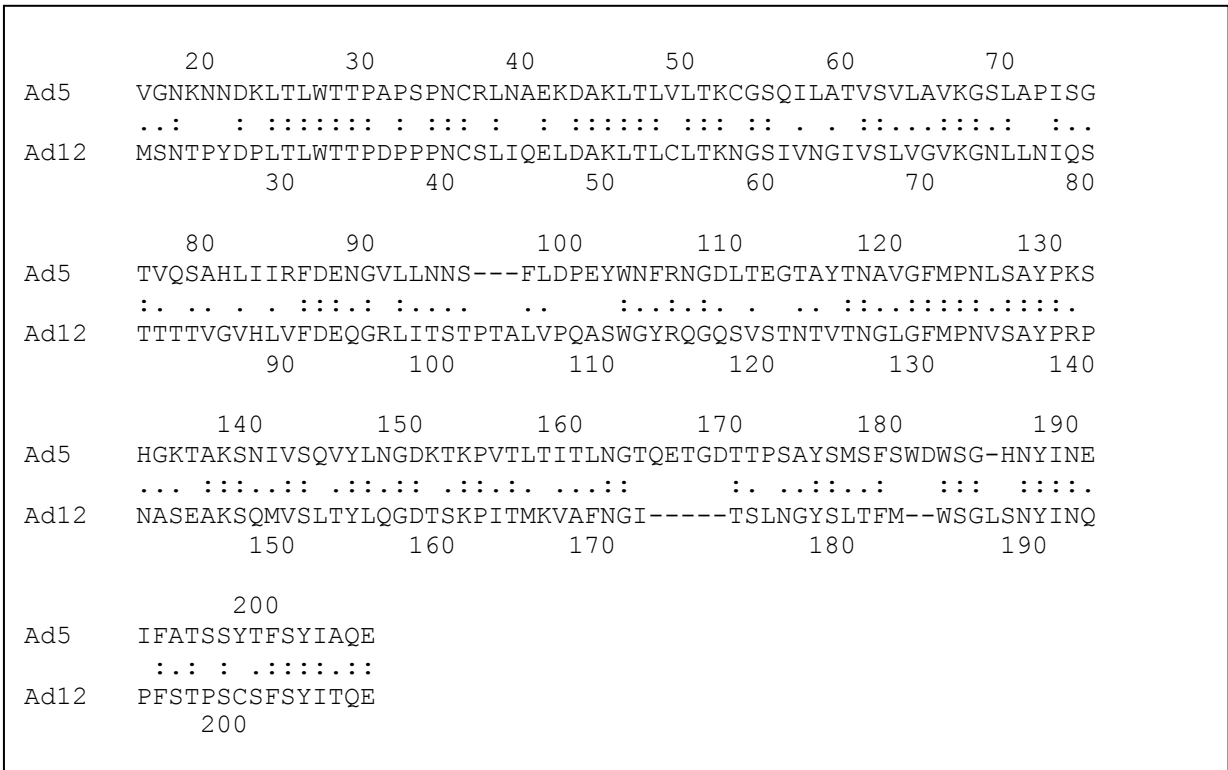


Figure 3-15. Sequence Alignment between Ad5 knob and Ad12 knob

The optimal alignment found when using LALIGN to align the sequences of Ad5 knob and Ad12 knob. The Ad12 knob showed high sequence homology to the Ad5 knob (45% identity, 73% similarity).

3.4.4.4 Targeting to the Human Glioma with RGD-Ad

In order to assess the targeting ability of our RGD-Ad to other therapeutically relevant cell lines, we chose two established human glioma cells (U87-MG and D65-MG), known to express high levels of $\alpha_v\beta_3$ integrin [74]. Glioblastoma (glioma), one of the most common primary and aggressive forms of brain cancer, is notoriously difficult to treat with conventional therapeutics and consequently have been a target for gene therapy [75-76]. Since those cells also express the natural primary receptor of Ad (CAR) in low (U87-MG) and medium (D65-MG) levels [76], causing unwanted background infections, a recombinant Ad12 knob was added to the medium as a CAR inhibitor, prior to the infection with RGD-Ad as described in Chapter 3.4.4.3. The results demonstrated a ~380-fold increase (D65-MG) and a ~1200-fold increase (U87-MG) in gene deliveries with *c*(RGDfK)-PEG-Ad in comparison with unmodified Ad, which is dependent of the expression levels of integrins in the cell lines [77-79]. In addition, despite different levels of CAR expressions on those cells (U87-MG and D65-MG), negligible backgrounds were observed in both cases, indicating Ad12 knob can effectively inhibit the CAR mediated infections of Ad vectors as shown in Figure 3-16. For the purpose of re-examining our hypothesis of $\alpha_v\beta_5$ -dependent transduction efficiencies in the cases of RGD-Ads, infection assays with IRGD-Ad and cRGD-Ad were performed simultaneously under the same condition. Different from B16BL6 cells (> 8-fold increased transduction efficiency with IRGD-Ad at MOI of 500), the similar transduction efficiencies was observed in U87-MG cells and ~ 25% increase in D65-MG was observed with IRGD-Ad as depicted in Figure 3-17. If we consider the higher affinity of cyclic RGD peptide (~ 100-fold) to $\alpha_v\beta_3$ integrin than linear RGD peptide, these results still can be explained by our hypothesis. Nevertheless, the amount of increase in U87-MG and D65-MG were only moderate when compared with B16BL6 cells. In general, higher

percentage (73%) of glioma cells are positive for $\alpha_v\beta_5$ integrin than $\alpha_v\beta_3$ (21%) integrin [74] and U87-MG expresses $\alpha_v\beta_5$ integrins in comparable level to $\alpha_v\beta_3$ integrins [78], which may mitigate the biased binding of cyclic RGD peptide to $\alpha_v\beta_3$ integrin receptors and reduce the difference in transduction efficiency when compared to B16BL6 cells.

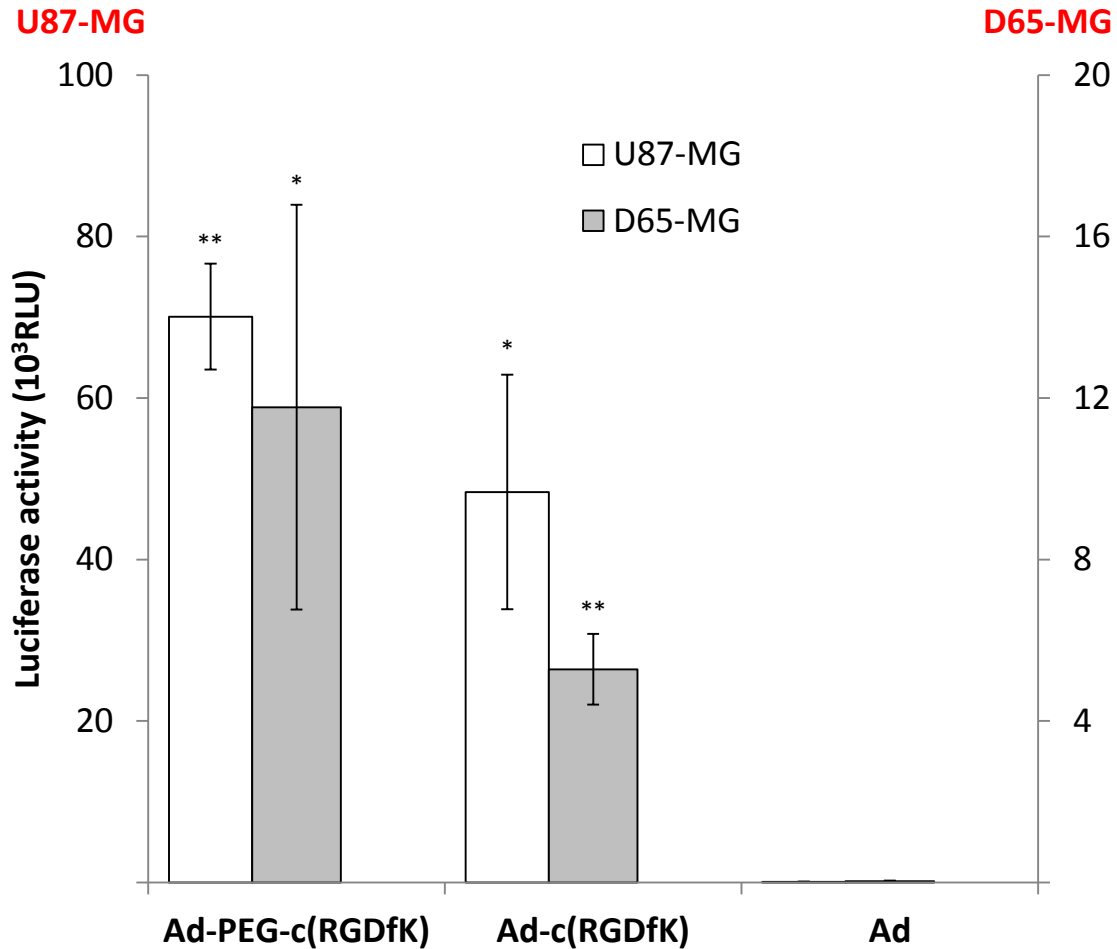


Figure 3-16. Infection Assay with cRGD-Ad to Human Glioma

Cells (U-87MG, D-65MG) were seeded in 96-well black and clear bottom plates at a density of 1×10^4 cells/well, respectively, 1 day before infection. Monolayer cells were washed with PBS and incubated in inhibition buffer ([Ad12 knob] $\approx 20 \mu\text{M}$ in PBS with 2% serum) for 1 h at RT. Virus stock was added to the inhibition buffer at a multiplicity of infection (MOI) of 500 and incubated at 37°C . After 1 h, cell growth media were added and cells were incubated at 37°C . 24 h post infection, the expression levels of luciferase transgene were determined by a photometer with the luciferase assay kit (Bright-Glo, Promega) Experiments were performed in triplicate and presented as mean \pm standard deviation. p -values were calculated by a two-tailed unpaired Student's t-test. **: $p < 0.01$, *: $p < 0.05$

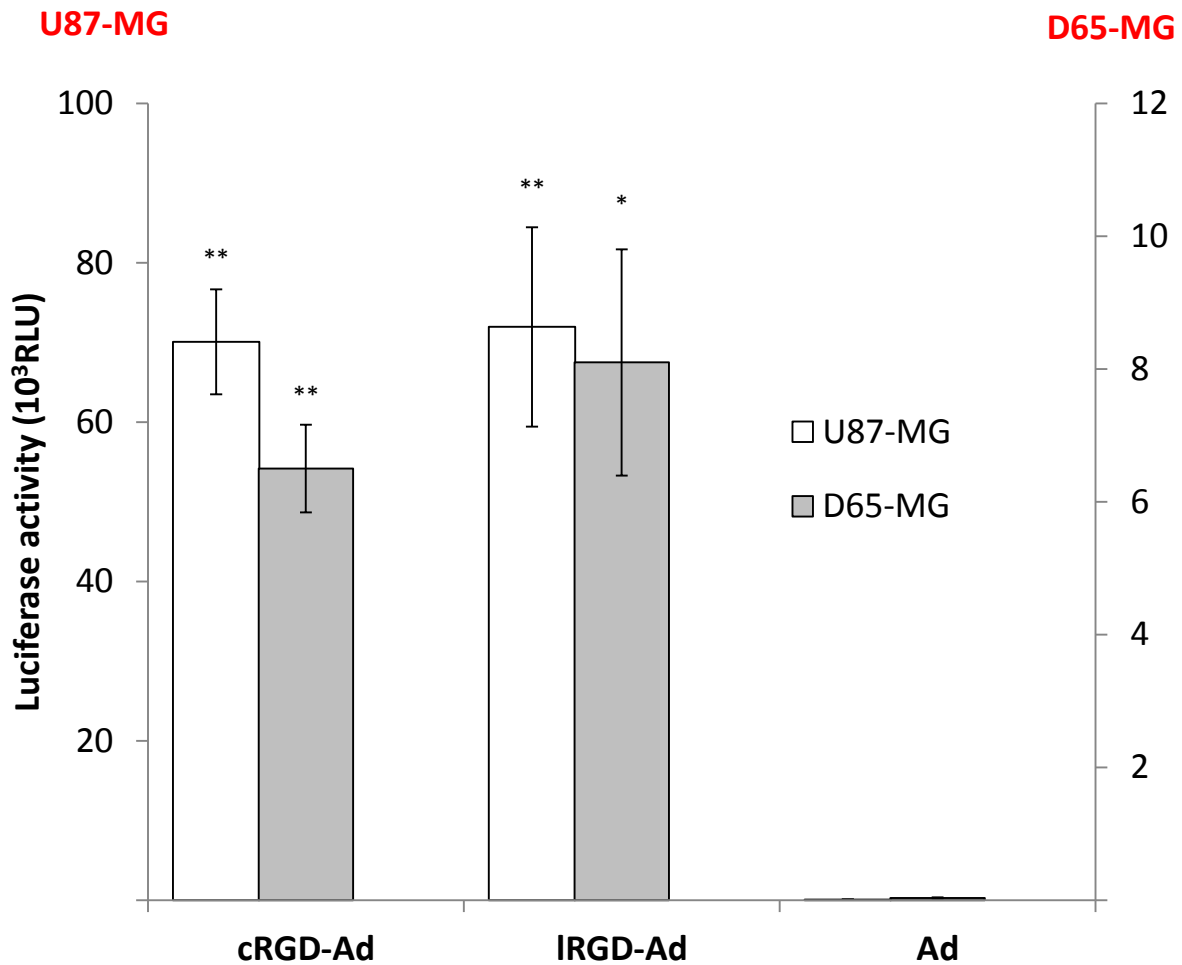


Figure 3-17. Infection Assays with cRGD-Ad and IRGD-Ad to Human Glioma

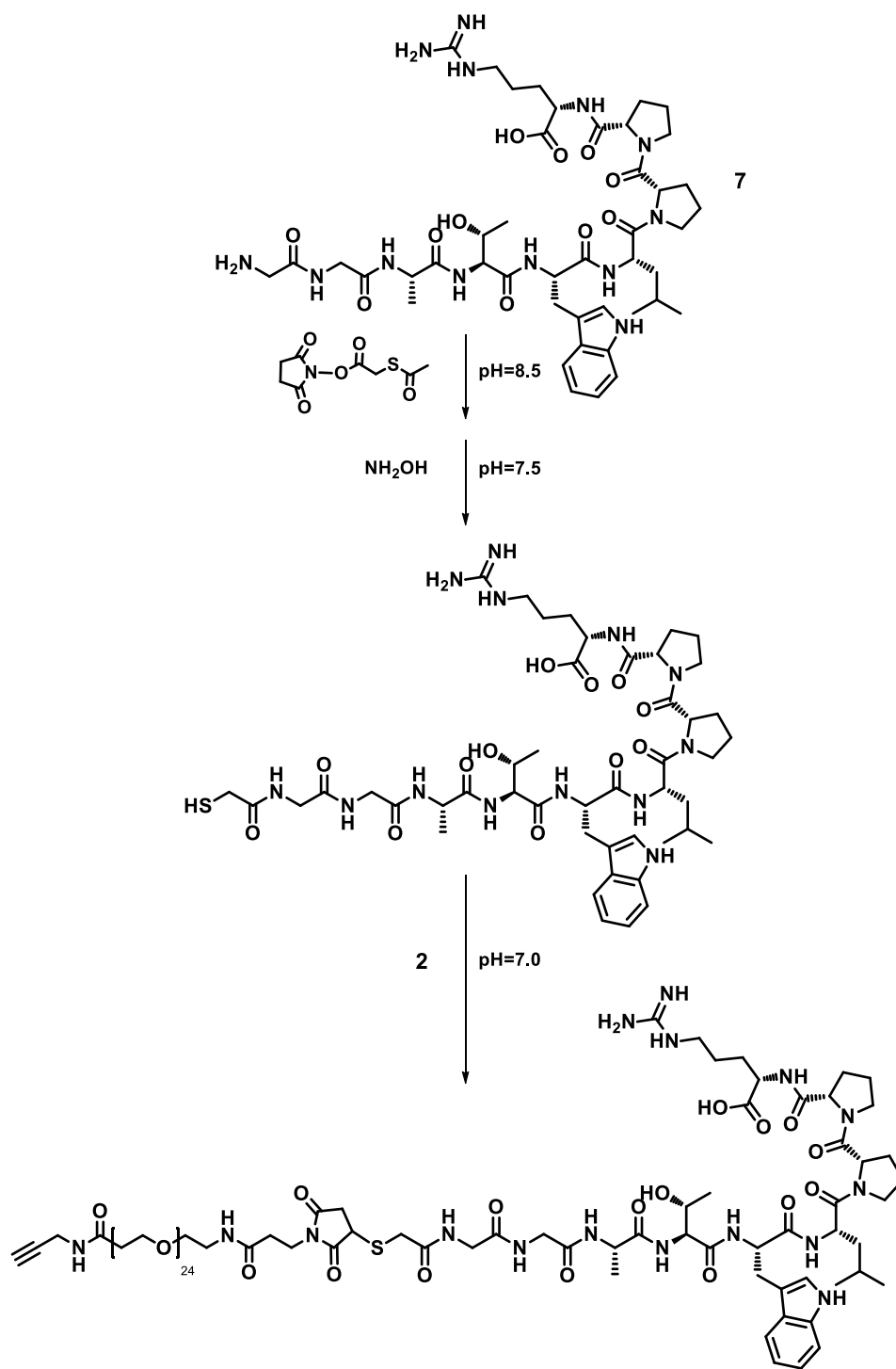
Cells (U-87MG, D-65MG) were seeded in 96-well black and clear bottom plates at a density of 1×10^4 cells/well, respectively, 1 day before infection. Monolayer cells were washed with PBS and incubated in inhibition buffer ([Ad12 knob] $\approx 20 \mu\text{M}$ in PBS with 2% serum) for 1 h at RT. Virus stock was added to the inhibition buffer at a multiplicity of infection (MOI) of 500 and incubated at 37 °C. After 1 h, cell growth media were added and cells were incubated at 37 °C. 24 h post infection, the expression levels of luciferase transgene were determined by a photometer with the luciferase assay kit (Bright-Glo, Promega). Experiments were performed in triplicate and presented as mean \pm standard deviation. *p*-values were calculated by a two-tailed unpaired Student's *t*-test. **: *p* < 0.01, *: *p* < 0.05.

3.4.5 Targeting to Angiogenesis

Angiogenesis, the growth of new blood vessels, is required for invasive tumor growth and metastasis [80-83]. Moreover, the tumor blood vessels display specific abnormalities including up-regulated protein markers usually negative in normal physiological conditions [84]. Hence, these proteins have been prospective targets for selective cancer therapy. In addition to $\alpha_v\beta_3$ integrin described in Chapter 3.2, the vascular endothelial growth factor receptor 2 (VEGFR2) [81] and the tyrosine kinase receptor Tie2 [85] are such hallmarks associated with tumor angiogenesis and over-expressed in tumor vessels. Recently, Haisma *et al.* reported selective targeting of Ad vectors to the endothelial receptors such as $\alpha_v\beta_3$ integrin, VEGFR2, and Tie2 in both mouse (H5V) and human cell lines (HUVEC) using a bifunctional single chain antibody expressing targeting peptides and α -knob domains (i.e., ‘adaptor’ approach) [86]. In the context of expanding Ad tropism and demonstrating the versatility of our approach, we desire to target the same receptors involved in angiogenesis using azide-enabled Ad (GlcNAz-Ad) and bioorthogonal “click” chemistry.

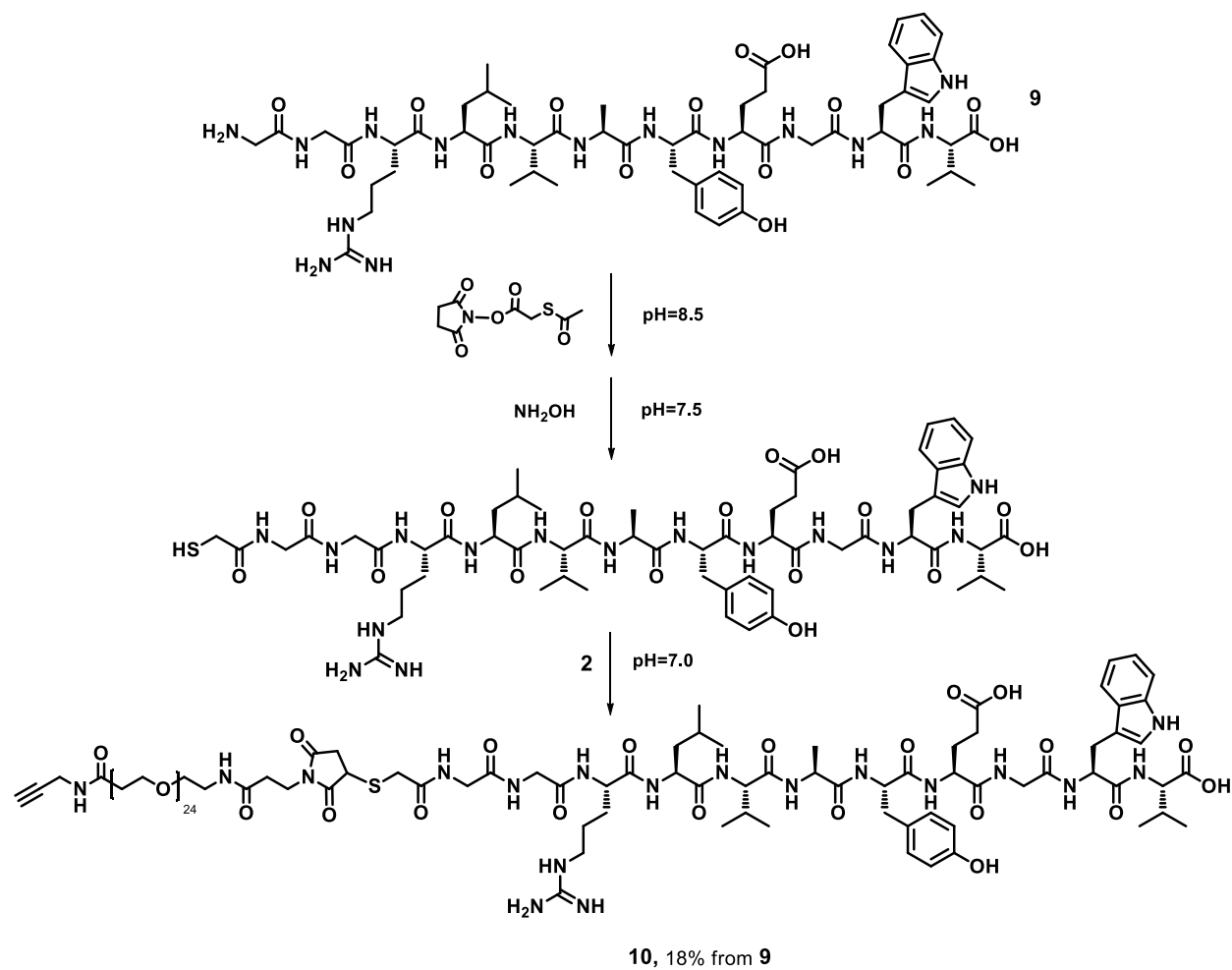
3.4.5.1 Synthesis of VEGFR2 and Tie2-Targeting Peptides-PEG-alkyne

The targeting peptides (ATWLPPR for VEGFR2 and RLVAYEGWV for Tie2) were identified by phase-display-library screening [87-88]. We prepared these peptides by standard Fmoc solid phase peptide synthesis with two *N*-terminal glycine spacers and coupled with alkyne-PEG-maleimide linker *via* the same chemistry described in Chapter 3.4.1 as depicted in Scheme 3-8 and Scheme 3-9.



8, 25% from 7

Scheme 3-8. Synthesis of VEGFR2 Targeting Peptide-PEG-alkyne



Scheme 3-9. Synthesis of Tie2 Receptor Targeting Peptide-PEG-alkyne

3.4.5.2 Infection Assays with Angiogenesis-targeting Ad to HUVEC *in vitro*

The azide-enabled Ad5 (GlcNAz-Ad) was conjugated with alkyne-PEG-GGATWLPPR and alkyne-PEG-GGRLVAYEGWV respectively *via* CuAAC as described in Chapter 3.4.3 (in detail in ‘Materials and methods’ section). To assess the targeting ability of peptide-conjugated Ads to human endothelial receptors, HUVEC (human umbilical vein endothelial cell), known to express VEGFR2, Tie2, and $\alpha_v\beta_3$ integrins receptors, was infected with corresponding targeting Ad vectors (Ad-PEG-GGATWLPPR, Ad-PEG-GGRLVAYEGWV, and Ad-PEG-*c*(RGDfK)) including luciferase reporter gene. To mitigate background infections mediated by CAR, cells were incubated with a recombinant Ad12 knob prior to infection with targeted Ad as described in Chapter 3.4.4.3. 24 h post-infection, the levels of luciferase transgene expression were measured by photometer, which showed ~7-fold (Tie2 targeting), ~5-fold (VEGFR2 targeting) and ~3-fold ($\alpha_v\beta_3$ integrin targeting) increases of gene deliveries with targeted Ads in comparison with non-targeted Ads as depicted in Figure 3-18. In this infection assay, as another control, alkyne-PEG-maleimide (**2** in Scheme 3-2) was also conjugated on GlcNAz-Ad *via* the same CuAAC condition, which can reveal the effect of a long PEG₂₄ linker without targeting peptide on transduction efficiency of Ad. The result presented the equal level of signal to the completely unmodified Ad as shown in Figure 3-18, indicating the increases of transgene expression resulted purely from targeting peptide moieties. In addition, the transduction efficiency of cRGD-Ad was compared with that of IRGD-Ad simultaneously under the same condition, showing the similar levels of increased gene delivery to HUVEC (data not shown), which can be explained by the same level of $\alpha_v\beta_5$ expression compared to $\alpha_v\beta_3$ in HUVEC [89-90] and the same rationale as in Chapter 3.4.4.4.

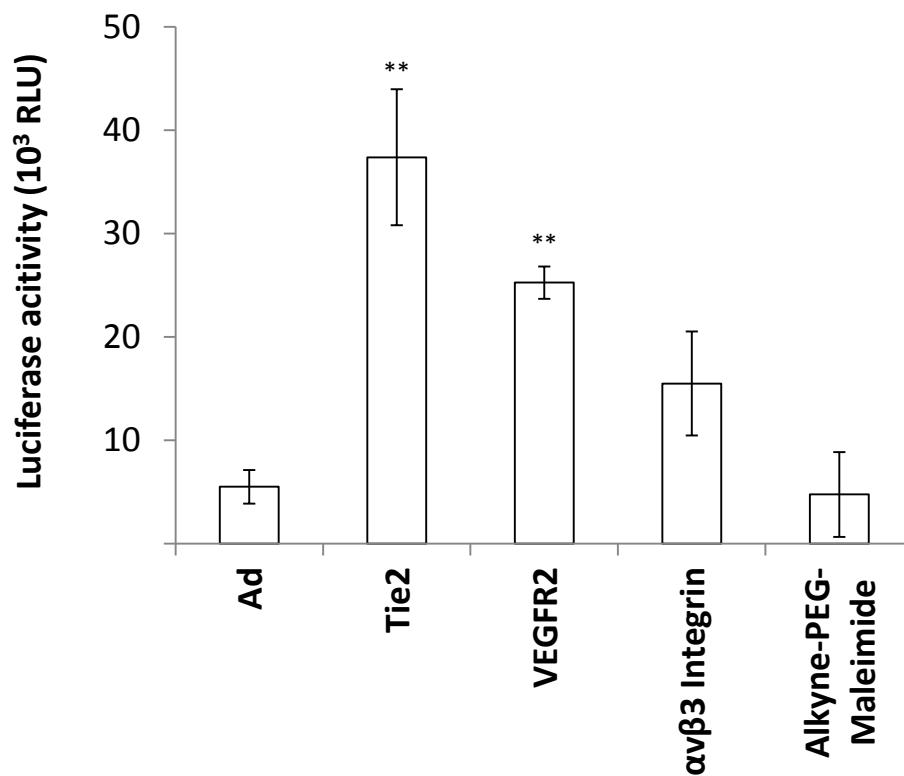


Figure 3-18. Infection Assays with Angiogenesis Targeting Ad

Cells (HUVEC) were seeded in 96-well black and clear bottom plates at a density of 1×10^4 cells/well, 1 day before infection. Monolayer cells were washed with PBS and incubated in inhibition buffer ([Ad12 knob] $\approx 20 \mu\text{M}$ in PBS with 2% serum) for 1 h at RT. Virus stock was added to the inhibition buffer at a multiplicity of infection (MOI) of 1000 and incubated at 37 °C. After 1 h, cell growth media were added and cells were incubated at 37 °C. 24 h post infection, the expression levels of luciferase transgene were determined by a photometer with the luciferase assay kit (Bright-Glo, Promega). Experiments were performed in triplicate and presented as mean \pm standard deviation. *p*-values were calculated by a two-tailed unpaired Student's t-test. **: *p* < 0.01, *: *p* < 0.05.

3.4.6 Conclusion

We demonstrated that adenoviruses bearing metabolically incorporated *O*-GlcNAz moiety, can be modified and targeted using synthetic peptides including alkyne moieties as “clickable” partner. Notably, this targeting strategy is exceedingly straightforward, requiring only minor modifications of Ad production protocol and “clickable” targeting molecules. We selectively targeted Ad vectors to the receptors up-regulated in cancer cells or tumor vessels, including $\alpha_v\beta_3$ integrin, VEGFR2, and Tie2 by virtue of affinities between targeting peptides and corresponding receptors. *Scilicet*, alkyne moiety was covalently linked with various targeting synthetic peptides which have specific affinities to the corresponding receptors over-expressed on different types of cancer cells. Then, the “click” reaction was performed between alkyne-peptides and azide-enabled (*O*-GlcNAz) Ad vectors containing a reporter transgene. Targeting studies indicated remarkable (~1000 fold) to modest (~3 fold) increases in infectivity dependent of the nature of the cell line. Interestingly, cyclic-RGD-peptide-conjugated Ad showed unexpected lower transductions to mouse melanoma cells (B16BL6) than linear-RGD-Ad whose ligand has lower affinity to the target receptor ($\alpha_v\beta_3$ integrin) than cyclic RGD peptides. Focusing on the selective role of homologous $\alpha_v\beta_5$ integrin which promotes Ad-mediated membrane permeabilization and subsequent endosome rupture, we hypothesized that the unexpected low transductions stemmed from $\alpha_v\beta_5$ -excluded endocytosis owing to the high binding specificity of cyclic RGD peptide to $\alpha_v\beta_3$ integrin, which was supported by our thin-sectioning TEM study. However, in the further infection studies using different cell lines, we observed that the opposite trend of infectivity with cyclic RGD-Ad were alleviated in a cell-specific manner, which probably due to the different expression level of $\alpha_v\beta_5$ integrins compared to $\alpha_v\beta_3$ integrins.

3.4.7 Materials and methods

General

All chemical reagents were obtained from commercial sources and used without further purification unless otherwise noted. Human adenovirus serotype 5 (Ad5) containing luciferase transgene was obtained from Vector Biolabs (Ad5-CMV-Luc) (Philadelphia, PA). Succinimidyl-([N-maleimidopropionamido]-24ethyleneglycol) ester (NHS-PEG₂₄-Maleimide) was purchased from Thermo Fisher Scientific Inc. (Rockford, IL). pET15b-Ad12 knob plasmid was kindly donated by Dr. P. Freimuth. Matrix assisted laser desorption-ionization time of flight (MALDI-TOF) mass spectra were obtained on a Bruker Autoflex II mass spectrometer (Bremen Germany). HPLC was performed on Shimadzu LG-20AB / SPD-20A system with a C18 column (250 × 4.6 mm, Varian). Size exclusion separation (SEP) columns were purchased from GE Healthcare (NAP-5 column, Sephadex G-25 DNA grade) (Pittsburgh, PA) and SEP spin columns from Princeton Separations (Centri-Sep column CS-400) (Adelphia, NJ). Transmission electron microscope (TEM) image was acquired with a FEI Tecnai BioTwinG2 and an AMT XR-60 CCD digital camera system. Luciferase activity was measured on a photometer (PerkinElmer 2030 multilabel reader) with luciferase assay kit (Bright-Glo, Promega).

Cell Culture

Eagle's Minimum Essential Media (MEM), Richter's Zinc option MEM and Penicillin/Streptomycin and 0.5% Trypsin-EDTA were purchased from GIBCO (Grand Island, NY). Fetal bovine serum (FBS) was purchased from HyClone (Logan, UT). B16BL6 (mouse melanoma) cell line was kindly donated by Prof. Nakagawa from Osaka University and D-65MG

(human glioma) by Prof. Darell D. Bigner from Duke University Medical Center. U-87MG (human glioma) and HUVEC (human umbilical vein endothelial cell) were obtained from Stony Brook University cell culture facility. B16BL6 and U-87MG cells were cultured in MEM and D-65MG cells in Richter's Zinc option MEM supplemented with 10% FBS, 100 IU/mL penicillin, 100 µg/mL streptomycin. HUVEC was cultured in EGM (endothelial cell growth medium, CC-3121: LONZA) supplemented with non-heat activated FBS 2%, Gentamicin sulfate & Amphotericin (GA-1000, CC-4081c: LONZA) 0.1%, rhEGF (recombinant human epidermal growth factor in buffered BSA saline solution (CC-4017c: LONZA) 0.1%, and BBE (Bovine Brain Extract) 0.4% (CC-4092c: LONZA). Cells were cultured at 37 °C in a humidified atmosphere containing 5% CO₂.

Synthesis of GalNAz (N-azidoacetyl- α,β -D-galactosamine)

First, azidoacetic acid was prepared as follows. Sodium azide (5.6 g, 86mmol) was added to iodoacetic acid (8.0g, 43mmol) in H₂O (100mL) and the reaction mixture was stirred at room temperature. After 4days, thin layer chromatography (TLC) analysis using detection by ultraviolet (UV) absorbance and staining with triphenylphosphine/toluene followed by ninhydrin indicates the reaction was complete. The solution was diluted with 1M HCl. The desired product was extracted into ethyl acetate, and the organic phase was washed with saturated NaHSO₃ and saturated NaCl. The solution was dried over MgSO₄, filtered, and concentrated to afford yellow oil (2.0g, 46% crude yield). Azidoacetic acid was volatile and therefore low vacuum was used when concentrating. The crude oil was used without further purification. D-Galactosamine hydrochloride (1.5g, 7.0mmol) was added to azidoacetic acid (0.98g, 9.7 mmol) in methanol (70mL). Triethylamine (2.5mL, 17 mmol) was added and the reaction mixture was stirred for 5

min at room temperature. The solution was cooled to 0°C and N-hydroxybenzotriazole (HOBt, 0.86g, 7.0mmol) was added, followed by 1-[3-(dimethylamino)propyl]-3-ethylcarbodiimide hydrochloride (2.68g, 14.0mmol). The reaction was allowed to warm to room temperature overnight, at which point TLC analysis with ceric ammonium molybdate (CAM) stain indicates that the reaction was complete. The compound was concentrated and purified by silica gel chromatography, eluting with CH₂Cl₂-methanol (9:1, v/v) and recrystallized (1.0g, 55% yield). ¹H NMR (300MHz, D₂O): δ 3.63 (2H, app t), 3.65-3.72 (1H, m), 3.77-3.84 (1H, m), 3.85-3.87 (2H, m), 3.89-3.91 (2H, m), 3.97 (2H, dd), 3.99 (1H, app d), 4.02 (1H, app d), 4.07-4.13 (4H, s), 5.14 (1H, d), 5.15 (1H, d) ppm.

Synthesis of Ac₄GalNAz (1,3,4,6-tetra-O-acetyl-N-azidoacetyl- α,β -D-galactosamine)

Acetic anhydride (1.0mL, 11mmol) was added to a solution of GalNAz (27.5mg, 1.05mmol) in pyridine (2mL) and the reaction mixture stirred overnight at room temperature. The solution was then concentrated and resuspended in ethyl acetate, followed by washing with 1M HCl, saturated NaHCO₃ and saturated NaCl. The organic layer was dried, filtered and concentrated. The crude peracetylated GalNAz was purified by silica gel chromatography eluting with 1:2 ethylacetate-hexane, with a 90% yield. ¹H NMR (300MHz, CDCl₃) mixture of anomers: δ 2.04 (3H, s), 2.06 (3H, s), 2.09 (6H, s), 2.13 (6H, s), 2.18 (3H, s), 2.19 (3H, s), 3.95 (1H, ddd), 4.07-4.12 (7H, m), 4.24-4.26 (2H, m), 4.68 (1H, ddd), 4.71 (1H, ddd), 5.00 (1H, dd), 5.25 (1H, app t), 5.29 (1H, dd), 5.50 (1H, d), 6.22 (1H, d), 6.23 (1H,d), 6.24 (1H, d) ppm.

Metabolic Labeling of Ad5 with N-azidoacetylgalactosamine

Metabolic labeling of Ad5 with *N*-azidoacetylgalactosamine was performed as described previously [53], that is, HEK 293 cells were infected with intact adenovirus particles with an MOI of 5 PFU/cell. The complete media was supplemented with 50 μ M peracetyl-*N*-azidoacetylgalactosamine or 50 μ M peracetyl-*N*-azidoacetylglucosamine and the infected cells were incubated at 37 °C. The plates were harvested 42-46 h post infection and virus particles were purified over a gradient of 1.4 g/mL and 1.25 g/mL CsCl centrifuged at 32,000 rpm for 1 h at 15 °C. The virus band at the boundary interface between the two CsCl layers was collected and further purified by an 18 h centrifugation at 35,000 rpm over 1.33 g/mL of CsCl.

Synthesis of cyclo(-Arg-Gly-Asp-D-Phe-Lys-) (3-1)

Cyclic pentapeptide *c*(RGDfK) was synthesized as described by Liu et al.[49], briefly, the linear peptide (GDfKR) was prepared by standard 9-fluorenylmethoxycarbonyl (Fmoc) solid phase peptide synthesis (SPPS) using 2-chlorotrityl chloride resin and cyclized with 1-propanephosphonic acid cyclic anhydride (T3P) as a coupling reagent. The cyclic peptide was purified by flash chromatography (methanol:ethyl acetate, 1:10) before deprotection. ESI *m/z* calcd for C₂₇H₄₁N₉O₇ [M] 603.3, obsd 604.3 [M + H]⁺.

Synthesis of Alkyne-PEG₂₄-maleimide (3-2)

NHS-PEG₂₄-maleimide (15 mg, 11 μ mol) was dissolved in anhydrous acetonitrile and propargylamine (0.6 mg, 11 μ mol) was added with 1.5 μ L of triethylamine. After 6 h, the reaction mixture was dried *in vacuo* and purified by reverse-phase HPLC with a C18 column and

elution with H₂O/acetonitrile gradient containing TFA (0.1% v/v) to afford **3-2** (9.2 mg, 63%). MALDI–TOF m/z calcd for C₆₁H₁₁₁N₃O₂₈ [M] 1333.74, obsd 1356.25 [M + Na]⁺.

Synthesis of alkyne-PEG₂₄-c(RGDfK) (3-3)

The conjugation of **2** with cyclic (RGDfK) peptide was realized by introduction of a sulfhydryl group to available lysine ε-amino group using *N*-succinimidyl-*S*-acetylthioacetate (SATA) and deprotection with hydroxylamine (NH₂OH), that is, c(RGDfK)•2TFA (5.5 mg, 6.6 μmol) was dissolved in 1 mL of Sodium Borate Buffer (pH 8.5) and 110 μL (7.15 μmol, 1.08 eq.) of 65 mM SATA in DMSO was added. After 2 h mixing at RT, 100 μL of 0.5 M hydroxylamine hydrochloride in 50 mM Sodium Phosphate, 25 mM EDTA, pH 7.5 buffer was added to the solution of SATA modified peptide. Reaction was performed for 2 h at RT and purified by HPLC (elution at 30% CH₃CN/ 70% H₂O, 0.1% TFA) ESI m/z calcd for C₂₉H₄₃N₉O₈ [M] 677.3, obsd 678.3 [M + H]⁺. Thiol c(RGDfK) eluate was dried *in vacuo* and redissolved in reduction buffer (50 mM sodium phosphate, 150 mM NaCl, 2 mM EDTA, pH 7.0) to obtain a final volume of 100 μL. The solution was incubated with immobilized TCEP (Tris[2-carboxyethyl] phosphine hydrochloride) disulfide reducing gel (Thermo Scientific) for 30 min at RT and centrifuged for 1 min. The supernatant containing the reduced peptide was mixed with **2** (8.8 mg, 6.6 μmol) in the same buffer solution immediately. After 2 h reaction at RT, the mixture was purified by HPLC (elution at 38% CH₃CN/ 62% H₂O, 0.1% TFA). MALDI–TOF (Matrix: DHB), m/z calcd [M] 2011.03, obsd 2012.84 [M + H]⁺.

Synthesis of alkyne-c(RGDfK) (3-4)

4-pentynoic acid (0.6 mg, 6.0 μmol) was dissolved in CH_2Cl_2 and *N*-hydroxy succinimide (NHS) (0.7 mg, 6.0 μmol) was added at 0 °C to form white slurry. *N,N'*-dicyclohexylcarbodiimide (DCC) (1.4 mg, 6.7 μmol) and 4-dimethylaminopyridine (DMAP) (0.1 mg, 0.8 μmol) was added to the slurry at 0 °C. The reaction mixture was stirred over night at RT and precipitation was filtered out. Without further purification, c(RGDfK)•2TFA (5.0 mg, 6.0 μmol) was added in dried DMSO with triethylamine 3 μL . The reaction was allowed to proceed 2 h at RT and recrystallized with diethyl ether, which afford yellow precipitation (3.6 mg, 88% yield). MALDI–TOF (Matrix: DHB), m/z calcd [M] 683.34, obsd 684.30 [M + H]⁺.

Synthesis of alkyne-PEG₂₄-GGRGDS (3-6)

Linear hexapeptide GGRGDS (**3-5**) was synthesized by standard Fmoc solid phase peptide synthesis (SPPS) using 2-chlorotrityl chloride resin as the synthesis of RGDfK peptide . The conjugation of **3-2** with GGRGDS peptide was realized by introduction of a sulfhydryl group to available N-terminal amino group of peptide using *N*-succinimidyl-*S*-acetylthioacetate (SATA) and deprotection with hydroxylamine (NH_2OH), that is, GGRGDS•TFA (4.4 mg, 6.6 μmol) was dissolved in 1 mL of Sodium Borate Buffer (pH 8.5) and 110 μL (7.15 μmol , 1.08 eq.) of 65 mM SATA in DMSO was added. After 2 h mixing at RT, 100 μL of 0.5 M hydroxylamine hydrochloride in 50 mM Sodium Phosphate, 25 mM EDTA , pH 7.5 buffer was added to the solution of SATA modified peptide. Reaction was performed for 2 h at RT and purified by HPLC. Thiol GGRGDS eluate was dried *in vacuo* and redissolved in reduction buffer (50 mM sodium phosphate, 150 mM NaCl, 2 mM EDTA, pH 7.0) to obtain a final volume of 100 μL . The solution was incubated with immobilized TCEP (Tris[2-carboxyethyl] phosphine

hydrochloride) disulfide reducing gel (Thermo Scientific) for 30 min at RT and centrifuged for 1 min. The supernatant containing the reduced peptide was mixed with **1** (8.8 mg, 6.6 μmol) in the same buffer solution of immediately. After 2 h reaction at RT, the mixture was purified by HPLC (elution at 38% CH_3CN / 62% H_2O , 0.1% TFA). MALDI-TOF (Matrix: DHB), m/z calcd [M] 1954.95, obsd 1973.22 [M + NH_4]⁺.

Synthesis of Alkyne-PEG₂₄-GGATWLPPR Peptide (3-8)

Linear peptide GGATWLPPR (**3-7**) was synthesized by standard solid phase peptide synthesis (SPPS) using an Applied Biosystems 433A peptide synthesizer, via 9-fluorenylmethoxycarbonyl (Fmoc) chemistry. The first residue was attached to the using 2-chlorotrityl chloride resin by shaking with the Fmoc-arginine (2.4 eq.) and DIEA (2.2 eq.) in dry DCM for 2.5 h at RT under argon, and all the following residues were coupled by standard Fmoc reaction cycles. Final peptide was cleaved from the resin using standard TFA methods (90% TFA, 10% H_2O). ESI m/z calcd for $\text{C}_{44}\text{H}_{67}\text{N}_{13}\text{O}_{11}$ [M] 953.5, obsd 477.9 [M + 2H]²⁺/2. The conjugation with **3-2** was realized by the same chemistry using SATA and NH_2OH as previous RGD peptides and purified by HPLC under the same conditions as synthesis of alkyne-PEG₂₄-c(RGDfK). HPLC (elution at 34% CH_3CN / 66% H_2O , 0.1% TFA). MALDI-TOF (Matrix: DHB), m/z calcd for $\text{C}_{107}\text{H}_{180}\text{N}_{16}\text{O}_{40}\text{S}$ [M] 2361.23, obsd 2361.67 [M + H]⁺.

Synthesis of Alkyne-PEG₂₄- GGRLVAYEGWV Peptide (3-10)

Linear peptide GGRLVAYEGWV (**3-9**) was synthesized by standard solid phase peptide synthesis (SPPS) using an Applied Biosystems 433A peptide synthesizer, via 9-fluorenylmethoxycarbonyl (Fmoc) chemistry. The first residue was attached to the using 2-

chlorotriyl chloride resin by shaking with the Fmoc-valine (2.4 eq.) and DIEA (2.2 eq.) in dry DCM for 2.5 h at RT under argon, and all the following residues were coupled by standard Fmoc reaction cycles. Final peptide was cleaved from the resin using standard TFA methods (90% TFA, 10% H₂O). MALDI–TOF (Matrix: DHB), m/z calcd for C₅₆H₈₃N₁₅O₁₅ [M] 1205.62, obsd 1205.60 [M + H]⁺. The conjugation with **3-2** was realized by the same chemistry using SATA and NH₂OH as previous RGD peptides and purified by HPLC under the same conditions as synthesis of alkyne-PEG₂₄-c(RGDfK). HPLC (elution at 34% CH₃CN / 66% H₂O, 0.1% TFA). MALDI–TOF (Matrix: DHB), m/z calcd for C₁₁₉H₁₉₆N₁₈O₄₄S [M] 2613.34, obsd 2616.64 [M + H]⁺.

“Click” Reaction between Azide-labeled Virus (Ad5-GalNAz) and Alkyne-PEG₂₄-Targeting Peptide (Targeting Peptide = c(RGDfK) or GGRGDS or GGATWLPPR or GGRLVAYEGWV)

50 µL of azide labeled virus stock (1×10^{12} particles/mL) in a 100 mM Tris-HCl buffer pH 8.0 was mixed with bathophenanthroline disulfonic acid disodium salt at a final concentration of 3 mM and alkyne-PEG₂₄-Targeting peptide at a final concentration of 100 µM. After the mixture was kept in a deoxygenated glove bag for 6 h, copper(I) bromide (CuBr) in dimethyl sulfoxide (DMSO) was added to a final concentration of 1 mM and the reaction was allowed to proceed for 12 h at RT in the deoxygenated glove bag. The reaction was quenched by bathocuproine-disulfonic acid disodium salt (BCS) at a final concentration of 10 mM. The “clicked” viruses were stored in PBS buffer with 0.9 mM CaCl₂ and 0.5 mM MgCl₂ containing 10% glycerol and kept in 4 °C for infection test up to 2 weeks.

Purification of Modified Viral Particles with Spin Columns

The viral particles were purified by Centri-Sep columns (CS-400, Princeton Separations, Adelphia, NJ), that is, the columns were gently tapped so that dry gels settle down at the bottom of spin columns and 0.8mL of buffer (PBS + 0.5mM MgCl₂ + 0.9mM CaCl₂ + 10% glycerol) was added to each column. The column caps were replaced and the gels were hydrated by shaking and inverting or brief vortexing. After 30 min at RT, air bubbles were removed from the top column. The top column caps were removed and excess fluid was drained into wash tube. The columns were spun at 3000 rpm for 2 min. and wash tubes were discarded. 50 µL of modified virus solutions were added and the columns were placed on sample collection tubes. After spinning at 3000 rpm for 2 min., the eluated solutions were collected. The purified “clicked” viruses were stored in PBS buffer with 0.9 mM CaCl₂ and 0.5 mM MgCl₂ containing 10% glycerol and kept in 4 °C for infection test. The purified viruses can be stored in 4 °C up to 2 weeks.

Quantitation of Viral Particles by PicoGreen Assay

The purified viruses were quantitated using PicoGreen reagent (Quant-iT, invitrogen, Carlsbad, CA) as described by M. T. McCaman *et al.*[91]. Briefly, 0.5 µL of 0.5 % SDS TE buffer was added to 4.5 µL of virus solution and incubated at 37 °C for 30 min. This virus lysis solution was diluted with 45 µL of TE. Working solution was prepared by adding 25 µL of Quant-iT PicoGreen in 4.975 mL of TE. 20 µL of diluted lysis solution and 180 µL of working solution was mixed and analyzed by fluorescence photometer. Using standard double stranded DNA, the fluorescence (excitation: 485 nm, emission: 538 nm) standard curve ($y = ax + b$; $x = \text{DNA ng}$, y

= fluorescence intensity) was obtained. The number of viral particle was calculated using the standard curve and a conversion factor (1 ng DNA = 2.6×10^7 Ad genome, i.e., Ad particles).

Subcellular Localization of Ad particles by Thin-sectioning Electron Microscopy

B16BL6 cells (2×10^6) were grown on ACLAR Embedding Film (Electron Microscopy Sciences, Fort Washington, PA) and incubated with modified Ad particles at a multiplicity of infection (MOI) of 1,000 in DMEM containing 10 mM HEPES (pH 7.5) and 0.5% BSA for 60 min at 4 °C and then warmed to 37 °C for 2 to 20 min. The cells were then washed with ice-cold PBS and fixed in 2% EM grade glutaraldehyde (Electron Microscopy Sciences, Fort Washington, PA) in 0.1M phosphate buffered saline (PBS). Cells were then processed using standard EM techniques. Briefly, after fixation, samples were washed in PBS and then placed in 1% osmium tetroxide in 0.1M PBS, en bloc stained with 1% aqueous uranyl acetate (Electron Microscopy Sciences, Fort Washington, PA), dehydrated in a graded series of ethyl alcohol and embedded in Durcupan resin (Sigma Aldrich Co., St Louis MO, USA). Areas of interest were blocked and 80 nm ultrathin sections were cut with a Reichert-Jung UltracutE ultramicrotome and placed on formvar coated slot copper grids. Sections were then counterstained with uranyl acetate and lead citrate and viewed with a FEI Tecnai BioTwinG² transmission electron microscope. Digital images were acquired with an AMT XR-60 CCD digital camera system and compiled using Adobe Photoshop.

Expression and Purification of Ad12 Knob

Ad12 knob was expressed and purified as described by P. Freimuth *et al.*[72]. Briefly, pET15b-Ad12 knob DNA plasmid which was kindly donated by Dr. Freimuth, was transformed into

strain BL21-DE3 competent cell by heat shock method (42 °C for 45 sec) for expression of the hexahistidine-tagged knob protein (MGSSHHHHHSSGLVPRGSHMSNTPYDPLTLWTPD-PPPNCSLIQELDAKLTCLCLKNGSIVNGIVSLVGVKGNLLNIQSTTTTVGVHLVFDEQGRLITSTPTALVPQASWGYRQGQSVSTNTVTNGLGFMPNVSA YPRPNASEAKSQMVSLTYL QGDTSKPITMKVAFNGITSLNGYSLTFMWSGLSNYINQPFSTPSCSFSYITQE). Overnight cultures in Luria-Bertani (LB) broth containing 150 mg of penicillin G (Sigma)/L were diluted 100-fold into fresh LB-penicillin broth and grown at 37 °C until mid-log phase (optical density of 0.8 at 600 nm), at which time they were chilled to 24 °C and adjusted to 50 mM isopropyl b-D-thiogalactopyranoside (IPTG) to induce knob expression. After shaking (250 rpm) overnight at 24 °C, the cells were collected by centrifugation, resuspended in 10% of the original culture volume of STE (10 mM Tris-HCl [pH 8.0], 100 mM NaCl, 1 mM EDTA) containing 100 mg of lysozyme/mL, and subjected to three cycles of freezing and thawing. The viscous cell lysate was then sonicated and cleared by centrifugation at 25,000 × g for 10 min. Knob was precipitated from the supernatant by the addition of solid ammonium sulfate to 35% saturation (25°C), dialyzed against several changes of 10 mM Tris-HCl (pH 7.5), and passed over a column of DEAE-cellulose (DE52; Whatman) equilibrated in the same buffer. Knob was recovered from the flowthrough fractions essentially free of contaminating *E. coli* proteins and nucleic acids, and was further purified by Ni-nitrilotriacetic acid (NTA) affinity chromatography according to the manufacturer's instructions (GE Healthcare).

Infection Assays

B16BL6

Cells (B16BL6) were seeded in 96-well black and clear bottom plates at a density of 1×10^4 cells/well, respectively, 1 day before infection. Virus stock was added to infection buffer (PBS, TC, and 2% serum) at a desired multiplicity of infection (MOI), the volume of virus stock needed was calculated by equations as followings, $MOI = PFU / \# \text{ of cells}$, ($PFU / \# \text{ of viral particles}$) = 20 for adenovirus, the volume of virus stock needed = $\# \text{ of viral particles needed} / \text{the titer of virus stock}$ (i.e., viral titer = $\# \text{ of viral particle/mL}$). Monolayer cells were washed with PBS and incubated in the infection buffer for 1 h at 37 °C. After 1 h, cell growth media were added and cells were incubated at 37 °C. 24 h post infection, the expression levels of luciferase transgene were determined by a photometer with the luciferase assay kit (Bright-Glo, Promega).

U-87MG, D-65MG, and HUVEC

Cells (U-87MG or D-65MG or HUVEC) were seeded in 96-well black and clear bottom plates at a density of 1×10^4 cells/well, respectively, 1 day before infection. Monolayer cells were washed with PBS and incubated in inhibition buffer ([Ad12 knob] $\approx 20 \mu\text{M}$ in PBS with 2% serum) for 1 h at RT. Virus stock was added to the inhibition buffer at a multiplicity of infection (MOI) of 500 (U-87MG, D-65MG) or 1000 (HUVEC) and incubated at 37 °C. After 1 h, cell growth media were added and cells were incubated at 37 °C. 24 h post infection, the expression levels of luciferase transgene were determined by a photometer with the luciferase assay kit (Bright-Glo, Promega).

Statistics

Experiments were performed in triplicate and presented as mean \pm standard deviation. *P*-values were calculated by a two-tailed unpaired Student's *t*-test. Data were considered to be significantly different when $P < 0.05$.

References

1. Flint, S. J.; Enquist, L. W.; Racaniello, V. R.; Skalka, A. M., *Principles of virology*. ASM Press: Washington, DC, **2009**.
2. Mateu, M. G., Virus engineering: functionalization and stabilization. *Protein Eng., Des. Sel.* **2011**, *24* (1-2), 53-63.
3. Asokan, A.; Conway, J. C.; Phillips, J. L.; Li, C.; Hegge, J.; Sinnott, R.; Yadav, S.; DiPrimio, N.; Nam, H. J.; Agbandje-McKenna, M., Reengineering a receptor footprint of adeno-associated virus enables selective and systemic gene transfer to muscle. *Nat. Biotechnol.* **2009**, *28* (1), 79-82.
4. Palucha, A.; Loniewska, A.; Satheshkumar, S.; Boguszewska-Chachulska, A. M.; Umashankar, M.; Milner, M.; Haenni, A. L.; Savithri, H. S., Virus-Like Particles: Models for Assembly Studies and Foreign Epitope Carriers. *Prog. Nucleic Acid Res. Mol. Biol.* **2005**, *80*, 135-168.
5. Inoue, T.; Kawano, M.; Takahashi, R.; Tsukamoto, H.; Enomoto, T.; Imai, T.; Kataoka, K.; Handa, H., Engineering of SV40-based nano-capsules for delivery of heterologous proteins as fusions with the minor capsid proteins VP2/3. *J. Biotechnol.* **2008**, *134* (1), 181-192.
6. Steinmetz, N. F.; Evans, D. J., Utilisation of plant viruses in bionanotechnology. *Org. Biomol. Chem.* **2007**, *5* (18), 2891-2902.
7. Krasnykh, V.; Dmitriev, I.; Mikheeva, G.; Miller, C. R.; Belousova, N.; Curiel, D. T., Characterization of an adenovirus vector containing a heterologous peptide epitope in the HI loop of the fiber knob. *J. Virol.* **1998**, *72* (3), 1844-1852.
8. Müller, O. J.; Kaul, F.; Weitzman, M. D.; Pasqualini, R.; Arap, W.; Kleinschmidt, J. A.; Trepel, M., Random peptide libraries displayed on adeno-associated virus to select for targeted gene therapy vectors. *Nat. Biotechnol.* **2003**, *21* (9), 1040-1046.
9. Miura, Y.; Yoshida, K.; Nishimoto, T.; Hatanaka, K.; Ohnami, S.; Asaka, M.; Douglas, J.; Curiel, D.; Yoshida, T.; Aoki, K., Direct selection of targeted adenovirus vectors by random peptide display on the fiber knob. *Gene Ther.* **2007**, *14* (20), 1448-1460.
10. Wu, P.; Xiao, W.; Conlon, T.; Hughes, J.; Agbandje-McKenna, M.; Ferkol, T.; Flotte, T.; Muzyczka, N., Mutational analysis of the adeno-associated virus type 2 (AAV2) capsid gene and construction of AAV2 vectors with altered tropism. *J. Virol.* **2000**, *74* (18), 8635-8647.

11. Maheshri, N.; Koerber, J. T.; Kaspar, B. K.; Schaffer, D. V., Directed evolution of adeno-associated virus yields enhanced gene delivery vectors. *Nat. Biotechnol.* **2006**, *24* (2), 198-204.
12. Schaffer, D. V.; Koerber, J. T.; Lim, K., Molecular engineering of viral gene delivery vehicles. *Annu. Rev. Biomed. Eng.* **2008**, *10*, 169.
13. Sen, S.; Venkata Dasu, V.; Mandal, B., Developments in Directed Evolution for Improving Enzyme Functions. *Appl. Biochem. Biotechnol.* **2007**, *143* (3), 212-223.
14. Bartel, M. A.; Weinstein, J. R.; Schaffer, D. V., Directed evolution of novel adeno-associated viruses for therapeutic gene delivery. *Gene Ther.* **2012**, *19* (6), 694-700.
15. Rüegg, C.; Postigo, A. A.; Sikorski, E. E.; Butcher, E. C.; Pytela, R.; Erle, D. J., Role of integrin alpha 4 beta 7/alpha 4 beta P in lymphocyte adherence to fibronectin and VCAM-1 and in homotypic cell clustering. *J. Cell Biol.* **1992**, *117* (1), 179-189.
16. Mizejewski, G. J., Role of Integrins in Cancer: Survey of Expression Patterns. *Proc. Soc. Exp. Biol. Med.* **1999**, *222* (2), 124-138.
17. Desgrosellier, J. S.; Cheresch, D. A., Integrins in cancer: biological implications and therapeutic opportunities. *Nat. Rev. Cancer* **2010**, *10* (1), 9-22.
18. Eliceiri, B. P.; Klemke, R.; Stromblad, S.; Cheresch, D. A., Integrin alphavbeta3 requirement for sustained mitogen-activated protein kinase activity during angiogenesis. *J. Cell Biol.* **1998**, *140* (5), 1255-63.
19. Hynes, R. O., Integrins: Bidirectional, Allosteric Signaling Machines. *Cell* **2002**, *110* (6), 673-687.
20. Guo, W.; Giancotti, F. G., Integrin signalling during tumour progression. *Nat. Rev. Mol. Cell Biol.* **2004**, *5* (10), 816-826.
21. Jin, H.; Varner, J., Integrins: roles in cancer development and as treatment targets. *Br. J. Cancer* **2004**, *90* (3), 561-565.
22. Niu, G.; Xiong, Z.; Cheng, Z.; Cai, W.; Gambhir, S. S.; Xing, L.; Chen, X., In vivo bioluminescence tumor imaging of RGD peptide-modified adenoviral vector encoding firefly luciferase reporter gene. *Mol. Imaging Biol.* **2007**, *9* (3), 126-34.
23. Huang, S.; Kamata, T.; Takada, Y.; Ruggeri, Z. M.; Nemerow, G. R., Adenovirus interaction with distinct integrins mediates separate events in cell entry and gene delivery to hematopoietic cells. *J. Virol.* **1996**, *70* (7), 4502-8.
24. Heckmann, D.; Kessler, H., Design and Chemical Synthesis of Integrin Ligands. In *Methods Enzymol.*, David, A. C., Ed. Academic Press: 2007; Vol. Volume 426, pp 463-503.

25. Kessler, H., Conformation and Biological Activity of Cyclic Peptides. *Angew. Chem., Int. Ed. Engl.* **1982**, *21* (7), 512-523.
26. Aumailley, M.; Gurrath, M.; Müller, G.; Calvete, J.; Timpl, R.; Kessler, H., Arg-Gly-Asp constrained within cyclic pentapeptides Strong and selective inhibitors of cell adhesion to vitronectin and laminin fragment P1. *FEBS Lett.* **1991**, *291* (1), 50-54.
27. Gurrath, M.; Müller, G.; Kessler, H.; Aumailley, M.; Timpl, R., Conformation/activity studies of rationally designed potent anti-adhesive RGD peptides. *Eur. J. Biochem.* **1992**, *210* (3), 911-921.
28. Geyer, A.; Mueller, G.; Kessler, H., Conformational Analysis of a Cyclic RGD Peptide Containing a ψ [CH₂-NH] Bond: A Positional Shift in Backbone Structure Caused by a Single Dipeptide Mimetic. *J. Am. Chem. Soc.* **1994**, *116* (17), 7735-7743.
29. Kessler, H.; Diefenbach, B.; Finsinger, D.; Geyer, A.; Gurrath, M.; Goodman, S. L.; Hölzemann, G.; Haubner, R.; Jonczyk, A.; Müller, G.; Roedern, E. G.; Wermuth, J., Design of superactive and selective integrin receptor antagonists containing the RGD sequence. *Lett. Pept. Sci.* **1995**, *2* (3), 155-160.
30. Haubner, R.; Gratias, R.; Diefenbach, B.; Goodman, S. L.; Jonczyk, A.; Kessler, H., Structural and Functional Aspects of RGD-Containing Cyclic Pentapeptides as Highly Potent and Selective Integrin $\alpha_v\beta_3$ Antagonists. *J. Am. Chem. Soc.* **1996**, *118* (32), 7461-7472.
31. Haubner, R.; Finsinger, D.; Kessler, H., Stereoisomeric Peptide Libraries and Peptidomimetics for Designing Selective Inhibitors of the $\alpha_v\beta_3$ Integrin for a New Cancer Therapy. *Angew. Chem., Int. Ed. Engl.* **1997**, *36* (13-14), 1374-1389.
32. Lohof, E.; Planker, E.; Mang, C.; Burkhart, F.; Dechantsreiter, M. A.; Haubner, R.; Wester, H.-J.; Schwaiger, M.; Hölzemann, G.; Goodman, S. L.; Kessler, H., Carbohydrate Derivatives for Use in Drug Design: Cyclic α_v -Selective RGD Peptides. *Angew. Chem., Int. Ed. Engl.* **2000**, *39* (15), 2761-2764.
33. C. Gilon, M. A. D., F. Burkhart, A. Friedler, H. Kessler, Synthesis of N-methylated peptides. In *"Houben-Weyl: Methods of Organic Chemistry"*, A.F.M. Goodmann, L. M., C. Toniolo, Ed. Thieme Verlag, Stuttgart, New York: **2003**.
34. Manavalan, P.; Momany, F. A., Conformational energy studies on N-methylated analogs of thyrotropin releasing hormone, enkephalin, and luteinizing hormone-releasing hormone. *Biopolymers* **1980**, *19* (11), 1943-1973.
35. Mazur, R. H.; James, P. A.; Tyner, D. A.; Hallinan, E. A.; Sanner, J. H.; Schulze, R., Bradykinin analogs containing N.alpha.-methyl amino acids. *J. Med. Chem.* **1980**, *23* (7), 758-763.

36. Tonelli, A. E., The effects of isolated N-methylated residues on the conformational characteristics of polypeptides. *Biopolymers* **1976**, *15* (8), 1615-1622.
37. Turker, R. K.; Hall, M. M.; Yamamoto, M.; Sweet, C. S.; Bumpus, F. M., A New, Long-Lasting Competitive Inhibitor of Angiotensin. *Science* **1972**, *177* (4055), 1203-1205.
38. Dechantsreiter, M. A.; Planker, E.; Mathä, B.; Lohof, E.; Hölzemann, G.; Jonczyk, A.; Goodman, S. L.; Kessler, H., N-Methylated Cyclic RGD Peptides as Highly Active and Selective $\alpha_v\beta_3$ Integrin Antagonists. *J. Med. Chem.* **1999**, *42* (16), 3033-3040.
39. Bauerschmitz, G. J.; Lam, J. T.; Kanerva, A.; Suzuki, K.; Nettelbeck, D. M.; Dmitriev, I., Treatment of ovarian cancer with a tropism modified oncolytic adenovirus. *Cancer Res.* **2002**, *62*, 1266-1270.
40. Rojas, J. J.; Gimenez-Alejandre, M.; Gil-Hoyos, R.; Cascallo, M.; Alemany, R., Improved systemic antitumor therapy with oncolytic adenoviruses by replacing the fiber shaft HSG-binding domain with RGD. *Gene Ther.* **2012**, *19* (4), 453-457.
41. Burkhardt, D. J.; Kalet, B. T.; Coleman, M. P.; Post, G. C.; Koch, T. H., Doxorubicin-formaldehyde conjugates targeting $\alpha_v\beta_3$ integrin. *Mol. Cancer Ther.* **2004**, *3* (12), 1593-1604.
42. Kok, R. J.; Schraa, A. J.; Bos, E. J.; Moorlag, H. E.; Ásgeirsdóttir, S. A.; Everts, M.; Meijer, D. K. F.; Molema, G., Preparation and Functional Evaluation of RGD-Modified Proteins as $\alpha_v\beta_3$ Integrin Directed Therapeutics. *Bioconjugate Chem.* **2001**, *13* (1), 128-135.
43. Krom, Y. D.; Gras, J. C. E.; Frants, R. R.; Havekes, L. M.; van Berkel, T. J.; Biessen, E. A. L.; van Dijk, K. W., Efficient targeting of adenoviral vectors to integrin positive vascular cells utilizing a CAR-cyclic RGD linker protein. *Biochem. Biophys. Res. Commun.* **2005**, *338* (2), 847-854.
44. Arosio, D.; Manzoni, L.; Araldi, E. M.; Caprini, A.; Monferini, E.; Scolastico, C., Functionalized cyclic RGD peptidomimetics: conjugable ligands for alphavbeta3 receptor imaging. *Bioconjugate Chem.* **2009**, *20* (8), 1611-7.
45. Merkel, O. M.; Germershaus, O.; Wada, C. K.; Tarcha, P. J.; Merdan, T.; Kissel, T., Integrin $\alpha_v\beta_3$ targeted gene delivery using RGD peptidomimetic conjugates with copolymers of PEGylated poly(ethylene imine). *Bioconjugate Chem.* **2009**, *20* (6), 1270-80.
46. Shi, J.; Kim, Y. S.; Chakraborty, S.; Jia, B.; Wang, F.; Liu, S., 2-Mercaptoacetylglucylglycyl (MAG2) as a bifunctional chelator for ^{99m}Tc -labeling of cyclic RGD dimers: effect of technetium chelate on tumor uptake and pharmacokinetics. *Bioconjugate Chem.* **2009**, *20* (8), 1559-68.

47. Aizpurua, J. M.; Ganboa, J. I.; Palomo, C.; Loinaz, I.; Oyarbide, J.; Fernandez, X.; Balentova, E.; Fratila, R. M.; Jimenez, A.; Miranda, J. I.; Laso, A.; Avila, S.; Castrillo, J. L., Cyclic RGD beta-lactam peptidomimetics induce differential gene expression in human endothelial cells. *ChemBioChem* **2011**, *12* (3), 401-5.
48. Fields, G.; Carr, S.; Marshak, D.; Smith, A.; Stults, J.; Williams, L.; Williams, K.; Young, J.; Angeletti, R., Techniques in Protein Chemistry IV. *RH Angeletti, Editor* **1993**, 229-238.
49. Dai, X.; Su, Z.; Liu, J. O., An improved synthesis of a selective $\alpha_v\beta_3$ -integrin antagonist cyclo(-RGDfK-). *Tetrahedron Lett.* **2000**, *41* (33), 6295-6298.
50. Xiong, Z.; Cheng, Z.; Zhang, X.; Patel, M.; Wu, J. C.; Gambhir, S. S.; Chen, X., Imaging chemically modified adenovirus for targeting tumors expressing integrin $\alpha_v\beta_3$ in living mice with mutant herpes simplex virus type 1 thymidine kinase PET reporter gene. *J. Nucl. Med.* **2006**, *47* (1), 130-139.
51. Hermanson, G. T., *Bioconjugate techniques*. 2nd ed.; Academic press: Rockford, Illinois, USA, 2008; p 719.
52. Cauet, G.; Strub, J.-M.; Leize, E.; Wagner, E.; Dorsselaer, A. V.; Lusky, M., Identification of the Glycosylation Site of the Adenovirus Type 5 Fiber Protein. *Biochemistry* **2005**, *44* (14), 5453-5460.
53. Banerjee, P. S.; Ostapchuk, P.; Hearing, P.; Carrico, I., Chemoselective Attachment of Small Molecule Effector Functionality to Human Adenoviruses Facilitates Gene Delivery to Cancer Cells. *J. Am. Chem. Soc.* **2010**, *132* (39), 13615-13617.
54. Laughlin, S. T.; Agard, N. J.; Baskin, J. M.; Carrico, I. S.; Chang, P. V.; Ganguli, A. S.; Hangauer, M. J.; Lo, A.; Prescher, J. A.; Bertozzi, C. R., Metabolic Labeling of Glycans with Azido Sugars for Visualization and Glycoproteomics. In *Methods Enzymol.*, Minoru, F., Ed. Academic Press: 2006; Vol. Volume 415, pp 230-250.
55. Rostovtsev, V. V.; Green, L. G.; Fokin, V. V.; Sharpless, K. B., A Stepwise Huisgen Cycloaddition Process: Copper(I)-Catalyzed Regioselective "Ligation" of Azides and Terminal Alkynes. *Angew. Chem., Int. Ed. Engl.* **2002**, *114* (14), 2708-2711.
56. Tornøe, C. W.; Christensen, C.; Meldal, M., Peptidotriazoles on Solid Phase: [1,2,3]-Triazoles by Regiospecific Copper(I)-Catalyzed 1,3-Dipolar Cycloadditions of Terminal Alkynes to Azides. *J. Org. Chem.* **2002**, *67* (9), 3057-3064.
57. Meldal, M.; Tornøe, C. W., Cu-Catalyzed Azide-Alkyne Cycloaddition. *Chem. Rev. (Washington, DC, U. S.)* **2008**, *108* (8), 2952-3015.

58. Wang, Q.; Chan, T. R.; Hilgraf, R.; Fokin, V. V.; Sharpless, K. B.; Finn, M., Bioconjugation by copper (I)-catalyzed azide-alkyne [3+ 2] cycloaddition. *J. Am. Chem. Soc.* **2003**, *125* (11), 3192-3193.
59. Gupta, S. S.; Kuzelka, J.; Singh, P.; Lewis, W. G.; Manchester, M.; Finn, M. G., Accelerated Bioorthogonal Conjugation: A Practical Method for the Ligation of Diverse Functional Molecules to a Polyvalent Virus Scaffold. *Bioconjugate Chem.* **2005**, *16* (6), 1572-1579.
60. Banerjee, P. S.; Ostapchuk, P.; Hearing, P.; Carrico, I. S., Unnatural Amino Acid Incorporation onto Adenoviral (Ad) Coat Proteins Facilitates Chemoselective Modification and Retargeting of Ad Type 5 Vectors. *J. Virol.* **2011**, *85* (15), 7546-7554.
61. Banerjee, P. S.; Zuniga, E. S.; Ojima, I.; Carrico, I. S., Targeted and armed oncolytic adenovirus via chemoselective modification. *Bioorg. Med. Chem. Lett.* **2011**, *21* (17), 4985-4988.
62. Koizumi, N.; Mizuguchi, H.; Hosono, T.; Ishii-Watabe, A.; Uchida, E.; Utoguchi, N.; Watanabe, Y.; Hayakawa, T., Efficient gene transfer by fiber-mutant adenoviral vectors containing RGD peptide. *Biochim. Biophys. Acta, Gen. Subj.* **2001**, *1568* (1), 13-20.
63. Wu, E.; Pache, L.; Von Seggern, D. J.; Mullen, T.-M.; Mikyas, Y.; Stewart, P. L.; Nemerow, G. R., Flexibility of the Adenovirus Fiber Is Required for Efficient Receptor Interaction. *J. Virol.* **2003**, *77* (13), 7225-7235.
64. Wickham, T. J.; Filardo, E. J.; Cheresch, D. A.; Nemerow, G. R., Integrin alpha v beta 5 selectively promotes adenovirus mediated cell membrane permeabilization. *J. Cell Biol.* **1994**, *127* (1), 257-264.
65. Wang, K.; Guan, T.; Cheresch, D. A.; Nemerow, G. R., Regulation of adenovirus membrane penetration by the cytoplasmic tail of integrin $\beta 5$. *J. Virol.* **2000**, *74* (6), 2731-2739.
66. Lyle, C.; McCormick, F., Integrin $\alpha_v\beta_5$ is a primary receptor for adenovirus in CAR-negative cells. *Virol. J.* **2010**, *7* (1), 148.
67. Gaertner, F.; Kessler, H.; Wester, H. J.; Schwaiger, M.; Beer, A., Radiolabelled RGD peptides for imaging and therapy. *Eur. J. Nucl. Med. Mol. Imaging* **2012**, 1-13.
68. Goodman, S. L.; Hölzemann, G.; Sulyok, G. A. G.; Kessler, H., Nanomolar small molecule inhibitors for $\alpha_v\beta_6$, $\alpha_v\beta_5$, and $\alpha_v\beta_3$ integrins. *J. Med. Chem.* **2002**, *45* (5), 1045-1051.
69. Hariharan, S.; Gustafson, D.; Holden, S.; McConkey, D.; Davis, D.; Morrow, M.; Basche, M.; Gore, L.; Zang, C.; O'Bryant, C., Assessment of the biological and pharmacological

- effects of the $\alpha_v\beta_3$ and $\alpha_v\beta_5$ integrin receptor antagonist, cilengitide (EMD 121974), in patients with advanced solid tumors. *Ann. Oncol.* **2007**, *18* (8), 1400-1407.
70. Schober, D.; Bayer, N.; Murphy, R. F.; Wagner, E.; Fuchs, R., Establishment of an assay to determine adenovirus-induced endosome rupture required for receptor-mediated gene delivery. *Gene Ther. Mol. Biol.* **1999**, *3*, 25-33.
 71. Bewley, M. C.; Springer, K.; Zhang, Y.-B.; Freimuth, P.; Flanagan, J. M., Structural Analysis of the Mechanism of Adenovirus Binding to Its Human Cellular Receptor, CAR. *Science* **1999**, *286* (5444), 1579-1583.
 72. Freimuth, P.; Springer, K.; Berard, C.; Hainfeld, J.; Bewley, M.; Flanagan, J., Coxsackievirus and Adenovirus Receptor Amino-Terminal Immunoglobulin V-Related Domain Binds Adenovirus Type 2 and Fiber Knob from Adenovirus Type 12. *J. Virol.* **1999**, *73* (2), 1392-1398.
 73. Bai, M.; Campisi, L.; Freimuth, P., Vitronectin receptor antibodies inhibit infection of HeLa and A549 cells by adenovirus type 12 but not by adenovirus type 2. *J. Virol.* **1994**, *68* (9), 5925-5932.
 74. Mattern, R. H.; Read, S. B.; Pierschbacher, M. D.; Sze, C. I.; Eliceiri, B. P.; Kruse, C. A., Glioma cell integrin expression and their interactions with integrin antagonists. *Cancer Ther.* **2005**, *3*, 325.
 75. Asaoka, K.; Tada, M.; Sawamura, Y.; Ikeda, J.; Abe, H., Dependence of efficient adenoviral gene delivery in malignant glioma cells on the expression levels of the Coxsackievirus and adenovirus receptor. *J. Neurosurg.* **2000**, *92* (6), 1002-1008.
 76. Van Houdt, W. J.; Wu, H.; Glasgow, J. N.; Lamfers, M. L.; Dirven, C. M.; Gillespie, G. Y.; Curiel, D. T.; Haviv, Y. S., Gene delivery into malignant glioma by infectivity-enhanced adenovirus: in vivo versus in vitro models. *Neuro-oncol.* **2007**, *9* (3), 280-290.
 77. Huang, R.; Vider, J.; Kovar, J. L.; Olive, D. M.; Mellinghoff, I. K.; Mayer-Kuckuk, P.; Kircher, M. F.; Blasberg, R. G., Integrin $\alpha_v\beta_3$ -Targeted IRDye 800CW Near-Infrared Imaging of Glioblastoma. *Clin. Cancer Res.* **2012**, *18* (20), 5731-5740.
 78. Monferran, S.; Nicolas, S.; Delmas, C.; Favre, G.; Bonnet, J.; E., C.-J.-M.; Toulas, C., $\alpha_v\beta_3$ and $\alpha_v\beta_5$ integrins control glioma cell response to ionising radiation through ILK and RhoB. *Int. J. Cancer* **2008**, *123*, 357-364.
 79. McCoy, E.; Sontheimer, H., Expression and function of water channels (aquaporins) in migrating malignant astrocytes. *Glia* **2007**, *55* (10), 1034-1043.
 80. Gutheil, J. C.; Campbell, T. N.; Pierce, P. R.; Watkins, J. D.; Huse, W. D.; Bodkin, D. J.; Cheresch, D. A., Targeted Antiangiogenic Therapy for Cancer Using Vitaxin: A

- Humanized Monoclonal Antibody to the Integrin $\alpha_v\beta_3$. *Clin. Cancer Res.* **2000**, 6 (8), 3056-3061.
81. Kowanzetz, M.; Ferrara, N., Vascular Endothelial Growth Factor Signaling Pathways: Therapeutic Perspective. *Clin. Cancer Res.* **2006**, 12 (17), 5018-5022.
 82. Villa, A.; Trachsel, E.; Kaspar, M.; Schliemann, C.; Somavilla, R.; Rybak, J.-N. L.; Borsi, C. R. I.; Neri, D., A high-affinity human monoclonal antibody specific to the alternatively spliced EDA domain of fibronectin efficiently targets tumor neo-vasculature *in vivo*. *Int. J. Cancer* **2008**, 122 (11), 2405-2413.
 83. Hodivala-Dilke, K., $\alpha_v\beta_3$ integrin and angiogenesis: a moody integrin in a changing environment. *Curr. Opin. Cell Biol.* **2008**, 20, 514–519.
 84. Ferrara, N.; Kerbel, R. S., Angiogenesis as a therapeutic target. *Nature* **2005**, 438 (7070), 967-974.
 85. Lewis, C. E.; De Palma, M.; Naldini, L., Tie2-expressing monocytes and tumor angiogenesis: regulation by hypoxia and angiopoietin-2. *Cancer Res.* **2007**, 67 (18), 8429-8432.
 86. Haismaa, H. J.; Kamps, G. K.; Boumaa, A.; Geelb, T. M.; Rotsb, M. G.; Kariatha, A.; Bellua, A. R., Selective targeting of adenovirus to $\alpha_v\beta_3$ integrins, VEGFR2 and Tie2 endothelial receptors by angio-adenobodies. *Int. J. Pharm.* **2010**, 391, 155–161.
 87. Binetruy-Tournaire, R.; Demangel, C.; Malavaud, B.; Vassy, R.; Rouyre, S.; Kraemer, M.; Plouet, J.; Derbin, C.; Perret, G.; Mazie, J. C., Identification of a peptide blocking vascular endothelial growth factor (VEGF)-mediated angiogenesis. *EMBO J.* **2000**, 19 (7), 1525-1533.
 88. Sj, D.; Liu, W.; Simmons, C. A.; Moore, J. T.; Tian, G., Identifying substrates for endothelium-specific Tie-2 receptor tyrosine kinase from phage-displayed peptide libraries for high throughput screening. *Comb. Chem. High Throughput Screen.* **2001**, 4 (6), 525-533.
 89. Alghisi, G. C.; Ponsonnet, L.; Rüegg, C., The Integrin Antagonist Cilengitide Activates $\alpha_v\beta_3$, Disrupts VE-Cadherin Localization at Cell Junctions and Enhances Permeability in Endothelial Cells. *PLoS One* **2009**, 4 (2), e4449.
 90. Brooks, P. C.; Montgomery, A. M. P.; Rosenfeld, M.; Reisfeld, R. A.; Hu, T.; Klier, G.; Cheresch, D. A., Integrin $\alpha_v\beta_3$ antagonists promote tumor regression by inducing apoptosis of angiogenic blood vessels. *Cell* **1994**, 79 (7), 1157-1164.
 91. Murakami, P.; McCaman, M. T., Quantitation of Adenovirus DNA and Virus Particles with the PicoGreen Fluorescent Dye. *Anal. Biochem.* **1999**, 274 (2), 283-288.

Chapter 4. Retargeting Adenoviral Vectors via Affibody “Click” Conjugation

Note: This chapter includes the material and direct excerpts from the manuscript which has been published (Oum, Y. H.; Carrico, I. S., Altering Adenoviral Tropism via Click Modification with ErbB Specific Ligands. *Bioconjugate Chem.* **2012**, *23* (7), 1370-1376).

4.1 Introduction

As described in the previous chapters, despite the significant losses in either particle production or infectivity that are typically associated with genetic insertion of targeting ligands, genetics remains the most prevalent form of transductional targeting [1-3]. In the context of modifying Ad vectors' natural tropism to the disease-relevant cells, hotspots for genetic manipulation have been identified allowing the insertion of targeting peptides without significant impact on viral fitness [5]. However, "the targeting peptide ligands screened by phage display showed very limited success due to the low affinities and frequent loss of their function upon fusion with the Ad fiber" [6-7]. Further, even at well-characterized sites, impact on viral fitness is generally a function of the size and physical properties of the insert. In other words, the genetic incorporation of the attractive ligand candidates such as antibodies and growth factors was limited by their large size and the incompatibility with biosynthesis of viral proteins. In order to move beyond these general restrictions, a number of labs have developed both chemical and non-covalent modification approaches. The former methodology typically takes advantage of surface exposed lysines for polyethylene glycol modification, which generates particles that are both efficiently "detargeted" and shielded from immune recognition [8-9]. Such "stealth" vectors can be armed with targeting moieties but lysine acylation precludes precise control and can lead to reduced infectivity [10-11]. Alternatively, bridging molecules composed of an Ad binding domain and a targeting domain have been used to create non-covalent targeted Ad complexes. In such a way antibodies bearing targeting motifs can both "detarget" and "retarget" in tandem, but *in vivo* stability remains a significant question. Avidin-bridged complexes have higher affinity and provide more flexibility but require the genetic introduction of biotin accepting peptides [12-13].

4.2 Targeting to the Epidermal Growth Factor Receptors (EGFR or ErbB)

The ErbB family consists of four closely related type1 transmembrane tyrosine kinase receptors, *videlicet*, epidermal growth factor receptor (EGFR, ErbB, Her1 in human), ErbB2 (Her2/Neu), ErbB3 (Her3) and ErbB4 (HER4), which dimerize upon binding to its ligand (EGF, TGF α , TGF β , and neureguline) and transduce signals to stimulate cell growth and differentiation [4] (Figure 4-1). EGFR, ErbB2 and ErbB3 are all associated with the development and progress of cancer. In addition, EGFR and ErbB2 receptors are frequently overexpressed on various cancers [14-15]. Accordingly, those receptors have been targets for cancer therapeutics. Especially, monoclonal antibodies (i.e., Trastuzumab, Herceptin[®]; Genentech) was employed to treat ErbB2-positive breast cancer and approved by FDA [16]. In this study, we chose EGFR and Her2, the verified cancer markers, as candidate receptors for our cancer retargeting Ad.

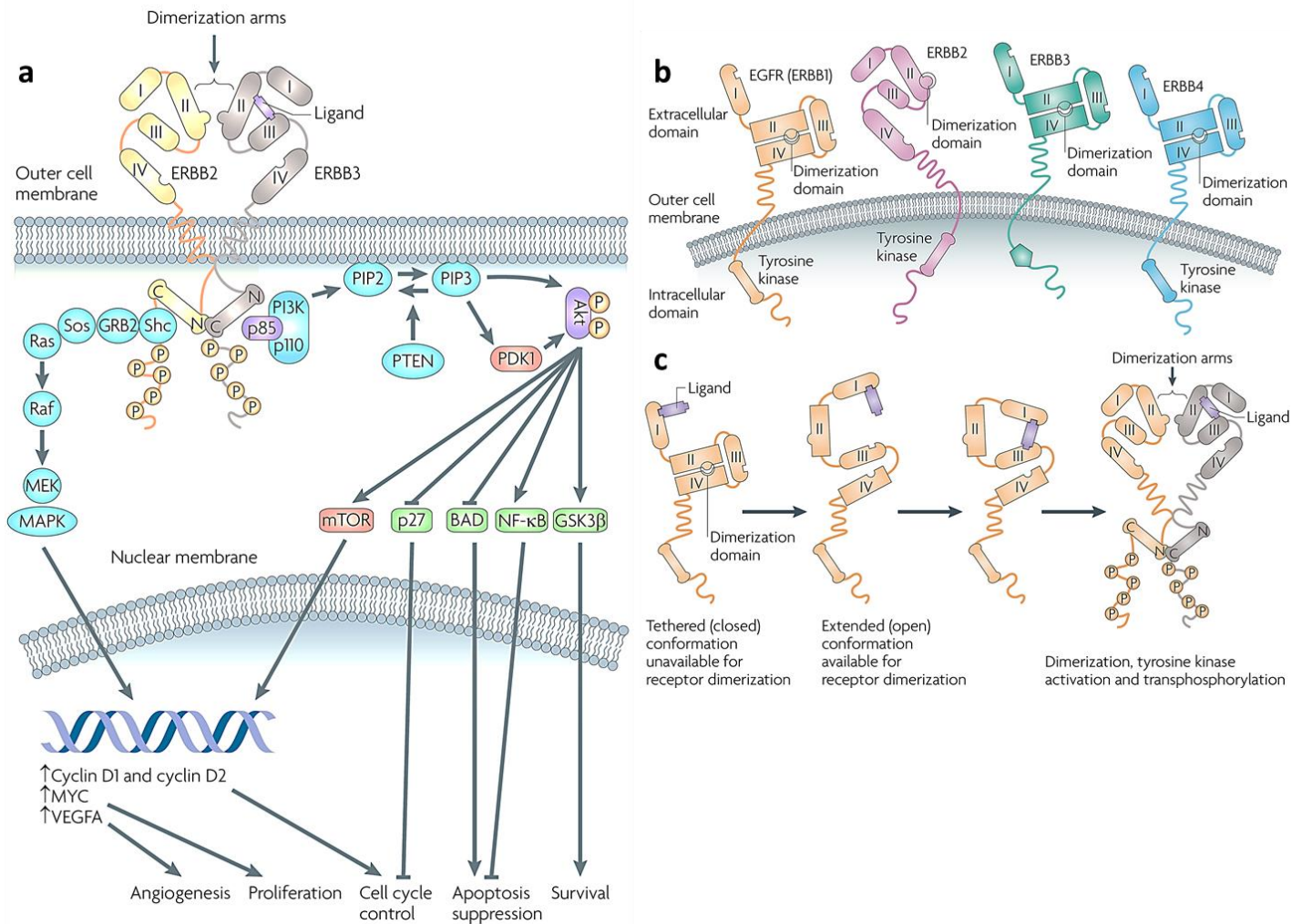


Figure 4-1. ErbB Receptors and Signalling Downstream

a) “Ligand binding and subsequent dimer formation initiates signaling through a complex array of intracellular pathway that initiate and control a range of cellular processes” [4], **b)** Four members of ErbB family, note that only ErbB2 exits in an active extended (“open”) conformation, which permanently available for dimerization, **c)** Conceptualization of the receptor conformational change on ligand binding *This figure was reprinted from reference [4] with the permission of publisher (“Nature Publishing Group”).

4.3 Affibody

Affibodies are engineered small protein domains derived from a 3-helix bundle domain Z of *Staphylococcus* protein A, having a specific affinity to a target protein, which is obtained by

combinatorial phage display selection based on 13 randomization out of a 58 amino acid scaffold [17-18] (Figure 4-2).

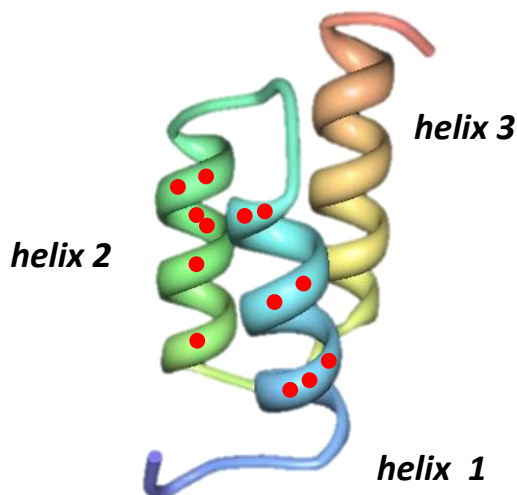


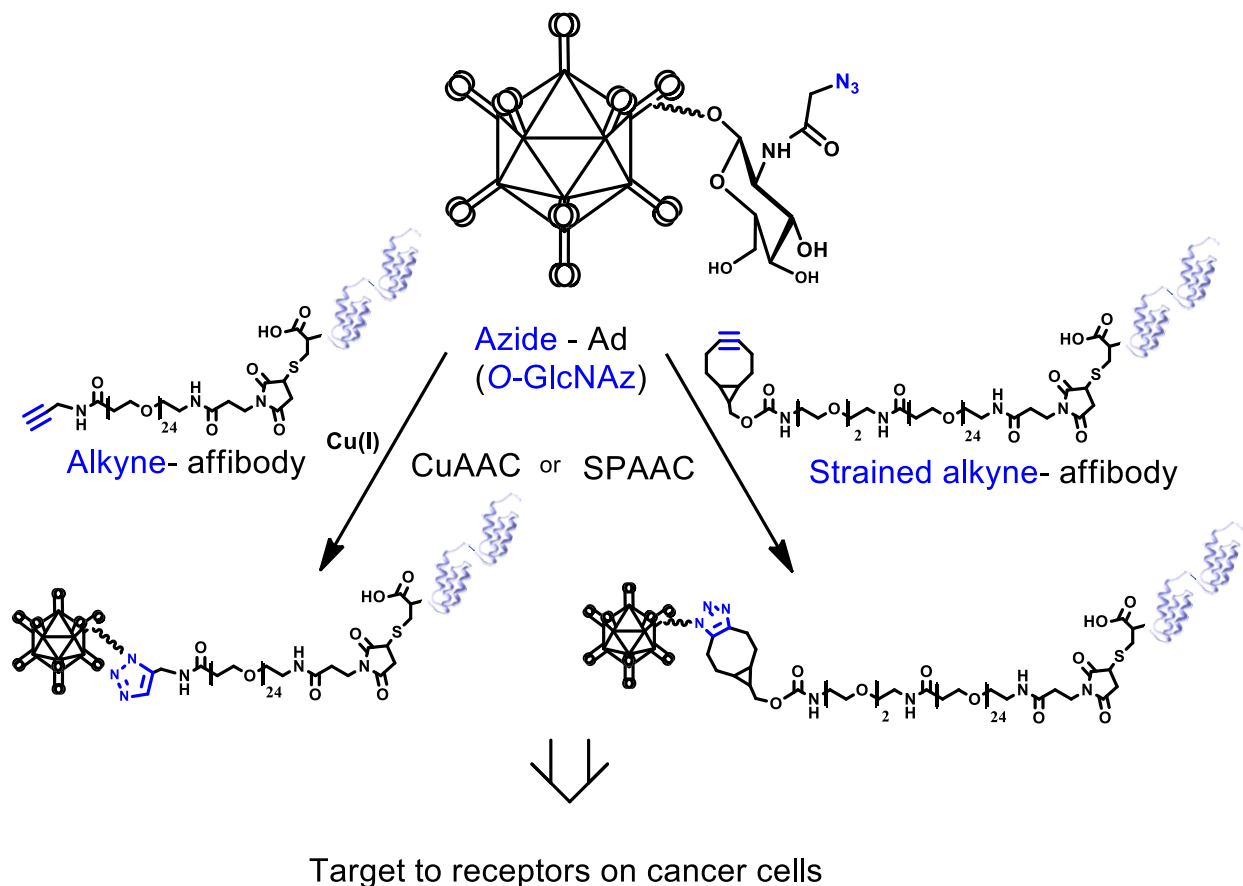
Figure 4-2. The Structure of Affibody

Z-domain of protein A (2SPZ). Graphical representations were prepared from the PDB information using the software “PDB Simple viewer”. The red dots indicate 13 preselected randomization positions for the combinatorial phage display selection.

Affibody has many advantages as a targeting molecule such as i) high affinity ($K_d \approx \text{nM} \sim \text{pM}$), ii) smaller size ($\sim 6 \text{ kDa}$) compared with antibody ($\sim 150 \text{ kDa}$) and scFv ($\sim 50 \text{ kDa}$), iii) no required post-translational modifications, iv) fast spontaneous refolding, v) excellent stability (at $90 \text{ }^\circ\text{C}$, $\text{pH } 2.5 \sim 11$), vi) high water solubility compared with modified scFv, and vii) physiological inactivity. Hence, these favorable properties rendered affibody an attractive alternative to natural targeting ligands including antibodies and scFvs.

In this study we use this two-step labeling procedure to alter the tropism of adenoviral vectors by appending affibodies selective for either Her2 (ErbB2) or EGFR (ErbB1) (Scheme 4-1). Both receptors are validated, high-value targets for cancer targeting [19-21]. Affibody modification does not significantly impact particle aggregation or stability. Infection of a panel of cancer cells with modified Ad demonstrates significant increases in gene delivery that

parallels known receptor availability. This work demonstrates the ease, speed and utility of chemoselective modification of adenoviruses with engineered antibody domains, which is expected to encourage the development of next generation therapeutic vectors.



Scheme 4-1. Overall Scheme of Cancer Targeting with Affibody-Clicked Ad

Note that head-to-tail dimeric affibodies were used to increase the avidity as demonstrated in the reference [22].

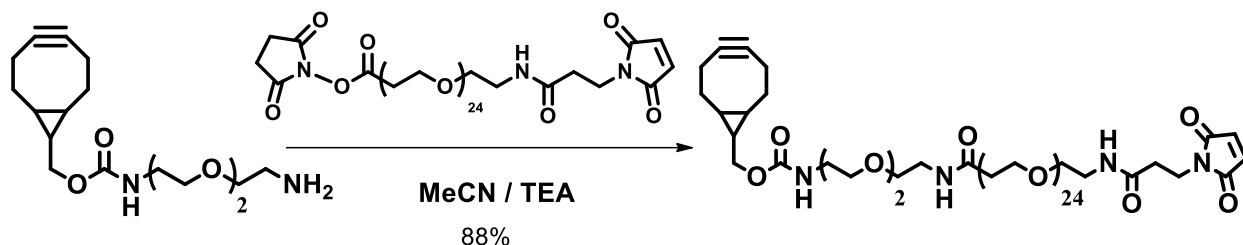
4.4 Results and Discussion

4.4.1 Preparation of Affibody-conjugated Ad *via* CuAAC or SPAAC

O-GlcNAz enabled viruses were produced by standard Ad protocol with one exception, 50 μ M Ac₄GalNAz was added to the media of Ad producer cells (*vid.* Chapter 3.4.2). Infection, production and purification were in all other ways identical to published protocol [23]. *O*-GlcNAz enabled Ad exposed to fluorescent Cu(I) promoted click reagents demonstrate ~22 dye molecules per viral particle [23]. This number is consistent with *O*-GlcNAc occupancy at Ser109 (~50%; 36 sites/particle) [24], indicating that both metabolic and chemical labeling are exceedingly efficient. Notably, treatment of these viruses with a glycosidase known to cleave *O*-GlcNAz abrogates chemical labeling, indicating that *O*-GlcNAz is the site for all click modification and that the reaction is exceedingly specific [23]. As Cu(I) promoted click chemistry is fast, robust and easy to access, we initially used this chemistry to produce affibody-modified particles. In order to access “click” chemistry competent affibodies, we created affibodies bearing a polyethylene glycol alkyne linker (PEG₂₄-CCH) **1** (Figure 4-3). Commercial affibodies with one available *C*-terminal cysteine (Abcam) were modified with maleimide-PEG₂₄-CCH which was obtained *via* reaction of commercially available maleimide-PEG₂₄-NHS with propargyl amine (Scheme 3-2).

While the ubiquity of Cu(I) promoted “click” chemistry makes it easily accessible, particularly to the biological labs, cytotoxic Cu(I) is notoriously difficult to remove from the resultant conjugates. As an alternative we explored the potential of strain-promoted “click” chemistry. While strain promoted reagents have been difficult to access in the past, new syntheses have made this set of reactions both faster and more accessible. Further, a few strained

alkyne reagents have recently become commercially available (Jena Bioscience) [25-26]. We synthesized the precursor amino-bicyclononyne (BCN) derivative *via* literature procedure [27] and cross-linked it with maleimide-PEG₂₄-NHS through the same chemistry used in synthesizing maleimide-PEG₂₄-CCH to afford maleimide-PEG-BCN. (Scheme 4-2)



Scheme 4-2. Synthesis of Maleimide-PEG-BCN

4.4.1.1 Quantifying “click” efficiency for Ad Fiber Modification via SPAAC

To quantify the efficiency of strain promoted “click” modification, azide-labeled viruses were exposed to a tetramethyl rhodamine BCN reagent. Chemical modification with this reagent allowed comparison of this fluorescently labeled sample, with quantified particle number, to a known tetramethyl rhodamine standard (Figure 4-4 and Table 4-1). Fluorescent gel scanning analysis revealed exclusive modification of a single protein with MW consistent with that of the fiber protein. Quantification demonstrated ~9 modifications per viral particle under standard conditions used for BCN labeling. Notably, the natural residue, GlcNAc, is present at ~20 residues per particle (50-60% occupancy of Ser109) [24] In previous studies, we determined that the metabolic replacement of *O*-GlcNAc with the azido surrogate, *O*-GlcNAz, was essentially complete. This indicates that the efficiency of strain promoted modification was ~45% of that of

that obtained for Cu(I) promoted modification, which is consistent with previous bioconjugation studies [28].

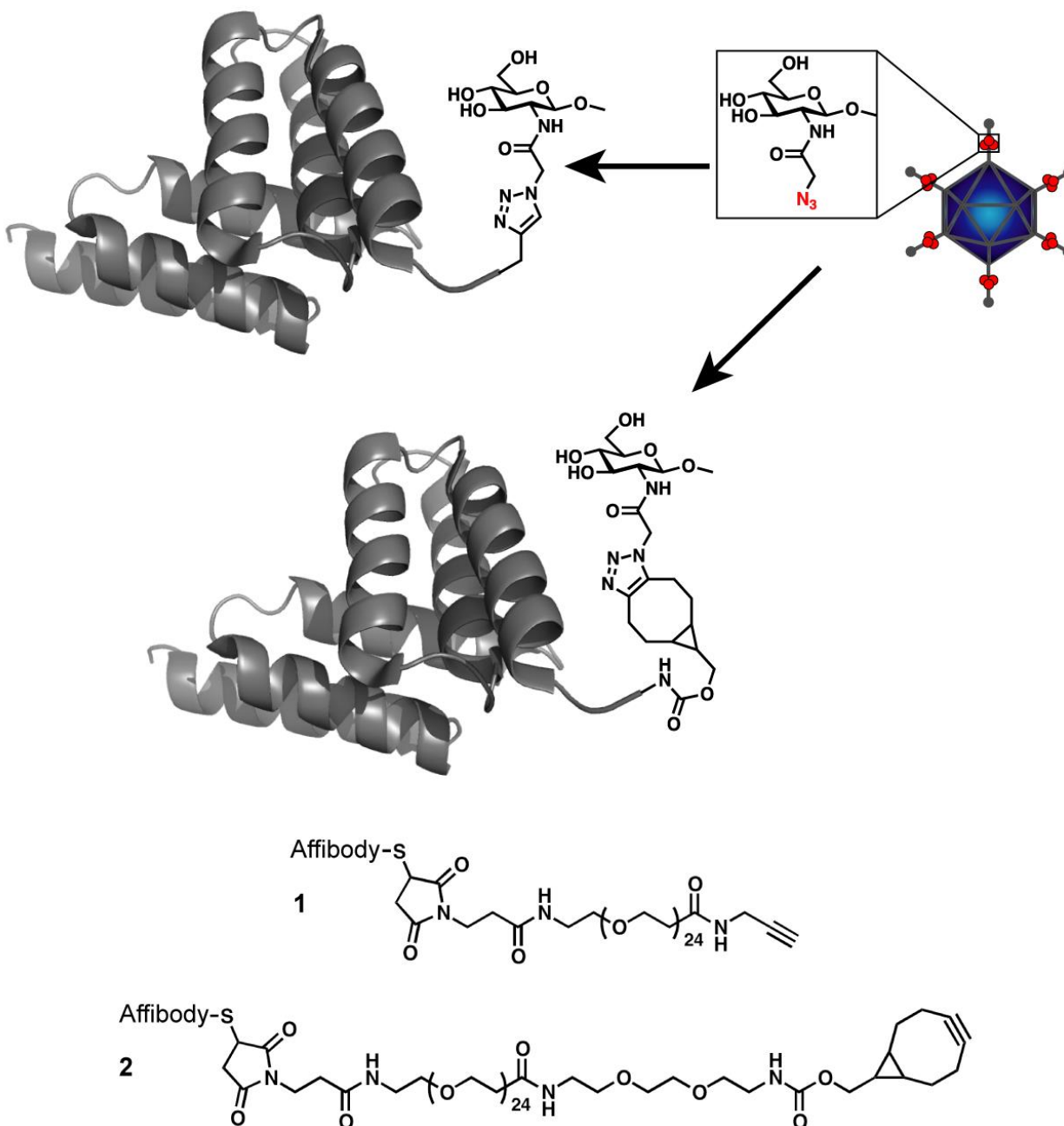
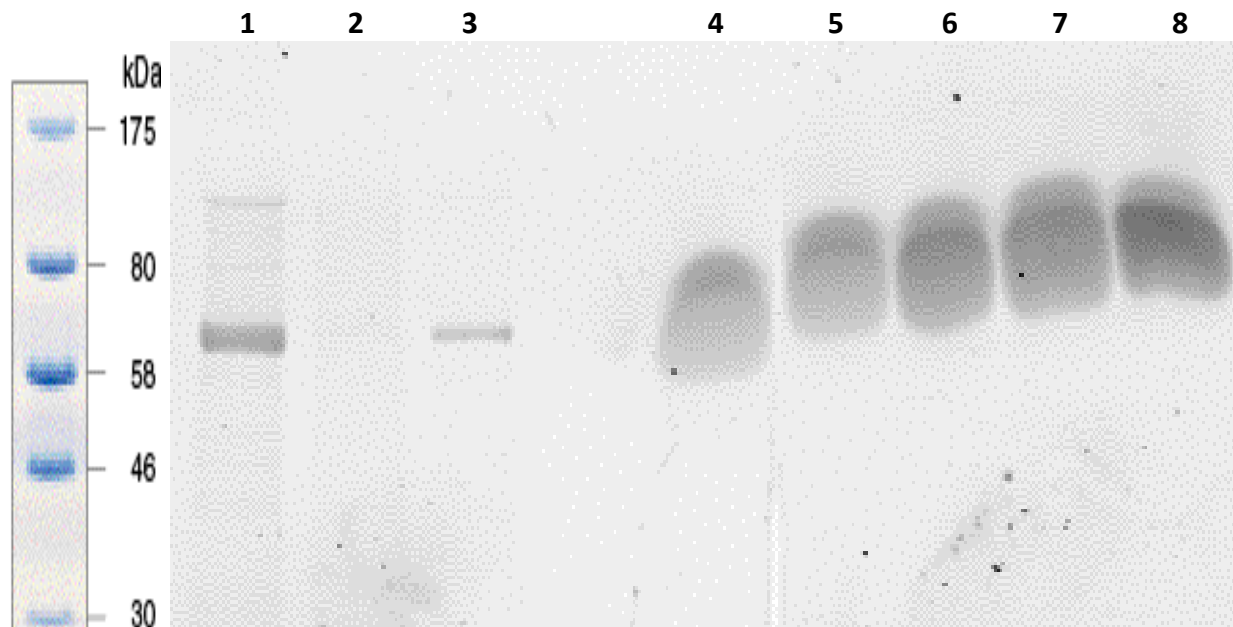


Figure 4-3. Illustration of Affibody Modification

A cartoon illustrating affibody modification of *O*-GlcNAz enabled Ad *via* either Cu(I) or strain promoted “click” chemistry. Note that head-to-tail dimeric affibodies were used to increase the avidity as demonstrated in the reference [22]



[TAMRA-BCN]	100 μM	100 μM	100 μM	0.4 nM	0.5 nM	1.0 nM	1.5 nM	2.0 nM
Virus	GlcNAz -Ad	Intact Ad	GlcNAz- Ad	-	-	-	-	-
Dialysis	-	-	+	-	-	-	-	-

Figure 4-4. Quantitation of Viral Fibers Labeled *via* SPAAC Using Gel Fluorescence Assay with TAMRA-BCN

lane1: TAMRA-BCN (20 mM) was added to *O*-GlcNAz labeled Ad stock (1.0×10^{12} particles/mL) to obtain final concentration 100 μM of TAMRA-BCN and the reaction was allowed to proceed for 2 h at RT; lane2: reaction was performed at the same conditions as lane 1 except using intact Ad (negative control); lane3: to support covalent conjugation between TAMRA-BCN and viral fiber of *O*-GlcNAz-Ad, adenoviral fiber was partially purified from lane 1 reaction mixture, to wit, TAMRA-BCN-GlcNAz labeled adenoviral particles were dialyzed overnight in a Tris-maleate (5 mM Tris, 5 mM maleic acid, 1 mM EDTA) buffer at pH 6.5. The dialyzed solution was centrifuged at 14,000 rpm for 1 h at 4 °C, after which the supernatant containing the labeled fiber proteins was separated from the precipitated viral capsids and run on the gel; lane 4~8: TAMRA-BCN standard solutions with different concentrations.

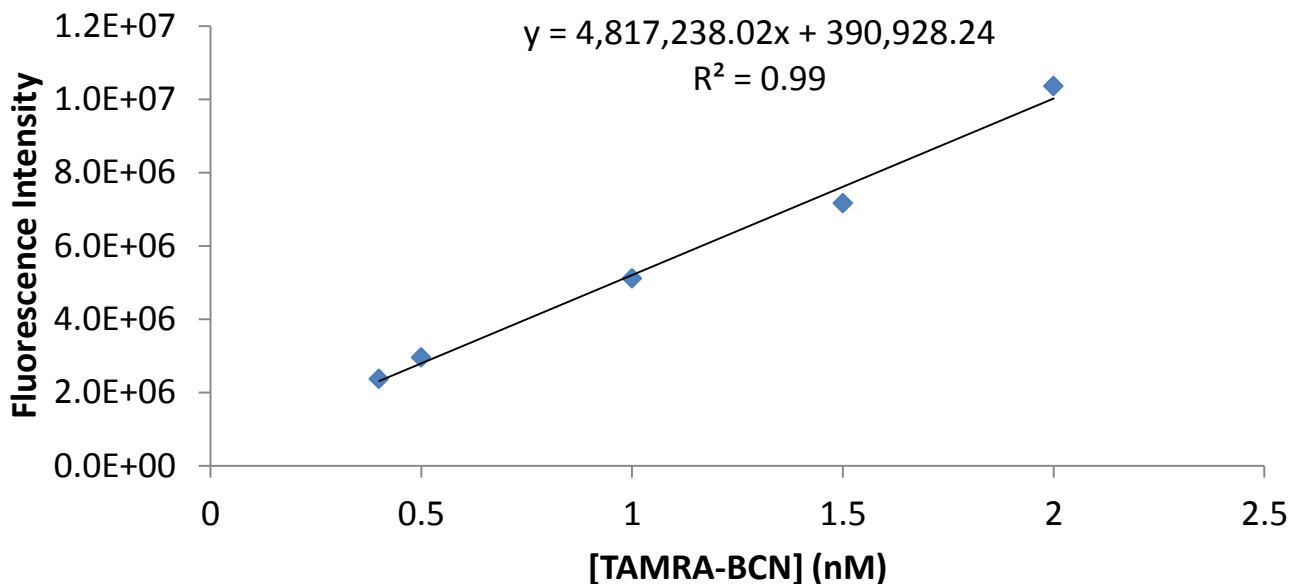


Figure 4-5. Standard calibration curve for determination of [TAMRA-BCN] conjugated on viral fibers

Table 4-1. The Number of Dye Molecules Conjugated on a Virion via SPAAC

Reaction time (h)	Concentration of dye on 10^{12} viral Fiber (nM)	Dye/ viral particle
2	1.69	1.01
16	14.7	8.84

* Column 1 shows reaction (strain-promoted alkyne-azide cycloaddition) time at RT; Column 2, the concentration of dye on viral fiber calculated from fluorescence gel scans and the standard calibration curve; column 3 shows the corresponding number of dye molecules per viral particle deduced from column 2 and the molarity of viral particles (1.00×10^{12} particles/ mL \approx 1.66 nM)

Maleimide-PEG₂₄-BCN was conjugated to the EGFR selective affibody **2** *via* modification of the reduced C-terminal cysteine (Figure 4-3). Analysis of the PD-10 purified constructs demonstrated masses that corresponded well with the theoretical values (Figure 4-6). Cu(I) mediated modification *O*-GlcNAz enabled Ad was accomplished by exposure to the affibody-CCH under conditions previously optimized for bioconjugation (1 mM CuBr; 3 mM bathophenanthroline disulfonate; 100 μ M alkyne; RT) [29-30]. In an effort to reduce the amount of copper in the final viral preparation, a Cu(I) specific chelator, bathocuproinedisulfonate, was added prior to desalting via size exclusion (Centri-Sep CS-901; Princeton separations) and virus quantitation by PicoGreen assay (Quant-iT; Invitrogen, *vid.* Materials and methods). Modification of *O*-GlcNAz enabled Ad with affiEGFR-BCN was achieved *via* incubation with 100 μ M of the strained alkyne at room temperature for 16 hours (PBS; pH = 7.4). After removal of excess affibody reagents via desalting spin column, viruses were stored at 4 °C for up to 2 weeks. In order to more directly assess anti-EGFR affibody attachment to Ad viral particles, via either Cu(I) or strain promoted click chemistry, anti-fiber western blotting was used. The results (Figure 4-8) demonstrate the appearance of a new band above that of the native fiber, which is consistent with the conjugation of a small protein. Further, Cu(I) mediated conjugation produces a significantly more intense band than the strain promoted reaction, consistent with our assessment of the relative conjugation efficiencies.

To assess the physical impact of affibody modification, viral particles were characterized for changes in size, oligomerization, and thermal stability. TEM was used to assess both changes in size and oligomerization state [31-32]. TEM of affiEGFR-CCH, affiEGFR-BCN modified particles revealed discrete, uniform and well dispersed particles that measured ~90 nm in diameter (Figure 4-7). Both were indistinguishable from unmodified particles indicating that

both oligomerization state and apparent size were largely unaffected by modification [31-32]. To further gauge the impact of modification on viral physiology we sought to assess differences in stability of the resultant particles. A standard assay for Ad thermal stability requires the addition of propidium iodide, a DNA binding fluorophore that is non-fluorescent prior to intercalation. As a result, heating Ad samples at neutral pH in the presence of propidium iodide yields an increase in fluorescence upon capsid breakdown [33]. We compared thermal degradation of three viral particles, completely unmodified Ad, Ad modified with affiEGFR-PEG-CCH and Ad modified with affiEGFR-PEG-BCN. (Figure 4-9) Comparison of T_2 transitions, the major structural transition for adenovirus thermal degradation, revealed that unmodified Ad ($T_2 = 67$ °C), affiEGFR-PEG-CCH modified Ad ($T_2 = 65$ °C) and affiEGFR-PEG-BCN modified Ad ($T_2 = 62$ °C) have similar stabilities and are comparable to literature values for unmodified particles [33].

The average size and surface charge in the solution were measured by dynamic light scattering (DLS) (Figure 4-10). AffiEFGR-PEG-CCH modified Ad showed the larger effective diameter than unmodified Ad due to the increased hydrodynamic volume of PEG₂₄-affiEFGR chains on the surface. Interestingly, unexpected moderate increase was also observed with *O*-GlcNAz enabled Ad, which leads to the hypothesis of the incorporation of more water molecules onto viral surfaces. AffiEFGR-PEG-CCH modified Ad demonstrated more negative surface charge values because antiERFG-affibody is negatively charged at physiological pH (\therefore pI = 4.4). However, it is not obvious why AffiEFGR-PEG-CCH modified Ad showed about 2-fold effective diameter than that of unmodified Ad, which was inconsistent with the results of our TEM study. It is likely that partial aggregations occurred during the measurement due to the repeated alternating electric field changes, which was also observed in other study [34].

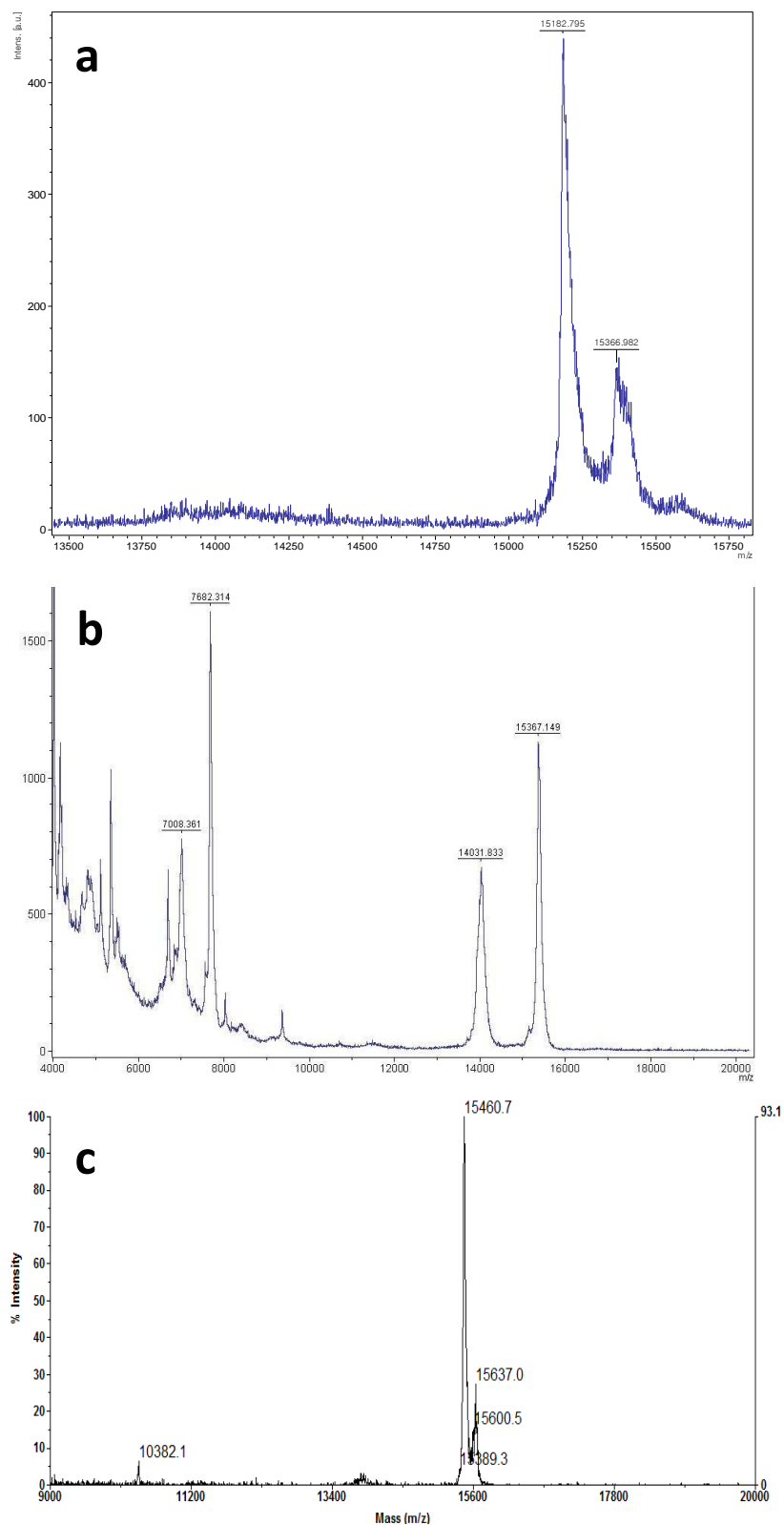


Figure 4-6. MALDI-TOF Spectra of Affibody-PEG-Alkyne

a) affiEGF-PEG₂₄-CCH, m/z [M + H]⁺, calcd 15186, obsd 15183; b) affiHer2-PEG₂₄-CCH, calcd 15364, obsd 15367 (unreacted affibody was removed by size-exclusion after “click” with virus); c) affiEGFR-PEG₂₆-BCN, calcd 15456, obsd 15461

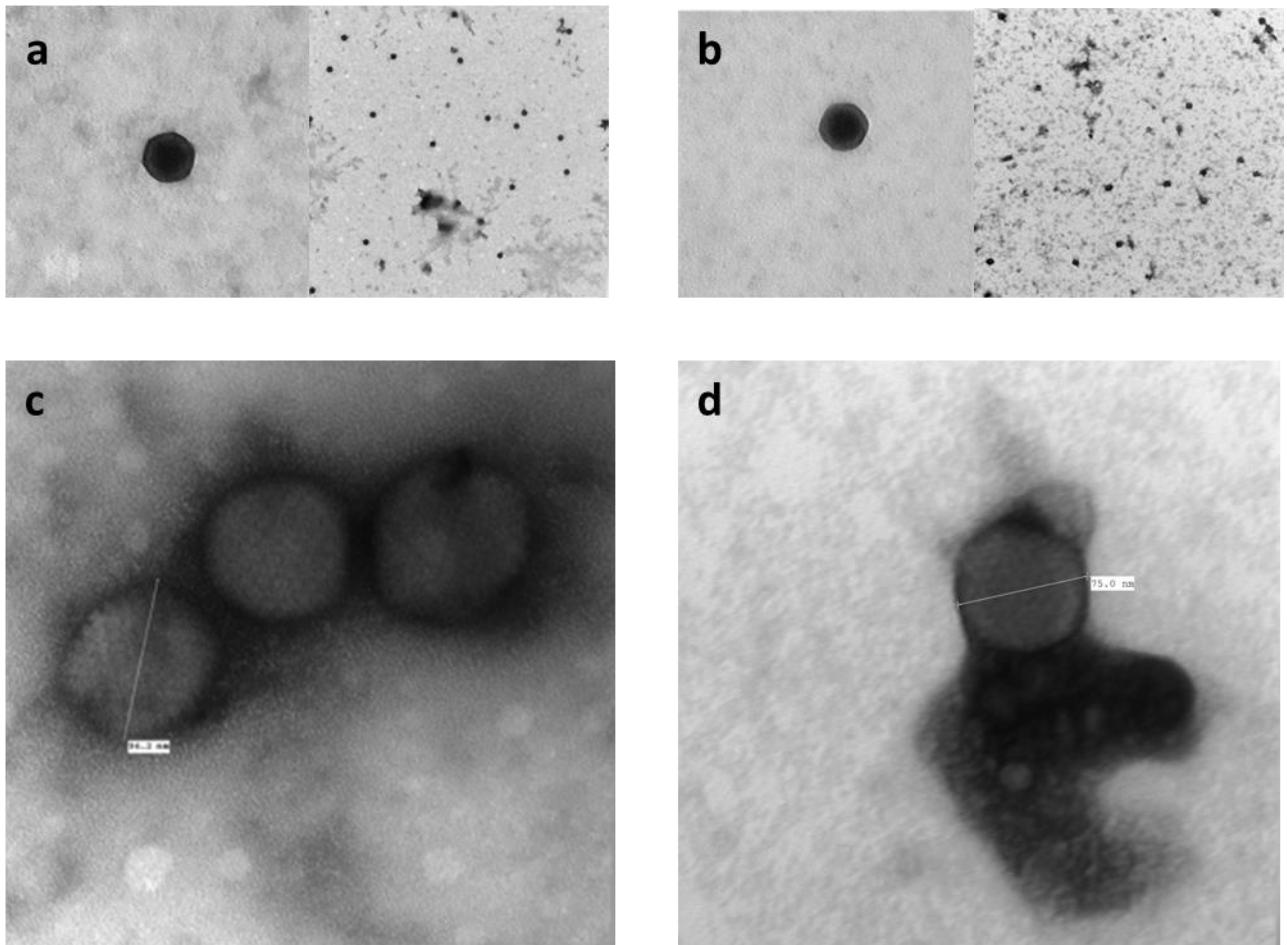


Figure 4-7. TEM Images of Ad Particles

a) Intact Ad, b) affiEGFR-PEG-CCH modified Ad *via* CuAAC, c) magnification of b) shows the diameter (96.2 nm) and hexons of virions d) affiEGFR-PEG-BCN modified Ad *via* SPAAC shows the diameter (75.0 nm) and hexons of a virion.

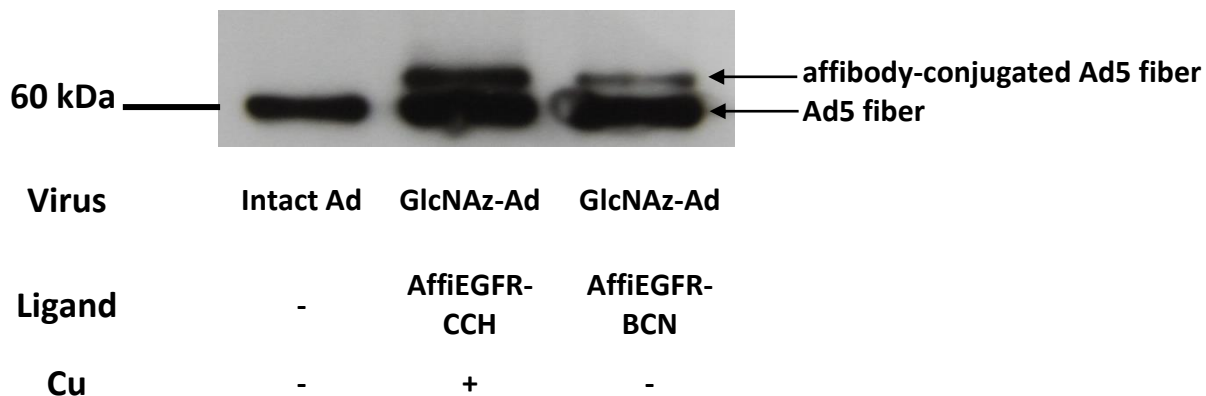


Figure 4-8. Western Blot against Ad Fiber

Western blotting was performed against Ad5 fibers using α -fiber (Ad5) antibody which was kindly donated by Prof. Patrick Hearing Lab.; intact virus (left, control), affiEGFR-PEG-CCH modified Ad via CuAAC (middle), and affiEGFR-PEG-BCN modified Ad via SPAAC (right).

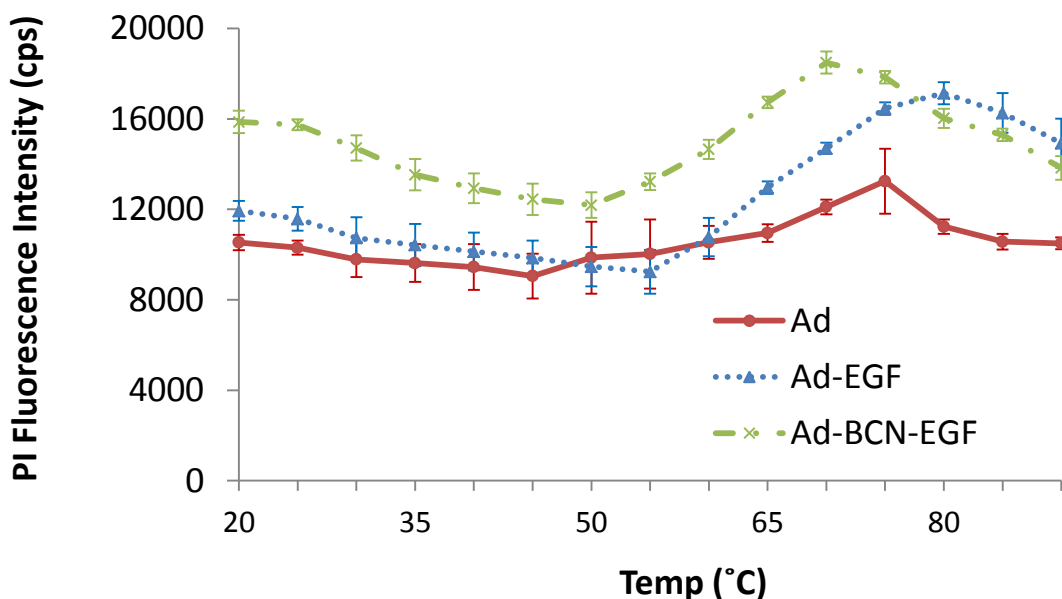


Figure 4-9. Thermal Stability Assays of Modified Ad Particles

Thermal stability assays of particles modified with either Cu(I) or strain promoted click. Fluorescence spectra (excitation at 535 nm, emission scan from 550 to 650 nm, $\lambda_{\max} = 613$, slit widths of 6 nm) of propidium iodide (7.5 μM) were collected at the viral concentration of 6.5×10^{10} particles /mL in 5 $^{\circ}\text{C}$ increments from 20 to 90 $^{\circ}\text{C}$ employing a QuantaMaster spectrofluorometer (Photon Technology International, Inc.). The T_2 were determined by calculating the point where the second derivatives of the λ_{\max} vs. temperature plots crossed the x-axis using Microcal Origin[®].

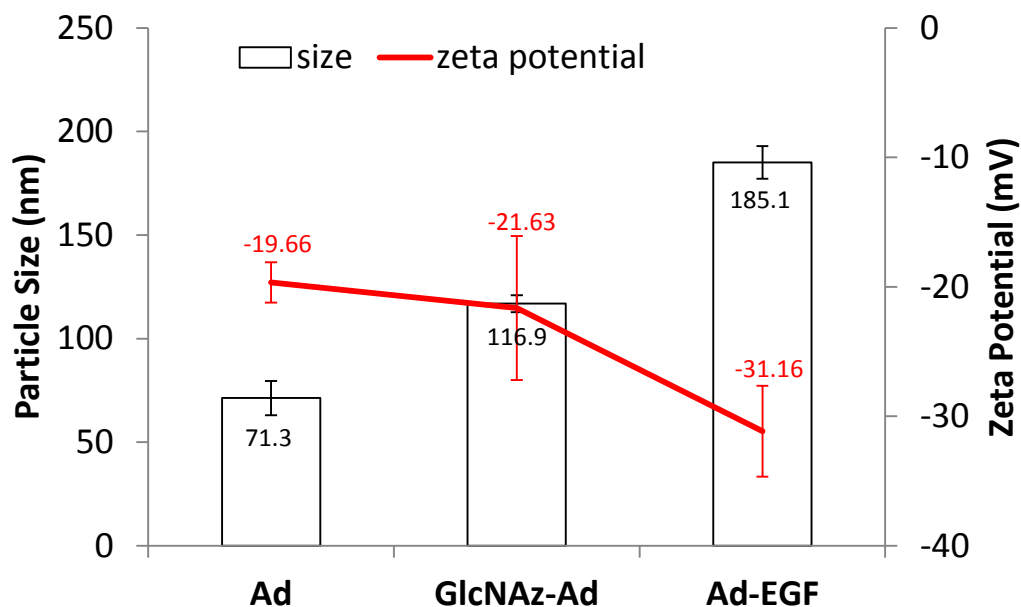


Figure 4-10. Zeta Potential and Particle Size of Virions Measured by Dynamic Light Scattering
 The instrument (Zeta plus, Brookhaven, New York) equipped with a He-Ne laser at a wavelength of 659 nm, 25 °C, pH 7.5 and zeta potential was calculated by Smoluchowski model. (Ad: unmodified Ad, GlcNAz-Ad: *O*-GlcNAz enabled Ad, Ad-EGF: affiEGFR-PEG-CCH modified Ad via CuAAC)

4.4.2 Infection Assays with Affibody-Clicked Ads

In order to examine affibody dependent increased infection of cancer cells, modified Ad5 particles were screened against a panel of well-established cancer lines for gene delivery. As these cells have different basal levels of the primary receptor for adenovirus, coxsackie adenovirus receptor (CAR), background infection is highly variable. To mitigate this background, a truncated soluble form of the fiber protein, which serves as the ligand for the primary adenovirus receptor (coxsackie adenovirus receptor), was added to the medium prior to infection with modified Ad particles. This soluble knob domain is readily overexpressed in *E. coli* and derived from a different serotype adenovirus, Ad12 [35]. However, the Ad12 knob has high

sequence homology to the Ad5 knob (46% identity) and binds to the same region of CAR. (*vid.* Chapter 3.4.4.3)

Ad5 bearing a luciferase transgene (AdLUC) and modified with affiEGFR-PEG-CCH via Cu(I) promoted click was screened against three cancer lines known to express high levels of EGFR (A431; SK-OV-3; PANC-1) in the presence of 20 μ M soluble Ad12 knob. After 24 hours cells were lysed and luciferase activity was measured. For these experiments virus produced in the absence of azido sugar was used as a control. Apart from omission of the azido sugar, all other processing was identical, including purification, exposure to click reagents and removal of these reagents. In all cases a \sim 7 fold increase in gene delivery was observed with affibody modified particles in comparison to unmodified particles (Figure 4-11).

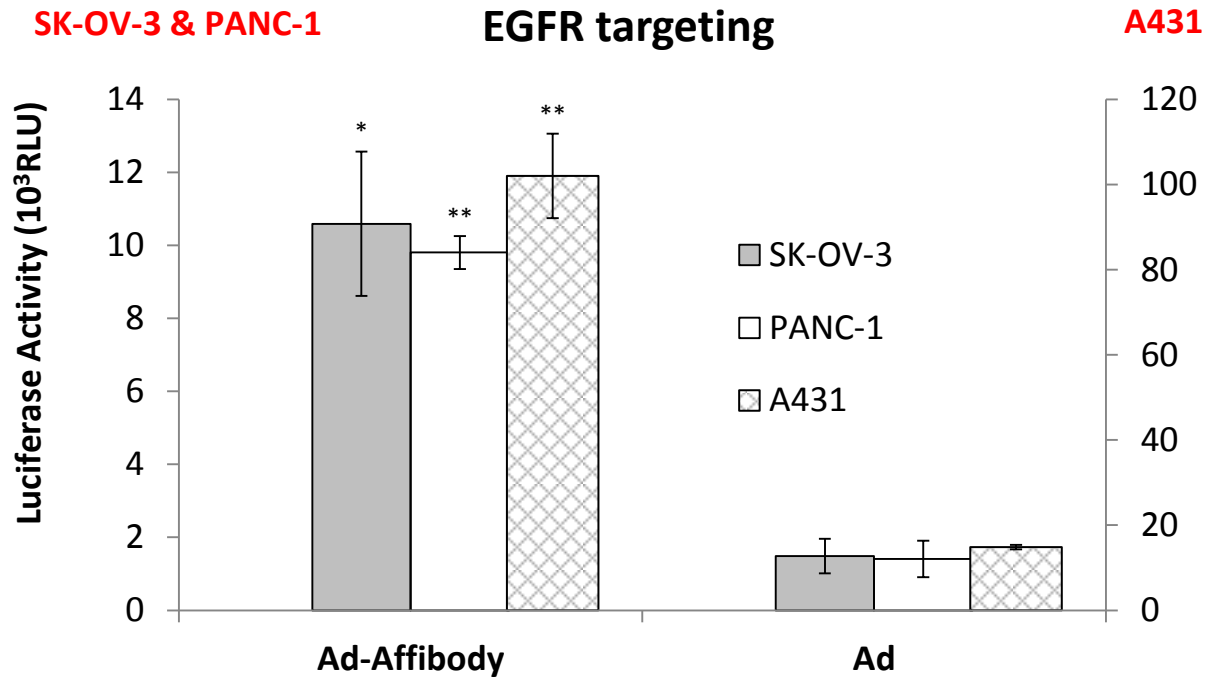


Figure 4-11. Comparison of Gene Delivery Capabilities of AffiEGFR-PEG-CCH Modified and Unmodified Ad

EGFR overexpressed cells (SK-OV-3: human ovarian adenocarcinoma; PANC-1: human pancreatic epithelioid carcinoma; A431: human epithelial carcinoma) were seeded in 96-well black and clear bottom plates at a density of 1×10^4 cells/well, respectively, 1 day before infection. Monolayer cells were washed with PBS and incubated in inhibition buffer ([Ad12 knob] $\approx 20 \mu\text{M}$ in PBS with 2% serum) for 1 h at 37 °C. Virus stocks were added to the inhibition buffer at a multiplicity of infection (MOI) of 1000 and incubated at 37 °C. After 1 h, cell growth media were added and cells were incubated at 37 °C. 24 h post infection, the expression levels of luciferase transgene were determined by a photometer with the luciferase assay kit (Bright-Glo, Promega). Experiments were performed in triplicate and presented as mean \pm standard deviation. *p*-values were calculated by a two-tailed unpaired Student's *t*-test. **: *p* < 0.01, *: *p* < 0.05

As an additional control, copper was omitted from the coupling solution. In the context of both SK-OV-3 and PANC-1 cells affibody modified virus demonstrated higher levels of gene delivery than either negative control (- Ac₄GalNAz or - Cu(I)) (Figure 4-12). However, A431 cells demonstrated much higher error and the level of gene delivery for affibody modified viruses was slightly less than virion not exposed to copper. This may be due to differences in copper sensitivity of the different cell lines used. In the context of these experiments the effect of copper is complicated due to partial oxidation of Cu(I) to Cu(II) in solution.

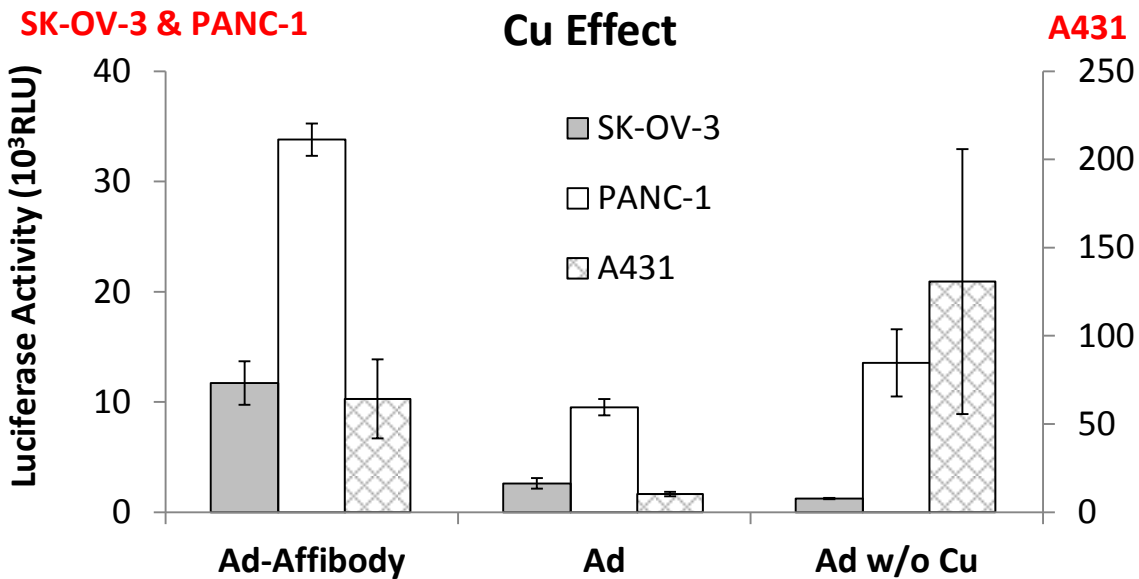


Figure 4-12. Effects of Cu(I) on Gene Delivery with AffiEGFR-PEG-CCH Modified Particles
 Ad-Affibody: anti-EGFR Affibody conjugated Ad *via* CuAAC; Ad: Intact Ad treated the same as Ad-Affibody without the AffiEGFR-PEG-CCH reagent; Ad w/o Cu: only copper was omitted.

AffiEGFR-PEG-BCN modified Ad screened against the same cell lines demonstrated more modest changes in gene delivery to SK-OV-3 and A431, and similar levels with PANC-1 cells (Figure 4-13), which is consistent with lower modification efficiency obtained with strain promoted “click” reactions. Completely untreated AdLUC and GlcNAz enabled AdLUC modified with BCN reagent without the affibody (maleimide-PEG-BCN), run as additional negative controls, demonstrated essentially equal signal to the – Ac₄GalNAz controls (Figure 4-13).

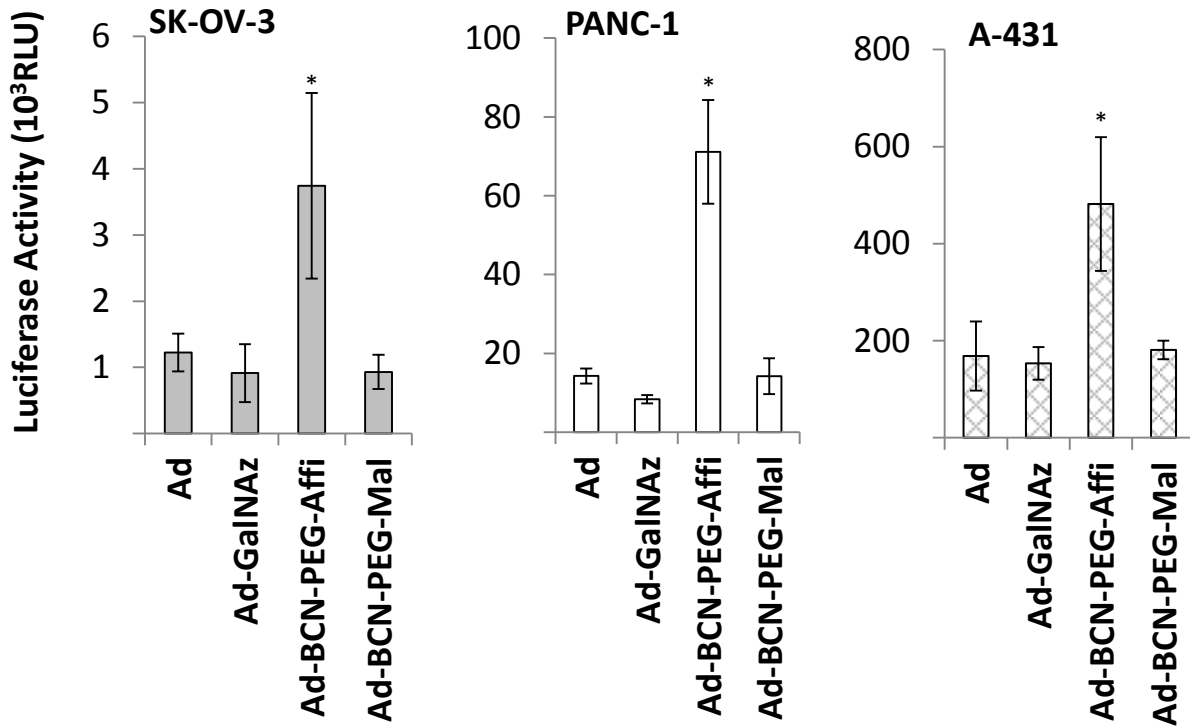


Figure 4-13. Infection Assays with affiEGFR-PEG-BCN “Clicked” Ad via SPAAC

Cells were infected and assayed in the same conditions as in **Figure 4-11**. (Ad: unmodified Ad, Ad-GalNAz: *O*-GlcNAz enabled Ad, Ad-BCN-PEG-Affi: affiEGFR-PEG-BCN modified Ad via SPAAC, Ad-BCN-PEG-Mal: maleimide-PEG-BCN modified Ad via SPAAC as a control)

Infectivity assays for affiHer2-PEG-CCH modified AdLUC were run in an identical manner to that described for affiEGFR-PEG-CCH modified Ad. These targeted viruses were screened against cells with high Her2 (MIA PaCa-2; SK-BR-3) and low Her2 (RD) levels (Figure 4-14 and Figure 4-15). Low Her2 cells demonstrated negligible increase in gene delivery over background, whereas the high Her2 cells demonstrated ~7 (MIA PaCa-2) and ~100 (SK-BR-3) fold increases in gene expression. Although no difference in receptor dependent targeting was seen for cells expressing different levels of EGFR, the differences in receptor levels were modest (A431 and SK-OV-3; ~820,000/cell and ~140,000/cell respectively)[36]. In contrast, Her2 targeted Ad demonstrated significant differences in gene delivery dependent on cell type, commensurate with receptor density that varies much more widely (SK-BR-3 and MIA PaCa-2; ~1,800,000/cell and ~21,000/cell respectively) [36].

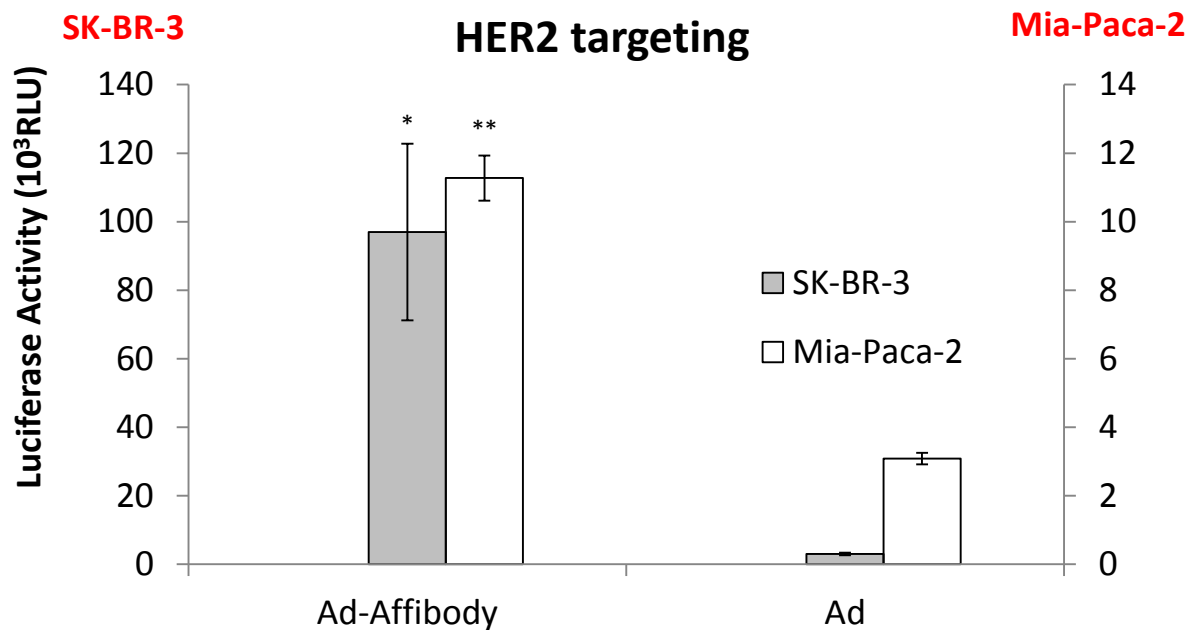


Figure 4-14. Gene Delivery with AffiHER2-PEG-CCH Modified and Unmodified Ad to Cells Expressing High Levels of Her2

Her2 overexpressed cells (SK-BR-3: human breast adenocarcinoma; MIA PaCa-2 (human pancreatic carcinoma)) were infected and assayed in the same conditions as in **Figure 4-11**.

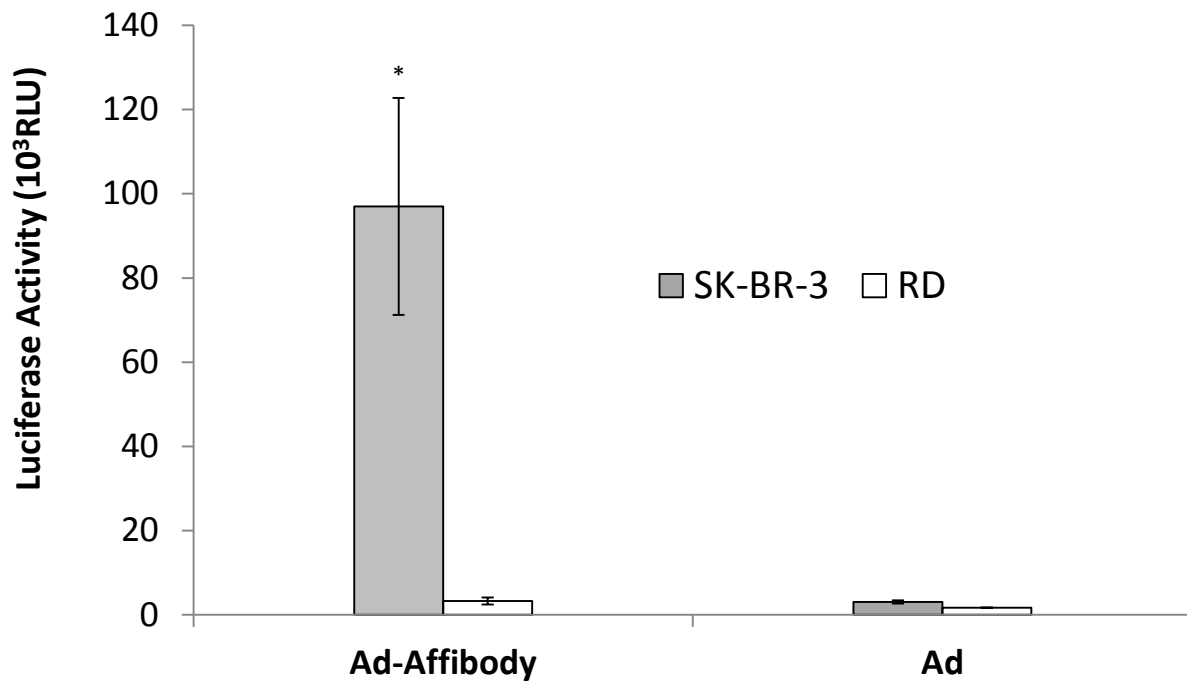


Figure 4-15. Comparison of Her2 Mediated Gene Delivery in Cells with High (SK-BR-3) and Low (RD) Her2 Levels

Her2-overexpressed cells (SK-BR-3) and Her2-negative cells (RD: human rhabdomyosarcoma) were infected and assayed in the same conditions as in **Figure 4-11**. Negligible transgene (luciferase) expressions were observed in Her2-negative RD cells in contrast to Her2-positive SK-BR-3.

Notably, in the absence of knob inhibition SK-BR-3 cells infected with Her2 modified Ad demonstrated a ~2 fold increase in gene delivery over unmodified Ad, which indicates affibody mediated cell entry can be even more efficient than the natural process (Figure 4-16).

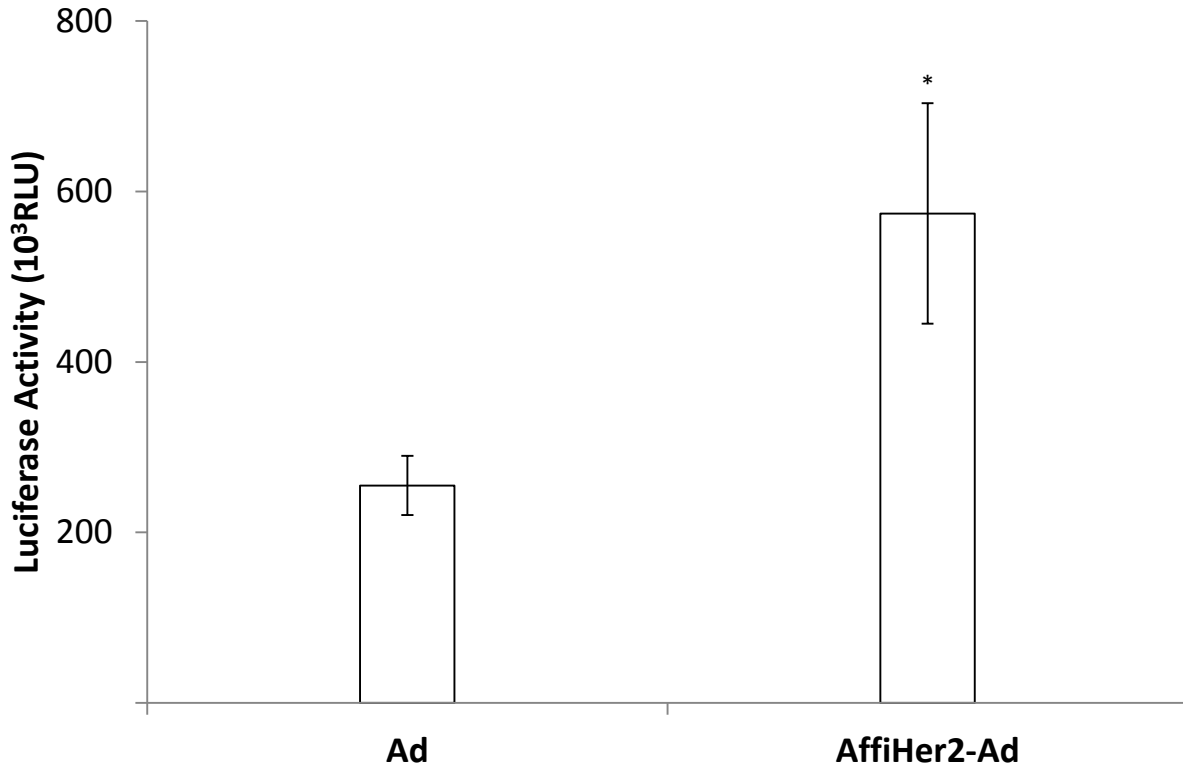


Figure 4-16. Comparison of Her2 Mediated Gene Delivery with Intact Ad (-Cu) and AffiHer2 “Clicked” Ad (+Cu)

SK-BR-3 cells were seeded in 96-well black and clear bottom plates at a density of 1×10^4 cells/well, 1 day before infection. Monolayer cells were washed with PBS. Virus stock was added to the infection buffer (PBS, TC, 2% serum) at a multiplicity of infection (MOI) of 1000 and cell were incubated in infection buffer at 37 °C. After 1 h, cell growth media were added and cells were incubated at 37°C. 24 h post infection, the expression levels of luciferase transgene were determined by a photometer with the luciferase assay kit (Bright-Glo, Promega). (Experiments were performed in triplicate and presented as mean \pm standard deviation. *p*-values were calculated by a two-tailed unpaired Student’s *t*-test. *: *p* < 0.05)

4.5 Conclusion

In summary we have demonstrated that adenoviruses bearing metabolically incorporated *O*-GlcNAz moieties can be modified and targeted using “clickable” affibody reagents. Notably, this targeting strategy is exceedingly straightforward, requiring only minor modifications of Ad production protocol and reagents. Enhancement with affibody or other antibody equivalents allows a high specificity approach to target essentially any cell surface receptors. Modification *via* either Cu(I) or strain promoted “click” yield particles with similar stability and aggregation state to unmodified particles, which was confirmed by our TEM studies and thermal stability assay using propidium iodide. Targeting studies indicate substantial (~100 fold) to modest (~3 fold) increases in infectivity dependent of both the nature of the cell line and the method of virus modification. These results are consistent with previous studies of affibody targeting and biomolecular modification [7]. The remarkable ease of implementation and broad availability of “click” reagents make this technique readily accessible.

4.6 Materials and methods

General

All chemical reagents were obtained from commercial sources and used without further purification unless otherwise noted. Human adenovirus serotype 5 (Ad5) containing luciferase transgene was obtained from Vector Biolabs (Ad5-CMV-Luc) (Philadelphia, PA). Anti-EGFR affibody (ab95116) and Anti-ErbB2 affibody (ab31889) were purchased from Abcam (Cambridge, MA). Succinimidyl-([N-maleimidopropionamido]-24ethyleneglycol) ester (NHS-PEG₂₄-Maleimide) was purchased from Thermo Fisher Scientific Inc. (Rockford, IL) and 5-Carboxytetramethylrhodamine, succinimidyl ester from AnaSpec (Fremont, CA). pET15b-Ad12 knob plasmid was kindly donated by Dr. P. Freimuth. Matrix assisted laser desorption-ionization time of flight (MALDI-TOF) mass spectra were obtained on a Bruker Autoflex II mass spectrometer (Bremen Germany). HPLC was performed on Shimadzu LG-20AB / SPD-20A system with a C18 column (250 × 4.6 mm, Varian). Size exclusion separation (SEP) columns were purchased from GE Healthcare (NAP-5 column, Sephadex G-25 DNA grade) (Pittsburgh, PA) and SEP spin columns from Princeton Separations (Centri-Sep column CS-400) (Adelphia, NJ). Transmission electron microscope (TEM) image was acquired with a FEI Tecnai BioTwinG² and an AMT XR-60 CCD digital camera system. Luciferase activity was measured on a photometer (PerkinElmer 2030 multilabel reader) with luciferase assay kit (Bright-Glo, Promega).

Cell Culture

Dulbecco's modified Eagle's medium (DMEM) with glutamine, McCoy's 5A medium modified, Penicillin/Streptomycin and 0.5% Trypsin-EDTA were purchased from GIBCO (Grand Island, NY). Fetal bovine serum (FBS) was purchased from HyClone (Logan, UT). A431 (human epithelial carcinoma), PANC-1 (human pancreatic epithelioid carcinoma), MIA PaCa-2 (human pancreatic carcinoma) and RD (human rhabdomyosarcoma) cell lines were cultured in DMEM supplemented with 10% FBS, 100 IU/mL penicillin, 100 µg/mL streptomycin. SK-OV-3 (human ovarian adenocarcinoma) and SK-BR-3 (human breast adenocarcinoma) cell lines were cultured in McCoy's 5A medium containing 10% FBS, 100 IU/mL penicillin, and 100 µg/mL streptomycin. Cells were cultured at 37 °C in a humidified atmosphere containing 5% CO₂.

Metabolic Labeling of Ad5 with N-azidoacetylgalactosamine.

Metabolic labeling of Ad5 with *N*-azidoacetylgalactosamine was performed as described previously[37], that is, HEK 293 cells were infected with intact adenovirus particles with a multiplicity of infection (MOI) of 5 PFU/cell. The complete media was supplemented with 50 µM peracetyl-*N*-azidoacetylgalactosamine or 50 µM peracetyl-*N*-azidoacetylglucosamine and the infected cells were incubated at 37 °C. The plates were harvested 42-46 h post infection and virus particles were purified over a gradient of 1.4 g/mL and 1.25 g/mL CsCl centrifuged at 32,000 rpm for 1 h at 15 °C. The virus band at the boundary interface between the two CsCl layers was collected and further purified by an 18 h centrifugation at 35,000 rpm over 1.33 g/mL of CsCl.

Synthesis of maleimide-PEG₂₄-CCH (3-2)

NHS-PEG₂₄-maleimide (15 mg, 11 μ mol) was dissolved in anhydrous acetonitrile and propargylamine (0.6 mg, 11 μ mol) was added with 1.5 μ L of triethylamine. After 6 h, the reaction mixture was dried *in vacuo* and purified by reverse-phase HPLC with a C18 column and elution with H₂O/acetonitrile gradient containing TFA (0.1% v/v) to afford **3-2** (9.2 mg, 63%). MALDI-TOF m/z calcd for C₆₁H₁₁₁N₃O₂₈ [M] 1333.74, obsd 1356.25 [M + Na]⁺.

Synthesis of Bicyclo[6.1.0]nonyne(BCN)-PEG-maleimide (4-1)

(1R,8S,9r)-bicyclo[6.1.0]non-4-yn-9-ylmethyl 3,6,9-trioxa-12-azadodecylcarbamate (BCN-PEG-NH₂) was synthesized as described by F. L. van Delft *et al.*[38] **4-1**(12 mg, 37 μ mol) was added to a solution of NHS-PEG₂₄-maleimide (52 mg, 37 μ mol) in anhydrous acetonitrile (1 mL) with 1.5 μ L of triethylamine. The reaction mixture was stirred for 12 h at room temperature (RT) and concentrated *in vacuo* then purified by HPLC to afford **3** (52 mg, 88%). MALDI-TOF m/z calcd for C₇₅H₁₃₄N₄O₃₂ [M] 1602.90, obsd 1626.28 [M + Na]⁺.

Conjugation of Affibody with maleimide-PEG₂₄-CCH(3-2)

Affibodies (100 μ g, 7.1 nmol) were dissolved in reduction buffer (50 mM sodium phosphate, 150 mM NaCl, 2 mM EDTA, pH 7.5) to obtain a final volume of 0.5 mL. Dithiothreitol (DTT) stock solution (0.5 M) was added to a final concentration of 20 mM DTT and incubated at RT for 2 h. Excess DTT was removed and changed to coupling buffer (PBS, pH 7.2, 5 mM EDTA) by passage through a NAP-5 column, pre-equilibrated with coupling buffer. maleimide-PEG₂₄-CCH (**3-2**) (1.0 mg, 0.75 μ mol) was added immediately after buffer change and the reaction was allowed to proceed for 2 h at RT with gentle mixing. After conjugation, the remaining excess **3-2**

was removed using NAP-5 column with water. MALDI-TOF m/z calcd for anti-EGFR affibody-PEG₂₄-CCH [M] 15185, obsd 15183 [M + H]⁺; calcd for anti-Her2 affibody-PEG₂₄-CCH [M] 15364, obsd 15367 [M + H]⁺.

Conjugation of Affibody with 4-1

The conjugation of affibody with **4-1** was performed in the same procedure and condition as with **3-2**. MALDI-TOF m/z calcd for anti-EGFR affibody-PEG-BCN [M] 15455, obsd 15461 [M + H]⁺.

“Click” Reaction between Azide-labeled Virus (Ad5-GalNAz) and Affibody-PEG₂₄-CCH

50 μ L of azide labeled virus stock (1.0×10^{12} particles/mL) in a 100 mM Tris-HCl buffer pH 8.0 was mixed with bathophenanthroline disulfonic acid disodium salt at a final concentration of 3 mM and affibody-PEG₂₄-CCH at a final concentration of 100 μ M. After the mixture was kept in a deoxygenated glove bag for 6 h, copper (I) bromide (CuBr) in dimethyl sulfoxide (DMSO) was added to a final concentration of 1 mM and the reaction was allowed to proceed for 12 h at RT in the deoxygenated glove bag. The reaction was quenched by bathocuproinedisulfonic acid disodium salt (BCS) at a final concentration of 10 mM.

Purification of Modified Viral Particles with Spin Columns

The viral particles were purified by Centri-Sep columns (CS-400, Princeton Separations, Adelphia, NJ), that is, the columns were gently tapped so that dry gels settle down at the bottom of spin columns and 0.8mL of buffer (PBS + 0.5 mM MgCl₂ + 0.9 mM CaCl₂ + 10% glycerol) was added to each column. The column caps were replaced and the gels were hydrated by

shaking and inverting or brief vortexing. After 30 min at RT, air bubbles were removed from the top column. The top column caps were removed and excess fluid was drained into wash tube. The columns were spun at 3000 rpm for 2 min. and wash tubes were discarded. 50 μ L of modified virus solutions were added and the columns were placed on sample collection tubes. After spinning at 3000 rpm for 2 min., the eluated solutions were collected. The purified “clicked” viruses were stored in PBS buffer with 0.9 mM CaCl₂ and 0.5 mM MgCl₂ containing 10% glycerol and kept in 4 °C for infection test. The purified viruses can be stored in 4 °C up to 2 weeks.

Quantitation of Viral Particles by PicoGreen Assay

The purified viruses were quantitated using PicoGreen reagent (Quant-iT, invitrogen, Carlsbad, CA) as described by M. T. McCaman *et al.*[39]. Briefly, 0.5 μ L of 0.5 % SDS TE buffer was added to 4.5 μ L of virus solution and incubated at 37 °C for 30 min. This virus lysis solution was diluted with 45 μ L of TE. Working solution was prepared by adding 25 μ L of Quant-iT PicoGreen in 4.975 mL of TE. 20 μ L of diluted lysis solution and 180 μ L of working solution was mixed and analyzed by fluorescence photometer. Using standard double stranded DNA, the fluorescence (excitation: 485 nm, emission: 538 nm) standard curve ($y = ax + b$; $x = \text{DNA ng}$, $y = \text{fluorescence intensity}$) was obtained. The number of viral particle was calculated using the standard curve and a conversion factor ($1 \text{ ng DNA} = 2.6 \times 10^7 \text{ Ad genome}$, i.e., Ad particles).

Synthesis of Tetramethylrhodamine-BCN (4-2) (TAMRA-BCN)

5-Carboxytetramethylrhodamine, succinimidyl ester (2.5 mg, 4.7 μ mol) was dissolved in anhydrous DMF and **4-1** (1.5 mg, 4.7 μ mol) was added with 1.5 μ L of triethylamine at RT.

After 6 h, the reaction mixture was dried *in vacuo* and purified by reverse-phase HPLC with a C18 column and elution with H₂O/acetonitrile gradient containing TFA (0.1% v/v) to afford **4-2** (2.8 mg, 80%). MALDI-TOF m/z calcd for C₄₂H₄₈N₄O₈ [M] 736.35, obsd 737.60 [M + H]⁺.

Fluorescent Gel Scanning Assay with TAMRA-BCN

Azide enabled viral particles (Ad5-GalNAz) were labeled with an TAMRA-BCN dye using strain promoted “Click” chemistry, that is, TAMRA-BCN (20 mM) was added to GalNAz labeled Ad stock (1.0×10^{12} particles/mL) to obtain final concentration of 100 μ M TAMRA-BCN and the reaction was allowed to proceed for 2 h at RT. After “Click” reaction viral particles were purified using Centri-Sep spin columns and quantitated with Quant-iT PicoGreen as described above. The purified viral stock (1×10^{12} viral particles/mL) was run on SDS-PAGE using the TAMRA-BCN dye as standard. Standard dye was loaded 15 min before the end of the run. Gels were scanned using a typhoon gel scanner in fluorescence mode with excitation filter at 532 nm and emission filter at 580 ± 15 nm. The fluorescence intensities of scans were subsequently analyzed with Image Quant TL 1D gel analyzer software. All gels were run at 4 °C for 60 min and scanned within 10 min after the end of run.

“Click” Reaction between Azide-labeled Virus (Ad5-GalNAz) and Affibody-PEG-BCN

100 μ L of azide labeled virus stock (1.0×10^{12} particles/mL) in a PBS buffer pH 7.4 was gently mixed with affibody-PEG-BCN (100 μ M) for 16 h at RT using LabQuake tube shaker. The viral particles were purified, quantitated and stored with the same method as described above (“Click” reaction between Ad5-GalNAz and Affibody-PEG₂₄-CCH).

Western Blotting for Viral Fiber

To all samples (10^9 viral particles of unmodified Ad, Affibody (anti-EGFR) conjugated Ads through Cu(I) promoted and strain promoted chemistry, respectively), loading dye was added and boiled at 95 °C for 10 min. The samples were run on a 10% polyacrylamide electrophoresis gel at 100 V for 3 h and transferred onto nitrocellulose membrane at 40 V over 2 h in a western transfer buffer (25 mM tris, 192 mM glycine, 0.5% SDS and 10% methanol). Blots were blocked by 5% skim milk in PBST for 1 h at RT on rocker and washed with PBST twice, then treated with primary α -Fiber (Ad5) rabbit antibody (kindly donated by Dr. Patrick Hearing, Stony Brook university) at a ratio of 1:1000 in 3% BSA for 1 h. Blots were washed 3 times with 5% skim milk and treated with secondary α -rabbit HRP conjugate antibody (GE Healthcare, Cat: NA934) at a ratio of 1:5000 with 5% skim milk in PBST for 1 h. The membrane was washed 3 times with 5% skim milk in PBST and twice with PBST. The chemiluminescent HRP substrate (Millipore Immobilon Western, Bilerica, MA) were introduced to the membranes for 2 min and the membranes were exposed to film in dark room for 20 sec.

TEM Image of Virus

Approximately 15 μ L of purified virus stock was placed on 400 mesh formvar coated copper grids for 1 min, fixed with 2% EM grade glutaraldehyde for 1 min and then counter stained with 2% phosphotungstic acid for 30 sec. Samples were then viewed with a FEI Tecnai BioTwinG² transmission electron microscope. Digital images were acquired with an AMT XR-60 CCD digital camera system and compiled using Adobe Photoshop.

Thermal Stability Assay of Virus

Thermal stability of virus was assayed as described by C. R. Middaugh [33] using propidium iodide (PI). Briefly, the fluorescence spectra (excitation at 535 nm, emission scan from 550 to 650 nm, $\lambda_{\max} = 613$, slit widths of 6 nm) of PI (7.5 μM) were collected at the viral concentration of 6.5×10^{10} particles /mL in 5 °C increments from 20 to 90 °C employing a QuantaMaster spectrofluorometer (Photon Technology International, Inc.) with a 5 min temperature equilibration time before data acquisition. The T_m was determined by calculating the point where the second derivatives of the λ_{\max} versus temperature plots crossed the x-axis using Microcal Origin.

Measurement of Average Size and Surface Charge

The sizes and zeta potentials of intact Ad, O-GlcNAz enabled Ad, and anti-EFGR-affibody conjugated Ad were measured using a dynamic light scattering instrument (Zeta plus, Brookhaven, New York) equipped with a He-Ne laser at a wavelength of 659 nm, 25 °C, pH 7.5 and calculated by Smoluchowski model (zeta potential).

Expression and Purification of Ad12 Knob.

Ad12 knob was expressed and purified as described by P. Freimuth *et al.*[40]. (in detail *vid.* Chapter 3, Materials and methods)

Infection Assay

Cells (A431, PANC-1, MIA PaCa-2, RD, SK-OV-3 and SK-BR-3) were seeded in 96-well black and clear bottom plates at a density of 1×10^4 cells/well, respectively, 1 day before infection.

Monolayer cells were washed with PBS and incubated in inhibition buffer ([Ad12 knob] \approx 20 μ M in PBS with 2% serum) for 1 h at 37 °C. Virus stocks were added to the inhibition buffer at a multiplicity of infection (MOI) of 1000 and incubated at 37 °C. After 1 h, cell growth media were added and cells were incubated at 37 °C. 24 h post infection, the expression levels of luciferase transgene were determined by a photometer with the luciferase assay kit (Bright-Glo, Promega).

Statistics

Experiments were performed in triplicate and presented as mean \pm standard deviation. *P*-values were calculated by a two-tailed unpaired Student's *t*-test. Data were considered to be significantly different when $P < 0.05$.

References

1. Magnusson, M. K. H., S.S.; Henning, P.; Boulanger, P.; Lindholm, L., Genetic retargeting of adenovirus vectors: functionality of targeting ligands and their influence on virus viability. *J. Gene Med.* **2002**, *4* (4), 356-370.
2. Henning, P.; Lundgren, E.; Carlsson, M.; Frykholm, K.; Johannisson, J.; Magnusson, M. K.; Tang, E.; Franqueville, L.; Hong, S. S.; Lindholm, L.; Boulanger, P., Adenovirus type 5 fiber knob domain has a critical role in fiber protein synthesis and encapsidation. *J. Gen. Virol.* **2006**, *87* (11), 3151-3160.
3. Matthews, Q. L.; Yang, P.; Wu, Q.; Belousova, N.; Rivera, A. A.; Stoff-Khalili, M. A.; Waehler, R.; Hsu, H. C.; Li, Z.; Li, J.; Mountz, J. D.; Wu, H. J.; Curiel, D. T., Optimization of capsid-incorporated antigens for a novel adenovirus vaccine approach. *J. Virol.* **2008**, *5*.
4. Baselga, J.; Swain, S. M., Novel anticancer targets: revisiting ERBB2 and discovering ERBB3. *Nat. Rev. Cancer* **2009**, *9* (7), 463-475.
5. Belousova, N.; Krendelchtchikova, V.; Curiel, D. T.; Krasnykh, V., Modulation of Adenovirus Vector Tropism via Incorporation of Polypeptide Ligands into the Fiber Protein. *J. Virol.* **2002**, *76* (17), 8621-8631.
6. Xia, H.; Anderson, B.; Mao, Q.; Davidson, B. L., Recombinant human adenovirus: targeting to the human transferrin receptor improves gene transfer to brain microcapillary endothelium. *J. Virol.* **2000**, *74*, 11359-11366.
7. Belousova, N.; Mikheeva, G.; Gelovani, J.; Krasnykh, V., Modification of Adenovirus Capsid with a Designed Protein Ligand Yields a Gene Vector Targeted to a Major Molecular Marker of Cancer. *J. Virol.* **2008**, *82* (2), 630-637.
8. Kreppel, F.; Gackowski, J.; Schmidt, E.; Stefan, K., Combined Genetic and Chemical Capsid Modifications Enable Flexible and Efficient De- and Retargeting of Adenovirus Vectors. *Mol. Ther.* **2005**, *12* (1), 107-117.
9. Kreppel, F.; Kochanek, S., Modification of Adenovirus Gene Transfer Vectors With Synthetic Polymers: A Scientific Review and Technical Guide. *Mol. Ther.* **2007**, *16* (1), 16-29.
10. Kreppel, F.; Gackowski, J.; Schmidt, E.; Kochanek, S., Combined genetic and chemical capsid modifications enable flexible and efficient de- and retargeting of adenovirus vectors. *Mol. Ther.* **2005**, *12* (1), 107-117.

11. Kreppel, F.; Kochanek, S., Modification of adenovirus gene transfer vectors with synthetic polymers: A scientific review and technical guide. *Molecular Therapy* **2008**, *16* (1), 16-29.
12. Campos, S. K.; Parrott, M. B.; Barry, M. A., Avidin-based Targeting and Purification of a Protein IX-modified, Metabolically Biotinylated Adenoviral Vector. *Mol. Ther.* **2004**, *9* (6), 942-954.
13. Pereboeva, L.; Komarova, S.; Roth, J.; Ponnazhagan, S.; Curiel, D. T., Targeting EGFR with metabolically biotinylated fiber-mosaic adenovirus. *Gene Ther* **2007**, *14* (8), 627-637.
14. Vincenzi, B.; Schiavon, G.; Silletta, M.; Santini, D.; Tonini, G., The biological properties of cetuximab. *Crit Rev Oncol Hematol* **2008**, *68* (2), 14-14.
15. Salomon, D. S.; Brandt, R.; Ciardiello, F.; Normanno, N., Epidermal growth factor-related peptides and their receptors in human malignancies. *Crit. Rev. Oncol. Hematol.* **1995**, *19* (3), 183-232.
16. Engel, R. H.; Kaklamani, V. G., HER2-positive breast cancer: current and future treatment strategies. *Drugs* **2007**, *67* (9), 1329-1341.
17. Nord, K.; Gunneriusson, E.; Ringdahl, J.; Ståhl, S.; Uhlén, M.; Nygren, P. Å., Binding proteins selected from combinatorial libraries of an α -helical bacterial receptor domain. *Nat. Biotechnol.* **1996**, *15* (8), 772-777.
18. Nygren, P. Å., Alternative binding proteins: Affibody binding proteins developed from a small three-helix bundle scaffold. *FEBS J.* **2008**, *275* (11), 2668-2676.
19. Dreux, A. C.; Lamb, D. J.; Modjtahedi, H.; Ferns, G. A. A., The epidermal growth factor receptors and their family of ligands: Their putative role in atherogenesis. *Atherosclerosis* **2006**, *186* (1), 38-53.
20. Belousova, N.; Mikheeva, G.; Gelovani, J.; Krasnykh, V., Modification of adenovirus capsid with a designed protein ligand yields a gene vector targeted to a major molecular marker of cancer. *J. Virol.* **2008**, *82* (2), 630-7.
21. Magnusson, M. K.; Henning, P.; Myhre, S.; Wikman, M.; Uil, T. G.; Friedman, M.; Andersson, K. M. E.; Hong, S. S.; Hoeben, R. C.; Habib, N. A.; Stahl, S.; Boulanger, P.; Lindholm, L., Adenovirus 5 vector genetically re-targeted by an affibody molecule with specificity for tumor antigen HER2/neu. *Cancer Gene Ther.* **2007**, *14* (5), 468-479.
22. Steffen, A. C.; Wikman, M.; Tolmachev, V.; Adams, G. P.; Nilsson, F. Y.; Stahl, S.; Carlsson, J., In vitro characterization of a bivalent anti-HER-2 affibody with potential for radionuclide-based diagnostics. *Cancer Biother. Radiopharm.* **2005**, *20* (3), 239-248.

23. Banerjee, P. S.; Ostapchuk, P.; Hearing, P.; Carrico, I., Chemoselective Attachment of Small Molecule Effector Functionality to Human Adenoviruses Facilitates Gene Delivery to Cancer Cells. *J. Am. Chem. Soc.* **2010**, *132* (39), 13615-13617.
24. Cauet, G.; Strub, J. M.; Leize, E.; Wagner, E.; Van Dorselaer, A.; Lusky, M., Identification of the glycosylation site of the adenovirus type 5 fiber protein. *Biochemistry* **2005**, *44* (14), 5453-5460.
25. Ning, X. H.; Guo, J.; Wolfert, M. A.; Boons, G. J., Visualizing metabolically labeled glycoconjugates of living cells by copper-free and fast huisgen cycloadditions. *Angew. Chem. Int. Ed. Eng.* **2008**, *47* (12), 2253-2255.
26. Debets, M. F.; van Berkel, S. S.; Schoffelen, S.; Rutjes, F.; van Hest, J. C. M.; van Delft, F. L., Aza-dibenzocyclooctynes for fast and efficient enzyme PEGylation via copper-free (3+2) cycloaddition. *Chem. Commun.* **2010**, *46* (1), 97-99.
27. Dommerholt, J.; Schmidt, S.; Temming, R.; Hendriks, L. J. A.; Rutjes, F.; van Hest, J. C. M.; Lefeber, D. J.; Friedl, P.; van Delft, F. L., Readily Accessible Bicyclononynes for Bioorthogonal Labeling and Three-Dimensional Imaging of Living Cells. *Angew. Chem. Int. Ed. Eng.* **2010**, *49* (49), 9422-9425.
28. Agard, N. J.; Baskin, J. M.; Prescher, J. A.; Lo, A.; Bertozzi, C. R., A Comparative Study of Bioorthogonal Reactions with Azides. *ACS Chem. Biol.* **2006**, *1* (10), 644-648.
29. Hong, V.; Presolski, S.; Ma, C.; Finn, M., Analysis and Optimization of Copper-Catalyzed Azide-Alkyne Cycloaddition for Bioconjugation. *Angew. Chem. Int. Ed. Eng.* **2009**, *48* (52), 9879-9883.
30. Hong, V.; Steinmetz, N. F.; Manchester, M.; Finn, M. G., Labeling Live Cells by Copper-Catalyzed Alkyne-Azide Click Chemistry. *Bioconjugate Chem.* **2010**, *21* (10), 1912-1916.
31. Chen, H.; Bartlett, J.; Wilcher, R.; Samulski, R.; Berns, K.; Bohenzky, R.; Liu, S.; Chen, L.; Huang, J., Comparative observation of the recombinant adeno-associated virus 2 using transmission electron microscopy and atomic force microscopy. *Microsc. Microanal.* **2007**, *13* (5), 384-389.
32. Rexroad, J.; Wiethoff, C. M.; Green, A. P.; Kierstead, T. D.; Scott, M. O.; Middaugh, C. R., Structural stability of adenovirus type 5. *J. Pharm. Sci.* **2003**, *92* (3), 665-678.
33. Rexroad, J.; Martin, T. T.; McNeilly, D.; Godwin, S.; Middaugh, C. R., Thermal stability of adenovirus type 2 as a function of pH. *J. Pharm. Sci.* **2006**, *95* (7), 1469-1479.
34. Oh, I. K.; Mok, H.; Park, T. G., Folate immobilized and PEGylated adenovirus for retargeting to tumor cells. *Bioconjugate Chem.* **2006**, *17* (3), 721-727.

35. Awasthi, V.; Meinken, G.; Springer, K.; Srivastava, S. C.; Freimuth, P., Biodistribution of radioiodinated adenovirus fiber protein knob domain after intravenous injection in mice. *J. Virol.* **2004**, *78* (12), 6431-8.
36. Gaborit, N.; Larbouret, C.; Vallaghe, J.; Peyrusson, F.; Bascoul-Mollevi, C.; Crapez, E.; Azria, D.; Chardès, T.; Poul, M. A.; Mathis, G., Time-resolved Fluorescence Resonance Energy Transfer (TR-FRET) to Analyze the Disruption of EGFR/HER2 Dimers. *J. Biol. Chem.* **2011**, *286* (13), 11337-45.
37. Banerjee, P. S.; Ostapchuk, P.; Hearing, P.; Carrico, I., Chemoselective Attachment of Small Molecule Effector Functionality to Human Adenoviruses Facilitates Gene Delivery to Cancer Cells. *J. Am. Chem. Soc.* **2010**, *132* (39), 13615-13617.
38. Dommerholt, J.; Schmidt, S.; Temming, R.; Hendriks, L. J. A.; Rutjes, F. P. J. T.; van Hest, J. C. M.; Lefeber, D. J.; Friedl, P.; van Delft, F. L., Readily Accessible Bicyclononynes for Bioorthogonal Labeling and Three-Dimensional Imaging of Living Cells. *Angew. Chem., Int. Ed. Engl.* **2010**, *49* (49), 9422-9425.
39. Murakami, P.; McCaman, M. T., Quantitation of Adenovirus DNA and Virus Particles with the PicoGreen Fluorescent Dye. *Anal. Biochem.* **1999**, *274* (2), 283-288.
40. Freimuth, P.; Springer, K.; Berard, C.; Hainfeld, J.; Bewley, M.; Flanagan, J., Coxsackievirus and Adenovirus Receptor Amino-Terminal Immunoglobulin V-Related Domain Binds Adenovirus Type 2 and Fiber Knob from Adenovirus Type 12. *J. Virol.* **1999**, *73* (2), 1392-1398.

Chapter 5. Labeling Ad with Positron Emitters for *In Vivo* Tracking

5.1 Introduction

We have demonstrated the successful targeting results *in vitro* using our retargeted Ad vectors as shown in the previous chapters. Accordingly, the next goal of our studies has focused on the vehicle's ability to reach the target area *in vivo* and the methods to visualize it. Viral vectors have the innate capability to deliver their genes into target cells, which allow 'reporter transgene approaches' to visualize viral distribution *in vivo* [1-3]. For example, the transgenes expressing the reporters such as fluorescent proteins (e.g., GFP), luminescent proteins (e.g., luciferase), radiotracer binding proteins (e.g., sodium iodide symporter [4]), and kinases promoting the accumulation of specific radioprobes (e.g., HSV1-tk [5]) were inserted into viral genomes to provide images of vector tracking and tropism *in vivo*. However, these reporter gene approaches do not address the initial kinetics and efficiency of gene delivery vehicle itself, which is essential for development and clinical translation of systemic nanoparticle-mediated gene therapy [6-7]. In other words, the majority of administered vectors are rapidly cleared or consumed through excretory or immune mechanism and sequestered by untargeted cells. Only small portion of vectors can reach the target cells and express the reporter proteins after a certain period of transduction time. Therefore, the transgene approaches can only present a minority report lacking an early history of most vehicles, and neither information about viral vectors' efficacy which is particularly important for controlling side effects such as immune responses. As an alternative, fluorescent molecules can be introduced onto viral capsid *via* chemical ligation or genetic engineering. Unfortunately, the high levels of autofluorescence in animal tissues hamper the application of this approach. To overcome this drawback, recently near-infrared (NIR,

$\lambda \approx 800$ nm where is little biological autofluorescence) fluorophores were chemically linked onto Adenovirus (Ad) particles and demonstrated better early kinetic images [6]. However, a fluorescence imaging *per se* has less sensitivity and brightness than other imaging methods such as positron emission tomography (PET) or single-photon emission computed tomography (SPECT), leading to the difficulty in tracking deep tissues and cancer-metastasis. Despite a few previous attempts, the current approaches for *in vivo* dynamic monitoring of viral particles are limited. Among the current noninvasive imaging techniques, PET is well suited for tracking of viral particles because it is incomparably sensitive along with SPECT (, but has better resolution than SPECT), can provide dynamic longitudinal images over the lifetime of radiotracers and quantifiable spatial images depending on the concentration of tracer. Thus, in this study, we aimed to demonstrate the feasibility of tracking Ad particles *in vivo* using PET imaging.

5.2 Labeling Ad with ^{18}F

Fluorine-18 (^{18}F) is one of the most commonly used positron emitting radioisotopes for PET imaging due to its advantageous radiochemical properties including a relatively long half-life ($t_{1/2} = 109.77$ min) among non-metallic radionuclides, a versatile synthetic applicability for labeling a radionuclide into target molecules, and a short positron range allowing better resolution images. Despite enormously wide usage of ^{18}F -labeled sugar, 2-deoxy-2- ^{18}F -fluoro-*D*-glucose (^{18}F FDG), direct incorporation of ^{18}F into biomolecules has foundered due to the interfering functionalities in target molecules, harsh reaction conditions, poor regioselectivity, and the low specific activity. Accordingly, the majority of ^{18}F -labeling methods have employed a prosthetic group such as *N*-succinimidyl 4- ^{18}F fluorobenzoate (^{18}F SFB) [8-10] or 4-

nitrophenyl 2-[¹⁸F]fluoropropionate ([¹⁸F]NPFP)[11] for fast and convenient radiolabelings under mild reaction conditions.

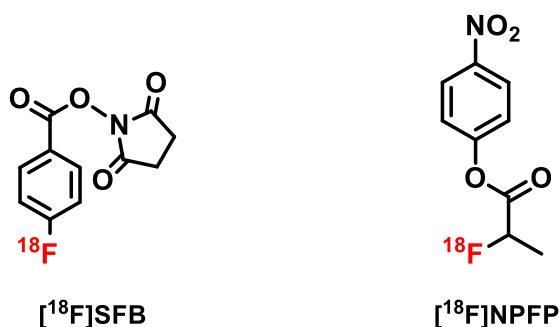


Figure 5-1. Prosthetic Groups Frequently Used for ¹⁸F-Labeling

Since the advent of copper-catalyzed azide–alkyne cycloaddition (CuAAC), efforts have been made to introduce “click” chemistry into the field of nuclear imaging, to take advantages of properties such as rapid kinetics (optimal $k \approx 10^4 \sim 10^5 \text{ M}^{-1} \text{ s}^{-1}$ at room temperature (RT) [12-13]), high yield even in very dilute conditions [14], unneeded protection / deprotection steps owing to virtually ideal chemoselectivity, and *in vivo* stability of linking unit (triazole) formed as a result of reaction, which have been desired for the ideal radiochemical reaction [15]. Moreover, a plethora of pharmacophores and targeting biomolecules already developed as “clickable” reagents can be readily accessible *via* “click” reactions. In this context, new prosthetic groups including alkyne or azide moieties were synthesized [16-17] as shown in Figure 5-2 a~d. However, the requirement for a cytotoxic cuprous catalyst restricts the utility of CuAAC in radiochemistry especially *in vivo* application. Therefore, copper-free “click” reactions such as strain-promoted alkyne-azide cycloaddition (SPAAC) was explored [18-20] as an alternative despite slower reaction rates (e.g., azadibenzocyclooctyne, ADIBO, $k \approx 0.31 \text{ M}^{-1} \text{ s}^{-1}$ in CD₃OD at RT [21]) than CuAAC (Figure 5-2 e, f). Recently, inverse-electron-demand Diels–Alder

cycloaddition between *trans*-cyclooctene (TCO) and tetrazine, known to have an unrivaled kinetics ($k \approx 2,000 \text{ M}^{-1} \text{ s}^{-1}$ in MeOH/H₂O = 9/1 [22]) among metal-free bioorthogonal reactions, was also employed to label peptides or proteins with ¹⁸F for PET imaging (Figure 5-2, g) [23-24], but the instability of TCO and tetrazine derivatives limits the wide application of this approach.

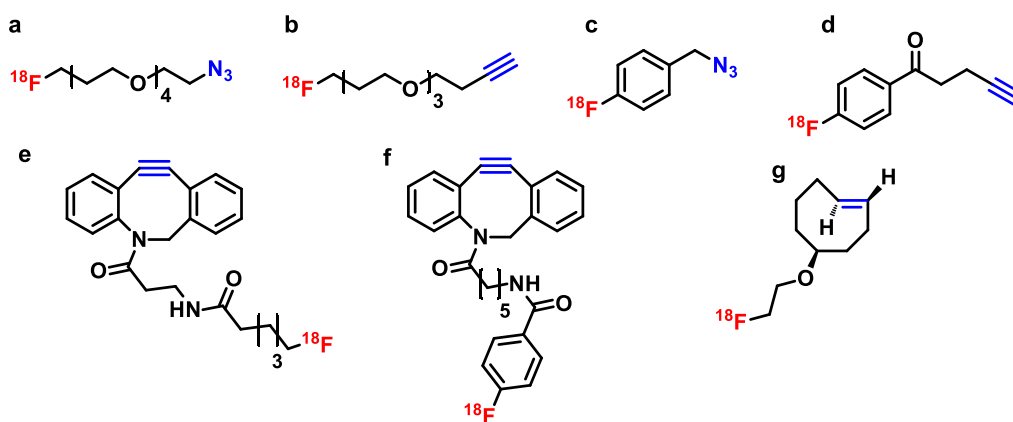
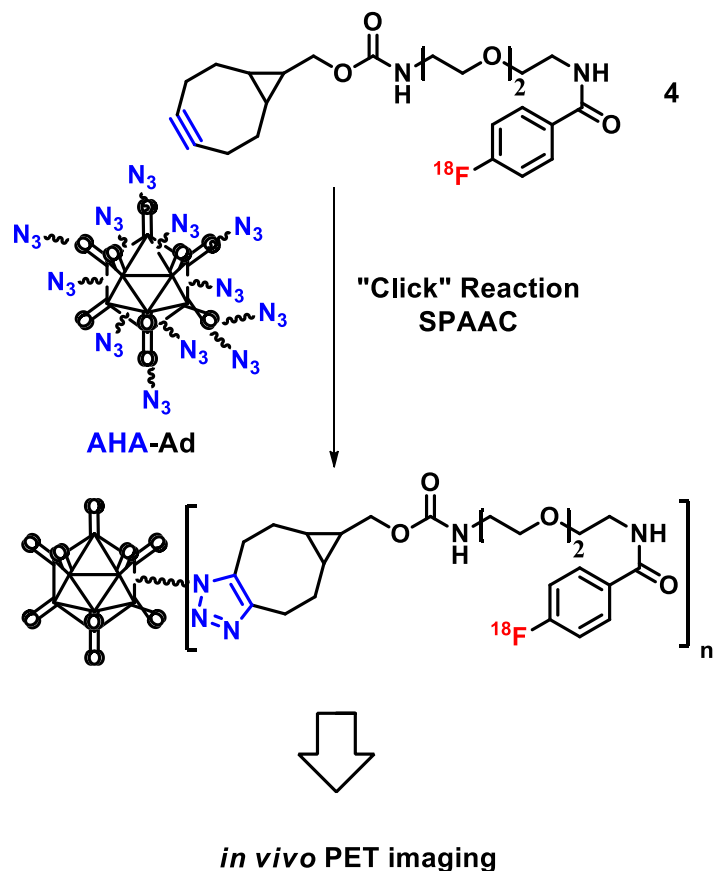


Figure 5-2. Examples of ¹⁸F-Labeling Prosthetic Groups for "Click" Reaction

a, b, c, d were synthesized for CuAAC [16-17, 20]; e, f for SPAAC [18-19]; and g for TCO-tetrazine ligation [23-24].

In this study, we adopted SPAAC to label Ad particles with ¹⁸F using the prosthetic group including a strained alkyne group, BCN-[¹⁸F]SFB, which can be synthesized in reaction conditions mild enough to leave strained alkyne functionality unperturbed as reported by Carpenter *et al.* [19] (Scheme 5-1). Bicyclonoyne (BCN) has comparable kinetics ($k \approx 0.14 \text{ M}^{-1} \text{ s}^{-1}$ in CD₃CN/D₂O = 3:1 at RT [25]) to ADIBO used in the precedents [18-20]. Further, our previous in-gel fluorescent assay showed a successful labeling of *O*-GlcNAz-Ad with micromolar (μM) Tetramethylrhodamine (TAMRA)-BCN dye *via* SPAAC under $\sim 40 \text{ nM}$ azide concentration (*vid.* Chapter 4) Therefore, we expected AHA-Ad bearing ~ 50 -fold more azide groups than *O*-GlcNAz-Ad (*vid.* Chapter 2), can be labeled with BCN-[¹⁸F]fluorobenzamide as depicted in Scheme 5-1. and provide positive radiosignals of viral particles *in vivo*.



Scheme 5-1. ^{18}F Labeling of Ad Particle via SPAAC

5.3 Labeling Ad with Longer-Lived Positron Emitters

The major challenge of PET imaging is the short half-lives of routinely used PET nuclides such as ^{18}F ($t_{1/2} = 1.8$ h) and ^{11}C ($t_{1/2} = 0.3$ h), particularly in the case where the half-lives of nuclides do not correspond with “the biological half-lives” and “pharmacokinetic parameters” of target molecules (e.g., antibodies have half-live up to several days and slowly localized on the targets.) [26-28]. To overcome this limitation, the use of longer-lived positron-emitting radionuclides has been explored for PET imaging as listed in Table 5-1.

Table 5-1. Characteristics of Selected Longer-Lived Positron-Emitting Radionuclides

radionuclide	half-life (h)	β^+ yields (%)	intrinsic resolution loss (mm)	human studies
^{18}F	1.83	97	0.7	Yes
^{124}I	100.2	24	2.3	Yes
^{76}Br	16.0	56	5.3	Yes
^{52}Mn	134.2	29	0.6	Yes
^{55}Co	17.5	76	1.6	Yes
^{66}Ga	9.4	56	5.8	Yes
^{72}As	25.9	88	3.6	Yes
^{64}Cu	12.7	18	0.7	Yes
^{86}Y	14.7	34	1.8	Yes
^{89}Zr	78.4	23	1.0	Yes

* This table was excerpted from the reference [28] with the permission of publisher (“ACS”).

Moreover, radioactive metal ions can be easily labeled by pre-conjugated chelators on the target molecules *via* much simpler procedures, compared to the time-consuming multi-step synthesis required for the incorporation of ^{18}F or ^{11}C , which is another advantage of longer-lived positron-emitter (LLPE) approach. Nevertheless, *in vivo* stability of the chelated metal complexes is the major issue needed to be conquered for the wide application of LLPE as imaging reagents. Among the listed LLPEs, ^{64}Cu has been investigated as a promising radionuclide for PET imaging due to its attractive radiochemical properties [29] such as long half-life (12.7 h), low positron energy (0.66 MeV) and no high-energy γ -emission, allowing high resolution images. Additionally, ^{64}Cu also emits Auger electrons and β^- particles (high energy electrons) during decay, which have the potential for radiotherapy. However, simple Cu(II) chelates are kinetically unstable in human serum and dissociated to form Cu(II)-albumin complex [30] due to

metabolic process of copper ions. To enhance the *in vivo* stability of Cu(II) complex, a variety of chelating agents have been explored and developed as exemplified in Figure 5-3.

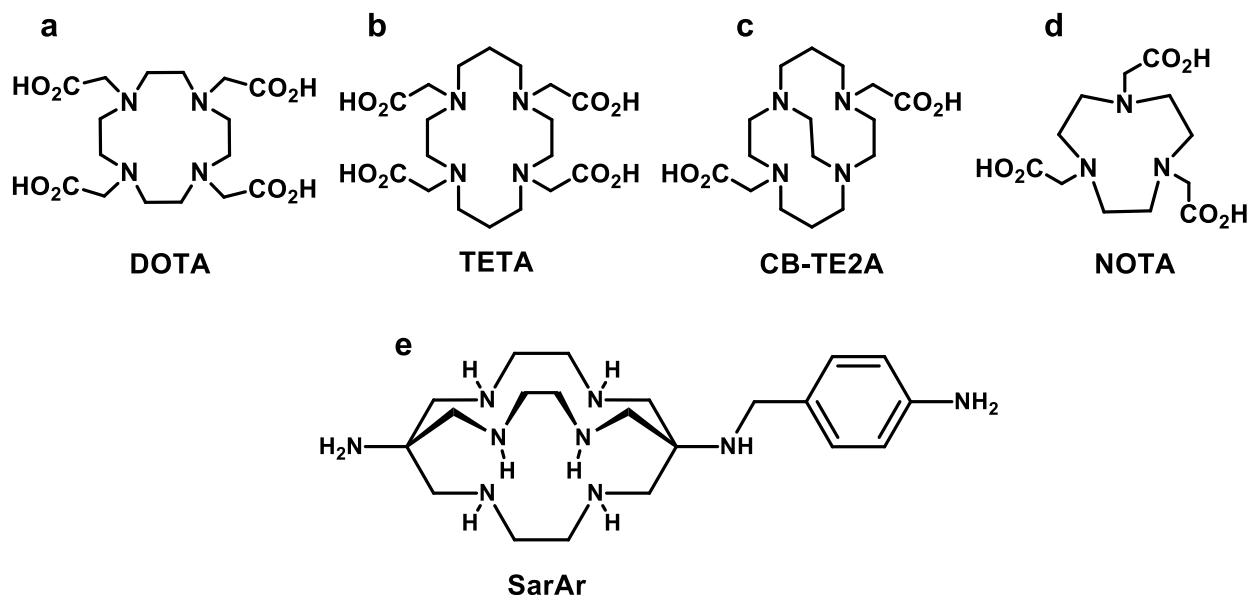
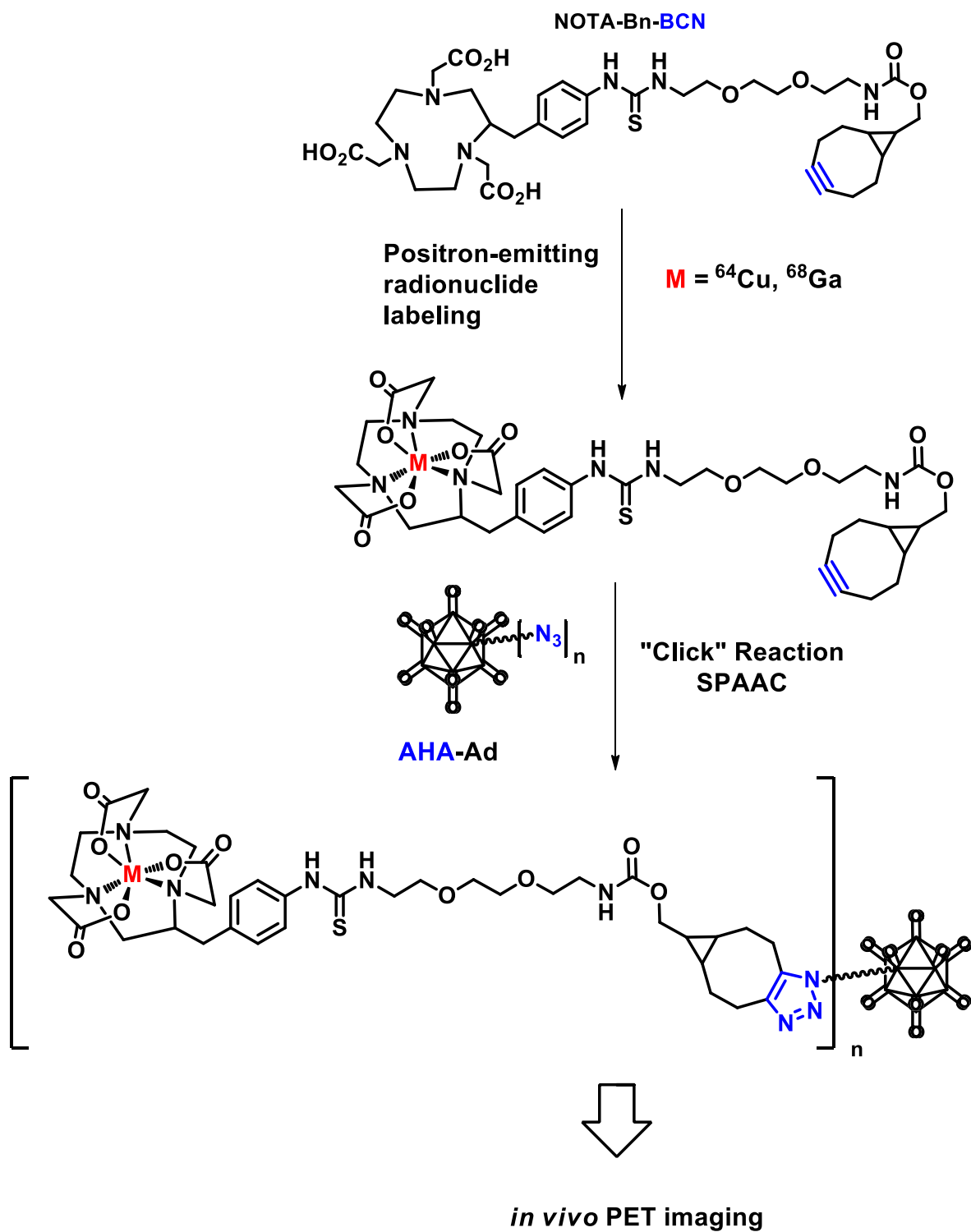


Figure 5-3. Different Copper Chelators for PET

a) DOTA (1,4,7,10-tetraazacyclododecane-1,4,7,10-tetraacetic acid), b) TETA (1,4,8,11-tetraazacyclotetradecane-1,4,8,11-tetraacetic acid), c) CB-TE2A (Cross-bridged 1,4,8,11-tetraazacyclotetradecane-1,8-diacetic acid), d) NOTA (1,4,7-triazacyclononane-1,4,7-triacetic acid, f) SarAr (1-N-(4-aminobenzyl)-3,6,10,13,16,19-hexaazabicyclo[6.6.6]eicosane-1,8-diamine)

While $^{64}\text{Cu(II)}$ complexes of DOTA and TETA showed only moderate *in vivo* stability, causing demetallation and elevated liver uptake, CB-TE2A complex demonstrated the resistance to dissociation in strong acid and serum [31] and the hexaazamacrobicyclic cage ligand, SarAr, displayed exceptional stability [32]. Furthermore, NOTA, known to form stable complexes with other metal ions (e.g. Ga(III), Gd(III), Zn(II), Mn(II), etc.), turned out to have the capacity to form stable complexes with $^{64}\text{Cu(II)}$ as well and the complex showed reduced accumulation in kidney and liver *in vivo* assay [33]. Considering the difficulties in synthesizing chelator conjugates retaining a strained alkyne functionality and labeling conditions which should be tolerable for viral particles, we chose a commercially available NOTA derivative containing

isothiocyanate group, as a chelator for ^{64}Cu as shown in Scheme 5-2. NOTA is also known to form a remarkably stable complex with $^{68}\text{Ga(III)}$ (^{68}Ga , $t_{1/2} = 1.13$ h, intrinsic resolution loss = 2.4 mm) which can be easily acquired from an in-house $^{68}\text{Ge}/^{68}\text{Ga}$ generator (^{68}Ge , $t_{1/2} = 270.8$ days) without the need of cyclotron [34-36]. Thus, we desired to prepare 3 different positron-emitter (i.e., ^{18}F , ^{64}Cu , and ^{68}Ga)-labeled Ads and compare their pharmacokinetics and tropism using PET imaging as shown in Scheme 5-1 and Scheme 5-2. To avoid the harsh labeling conditions which can perturb the physiology of virus, a metal-complexation step was schemed to precede SPAAC as shown in Scheme 5-2.



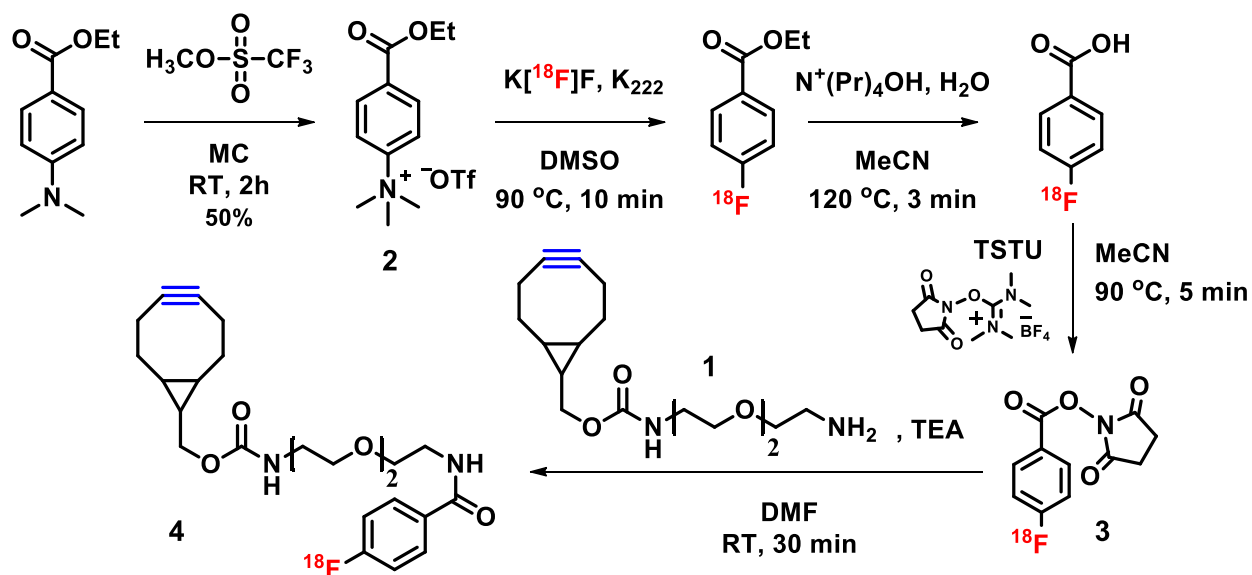
Scheme 5-2. ⁶⁴Cu and ⁶⁸Ga Labeling of Ad via SPAAC

5.4 Results and Discussion

5.4.1 ^{18}F Labeling

5.4.1.1 Synthesis of BCN- ^{18}F fluorobenzamide

^{18}F SFB (**3**) was synthesized as described by Tang *et al.* [8, 37] and reacted with BCN-PEG-NH₂ (**1**) to afford a “clickable” new prosthetic group, BCN- ^{18}F fluorobenzamide, as shown in Scheme 5-3. Separately, the radio-inactive “cold” compound, BCN-fluorobenzamide, was also synthesized *via* the same procedure using radio-inactive K¹⁹F instead of K[¹⁸F]¹⁹F to characterize the radioactive “hot” compound before decay by comparing chemical properties such as a chromatographic retention time.



Scheme 5-3. Synthesis of BCN- ^{18}F fluorobenzamide

All the reactions involving radioactive chemicals, were monitored by radio TLC scanning as shown in Figure 5-4. After fluorination, *N*-succinimidylation, and hydrolysis of excess [¹⁸F]SFB,

the reaction mixtures were purified by C18 Sep-Pak cartridge to remove unreacted reactants. The final Sep-Pak eluate was repurified by HPLC using a C18 semi-Prep column to obtain pure compound **4** which eluted at the same retention time using an isocratic solvent (50% MeCN/H₂O, 0.1% formic acid) as standard radio-inactive (“cold”) compound (**4'**) as demonstrated in Figure 5-5.

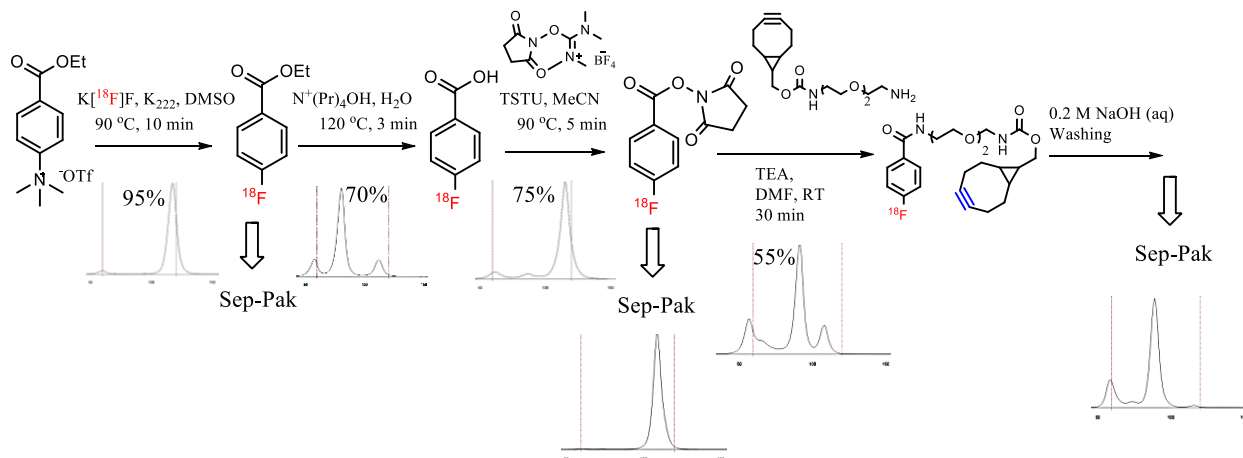


Figure 5-4. Reaction Monitoring by Radio TLC Scanning

All TLCs were developed with 100% Ethyl acetate using normal phase silica plates, which revealed overall yield as 27%.

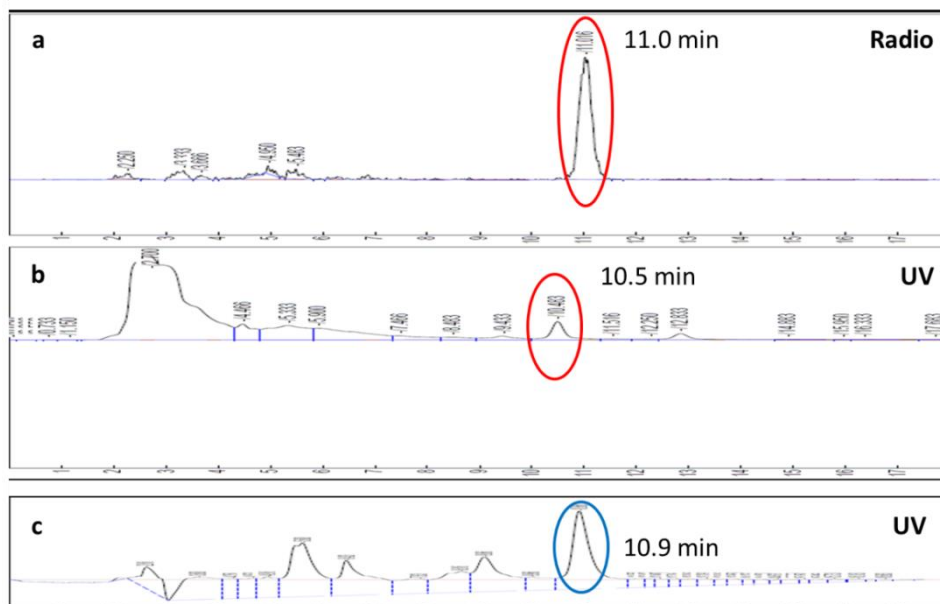


Figure 5-5. HPLC Traces of BCN-fluorobenzamide

a) radioactive trace of BCN- ^{18}F fluorobenzamide (**4**), b) UV ($\lambda=220$ nm) trace of radioactive “hot” compound **4**, c) UV ($\lambda=220$ nm) trace of radioinactive “cold” BCN-fluorobenzamide which was characterized by mass spectrometry (*vid. Appendix*)

After decay, the compound **4** was re-characterized by mass spectrometry as shown in Figure 5-6, which confirmed the correct molecular weight.

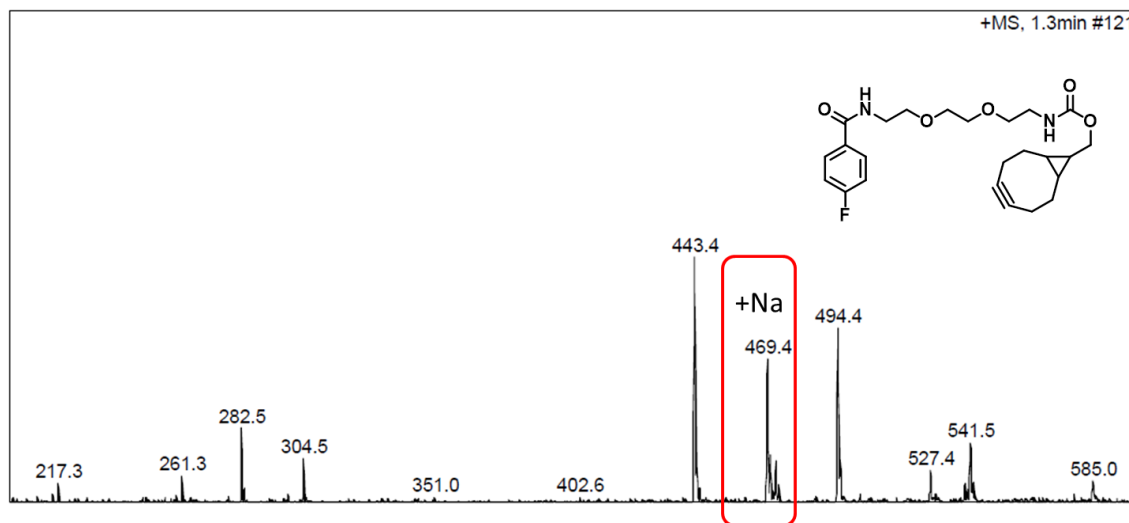


Figure 5-6. ESI-Mass Spectrum of Decayed Compound 4

HPLC-purified compound **4** was decayed (2 days) and characterized by ESI mass. (Calculated monoisotopic m/z for $[\text{M}+\text{Na}]^+ = 469.2$, observed $[\text{M}+\text{Na}]^+ = 469.4$)

Before the “click” reaction with azide-enabled Ad, the solubility of compound **4** in the reaction condition (5% DMSO, RT) was estimated using UV detector in HPLC. To wit, first, the known amount of standard ¹⁹F compound **4'** was dissolved in 100% acetonitrile and analyzed by HPLC, and then the excess amount of **4'** was dissolved in 5% DMSO/water solution and filtered by a 0.45 μm pore-sized membrane and analyzed in the same HPLC condition. By comparing the areas of corresponding UV peaks, the solubility of compound **4** in 5% DMSO/water solution was calculated as 0.5 mg/mL which met the empirical minimum solubility required for detecting ¹⁸F compound.

5.4.1.2 SPAAC between AHA-Ad and BCN-¹⁸F]fluorobenzamide

HPLC-purified “clickable” prosthetic group, BCN-¹⁸F]fluorobenzamide (~300 μCi), was reacted with azide-enabled Ad (150 μL of 3.0×10^{12} particles/mL \approx 5 nM) which was labeled with 32 mM azidohomoalanine (AHA) and assayed previously to bear ~500 accessible azide groups on a viral capsid [38] (\therefore $[N_3] \approx 2.5 \mu\text{M}$) in 5% DMSO/ PBS buffer, pH 7.4 at RT. The reaction was monitored by radio TLC up to 1 h, but the ¹⁸F-labeled virion was not detected by radio TLC as shown in Figure 5-7.

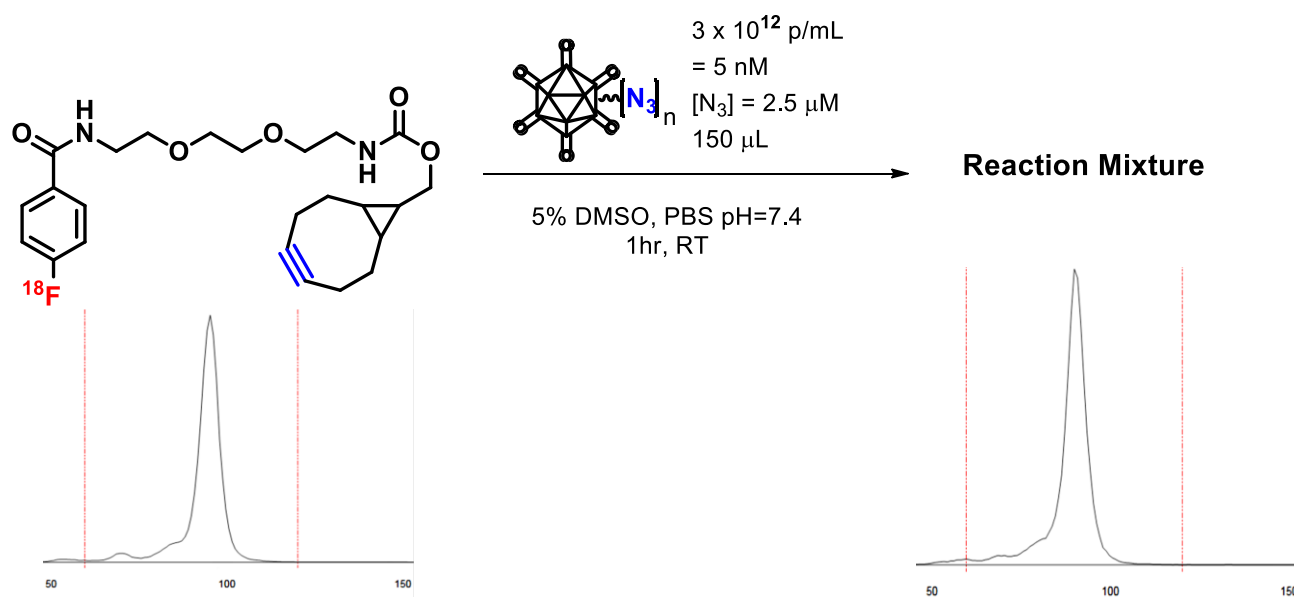


Figure 5-7. SPAAC Reaction between BCN-¹⁸F]fluorobenzamide and AHA-Ad Monitored by Radio TLC

TLC was developed with 100% Ethyl acetate using normal phase silica plates and showed no radioactivity on the base line corresponding to the labeled virions.

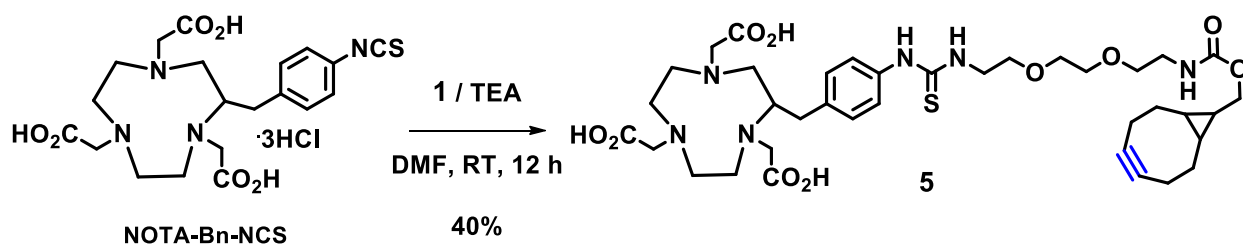
The slow diffusion ($D = 4.46 \times 10^{-12}$ m²/s for Ad particle) of nanoparticles could be a possible reason for the late kinetics. Therefore, the reaction with azidohomoalanine (AHA) as a small molecule containing an azide group was also performed in the same reaction conditions, but no reaction was detected by radio TLC as well. Considering the low solubility of BCN-

fluorobenzamide in aqueous solution and the trace level radioactive portion of it (i.e., low specific activity), we suppose very rarefied concentration of “clickable” prosthetic group might affect the reaction kinetics of copper-free “click” reaction using BCN (**4**).

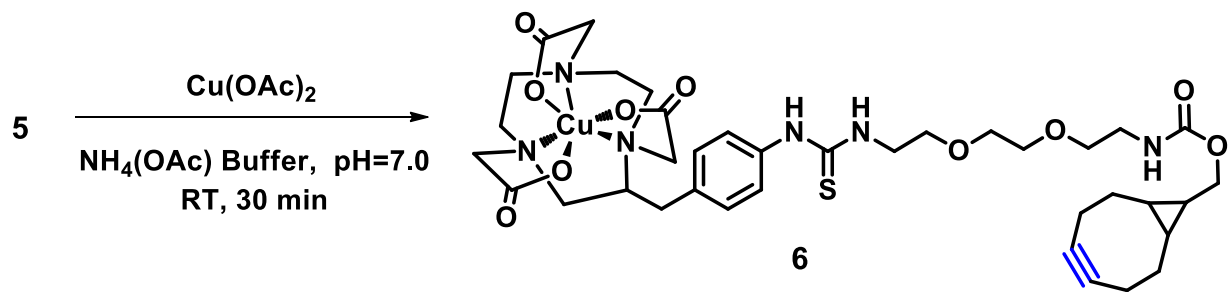
5.4.2 $^{64}\text{Cu}/^{68}\text{Ga}$ Labeling

5.4.2.1 Synthesis of NOTA-BCN

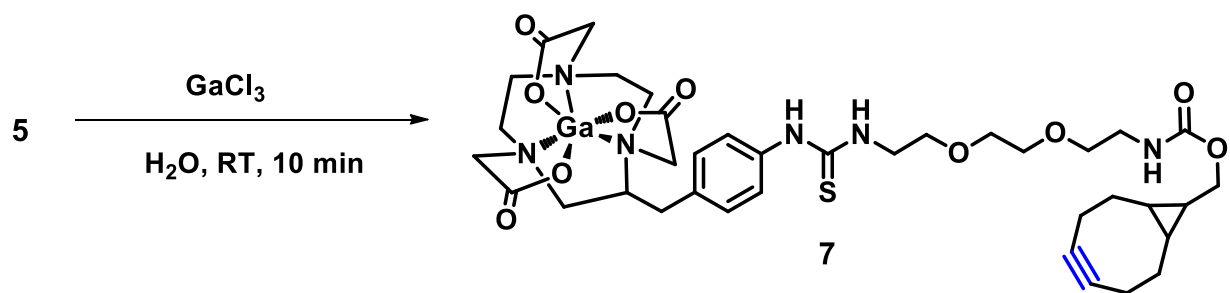
In an effort to label Ad particles with long-lived positron emitters such as ^{64}Cu and ^{68}Ga , NOTA chelator was cross-linked with BCN moiety, *videlicet*, the isothiocyanate group of a NOTA derivative was used for nucleophilic addition reactions with primary amine group of BCN-PEG-NH₂ (**1**) to form stable thiourea bond as shown in Scheme 5-4. Compound **5** was purified by HPLC and characterized by mass spectrometry. The metal-complexations were tested using radio-inactive “cold” ^{63}Cu and ^{69}Ga compounds as shown in Scheme 5-5 and Scheme 5-6.



Scheme 5-4. Synthesis of NOTA-PEG-BCN



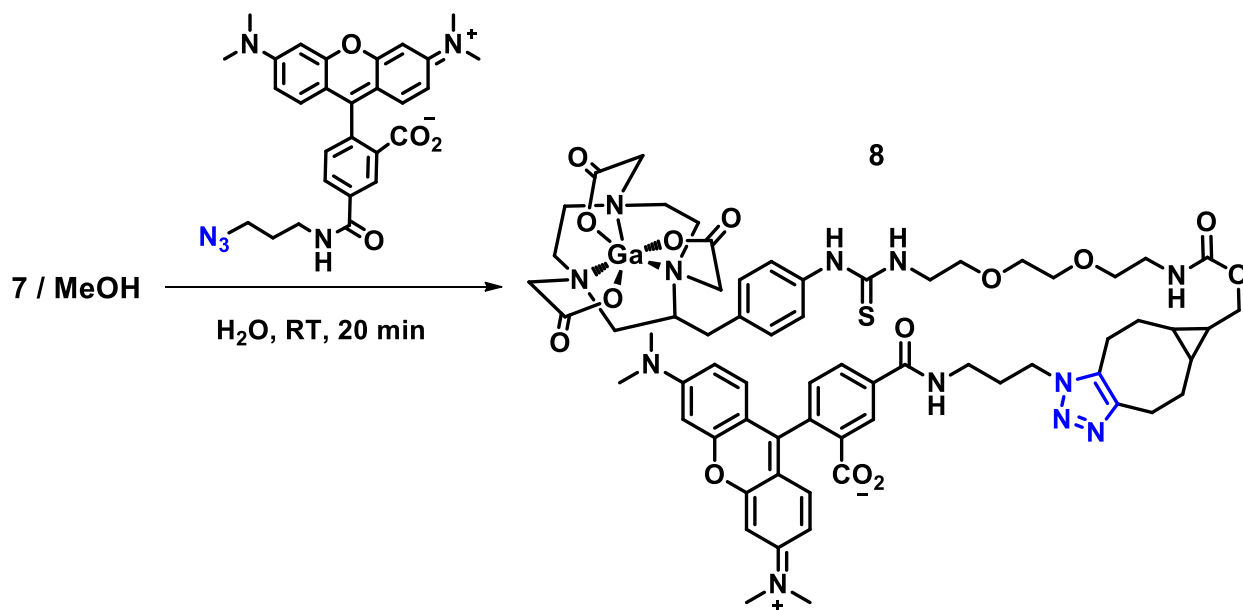
Scheme 5-5. ^{63}Cu -Complexation of NOTA-BCN



Scheme 5-6. ^{69}Ga -Complexation of NOTA-BCN

5.4.2.2 "Click" Test of ^{69}Ga -NOTA-BCN with TAMRA-azide

Due to the instability of the strained alkyne moiety [39], we desired to assess the retention of functionality after the acidic metal-complexation step, which is required for the next conjugation step with virus. Under the same "click" condition as the viral conjugation, the TAMRA-azide dye was reacted with Ga-NOTA-BCN (**7**) as shown in Scheme 5-7 and purified by HPLC and characterized by MALDI-TOF as demonstrated in Figure 5-8.



Scheme 5-7. "Click" Test of ^{69}Ga -NOTA-BCN (**7**) with TAMRA-azide

20 nmole of **7** was dissolved in 110 μL (18 μM) of methanol and mixed with 130 μL of aqueous TAMRA-azide solution (15 μM) and proceed to react at RT for 20 min.

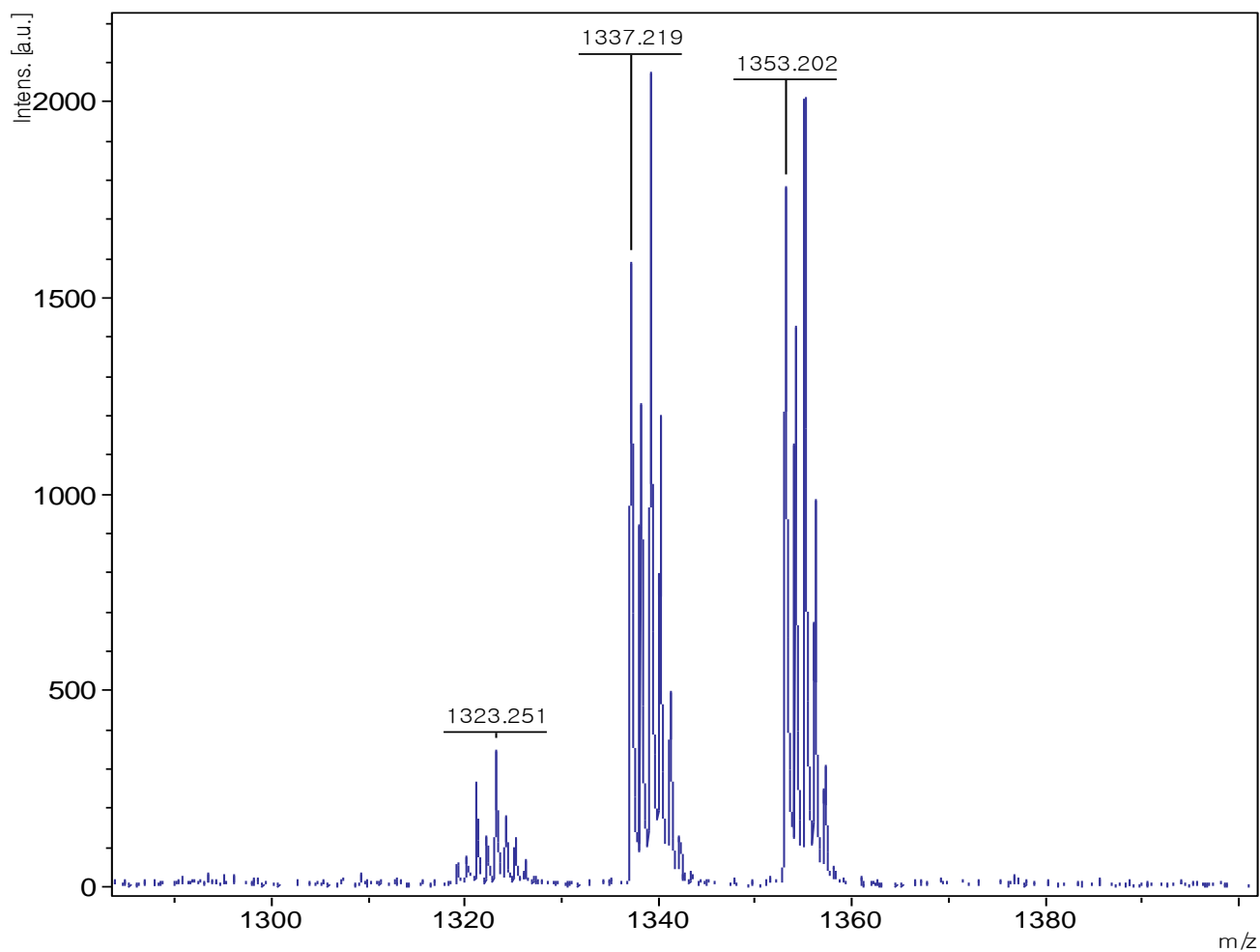


Figure 5-8. MALDI-TOF Spectrum of ⁶⁹Ga-NOTA-TAMRA (8)

Strain promoted “click” reaction between ⁶⁹Ga-NOTA-BCN and TAMRA-azide was performed to assess the retention of bicyclononyne functionality after the metal-complexation in acidic condition, then purified by HPLC and characterized by MALDI-TOF. monoisotopic m/z calculated for [M+H]⁺ = 1353.48, observed for [M+H]⁺ = 1353.20, Matrix (SA).

5.4.2.3 *In vitro* Infection Assay Using $^{63}\text{Cu}/^{69}\text{Ga}$ -Labeled Ad without HPLC

One advantage of using metal positron emitters is that only small amount of chelators are necessary to acquire high level yield, permitting the preparation of radiotracer without HPLC purification, which can considerably reduce the processing time, while retaining effective specific activity levels. Several tumor imaging studies using ^{68}Ga -labeled NOTA-tracers demonstrated the promising results without HPLC purification steps [36, 40-41]. Accordingly, we also desired to examine the potential for omitting HPLC purification as shown in Figure 5-9 by *in vitro* infection assays. After metal-complexation, the half of reaction mixture was purified by HPLC and used for conjugating with viruses *via* SPAAC, whereas the other half was used *in situ*. All the viruses were purified by size exclusion columns after SPAAC reaction. While the same level of reporter transgene expression was observed with ^{69}Ga -NOTA-Ad in both cases, only marginal transgene expression was observed with ^{63}Cu -NOTA-Ad in the absence of HPLC purification, probably due to the cytotoxic copper effect. This result suggests that the cytotoxic metals labeling requires HPLC purification for cellular assays besides size exclusion despite sub-micromolar amount of labeling reagents. The concentrations of ^{63}Cu and ^{69}Ga in the “clicked” viral stocks were quantitated by inductively coupled plasma mass spectrometry (ICP-MS) to assess the amount of residual metal ions, but the data represented inconsistent results due to the natural abundance of corresponding elements. (data not shown)

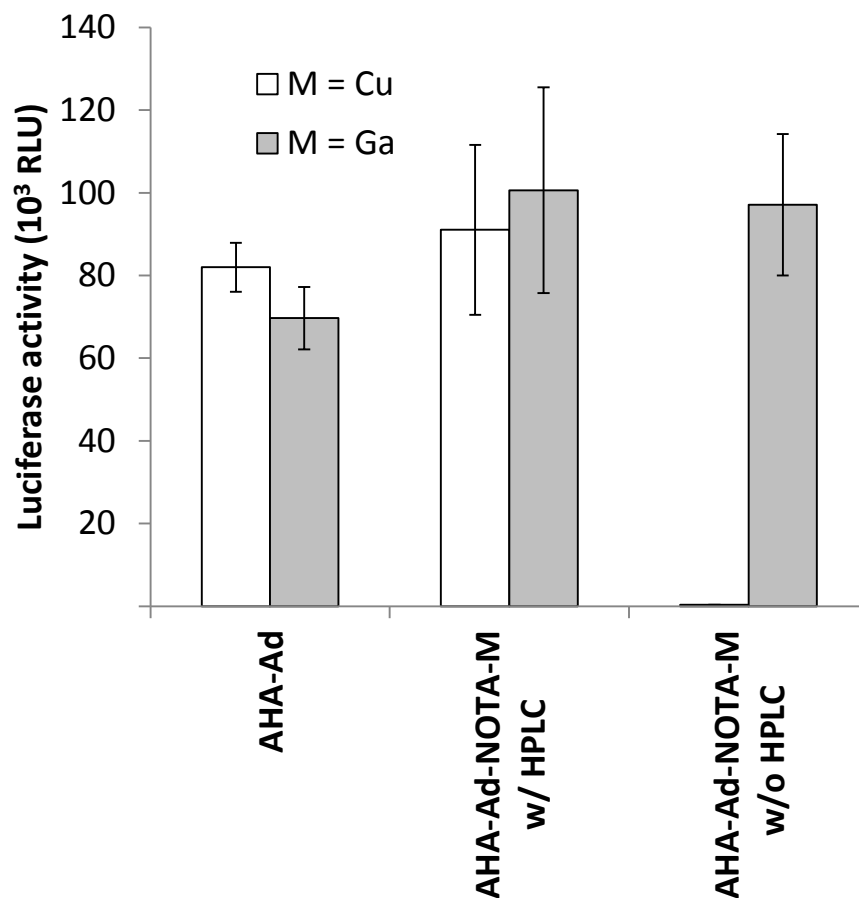


Figure 5-9. Infection Assays with "Clicked" Metal-Chelated Ad

HEK 293 cells were seeded in 96-well black and clear bottom plates at a density of 1×10^4 cells/well, 1 day before infection. Monolayer cells were washed with PBS. Virus stock was added to the infection buffer (PBS, TC, 2% serum) at a multiplicity of infection (MOI) of 500 and cell were incubated in infection buffer at 37 °C. After 1 h, cell growth media were added and cells were incubated at 37°C. 24 h post infection, the expression levels of luciferase transgene were determined by a photometer with the luciferase assay kit (Bright-Glo, Promega).

5.4.3 Labeling Folate-Targeting Ad with ^{89}Zr

^{89}Zr appeared recently in the field of PET imaging due to its favorable radiochemical properties such as a long half-life ($t_{1/2} = 3.27$ d), a high resolution (intrinsic loss = 1.0 mm) as shown in Table 5-1. Moreover, compared with expensive ^{124}I ($t_{1/2} = 4.18$ d, resolution loss = 2.4 mm), ^{89}Zr can be produced at a reasonable cost for routine clinical application and allow a better resolution image. $^{89}\text{Zr(IV)}$ shows very high affinity for the multiple oxygen donors of the chelator, deferoxamine (DFO), which is a bacterial siderophore, *scilicet*, a natural chelator for iron(III). In the context of tracking cancer-targeting Ad vector *in vivo* by PET, we prepared a folate-receptor targeting Ad vector adorned with DFO ligands for chelating ^{89}Zr positron emitter using our dually modified *O*-GlcNAz/HPG-Ad [42] *via* two successive orthogonal “click” reactions as depicted in Scheme 5-8. Notably, ^{89}Zr can be labeled in physiological pH using ^{89}Zr -oxalate without impairing viral fitness, allowing metal-labeling as a final step which has an advantage in retaining radioactivity longer, compared with our preceding labeling procedures.

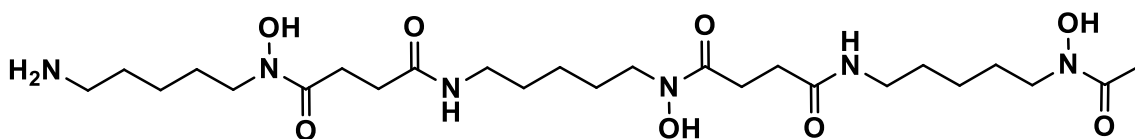
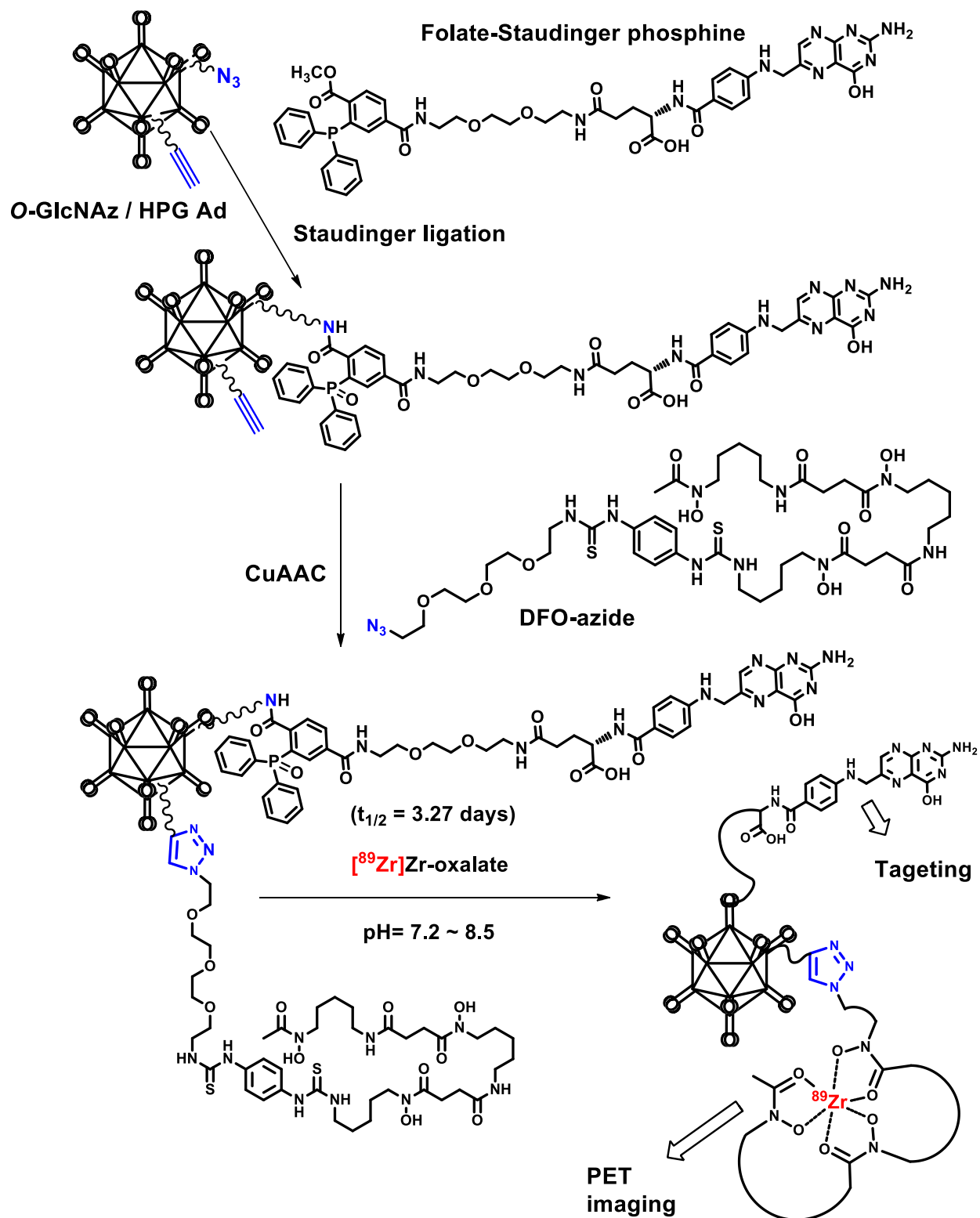


Figure 5-10. Structure of DFO

Deferoxamine (also known as desferrioxamine B, desferoxamine B, DFO-B, DFOA, DFB or desferal) is synthesized by the actinobacteria *Streptomyces pilosus*, IUPAC name: *N'*-[5-(Acetyl-hydroxy-amino)pentyl]-*N*-[5-[3-(5-aminopentyl-hydroxy-carbamoyl) propanoylamino]pentyl]-*N*-hydroxy-butane diamide



Scheme 5-8. ^{89}Zr -Labeling of Folate-Receptor-Targeting Ad Using DFO Chelator

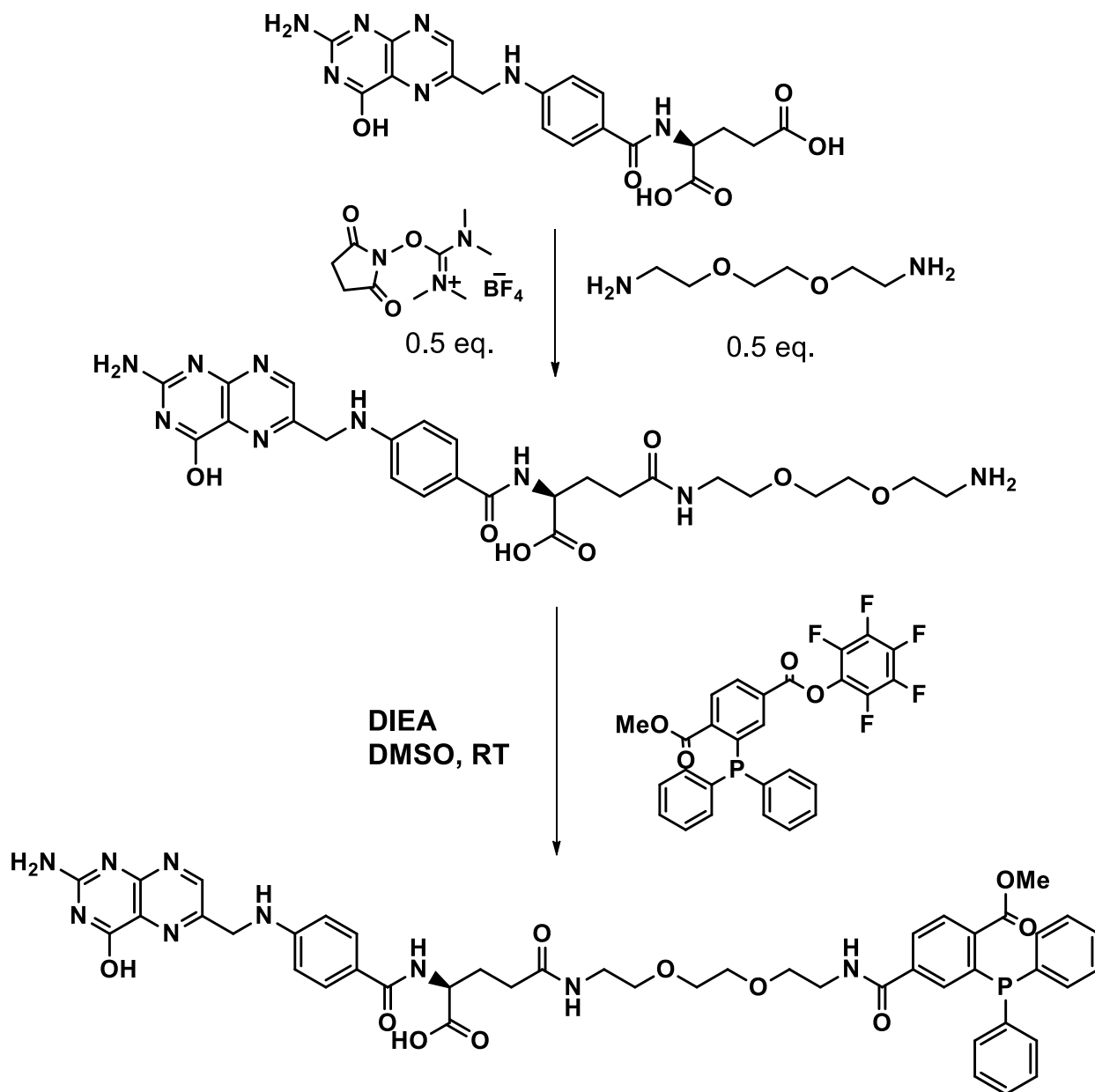
5.4.3.1 Usage of Azide/Alkyne-enabled Ad for Labeling Retargeted Ad

In order to conjugate the targeting and imaging group selectively as shown in Scheme 5-8, we used dually modified azide/alkyne-enabled Ad which was reported by our group recently [42]. To wit, these viruses were prepared *via* the simultaneous metabolic labeling with azide-bearing unnatural sugar residue, peracetylated *N*-azidoacetylgalactosamine (Ac₄GalNAz) as a substrate for *O*-Glycosylation at viral fiber, and an alkyne-bearing unnatural amino acid, homopropargylglycine (HPG) as a methionine surrogate in protein biosynthesis. Introduction of these surrogates into Ad particles allows sequential Staudinger ligation of *O*-GlcNAz followed by copper assisted “click” modification of homopropargylglycine (HPG). Moreover, the two chemically orthogonal ligation reactions (Staudinger and CuAAC) were envisioned to permit the specific conjugation of the targeting and imaging ligand with a viral capsid without mutual interference.

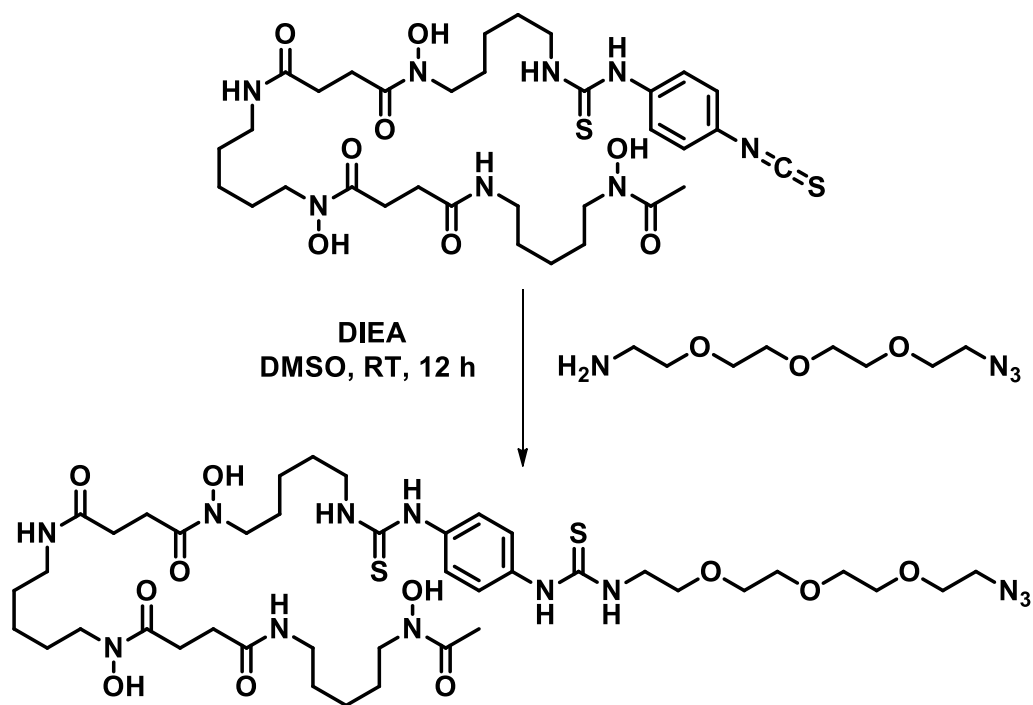
5.4.3.2 Synthesis of Folate-Staudinger Phosphine and DFO-azide

The folate-Staudinger phosphine to be used for viral targeting towards tumorous tissues was synthesized as shown in Scheme 5-9. Briefly, folic acid was linked with 1,8-diamino-3,6-dioxaoctane using 0.5 equivalent coupling agent, *O*-(*N*-Succinimidyl)-1,1,3,3-tetramethyl uranium tetrafluoroborate (TSTU), to induce a mono-amine coupled compound as major, and purified by HPLC. Then, the purified folate-PEG-amine was reacted with Staudinger phosphine-pentafluorophenyl (PFP) active ester to afford folate-Staudinger phosphine and purified again by HPLC. After lyophilization, the product was stored at -80 °C. The DFO-PEG-azide for chelating positron emitter (⁸⁹Zr) as a PET imaging agent was synthesized as in Scheme 5-10. In short, DFO ligand was cross-linked with azide group *via* the thiourea bond formed as a result of nucleophilic addition reaction between the isothiocyanate group of DFO ligand and primary

amine group of azide-PEG-NH₂. The reaction mixture was purified by HPLC. Both products were characterized by mass spectroscopy and ¹H-NMR. (*vid.* Appendix)



Scheme 5-9. Synthesis of Folate-Staudinger Phosphine



Scheme 5-10. Synthesis of DFO-PEG-N₃

5.4.3.3 “Click” reaction of HPG/GlcNAz-Ad with folate-phosphine and DFO-azide

First, folate-phosphine was conjugated first with the azide groups (*O*-GlcNAz) on viral fiber *via* Staudinger ligation as shown in Scheme 5-8. Sequential chemistry on the dual labeled vectors is important for introducing effective modifications. The excess use of 300 μM phosphine ligand helps to saturate the available azides ($[\textit{O}\text{-GlcNAz}] \approx 0.1 \mu\text{M}$ when using 3×10^{12} particles/mL viral stock, \therefore ~ 22 azides per particle was assayed [43]) on the viral capsid. After oxidation of excess phosphine by opening the reaction tubes to the air for 5 h and size exclusion, 400 μM of DFO-azide was “clicked” with alkyne groups of HPG residues (solvent exposed [alkyne] $\approx 1.0 \mu\text{M}$ based on our TAMRA-azide assay [42]) on the viral surface under the same reaction conditions described in Chap 3.4.3 [38]. A higher concentration of DFO-azide was used to scavenge any remaining phosphine derivatives and prevent particle aggregation *via* inter-virion “click” reactions. The “clicked” viruses

were repurified using size exclusion columns to remove remaining small molecules and stored at 4 °C up to 2 weeks.

5.4.3.4 Labeling DFO/Folate-Ad with ^{89}Zr

The labeling of ^{89}Zr was performed by mixing ^{89}Zr -oxalate (300 μCi , pH 7.7) with DFO/Folate-Ad (150 μL , 0.05 mg/mL, in PBS pH 7.4). Then, the mixture was incubated at RT and metal-complexation progress was monitored up to 2 h by radio TLC. Surprisingly, a perfect radiolabeling (100%) was observed with DFO/Folate-Ad in contrast to the control (0% labeling) as shown in Figure 5-11.

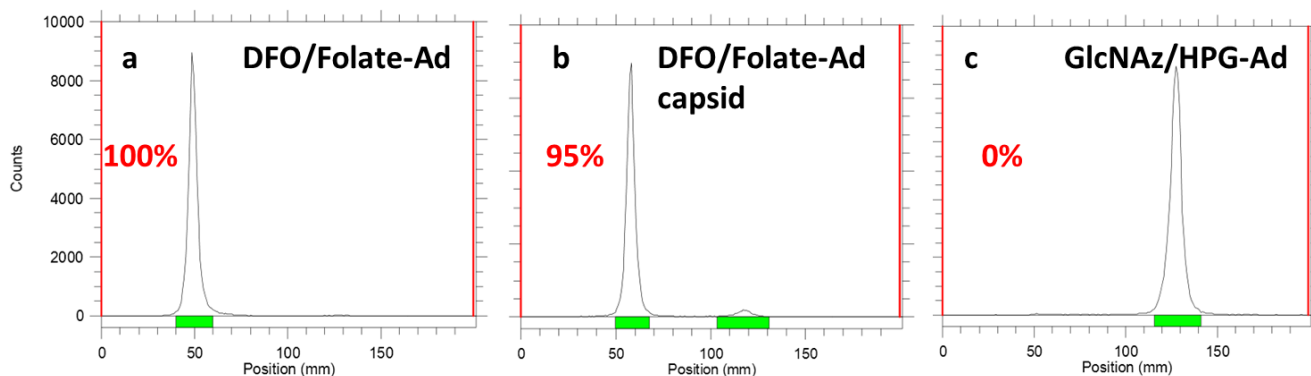


Figure 5-11. ^{89}Zr Labeling Monitored by radio TLC

^{89}Zr -complexation was up to 1 h by ITLC (silica-gel impregnated glass-fiber instant thin-layer chromatography, diethylenetriamine pentaacetate (DTPA), 50 mM, pH7), which shows crude radiolabeling yields and radiochemical purity (RCP). a) DFO/Folate-Ad: 100% RCP, b) DFO/Folate-Ad capsid: 95% RCP, and c) GlcNAz/HPG-Ad as a control: 0%.

5.5 Conclusion

In summary, with the aim of tracking Ad particles *in vivo* using real-time dynamic PET imaging, we attempted to introduce a variety of positron emitters onto viral capsid *via* “click” reactions such as CuAAC and SPAAC. First, in an effort to label Ad with a commonly used

positron emitter (^{18}F), a novel metal-free “clickable” ^{18}F -prosthetic group, BCN- ^{18}F fluorobenzamide, was synthesized and SPAAC was performed to label azide-enabled Ad (AHA-Ad) with BCN- ^{18}F -prosthetic group. However, the ^{18}F -labeled virion was not detected by radio TLC, probably due to the low solubility and specific activity of the new “clickable” prosthetic group. Second, in the context of labeling Ad with a longer-lived positron emitter, a novel bifunctional NOTA-BCN ligand was synthesized, which can chelate ^{64}Cu ($t_{1/2} = 12.7$ h) and conjugate AHA-Ad particles *via* SPAAC. After the metal-complexation, the retention of strained alkyne functionality was confirmed by characterizing the “clicked” product using mass spectrometry. The indispensability of additional HPLC purification to eliminate residual cytotoxic copper ions even after sub-micromolar scale metallation reactions, was reaffirmed by *in vitro* infection assays. Lastly, in order for the real-time dynamic tracking of cancer-targeting Ad vectors *in vivo* by PET, our dually modified, azide/alkyne-enabled-Ad (*O*-GlcNAz/HPG-Ad) was “clicked” with folate-Staudinger phosphine first *via* Staudinger ligation, to target the folate receptors on cancer cells, then DFO, the ligand for longer-lived positron emitter ^{89}Zr ($t_{1/2} = 78.4$ h), was conjugated onto Ad capsid *via* CuAAC. Astonishingly, folate/DFO-Ad showed 100% radiolabeling yield with ^{89}Zr . The *in vivo* PET imaging experiment will be performed in tumor-implanted mouse models in the near future.

5.6 Materials and methods

General

All chemical reagents were obtained from commercial sources and used without further purification unless otherwise noted. Human adenovirus serotype 5 (Ad5) containing luciferase transgene was obtained from Vector Biolabs (Ad5-CMV-Luc) (Philadelphia, PA). ^1H and ^{13}C -NMR data were obtained either using 300 MHz Varian Gemini 2300 or Oxford AS 400 MHz spectrometer, ESI-Mass spectra were obtained using an Agilent 1100 LC/MSD VL instrument and Matrix assisted laser desorption-ionization time of flight (MALDI-TOF) mass spectra were obtained on a Bruker Autoflex II mass spectrometer (Bremen Germany). HPLC was performed on Shimadzu LG-20AB / SPD-20A system with a C18 column (250×4.6 mm, Varian). Size exclusion separation (SEP) columns were purchased from GE Healthcare (NAP-5 column, Sephadex G-25 DNA grade) (Pittsburgh, PA) and SEP spin columns from Princeton Separations (Centri-Sep column CS-400) (Adelphia, NJ). Electrophoresis gels were scanned on a Typhoon 9400 fluorescent gel scanner and luciferase activity was measured on a photometer (PerkinElmer 2030 multilabel reader) with luciferase assay kit (Bright-Glo, Promega). For ^{18}F labeling, Radiochemical purity was also determined by thin layer chromatography (TLC) using and measuring radioactivity distribution on Macherey–Nagel polygram sil G/UV254 plastic-back TLC plate with Bioscan system 200 imaging scanner (Bioscan Inc., Washington, DC). For ^{89}Zr labeling, Radioactivity measurements were made by using a Capintec CRC-15R Dose Calibrator (Capintec, Ramsey, NJ) with a calibration factor of 465 for ^{89}Zr . For accurate quantification of radioactivities, experimental samples were counted for 1 min. on a calibrated Perkin Elmer (Waltham, MA) Automatic Wizard2 Gamma Counter by using a dynamic energy window of 800–1000 keV for ^{89}Zr (909 keV emission). ^{89}Zr -radiolabeling reactions were monitored by

using silica-gel impregnated glass-fiber instant thin-layer chromatography (ITLC-SG) paper (Pall Corp., East Hills, NY) and analyzed on a radio-TLC plate reader (Bioscan System 200 Imaging Scanner) coupled to a Bioscan Auto-changer 1000 (Bioscan Inc., Washington, DC, using Win-Scan Radio-TLC software version 2.2).

K₂₂₂/K[¹⁸F]F complex

No-carrier-added [¹⁸F]F⁻ was obtained through the nuclear reaction ¹⁸O(p, n)¹⁸F by irradiation of >95% ¹⁸O-enriched water with an 11 MeV proton beam using BNL EBCO TR-19 cyclotron (17.4 MeV) cyclotron. After the delivery of [¹⁸F]F⁻ from the cyclotron, the radioactivity was passed through a Sep-Pak light QMA cartridge to trap [¹⁸F]F⁻ ([¹⁸O]water was collected for recycling). [The Sep-Pak light QMA cartridge was pre-conditioned sequentially with 5 mL of 0.5 M potassium bicarbonate, 10 mL of deionized water, and 10 mL of acetonitrile before use.] The [¹⁸F]F⁻ was eluted with 1.5 mL of a solution prepared by mixing aqueous K₂CO₃ (0.11 g, 0.8 mmol in 1.0 mL of water) with Kryptofix 222(K₂₂₂) (0.60 g, 1.6 mmol in 19 mL of acetonitrile). The solvent was evaporated under a stream of argon at 120 °C. Azeotropic drying was repeated twice with 1 mL portions of MeCN to generate the anhydrous K₂₂₂/K[¹⁸F]F complex.

Synthesis of Ethyl 4-trimethylammoniumbenzoate trifluoromethanesulfonate (5-2)

Ethyl 4-trimethylammoniumbenzoate trifluoromethanesulfonate was synthesized according to the procedure reported by Hatanaka *et al.* [37]. *Scilicet*, ethyl 4-dimethylaminobenzoate 11.4 g (59 mmol) was dissolved in 70 mL anhydrous CH₂Cl₂. 10 g of CF₃SO₃CH₃ (64.9 mmol) was added dropwise to the solution, and the mixture was stirred overnight at RT. A crystalline precipitate was formed by the addition of Et₂O (100 mL) and collected by vacuum filtration.

Recrystallization from CH₂Cl₂/Et₂O afforded 10.6 g of product. (Yield: 50%). ¹H NMR (400MHz, CDCl₃): δ 8.23 (2H, m), 7.93 (2H, m), 4.39 (3H, q, *J* = 7.16 Hz), 3.77 (9H, s), 1.40 (3H, t, *J* = 7.16 Hz) ppm. ¹³C NMR (400MHz, CDCl₃): δ 164.4, 149.8, 132.7, 132.0, 120.0, 61.9, 57.3, 14.2 ppm.

Radiosynthesis of [¹⁸F]SFB (5-3)

[¹⁸F]SFB was prepared as described by Tang *et al.* [8] with some modifications. Briefly, ethyl 4-(trimethylammonium triflate)benzoate (5.0 mg, 20 μmol) in anhydrous DMSO (500 μL) was added to the dried K₂₂₂/K[¹⁸F]F and the mixture heated at 90 °C for 10 min to produce ethyl 4-[¹⁸F]fluorobenzoate and purified by a C18 Sep-Pak cartridge to remove unreacted reagents, that is, the reaction mixture was loaded on the cartridges and washed with water (10 mL), dried with air thrice, then eluted with MeCN (2 mL). The ethyl ester was subsequently hydrolyzed to form 4-[¹⁸F]fluorobenzoic acid using 20 μL of tetrapropylammonium hydroxide (1.0M in water) at 120 °C for 3 min in a sealed vial, and then the mixture was azeotropically dried using MeCN (1 mL). Subsequently, a solution of *N,N,N',N'*-tetramethyl-*O*-(*N*-succinimidyl)uronium tetrafluoroborate (TSTU) (12 mg, 33 μmol) in MeCN (500 μL) was added and the solution heated at 90 °C for 5 min in the sealed vial. After cooling, 5% aqueous acetic acid (9 mL) and water (15 mL) were added. The reaction mixture was passed through a C18 Sep-Pak cartridge to trap the [¹⁸F]SFB. The cartridges were washed with 10% aqueous MeCN (15 mL), dried with air thrice and then the product [¹⁸F]SFB eluted with MeCN (2 mL). The solvent was removed under a stream of argon at 60 °C to provide the dry [¹⁸F]SFB.

Radiosynthesis of BCN-[¹⁸F]fluorobenzamide (5-4)

(1R,8S,9r)-bicyclo[6.1.0]non-4-yn-9-ylmethyl 3,6,9-trioxa-12-azadodecylcarbamate (**4-1**) (3.0 mg, 9 μmol in anhydrous DMF 500 μL) which was synthesized as described by F. L. van Delft *et al.*[25] (*vid.* Chapter 4, Materials and methods), were added to the dried [¹⁸F]SFB residue. The mixture was allowed to react at RT for 15 min with 1.5 μL of triethylamine and then 4.5 mL of 0.2 M NaOH solution was added. After 2 min, the reaction mixture was filtered by 0.45 μm pore-sized membrane to remove unreacted excess reagents and loaded on C18 Sep-Pak cartridge, then washed with water (10 mL), dried with air thrice, and eluted with Et₂O (2mL). The solvent was removed under a stream of argon at 40 °C and re-purified by HPLC (isocratic 50% MeCN/water, 0.1% TFA with radiodetector and UV detector, λ = 220 nm) using C18 semi-Prep column (Jupiter, phenomenex) to provide BCN-[¹⁸F]fluorobenzamide.

SPAAC between BCN-[¹⁸F]fluorobenzamide and AHA-Ad

The HPLC eluate containing compound **5-4** was collected and loaded onto a C18 Sep-Pak cartridge and eluted with Et₂O (2 mL). The solvent was removed under a stream of argon at 40 °C and redissolved in 7.5 μL of DMSO, then radioactivity was measured (~300 μCi) and 142.5 μL of AHA-Ad (labeled in 32 mM AHA) stock was added. The reaction was monitored by radio TLC every 20 min up to 1 h.

Synthesis of NOTA-BCN (5-5)

4-1 (10 mg, 30.8 μmol) was dissolved in anhydrous DMF (200 μL) and added dropwise to the DMF solution (200 μL) of NOTA-Bn-NCS ·3HCl (17.1 mg, 30 μmol) with TEA (17 μL, 127 μmol) and allowed to react for overnight at RT, observing the appearance of a yellow color.

Dried *in vacuo* and re-dissolved in pH = 9 buffer with 10% MeCN and purified by HPLC (MeCN/H₂O gradient 5% ~ 50%, 0.1% TFA, UV detector at $\lambda=270$ nm) afforded 9.6 mg of product. Yield 40%. ESI m/z calcd for [M + H]⁺ 775.36, obsd 775.37 [M + H]⁺.

Cu(II) chelation with 5-5

CuCl₂·2H₂O (18.8 μ g (110 nmol) in 10 μ L of 0.1 M ammonium acetate Buffer, pH 7.5) was added to **5-5** (20 nmol, 15.5 μ g in 100 μ L of 0.1M ammonium acetate buffer, pH 7.5) and incubated for 30 min at RT. The reaction mixture was analyzed with TLC (MeOH/ 10% 0.1M ammonium acetate buffer = 1/1) and purified by HPLC (MeCN/H₂O gradient 5% ~ 50%, 0.1% TFA, UV detector at $\lambda=270$ nm)

Ga(III) chelation with 5-5

GaCl₃ (19.4 μ g (110 nmol) in 10 μ L of 0.1N HCl adjusted to pH 2.3) was added to **5-5** (20 nmole, 15.5 μ g in 100 μ L of ammonium acetate buffer, pH 7.5) and incubated for 10 min at RT. The reaction mixture was purified by HPLC (MeCN/H₂O gradient 5% ~ 50%, 0.1% TFA, UV detector at $\lambda=270$ nm).

“Click” reaction of Ga-NOTA-BCN with TAMRA-azide

After 10 min reaction of GaCl₃ and **5-5**, 20 μ L solution of 1.0 mM TAMRA-azide in MeOH was added and allowed to react for 20 min at RT, purified by HPLC (MeCN/H₂O gradient 5% ~ 50%,

0.1% TFA, UV detector at $\lambda=270$ nm). The product was characterized by MALDI-TOF m/z calculated for $[M+H]^+ = 1353.48$, observed for $[M+H]^+ = 1353.20$.

Infection Assays using Metal-Chelated-Ad with and without HPLC Purification

HEK 293 cells were seeded in 96-well black and clear bottom plates at a density of 1×10^4 cells/well, respectively, 1 day before infection. Virus stock was added to infection buffer (PBS, TC, and 2% serum) at a desired multiplicity of infection (MOI), the volume of virus stock needed was calculated by equations as followings, $MOI = PFU / \# \text{ of cells}$, $(PFU / \# \text{ of viral particles}) = 20$ for adenovirus, the volume of virus stock needed = $\# \text{ of viral particles needed} / \text{the titer of virus stock}$ (i.e., viral titer = $\# \text{ of viral particle/mL}$). Monolayer cells were washed with PBS and incubated in the infection buffer for 1 h at 37 °C. After 1 h, cell growth media were added and cells were incubated at 37 °C. 24 h post infection, the expression levels of luciferase transgene were determined by a photometer with the luciferase assay kit (Bright-Glo, Promega).

Synthesis of Folate-PEG-Staudinger phosphine (5-6)

Folic acid (161.3 mg, 365 μmol) was dissolved in anhydrous DMSO with 0.5 eq. *O*-(*N*-Succinimidyl)-1,1,3,3-tetramethyl uranium tetrafluoroborate (TSTU) and stirred for 1h, then 0.5 eq. of 1,8-diamino-3,6-dioxaoctane was added dropwise with TEA. The reaction was allowed to proceed at RT for 12 h and purified by HPLC (eluted btw. 10% ~ 20% MeCN/H₂O, 0.1% TFA, $\lambda = 370$ nm) and characterized by mass spectrometry. m/z cald. for $[M] = 571.25$, obsd. for $[M+H]^+ = 572.76$ Then, the purified folate-PEG-amine (2.6 mg, 4.5 μmol) was reacted with 2-(diphenylphosphino)terephthalic acid 1-methyl 4-pentafluorophenyl diester (5.0 mg, 9.0 μmol)

in anhydrous (important!) DMSO 500 μL with 10 μL of dry DIEA for 2 h under argon atmosphere and purified by HPLC (eluted btw. 35% ~ 50% MeCN/H₂O, 0.1% TFA, $\lambda = 370$ nm). The collected fractions were immediately frozen by liquid nitrogen and lyophilized. Stored at -80 °C. ¹H NMR (400MHz, (CD₃)₂SO): δ 8.63 (2H, m), 8.30 (2H, m), 7.95-7.88 (4H, m), 7.65-7.54 (6H, m), 7.42 (2H, m), 7.19 (1H, m), 6.29 (2H, s), 4.47 (2H, m), 4.03 (1H, m), 3.64-3.35 (5H, m), 2.88 (3H, m), 2.72 (2H, m), 2.66 (1H, m), 2.33-2.32 (1H, m), 2.07 (1H, m), 1.98 (1H, m), 1.75 (1H, m), 1.55 (2H, m), 1.23-1.04 (7H, m), 0.83 (2H, m) ppm. m/z calcd. for [M] = 917.33, obsd. for [M+H]⁺ = 918.86.

Synthesis of DFO-PEG-N₃

Azido-PEG₃-amine (5.1 μL , 26 μmol) was added to the solution of deferoxamine-Bn-isothiocyanate (DFO-p-SCN) (19.3 mg, 26 μmol in 0.5 mL dry DMSO) with DIEA 10 μL and allowed to react at RT for 12 h and purified by HPLC (eluted ~ 35% MeCN/H₂O, 0.1% TFA, $\lambda = 238$ nm). ¹H NMR (400MHz, (CD₃)₂SO): δ 9.62 (4H, m), 9.40 (1H, b), 7.77 (2H, m), 7.64 (2H, m), 7.34 (4H, s), 6.53 (1H, s), 5.75 (1H, s), 3.56-3.55 (8H, m), 3.00 (4H, m), 2.57 (4H, m), 2.26 (4H, m), 1.96 (3H, m), 1.51 (8H, m), 1.38 (4H, m), 1.23 (6H, m) ppm. m/z calcd. for [M] = 970.47, obsd. for [M+H]⁺ = 971.53

⁸⁹Zr Production

Zirconium-89 was produced via the ⁸⁹Y(*p,n*)⁸⁹Zr transmutation reaction on an EBCO TR19/9 variable beam energy cyclotron (EbcO Industries Inc., Richmond, British Columbia, Canada) in accordance with previously reported methods [44-45]. The ⁸⁹Zr-oxalate was isolated in high

radionuclidic and radiochemical purity (RCP) >99.9%, with an effective specific-activity of 195–497 MBq/μg, (5.28–13.43 mCi/μg) [44].

⁸⁹Zr Labelling of DFO/Folate-Ad

⁸⁹Zr-DFO/Folate-Ad was prepared by the metal-complexation of ⁸⁹Zr-oxalate with DFO/Folate-Ad. Typical radiolabeling reactions were conducted in accordance with the following procedure. Briefly, ⁸⁹Zr-oxalate (300 μCi) in 1.0 M oxalic acid (170 μL) was adjusted to pH 7.7–8.1 with 1.0 M Na₂CO₃(aq.). CAUTION: Acid neutralization releases CO₂(g) and care should be taken to ensure that no radioactivity escapes the microcentrifuge vial. After CO₂ evolution ceased, DFO/Folate-Ad (150 μL, 0.05 mg/mL, in PBS) was added and the reaction was mixed gently by aspirating with a pipette. The reaction was incubated at RT for between 1–2 h and metal-complexation progress was monitored with respect to time by ITLC (DTPA, 50 mM, pH7). After 1 h, crude radiolabeling yields and radiochemical purity (RCP) was assessed as ~100%.

References

1. Douglas, J. T.; Rogers, B. E.; Rosenfeld, M. E.; Michael, S. I.; Feng, M. Z.; Curiel, D. T., Targeted gene delivery by tropism-modified adenoviral vectors. *Nat. Biotechnol.* **1996**, *14* (11), 1574-1578.
2. Reynolds, P. N.; Zinn, K. R.; Gavrilyuk, V. D.; Balyasnikova, I. V.; Rogers, B. E.; Buchsbaum, D. J.; Wang, M. H.; Miletich, D. J.; Grizzle, W. E.; Douglas, J. T., A targetable, injectable adenoviral vector for selective gene delivery to pulmonary endothelium in vivo. *Mol. Ther.* **2000**, *2* (6), 562-578.
3. Shashkova, E. V.; Doronin, K.; Senac, J. S.; Barry, M. A., Macrophage depletion combined with anticoagulant therapy increases therapeutic window of systemic treatment with oncolytic adenovirus. *Cancer Res.* **2008**, *68* (14), 5896-5904.
4. Groot-Wassink, T.; Aboagye, E. O.; Wang, Y.; Lemoine, N. R.; Reader, A. J.; Vassaux, G., Quantitative Imaging of Na/I Symporter Transgene Expression Using Positron Emission Tomography in the Living Animal. *Mol. Ther.* **2004**, *9* (3), 436-442.
5. Gambhir, S. S.; Barrio, J. R.; Wu, L.; Iyer, M.; Namavari, M.; Satyamurthy, N.; Bauer, E.; Parrish, C.; MacLaren, D. C.; Borghei, A. R., Imaging of adenoviral-directed herpes simplex virus type 1 thymidine kinase reporter gene expression in mice with radiolabeled ganciclovir. *J. Nucl. Med.* **1998**, *39* (11), 2003.
6. Hofherr, S. E.; Adams, K. E.; Chen, C. Y.; May, S.; Weaver, E. A.; Barry, M. A., Real-Time Dynamic Imaging of Virus Distribution *In Vivo*. *PLoS One* **2011**, *6* (2), e17076.
7. Flexman, J. A.; Cross, D. J.; Lewellen, B. L.; Miyoshi, S.; Kim, Y.; Minoshima, S., Magnetically Targeted Viral Envelopes: A PET Investigation of Initial Biodistribution. *NanoBioscience, IEEE Transactions on* **2008**, *7* (3), 223-232.
8. Tang, G.; Zeng, W.; Yu, M.; Kabalka, G., Facile synthesis of *N*-succinimidyl 4-^[18F]fluorobenzoate (^[18F]SFB) for protein labeling. *J. Labelled Compd. Radiopharm.* **2008**, *51* (1), 68-71.
9. Glaser, M.; Årstad, E.; Luthra, S. K.; Robins, E. G., Two-step radiosynthesis of [^{18F}]N-succinimidyl-4-fluorobenzoate (^[18F]SFB). *J. Labelled Compd. Radiopharm.* **2009**, *52* (8), 327-330.
10. Scott, P. J. H.; Shao, X., Fully automated, high yielding production of *N*-succinimidyl 4-^[18F]fluorobenzoate (^[18F]SFB), and its use in microwave-enhanced radiochemical coupling reactions. *J. Labelled Compd. Radiopharm.* **2010**, *53* (9), 586-591.

11. Wester, H.-J.; Hamacher, K.; Stöcklin, G., A comparative study of N.C.A. Fluorine-18 labeling of proteins via acylation and photochemical conjugation. *Nucl. Med. Biol.* **1996**, *23* (3), 365-372.
12. Chigrinova, M.; Blake, J. A.; Pezacki, J. P., Kinetics studies of rapid strain-promoted [3+2]-cycloadditions of nitrones with biaryl-aza-cyclooctynone. *Org. Biomol. Chem.* **2012**, *10* (15), 3066-3070.
13. Presolski, S. I.; Hong, V.; Cho, S.-H.; Finn, M. G., Tailored Ligand Acceleration of the Cu-Catalyzed Azide–Alkyne Cycloaddition Reaction: Practical and Mechanistic Implications. *J. Am. Chem. Soc.* **2010**, *132* (41), 14570-14576.
14. Meldal, M.; Tornøe, C. W., Cu-Catalyzed Azide–Alkyne Cycloaddition. *Chem. Rev. (Washington, DC, U. S.)* **2008**, *108* (8), 2952-3015.
15. Glaser, M.; Robins, E. G., ‘Click labelling’ in PET radiochemistry. *J. Labelled Compd. Radiopharm.* **2009**, *52* (10), 407-414.
16. Marik, J.; Sutcliffe, J. L., Click for PET: rapid preparation of [¹⁸F]fluoropeptides using CuI catalyzed 1,3-dipolar cycloaddition. *Tetrahedron Lett.* **2006**, *47* (37), 6681-6684.
17. Glaser, M.; Årstad, E., “Click Labeling” with 2-[¹⁸F]Fluoroethylazide for Positron Emission Tomography. *Bioconjugate Chem.* **2007**, *18* (3), 989-993.
18. Arumugam, S.; Chin, J.; Schirmacher, R.; Popik, V. V.; Kostikov, A. P., [¹⁸F]Azadibenzocyclooctyne ([¹⁸F]ADIBO): A biocompatible radioactive labeling synthon for peptides using catalyst free [3+2] cycloaddition. *Bioorg. Med. Chem. Lett.* **2011**, *21* (23), 6987-6991.
19. Carpenter, R. D.; Hausner, S. H.; Sutcliffe, J. L., Copper-free click for PET: Rapid 1, 3-dipolar cycloadditions with a fluorine-18 cyclooctyne. *ACS Med. Chem. Lett.* **2011**, *2* (12), 885-889.
20. Sachin, K.; Jadhav, V. H.; Kim, E.-M.; Kim, H. L.; Lee, S. B.; Jeong, H.-J.; Lim, S. T.; Sohn, M.-H.; Kim, D. W., F-18 Labeling Protocol of Peptides Based on Chemically Orthogonal Strain-Promoted Cycloaddition under Physiologically Friendly Reaction Conditions. *Bioconjugate Chem.* **2012**, *23* (8), 1680-1686.
21. Debets, M. F.; van Berkel, S. S.; Schoffelen, S.; Rutjes, F. P. J. T.; van Hest, J. C. M.; van Delft, F. L., Aza-dibenzocyclooctynes for fast and efficient enzyme PEGylation via copper-free (3+2) cycloaddition. *Chem. Commun. (Cambridge, U. K.)* **2010**, *46* (1), 97.
22. Debets, M. F.; van Berkel, S. S.; Dommerholt, J.; Dirks, A. J.; Rutjes, F. P. J. T.; van Delft, F. L., Bioconjugation with Strained Alkenes and Alkynes. *Acc. Chem. Res.* **2011**, *44* (9), 805-815.

23. Selvaraj, R.; Liu, S.; Hassink, M.; Huang, C.-w.; Yap, L.-p.; Park, R.; Fox, J. M.; Li, Z.; Conti, P. S., Tetrazine-trans-cyclooctene ligation for the rapid construction of integrin $\alpha_v\beta_3$ targeted PET tracer based on a cyclic RGD peptide. *Bioorg. Med. Chem. Lett.* **2011**, *21* (17), 5011-5014.
24. Reiner, T.; Keliher, E. J.; Earley, S.; Marinelli, B.; Weissleder, R., Synthesis and *In Vivo* Imaging of a ^{18}F -Labeled PARP1 Inhibitor Using a Chemically Orthogonal Scavenger-Assisted High-Performance Method. *Angew. Chem., Int. Ed. Engl.* **2011**, *50* (8), 1922-1925.
25. Dommerholt, J.; Schmidt, S.; Temming, R.; Hendriks, L. J. A.; Rutjes, F. P. J. T.; van Hest, J. C. M.; Lefeber, D. J.; Friedl, P.; van Delft, F. L., Readily Accessible Bicyclononynes for Bioorthogonal Labeling and Three-Dimensional Imaging of Living Cells. *Angew. Chem., Int. Ed. Engl.* **2010**, *49* (49), 9422-9425.
26. Otsuka, F. L.; Welch, M. J.; Kilbourn, M. R.; Dence, C. S.; Dille, W. G.; Wells, S. A., Antibody fragments labeled with fluorine-18 and gallium-68: *In vivo* comparison with indium-111 and iodine-125-labeled fragments. *Int. J. Rad. Appl. Instrum. B* **1991**, *18* (7), 813-816.
27. Garg, P. K.; Garg, S.; Bigner, D. D.; Zalutsky, M. R., Localization of fluorine-18-labeled Mel-14 monoclonal antibody F (ab')₂ fragment in a subcutaneous xenograft model. *Cancer Res.* **1992**, *52* (18), 5054-5060.
28. Nayak, T. K.; Brechbiel, M. W., Radioimmunoimaging with Longer-Lived Positron-Emitting Radionuclides: Potentials and Challenges. *Bioconjugate Chem.* **2009**, *20* (5), 825-841.
29. Anderson, C. J.; Welch, M. J., Radiometal-Labeled Agents (Non-Technetium) for Diagnostic Imaging. *Chem. Rev. (Washington, DC, U. S.)* **1999**, *99* (9), 2219-2234.
30. Cole, W. C.; DeNardo, S. J.; Meares, C. F.; McCall, M. J.; DeNardo, G. L.; Epstein, A. L.; O'Brien, H. A.; Moi, M. K., Serum stability of ^{67}Cu chelates: comparison with ^{111}In and ^{57}Co . *Int. J. Rad. Appl. Instrum. B* **1986**, *13* (4), 363.
31. Woodin, K. S.; Heroux, K. J.; Boswell, C. A.; Wong, E. H.; Weisman, G. R.; Niu, W.; Tomellini, S. A.; Anderson, C. J.; Zakharov, L. N.; Rheingold, A. L., Kinetic Inertness and Electrochemical Behavior of Copper(II) Tetraazamacrocyclic Complexes: Possible Implications for *In Vivo* Stability. *Eur. J. Inorg. Chem.* **2005**, *2005* (23), 4829-4833.
32. Di Bartolo, N. M.; Sargeson, A. M.; Donlevy, T. M.; Smith, S. V., Synthesis of a new cage ligand, SarAr, and its complexation with selected transition metal ions for potential use in radioimaging. *J. Chem. Soc., Dalton Trans.* **2001**, (15), 2303-2309.

33. Prasanphanich, A. F.; Nanda, P. K.; Rold, T. L.; Ma, L.; Lewis, M. R.; Garrison, J. C.; Hoffman, T. J.; Sieckman, G. L.; Figueroa, S. D.; Smith, C. J., [⁶⁴Cu-NOTA-8-Aoc-BBN (7-14) NH₂] Targeting Vector for Positron-Emission Tomography Imaging of Gastrin-Releasing Peptide Receptor-Expressing Tissues. *Proc. Natl. Acad. Sci. U. S. A.* **2007**, 12462-12467.
34. Lang, L.; Li, W.; Guo, N.; Ma, Y.; Zhu, L.; Kiesewetter, D. O.; Shen, B.; Niu, G.; Chen, X., Comparison study of [¹⁸F] FAI-NOTA-PRGD₂, [¹⁸F] FPPRGD₂, and [⁶⁸Ga] Ga-NOTA-PRGD₂ for PET imaging of U87-MG tumors in mice. *Bioconjugate Chem.* **2011**, 22 (12), 2415-2422.
35. Alshoukr, F.; Prignon, A.; Brans, L.; Jallane, A.; Mendes, S.; Talbot, J. N.; Tourwé, D.; Barbet, J.; Gruaz-Guyon, A., Novel DOTA-neurotensin analogues for ¹¹¹In scintigraphy and ⁶⁸Ga PET imaging of neurotensin receptor-positive tumors. *Bioconjugate Chem.* **2011**, 22 (7), 1374-1385.
36. Jeong, J. M.; Hong, M. K.; Chang, Y. S.; Lee, Y.-S.; Kim, Y. J.; Cheon, G. J.; Lee, D. S.; Chung, J.-K.; Lee, M. C., Preparation of a Promising Angiogenesis PET Imaging Agent: ⁶⁸Ga-Labeled c(RGDyK)-Isothiocyanatobenzyl-1,4,7-Triazacyclononane-1,4,7-Triacetic Acid and Feasibility Studies in Mice. *J. Nucl. Med.* **2008**, 49 (5), 830-836.
37. Hatanaka, K.; Asai, T.; Koide, H.; Kenjo, E.; Tsuzuku, T.; Harada, N.; Tsukada, H.; Oku, N., Development of double-stranded siRNA labeling method using positron emitter and its in vivo trafficking analyzed by positron emission tomography. *Bioconjugate Chem.* **2010**, 21 (4), 756-763.
38. Banerjee, P. S.; Ostapchuk, P.; Hearing, P.; Carrico, I. S., Unnatural Amino Acid Incorporation onto Adenoviral (Ad) Coat Proteins Facilitates Chemoselective Modification and Retargeting of Ad Type 5 Vectors. *J. Virol.* **2011**, 85 (15), 7546-7554.
39. Chang, P. V.; Prescher, J. A.; Sletten, E. M.; Baskin, J. M.; Miller, I. A.; Agard, N. J.; Lo, A.; Bertozzi, C. R., Copper-free click chemistry in living animals. *Proc. Natl. Acad. Sci. U. S. A.* **2010**, 107 (5), 1821-1826.
40. Li, Z. B.; Chen, K.; Chen, X., ⁶⁸Ga-labeled multimeric RGD peptides for microPET imaging of integrin $\alpha_v\beta_3$ expression. *Eur. J. Nucl. Med. Mol. Imaging* **2008**, 35 (6), 1100-1108.
41. Liu, Z.; Niu, G.; Shi, J.; Liu, S.; Wang, F.; Chen, X., ⁶⁸Ga-labeled cyclic RGD dimers with Gly3 and PEG4 linkers: promising agents for tumor integrin $\alpha_v\beta_3$ PET imaging. *Eur. J. Nucl. Med. Mol. Imaging* **2009**, 36 (6), 947-957.
42. Banerjee, P. S.; Zuniga, E. S.; Ojima, I.; Carrico, I. S., Targeted and armed oncolytic adenovirus via chemoselective modification. *Bioorg. Med. Chem. Lett.* **2011**, 21 (17), 4985-4988.

43. Banerjee, P. S.; Ostapchuk, P.; Hearing, P.; Carrico, I., Chemoselective Attachment of Small Molecule Effector Functionality to Human Adenoviruses Facilitates Gene Delivery to Cancer Cells. *J. Am. Chem. Soc.* **2010**, *132* (39), 13615-13617.
44. Holland, J. P.; Sheh, Y.; Lewis, J. S., Standardized methods for the production of high specific-activity zirconium-89. *Nucl. Med. Biol.* **2009**, *36* (7), 729-739.
45. Verel, I.; Visser, G. W. M.; Boellaard, R.; Stigter-van Walsum, M.; Snow, G. B.; van Dongen, G. A. M. S., ⁸⁹Zr Immuno-PET: Comprehensive Procedures for the Production of ⁸⁹Zr-Labeled Monoclonal Antibodies. *J. Nucl. Med.* **2003**, *44* (8), 1271-1281.

General Conclusion and Future Direction

In summary, we have demonstrated that metabolically incorporated chemical handles such as unnatural sugars and/or amino acids can be facilely harnessed to retarget adenoviral vectors onto cancer cells and monitor the biodistribution of viral particles *via* Cu(I)- or strain-promoted “click chemistry” and corresponding reagents. Moreover, this strategy is readily expandable to other viral vectors and applications such as immunotherapy, requiring only minor modifications of Ad production protocol.

A few challenges remain in this strategy. First, the heterogeneous population of modified virions could be an issue for a clinical trial as in the case of simple chemical conjugation. Second, detargeting from native viral tropism still represents a critical hurdle particularly for *in vivo* studies, which could be addressed by the combination of a number of previously developed genetic and chemical detargeting approaches. However, those detargeting methods could also affect viral production methods and physiology, undermining the utility of our approach. Third, copper toxicity of CuAAC and low efficiency of SPAAC are caveats to be improved for *in vivo* applications. Thus, employing better bioorthogonal reactions should be a continuous effort.

One of the major advantages of our strategy is the facile conjugations of different targeting motifs without losing their biological activities, which cannot be easily achieved by genetic approach. Hence, interesting future directions include multi-component approaches for cancer targeting and vaccine development. Many tumors are known to be very heterogeneous and contain multiple cell types originated from the host organ. Therefore, the vector armed with multi-components against distinct cell surface receptors could increase the efficiency of gene delivery to target area.

An immune reaction is the major hurdle for gene delivery vectors, but ironically is the desired response for vaccine scaffolds. Therefore, conceptually, the least efficient gene delivery vectors could be a promising candidate as vaccine scaffolds. Recently, to overcome the drawbacks associated with conventional approaches such as a transgene expression of antigen, new strategies involving “antigen capsid-incorporation” and "multi-component" have been developed. In this context, our strategy could be applied to this field, which grants versatility and flexibility in terms of epitope conjugation on viral surfaces in a residue specific or site specific manner. Moreover, when combined with stochastic screening of multi-epitope displaying vectors and mass spectrometry-based proteomics, our approach could provide information about the best combination and optimal insertion site of epitopes with enhanced efficiency.

Bibliography

1. Flint, S. J.; Enquist, L. W.; Racaniello, V. R.; Skalka, A. M., *Principles of virology*. ASM Press: Washington, DC, **2009**.
2. Baselga, J.; Swain, S. M., Novel anticancer targets: revisiting ERBB2 and discovering ERBB3. *Nat. Rev. Cancer* **2009**, *9* (7), 463-475.
3. Victor N. Krasnykh, J. T. D., Victor W. van Beusechem, Genetic Targeting of Adenoviral Vectors. *Mol. Ther.* **2000**, *1* (5), 391-405.
4. Vocadlo, D. J.; Hang, H. C.; Kim, E. J.; Hanover, J. A.; Bertozzi, C. R., A chemical approach for identifying O-GlcNAc-modified proteins in cells. *Proc. Natl. Acad. Sci. U. S. A.* **2003**, *100* (16), 9116-9121.
5. Curiel, D. T.; Douglas, J. T., Adenoviral vectors for gene therapy. 2002; p 165.
6. Boyce, M.; Carrico, I. S.; Ganguli, A. S.; Yu, S.-H.; Hangauer, M. J.; Hubbard, S. C.; Kohler, J. J.; Bertozzi, C. R., Metabolic cross-talk allows labeling of O-linked β -N-acetylglucosamine-modified proteins via the N-acetylgalactosamine salvage pathway. *Proc. Natl. Acad. Sci. U. S. A.* **2011**, *108* (8), 3141-3146.
7. *Report and Recommendations of the Gene Therapy Working Group*; National Institutes of Health: Bethesda, Maryland, November 1, 2005.
8. Stuart H. Orkin, A. G. M. *Report and recommendations of the panel to assess the NIH investment in research gene therapy*; National Institutes of Health: December 7, 1995.
9. Hitt, M. M.; Addison, C. L.; Graham, F. L., Human adenovirus vectors for gene transfer into mammalian cells. *Adv Pharmacol* **1997**, *40*, 137-206.
10. Graham, F. L.; Prevec, L., Methods for construction of adenovirus vectors. *Mol. Biotechnol.* **1995**, *3* (3), 207-20.
11. Yeh, P.; Perricaudet, M., Advances in adenoviral vectors: from genetic engineering to their biology. *FASEB J.* **1997**, *11* (8), 615-623.
12. Toth, K.; Dhar, D.; Wold, W. S., Oncolytic (replication-competent) adenoviruses as anticancer agents. *Expert Opin. Biol. Ther.* **2010**, *10* (3), 353-368.
13. Cervantes-García, D.; Ortiz-López, R.; Mayek-Pérez, N.; Rojas-Martínez, A., Oncolytic virotherapy. *Ann. Hepatol* **2008**, *7*, 34-45.

14. Rux, J. J.; Burnett, R. M., Adenovirus Structure. *Hum. Gene Ther.* **2004**, *15* (12), 1167-1176.
15. Stewart, P. L.; Burnett, R. M.; Cyrklaff, M.; Fuller, S. D., Image reconstruction reveals the complex molecular organization of adenovirus. *Cell* **1991**, *67* (1), 145-154.
16. Reddy, V. S.; Natchiar, S. K.; Stewart, P. L.; Nemerow, G. R., Crystal Structure of Human Adenovirus at 3.5 Å Resolution. *Science* **2010**, *329* (5995), 1071-1075.
17. Saban, S.; Silvestry, M.; Nemerow, G.; Stewart, P., Visualization of α -helices in a 6 Å resolution cryoEM structure of adenovirus allows refinement of capsid protein assignments. *J. Virol.* **2006**, *80*, 12049-12059.
18. Norrby, E.; van der Veen, J.; Espmark, A., A new serological technique for identification of adenovirus infections. *Proc. Soc. Exp. Biol. Med.* **1970**, *134* (3), 889-95.
19. Belousova, N.; Mikheeva, G.; Gelovani, J.; Krasnykh, V., Modification of Adenovirus Capsid with a Designed Protein Ligand Yields a Gene Vector Targeted to a Major Molecular Marker of Cancer. *J. Virol.* **2008**, *82* (2), 630-637.
20. Zhang, Y.; Bergelson, J. M., Adenovirus receptors. *J. Virol.* **2005**, *79* (19), 12125-12131.
21. Arnberg, N., Adenovirus receptors: implications for tropism, treatment and targeting. *Rev. Med. Virol.* **2009**, *19* (3), 165-178.
22. Dehecchi, M. C.; Tamanini, A.; Bonizzato, A.; Cabrini, G., Heparan sulfate glycosaminoglycans are involved in adenovirus type 5 and 2-host cell interactions. *Virology* **2000**, *268* (2), 382-390.
23. Parker, A. L.; Waddington, S. N.; Nicol, C. G.; Shayakhmetov, D. M.; Buckley, S. M.; Denby, L.; Kembell-Cook, G.; Ni, S.; Lieber, A.; McVey, J. H., Multiple vitamin K-dependent coagulation zymogens promote adenovirus-mediated gene delivery to hepatocytes. *Blood* **2006**, *108* (8), 2554-2561.
24. Waddington, S. N.; McVey, J. H.; Bhella, D.; Parker, A. L.; Barker, K.; Atoda, H.; Pink, R.; Buckley, S. M. K.; Greig, J. A.; Denby, L.; Custers, J.; Morita, T.; Francischetti, I. M. B.; Monteiro, R. Q.; Barouch, D. H.; van Rooijen, N.; Napoli, C.; Havenga, M. J. E.; Nicklin, S. A.; Baker, A. H., Adenovirus Serotype 5 Hexon Mediates Liver Gene Transfer. *Cell* **2008**, *132* (3), 397-409.
25. Haisma, H. J.; Boesjes, M.; Beerens, A. M.; van der Strate, B. W. A.; Curiel, D. T.; Plüddemann, A.; Gordon, S.; Bellu, A. R., Scavenger Receptor A: A New Route for Adenovirus 5. *Mol. Pharm.* **2009**, *6* (2), 366-374.
26. Blumenthal, R.; Seth, P.; Willingham, M. C.; Pastan, I., pH-dependent lysis of liposomes by adenovirus. *Biochemistry* **1986**, *25* (8), 2231-2237.

27. Greber, U. F.; Willetts, M.; Webster, P.; Helenius, A., Stepwise dismantling of adenovirus 2 during entry into cells. *Cell* **1993**, *75* (3), 477-486.
28. Wickham, T. J.; Filardo, E. J.; Cheresch, D. A.; Nemerow, G. R., Integrin alpha v beta 5 selectively promotes adenovirus mediated cell membrane permeabilization. *J. Cell Biol.* **1994**, *127* (1), 257-264.
29. Strunze, S.; Trotman, L. C.; Boucke, K.; Greber, U. F., Nuclear Targeting of Adenovirus Type 2 Requires CRM1-mediated Nuclear Export. *Mol. Biol. Cell* **2005**, *16* (6), 2999-3009.
30. Bewley, M. C.; Springer, K.; Zhang, Y.-B.; Freimuth, P.; Flanagan, J. M., Structural Analysis of the Mechanism of Adenovirus Binding to Its Human Cellular Receptor, CAR. *Science* **1999**, *286* (5444), 1579-1583.
31. Howitt, J.; Bewley, M. C.; Graziano, V.; Flanagan, J. M.; Freimuth, P., Structural Basis for Variation in Adenovirus Affinity for the Cellular Coxsackievirus and Adenovirus Receptor. *J. Biol. Chem.* **2003**, *278* (28), 26208-26215.
32. Chiu, C. Y.; Wu, E.; Brown, S. L.; Von Seggern, D. J.; Nemerow, G. R.; Stewart, P. L., Structural Analysis of a Fiber-Pseudotyped Adenovirus with Ocular Tropism Suggests Differential Modes of Cell Receptor Interactions. *J. Virol.* **2001**, *75* (11), 5375-5380.
33. Zubieta, C.; Schoehn, G.; Chroboczek, J.; Cusack, S., The Structure of the Human Adenovirus 2 Penton. *Mol. Cell* **2005**, *17* (1), 121-135.
34. Chiu, C. Y.; Wu, E.; Brown, S. L.; Von Seggern, D. J.; Nemerow, G. R.; Stewart, P. L., Structural analysis of a fiber-pseudotyped adenovirus with ocular tropism suggests differential modes of cell receptor interactions. *J. Virol.* **2001**, *75* (11), 5375-5380.
35. Raper, S. E.; Chirmule, N.; Lee, F. S.; Wivel, N. A.; Bagg, A.; Gao, G.-p.; Wilson, J. M.; Batshaw, M. L., Fatal systemic inflammatory response syndrome in a ornithine transcarbamylase deficient patient following adenoviral gene transfer. *Mol. Genet. Metab.* **2003**, *80* (1-2), 148-158.
36. O'Riordan, C. R.; Lachapelle, A.; Delgado, C.; Parkes, V.; Wadsworth, S. C.; Smith, A. E.; Francis, G. E., PEGylation of adenovirus with retention of infectivity and protection from neutralizing antibody in vitro and in vivo. *Hum. Gene Ther.* **1999**, *10* (8), 1349-1358.
37. Magnusson, M. K.; Hong, S. S.; Boulanger, P.; Lindholm, L., Genetic Retargeting of Adenovirus: Novel Strategy Employing "Deknobbing" of the Fiber. *J. Virol.* **2001**, *75* (16), 7280-7289.

38. Magnusson, M. K.; See Hong, S.; Henning, P.; Boulanger, P.; Lindholm, L., Genetic retargeting of adenovirus vectors: functionality of targeting ligands and their influence on virus viability. *J. Gene Med.* **2002**, *4* (4), 356-370.
39. Henning, P.; Lundgren, E.; Carlsson, M.; Frykholm, K.; Johannisson, J.; Magnusson, M. K.; Tång, E.; Franqueville, L.; Hong, S. S.; Lindholm, L.; Boulanger, P., Adenovirus type 5 fiber knob domain has a critical role in fiber protein synthesis and encapsidation. *J. Gen. Virol.* **2006**, *87* (11), 3151-3160.
40. Magnusson, M. K.; Henning, P.; Myhre, S.; Wikman, M.; Uil, T. G.; Friedman, M.; Andersson, K. M. E.; Hong, S. S.; Hoeben, R. C.; Habib, N. A.; Stahl, S.; Boulanger, P.; Lindholm, L., Adenovirus 5 vector genetically re-targeted by an Affibody molecule with specificity for tumor antigen HER2//neu. *Cancer Gene Ther.* **2007**, *14* (5), 468-479.
41. Douglas, J. T.; Rogers, B. E.; Rosenfeld, M. E.; Michael, S. I.; Feng, M. Z.; Curiel, D. T., Targeted gene delivery by tropism-modified adenoviral vectors. *Nat. Biotechnol.* **1996**, *14* (11), 1574-1578.
42. Kreppel, F.; Gackowski, J.; Schmidt, E.; Kochanek, S., Combined genetic and chemical capsid modifications enable flexible and efficient de- and retargeting of adenovirus vectors. *Mol. Ther.* **2005**, *12* (1), 107-17.
43. Belousova, N.; Mikheeva, G.; Gelovani, J.; Krasnykh, V., Modification of adenovirus capsid with a designed protein ligand yields a gene vector targeted to a major molecular marker of cancer. *J. Virol.* **2008**, *82* (2), 630-7.
44. Haismaa, H. J.; Kamps, G. K.; Boumaa, A.; Geelb, T. M.; Rotsb, M. G.; Kariatha, A.; Bellua, A. R., Selective targeting of adenovirus to $\alpha_v\beta_3$ integrins, VEGFR2 and Tie2 endothelial receptors by angio-adenobodies. *Int. J. Pharm.* **2010**, *391*, 155-161.
45. Watkins, S.; Mesyanzhinov, V.; Kurochkina, L.; Hawkins, R., The 'adenobody' approach to viral targeting: specific and enhanced adenoviral gene delivery. *Gene Ther.* **1997**, *4* (10), 1004.
46. Dmitriev, I.; Kashentseva, E.; Rogers, B. E.; Krasnykh, V.; Curiel, D. T., Ectodomain of coxsackievirus and adenovirus receptor genetically fused to epidermal growth factor mediates adenovirus targeting to epidermal growth factor receptor-positive cells. *J. Virol.* **2000**, *74* (15), 6875-6884.
47. Li, E.; Brown, S.; Von Seggern, D.; Brown, G.; Nemerow, G., Signaling antibodies complexed with adenovirus circumvent CAR and integrin interactions and improve gene delivery. *Gene Ther.* **2000**, *7* (18), 1593.
48. Kolb, H. C.; Finn, M. G.; Sharpless, K. B., Click Chemistry: Diverse Chemical Function from a Few Good Reactions. *Angew. Chem., Int. Ed. Engl.* **2001**, *40* (11), 2004-2021.

49. Rostovtsev, V. V.; Green, L. G.; Fokin, V. V.; Sharpless, K. B., A Stepwise Huisgen Cycloaddition Process: Copper(I)-Catalyzed Regioselective “Ligation” of Azides and Terminal Alkynes. *Angew. Chem., Int. Ed. Engl.* **2002**, *114* (14), 2708-2711.
50. Tornøe, C. W.; Christensen, C.; Meldal, M., Peptidotriazoles on Solid Phase: [1,2,3]-Triazoles by Regiospecific Copper(I)-Catalyzed 1,3-Dipolar Cycloadditions of Terminal Alkynes to Azides. *J. Org. Chem.* **2002**, *67* (9), 3057-3064.
51. Lemieux, G. A.; Bertozzi, C. R., Chemoselective ligation reactions with proteins, oligosaccharides and cells. *Trends Biotechnol.* **1998**, *16* (12), 506-513.
52. Prescher, J. A.; Bertozzi, C. R., Chemistry in living systems. *Nat. Chem. Biol.* **2005**, *1*, 13-21.
53. Chigrinova, M.; Blake, J. A.; Pezacki, J. P., Kinetics studies of rapid strain-promoted [3+2]-cycloadditions of nitrones with biaryl-aza-cyclooctynone. *Org. Biomol. Chem.* **2012**, *10* (15), 3066-3070.
54. Presolski, S. I.; Hong, V.; Cho, S.-H.; Finn, M. G., Tailored Ligand Acceleration of the Cu-Catalyzed Azide–Alkyne Cycloaddition Reaction: Practical and Mechanistic Implications. *J. Am. Chem. Soc.* **2010**, *132* (41), 14570-14576.
55. Arumugam, S.; Chin, J.; Schirmmacher, R.; Popik, V. V.; Kostikov, A. P., [¹⁸F]Azadibenzocyclooctyne ([¹⁸F]ADIBO): A biocompatible radioactive labeling synthon for peptides using catalyst free [3+2] cycloaddition. *Bioorg. Med. Chem. Lett.* **2011**, *21* (23), 6987-6991.
56. Carpenter, R. D.; Hausner, S. H.; Sutcliffe, J. L., Copper-free click for PET: Rapid 1, 3-dipolar cycloadditions with a fluorine-18 cyclooctyne. *ACS Med. Chem. Lett.* **2011**, *2* (12), 885-889.
57. Sachin, K.; Jadhav, V. H.; Kim, E.-M.; Kim, H. L.; Lee, S. B.; Jeong, H.-J.; Lim, S. T.; Sohn, M.-H.; Kim, D. W., F-18 Labeling Protocol of Peptides Based on Chemically Orthogonal Strain-Promoted Cycloaddition under Physiologically Friendly Reaction Conditions. *Bioconjugate Chem.* **2012**, *23* (8), 1680-1686.
58. Debets, M. F.; van Berkel, S. S.; Schoffelen, S.; Rutjes, F. P. J. T.; van Hest, J. C. M.; van Delft, F. L., Aza-dibenzocyclooctynes for fast and efficient enzyme PEGylation via copper-free (3+2) cycloaddition. *Chem. Commun. (Cambridge, U. K.)* **2010**, *46* (1), 97.
59. Debets, M. F.; van Berkel, S. S.; Dommerholt, J.; Dirks, A. J.; Rutjes, F. P. J. T.; van Delft, F. L., Bioconjugation with Strained Alkenes and Alkynes. *Acc. Chem. Res.* **2011**, *44* (9), 805-815.
60. Chen, I.; Howarth, M.; Lin, W.; Ting, A. Y., Site-specific labeling of cell surface proteins with biophysical probes using biotin ligase. *Nat. Methods* **2005**, *2*, 99-104.

61. Zhang, Z.; Smith, B. A. C.; Wang, L.; Brock, A.; Cho, C.; Schultz, P. G., A new strategy for the site-specific modification of proteins in vivo. *Biochemistry* **2003**, *42* (22), 6735-6746.
62. Mahal, L. K.; Yarema, K. J.; Bertozzi, C. R., Engineering chemical reactivity on cell surfaces through oligosaccharide biosynthesis. *Science* **1997**, *276* (5315), 1125-1128.
63. Saxon, E.; Bertozzi, C. R., Cell Surface Engineering by a Modified Staudinger Reaction. *Science* **2000**, *287* (5460), 2007.
64. Jewett, J. C.; Sletten, E. M.; Bertozzi, C. R., Rapid Cu-Free Click Chemistry with Readily Synthesized Biarylazacyclooctynones. *J. Am. Chem. Soc.* **2010**, *132* (11), 3688-3690.
65. Sletten, E. M.; Nakamura, H.; Jewett, J. C.; Bertozzi, C. R., Difluorobenzocyclooctyne: Synthesis, Reactivity, and Stabilization by β -Cyclodextrin. *J. Am. Chem. Soc.* **2010**, *132* (33), 11799-11805.
66. Dommerholt, J.; Schmidt, S.; Temming, R.; Hendriks, L. J. A.; Rutjes, F. P. J. T.; van Hest, J. C. M.; Lefeber, D. J.; Friedl, P.; van Delft, F. L., Readily Accessible Bicyclononynes for Bioorthogonal Labeling and Three-Dimensional Imaging of Living Cells. *Angew. Chem., Int. Ed. Engl.* **2010**, *49* (49), 9422-9425.
67. van Berkel, S. S.; Dirks, A. J.; Debets, M. F.; van Delft, F. L.; Cornelissen, J. J. L. M.; Nolte, R. J. M.; Rutjes, F. P. J. T., Metal-Free Triazole Formation as a Tool for Bioconjugation. *ChemBioChem* **2007**, *8* (13), 1504-1508.
68. Ning, X.; Temming, R. P.; Dommerholt, J.; Guo, J.; Ania, D. B.; Debets, M. F.; Wolfert, M. A.; Boons, G.-J.; van Delft, F. L., Protein Modification by Strain-Promoted Alkyne-Nitrone Cycloaddition. *Angew. Chem., Int. Ed. Engl.* **2010**, *49* (17), 3065-3068.
69. Gutmiedl, K.; Wirges, C. T.; Ehmke, V.; Carell, T., Copper-Free "Click" Modification of DNA via Nitrile Oxide-Norbornene 1,3-Dipolar Cycloaddition. *Org. Lett.* **2009**, *11* (11), 2405-2408.
70. Blackman, M. L.; Royzen, M.; Fox, J. M., Tetrazine Ligation: Fast Bioconjugation Based on Inverse-Electron-Demand Diels-Alder Reactivity. *J. Am. Chem. Soc.* **2008**, *130* (41), 13518-13519.
71. Devaraj, N. K.; Weissleder, R.; Hilderbrand, S. A., Tetrazine-based cycloadditions: application to pretargeted live cell imaging. *Bioconjugate Chem.* **2008**, *19* (12), 2297.
72. Yang, J.; Šečkutè, J.; Cole, C. M.; Devaraj, N. K., Live-Cell Imaging of Cyclopropene Tags with Fluorogenic Tetrazine Cycloadditions. *Angew. Chem.* **2012**, *124* (30), 7594-7597.

73. Stockmann, H.; Neves, A. A.; Stairs, S.; Brindle, K. M.; Leeper, F. J., Exploring isonitrile-based click chemistry for ligation with biomolecules. *Org. Biomol. Chem.* **2011**, *9* (21), 7303-7305.
74. Sletten, E. M.; Bertozzi, C. R., A Bioorthogonal Quadricyclane Ligation. *J. Am. Chem. Soc.* **2011**, *133* (44), 17570-17573.
75. Weisbrod, S. H.; Marx, A., Novel strategies for the site-specific covalent labelling of nucleic acids. *Chem. Commun. (Cambridge, U. K.)* **2008**, (44), 5675-5685.
76. Sletten, E. M.; Bertozzi, C. R., Bioorthogonal chemistry: fishing for selectivity in a sea of functionality. *Angew. Chem., Int. Ed. Engl.* **2009**, *48* (38), 6974-6998.
77. Fernandez-Suarez, M.; Baruah, H.; Martinez-Hernandez, L.; Xie, K. T.; Baskin, J. M.; Bertozzi, C. R.; Ting, A. Y., Redirecting lipoic acid ligase for cell surface protein labeling with small-molecule probes. *Nat Biotech* **2007**, *25* (12), 1483-1487.
78. Ochiai, H.; Huang, W.; Wang, L.-X., Expedient Chemoenzymatic Synthesis of Homogeneous N-Glycoproteins Carrying Defined Oligosaccharide Ligands. *J. Am. Chem. Soc.* **2008**, *130* (41), 13790-13803.
79. Lapinsky, D. J., Tandem photoaffinity labeling–bioorthogonal conjugation in medicinal chemistry. *Bioorg. Med. Chem.* **2012**, *20* (21), 6237-6247.
80. Dieterich, D. C.; Link, A. J.; Graumann, J.; Tirrell, D. A.; Schuman, E. M., Selective identification of newly synthesized proteins in mammalian cells using bioorthogonal noncanonical amino acid tagging (BONCAT). *Proc. Natl. Acad. Sci. U. S. A.* **2006**, *103* (25), 9482-9487.
81. Dube, D. H.; Bertozzi, C. R., Metabolic oligosaccharide engineering as a tool for glycobiology. *Curr. Opin. Chem. Biol.* **2003**, *7* (5), 616-625.
82. Johnson, J. A.; Lu, Y. Y.; Van Deventer, J. A.; Tirrell, D. A., Residue-specific incorporation of non-canonical amino acids into proteins: recent developments and applications. *Curr. Opin. Chem. Biol.* **2010**, *14* (6), 774-780.
83. Dieterich, D. C.; Lee, J. J.; Link, A. J.; Graumann, J.; Tirrell, D. A.; Schuman, E. M., Labeling, detection and identification of newly synthesized proteomes with bioorthogonal non-canonical amino-acid tagging. *Nat. Protoc.* **2007**, *2* (3), 532-540.
84. Prescher, J. A.; Bertozzi, C. R., Chemistry in living systems. *Nat. Chem. Biol.* **2005**, *1* (1), 13-21.
85. Mahal, L. K.; Yarema, K. J.; Bertozzi, C. R., Engineering Chemical Reactivity on Cell Surfaces Through Oligosaccharide Biosynthesis. *Science* **1997**, *276* (5315), 1125.

86. Hang, H. C.; Yu, C.; Kato, D. L.; Bertozzi, C. R., A metabolic labeling approach toward proteomic analysis of mucin-type O-linked glycosylation. *Proc. Natl. Acad. Sci. U. S. A.* **2003**, *100* (25), 14846-14851.
87. Banerjee, P. S.; Ostapchuk, P.; Hearing, P.; Carrico, I., Chemoselective Attachment of Small Molecule Effector Functionality to Human Adenoviruses Facilitates Gene Delivery to Cancer Cells. *J. Am. Chem. Soc.* **2010**, *132* (39), 13615-13617.
88. Banerjee, P. S.; Zuniga, E. S.; Ojima, I.; Carrico, I. S., Targeted and armed oncolytic adenovirus via chemoselective modification. *Bioorg. Med. Chem. Lett.* **2011**, *21* (17), 4985-4988.
89. Cauet, G.; Strub, J. M.; Leize, E.; Wagner, E.; Van Dorselaer, A.; Lusky, M., Identification of the glycosylation site of the adenovirus type 5 fiber protein. *Biochemistry* **2005**, *44* (14), 5453-5460.
90. Banerjee, P. S.; Ostapchuk, P.; Hearing, P.; Carrico, I. S., Unnatural Amino Acid Incorporation onto Adenoviral (Ad) Coat Proteins Facilitates Chemoselective Modification and Retargeting of Ad Type 5 Vectors. *J. Virol.* **2011**, *85* (15), 7546-7554.
91. Banerjee, P. S. Development of novel gene therapy vectors via metabolic labeling and chemoselective modification of adenovirus capsid. State University of New York at Stony Brook, 2011.
92. Roth, S.; Thomas, N. R., A concise route to L-azidoamino acids: L-azidoalanine, L-azidohomoalanine and L-azidonorvaline. *Synlett* **2010**, *2010* (4), 607.
93. Mateu, M. G., Virus engineering: functionalization and stabilization. *Protein Eng., Des. Sel.* **2011**, *24* (1-2), 53-63.
94. Asokan, A.; Conway, J. C.; Phillips, J. L.; Li, C.; Hegge, J.; Sinnott, R.; Yadav, S.; DiPrimio, N.; Nam, H. J.; Agbandje-McKenna, M., Reengineering a receptor footprint of adeno-associated virus enables selective and systemic gene transfer to muscle. *Nat. Biotechnol.* **2009**, *28* (1), 79-82.
95. Palucha, A.; Loniewska, A.; Satheshkumar, S.; Boguszewska-Chachulska, A. M.; Umashankar, M.; Milner, M.; Haenni, A. L.; Savithri, H. S., Virus-Like Particles: Models for Assembly Studies and Foreign Epitope Carriers. *Prog. Nucleic Acid Res. Mol. Biol.* **2005**, *80*, 135-168.
96. Inoue, T.; Kawano, M.; Takahashi, R.; Tsukamoto, H.; Enomoto, T.; Imai, T.; Kataoka, K.; Handa, H., Engineering of SV40-based nano-capsules for delivery of heterologous proteins as fusions with the minor capsid proteins VP2/3. *J. Biotechnol.* **2008**, *134* (1), 181-192.

97. Steinmetz, N. F.; Evans, D. J., Utilisation of plant viruses in bionanotechnology. *Org. Biomol. Chem.* **2007**, *5* (18), 2891-2902.
98. Krasnykh, V.; Dmitriev, I.; Mikheeva, G.; Miller, C. R.; Belousova, N.; Curiel, D. T., Characterization of an adenovirus vector containing a heterologous peptide epitope in the HI loop of the fiber knob. *J. Virol.* **1998**, *72* (3), 1844-1852.
99. Müller, O. J.; Kaul, F.; Weitzman, M. D.; Pasqualini, R.; Arap, W.; Kleinschmidt, J. A.; Trepel, M., Random peptide libraries displayed on adeno-associated virus to select for targeted gene therapy vectors. *Nat. Biotechnol.* **2003**, *21* (9), 1040-1046.
100. Miura, Y.; Yoshida, K.; Nishimoto, T.; Hatanaka, K.; Ohnami, S.; Asaka, M.; Douglas, J.; Curiel, D.; Yoshida, T.; Aoki, K., Direct selection of targeted adenovirus vectors by random peptide display on the fiber knob. *Gene Ther.* **2007**, *14* (20), 1448-1460.
101. Wu, P.; Xiao, W.; Conlon, T.; Hughes, J.; Agbandje-McKenna, M.; Ferkol, T.; Flotte, T.; Muzyczka, N., Mutational analysis of the adeno-associated virus type 2 (AAV2) capsid gene and construction of AAV2 vectors with altered tropism. *J. Virol.* **2000**, *74* (18), 8635-8647.
102. Maheshri, N.; Koerber, J. T.; Kaspar, B. K.; Schaffer, D. V., Directed evolution of adeno-associated virus yields enhanced gene delivery vectors. *Nat. Biotechnol.* **2006**, *24* (2), 198-204.
103. Schaffer, D. V.; Koerber, J. T.; Lim, K., Molecular engineering of viral gene delivery vehicles. *Annu. Rev. Biomed. Eng.* **2008**, *10*, 169.
104. Sen, S.; Venkata Dasu, V.; Mandal, B., Developments in Directed Evolution for Improving Enzyme Functions. *Appl. Biochem. Biotechnol.* **2007**, *143* (3), 212-223.
105. Bartel, M. A.; Weinstein, J. R.; Schaffer, D. V., Directed evolution of novel adeno-associated viruses for therapeutic gene delivery. *Gene Ther.* **2012**, *19* (6), 694-700.
106. Rüegg, C.; Postigo, A. A.; Sikorski, E. E.; Butcher, E. C.; Pytela, R.; Erle, D. J., Role of integrin $\alpha 4 \beta 7 / \alpha 4 \beta P$ in lymphocyte adherence to fibronectin and VCAM-1 and in homotypic cell clustering. *J. Cell Biol.* **1992**, *117* (1), 179-189.
107. Mizejewski, G. J., Role of Integrins in Cancer: Survey of Expression Patterns. *Proc. Soc. Exp. Biol. Med.* **1999**, *222* (2), 124-138.
108. Desgrosellier, J. S.; Cheresch, D. A., Integrins in cancer: biological implications and therapeutic opportunities. *Nat. Rev. Cancer* **2010**, *10* (1), 9-22.
109. Eliceiri, B. P.; Klemke, R.; Stromblad, S.; Cheresch, D. A., Integrin $\alpha v \beta 3$ requirement for sustained mitogen-activated protein kinase activity during angiogenesis. *J. Cell Biol.* **1998**, *140* (5), 1255-63.

110. Hynes, R. O., Integrins: Bidirectional, Allosteric Signaling Machines. *Cell* **2002**, *110* (6), 673-687.
111. Guo, W.; Giancotti, F. G., Integrin signalling during tumour progression. *Nat. Rev. Mol. Cell Biol.* **2004**, *5* (10), 816-826.
112. Jin, H.; Varner, J., Integrins: roles in cancer development and as treatment targets. *Br. J. Cancer* **2004**, *90* (3), 561-565.
113. Niu, G.; Xiong, Z.; Cheng, Z.; Cai, W.; Gambhir, S. S.; Xing, L.; Chen, X., In vivo bioluminescence tumor imaging of RGD peptide-modified adenoviral vector encoding firefly luciferase reporter gene. *Mol. Imaging Biol.* **2007**, *9* (3), 126-34.
114. Huang, S.; Kamata, T.; Takada, Y.; Ruggeri, Z. M.; Nemerow, G. R., Adenovirus interaction with distinct integrins mediates separate events in cell entry and gene delivery to hematopoietic cells. *J. Virol.* **1996**, *70* (7), 4502-8.
115. Heckmann, D.; Kessler, H., Design and Chemical Synthesis of Integrin Ligands. In *Methods Enzymol.*, David, A. C., Ed. Academic Press: 2007; Vol. Volume 426, pp 463-503.
116. Kessler, H., Conformation and Biological Activity of Cyclic Peptides. *Angew. Chem., Int. Ed. Engl.* **1982**, *21* (7), 512-523.
117. Aumailley, M.; Gurrath, M.; Müller, G.; Calvete, J.; Timpl, R.; Kessler, H., Arg-Gly-Asp constrained within cyclic pentapeptides Strong and selective inhibitors of cell adhesion to vitronectin and laminin fragment P1. *FEBS Lett.* **1991**, *291* (1), 50-54.
118. Gurrath, M.; Müller, G.; Kessler, H.; Aumailley, M.; Timpl, R., Conformation/activity studies of rationally designed potent anti-adhesive RGD peptides. *Eur. J. Biochem.* **1992**, *210* (3), 911-921.
119. Geyer, A.; Mueller, G.; Kessler, H., Conformational Analysis of a Cyclic RGD Peptide Containing a ψ .[CH₂-NH] Bond: A Positional Shift in Backbone Structure Caused by a Single Dipeptide Mimetic. *J. Am. Chem. Soc.* **1994**, *116* (17), 7735-7743.
120. Kessler, H.; Diefenbach, B.; Finsinger, D.; Geyer, A.; Gurrath, M.; Goodman, S. L.; Hölzemann, G.; Haubner, R.; Jonczyk, A.; Müller, G.; Roedern, E. G.; Wermuth, J., Design of superactive and selective integrin receptor antagonists containing the RGD sequence. *Lett. Pept. Sci.* **1995**, *2* (3), 155-160.
121. Haubner, R.; Gratias, R.; Diefenbach, B.; Goodman, S. L.; Jonczyk, A.; Kessler, H., Structural and Functional Aspects of RGD-Containing Cyclic Pentapeptides as Highly Potent and Selective Integrin $\alpha_v\beta_3$ Antagonists. *J. Am. Chem. Soc.* **1996**, *118* (32), 7461-7472.

122. Haubner, R.; Finsinger, D.; Kessler, H., Stereoisomeric Peptide Libraries and Peptidomimetics for Designing Selective Inhibitors of the $\alpha_v\beta_3$ Integrin for a New Cancer Therapy. *Angew. Chem., Int. Ed. Engl.* **1997**, *36* (13-14), 1374-1389.
123. Lohof, E.; Planker, E.; Mang, C.; Burkhart, F.; Dechantsreiter, M. A.; Haubner, R.; Wester, H.-J.; Schwaiger, M.; Hölzemann, G.; Goodman, S. L.; Kessler, H., Carbohydrate Derivatives for Use in Drug Design: Cyclic α_v -Selective RGD Peptides. *Angew. Chem., Int. Ed. Engl.* **2000**, *39* (15), 2761-2764.
124. C. Gilon, M. A. D., F. Burkhart, A. Friedler, H. Kessler, Synthesis of N-methylated peptides. In *"Houben-Weyl: Methods of Organic Chemistry"*, A.F.M. Goodman, L. M., C. Toniolo, Ed. Thieme Verlag, Stuttgart, New York: **2003**.
125. Manavalan, P.; Momany, F. A., Conformational energy studies on N-methylated analogs of thyrotropin releasing hormone, enkephalin, and luteinizing hormone-releasing hormone. *Biopolymers* **1980**, *19* (11), 1943-1973.
126. Mazur, R. H.; James, P. A.; Tyner, D. A.; Hallinan, E. A.; Sanner, J. H.; Schulze, R., Bradykinin analogs containing N.alpha.-methyl amino acids. *J. Med. Chem.* **1980**, *23* (7), 758-763.
127. Tonelli, A. E., The effects of isolated N-methylated residues on the conformational characteristics of polypeptides. *Biopolymers* **1976**, *15* (8), 1615-1622.
128. Turker, R. K.; Hall, M. M.; Yamamoto, M.; Sweet, C. S.; Bumpus, F. M., A New, Long-Lasting Competitive Inhibitor of Angiotensin. *Science* **1972**, *177* (4055), 1203-1205.
129. Dechantsreiter, M. A.; Planker, E.; Mathä, B.; Lohof, E.; Hölzemann, G.; Jonczyk, A.; Goodman, S. L.; Kessler, H., N-Methylated Cyclic RGD Peptides as Highly Active and Selective $\alpha_v\beta_3$ Integrin Antagonists. *J. Med. Chem.* **1999**, *42* (16), 3033-3040.
130. Bauerschmitz, G. J.; Lam, J. T.; Kanerva, A.; Suzuki, K.; Nettelbeck, D. M.; Dmitriev, I., Treatment of ovarian cancer with a tropism modified oncolytic adenovirus. *Cancer Res.* **2002**, *62*, 1266-1270.
131. Rojas, J. J.; Gimenez-Alejandre, M.; Gil-Hoyos, R.; Cascallo, M.; Alemany, R., Improved systemic antitumor therapy with oncolytic adenoviruses by replacing the fiber shaft HSG-binding domain with RGD. *Gene Ther.* **2012**, *19* (4), 453-457.
132. Burkhart, D. J.; Kalet, B. T.; Coleman, M. P.; Post, G. C.; Koch, T. H., Doxorubicin-formaldehyde conjugates targeting $\alpha_v\beta_3$ integrin. *Mol. Cancer Ther.* **2004**, *3* (12), 1593-1604.
133. Kok, R. J.; Schraa, A. J.; Bos, E. J.; Moorlag, H. E.; Ásgeirsdóttir, S. A.; Everts, M.; Meijer, D. K. F.; Molema, G., Preparation and Functional Evaluation of RGD-Modified

- Proteins as $\alpha_v\beta_3$ Integrin Directed Therapeutics. *Bioconjugate Chem.* **2001**, *13* (1), 128-135.
134. Krom, Y. D.; Gras, J. C. E.; Frants, R. R.; Havekes, L. M.; van Berkel, T. J.; Biessen, E. A. L.; van Dijk, K. W., Efficient targeting of adenoviral vectors to integrin positive vascular cells utilizing a CAR-cyclic RGD linker protein. *Biochem. Biophys. Res. Commun.* **2005**, *338* (2), 847-854.
135. Arosio, D.; Manzoni, L.; Araldi, E. M.; Caprini, A.; Monferini, E.; Scolastico, C., Functionalized cyclic RGD peptidomimetics: conjugable ligands for $\alpha_v\beta_3$ receptor imaging. *Bioconjugate Chem.* **2009**, *20* (8), 1611-7.
136. Merkel, O. M.; Germershaus, O.; Wada, C. K.; Tarcha, P. J.; Merdan, T.; Kissel, T., Integrin $\alpha_v\beta_3$ targeted gene delivery using RGD peptidomimetic conjugates with copolymers of PEGylated poly(ethylene imine). *Bioconjugate Chem.* **2009**, *20* (6), 1270-80.
137. Shi, J.; Kim, Y. S.; Chakraborty, S.; Jia, B.; Wang, F.; Liu, S., 2-Mercaptoacetylglycylglycyl (MAG2) as a bifunctional chelator for ^{99m}Tc -labeling of cyclic RGD dimers: effect of technetium chelate on tumor uptake and pharmacokinetics. *Bioconjugate Chem.* **2009**, *20* (8), 1559-68.
138. Aizpurua, J. M.; Ganboa, J. I.; Palomo, C.; Loinaz, I.; Oyarbide, J.; Fernandez, X.; Balentova, E.; Fratila, R. M.; Jimenez, A.; Miranda, J. I.; Laso, A.; Avila, S.; Castrillo, J. L., Cyclic RGD beta-lactam peptidomimetics induce differential gene expression in human endothelial cells. *ChemBioChem* **2011**, *12* (3), 401-5.
139. Fields, G.; Carr, S.; Marshak, D.; Smith, A.; Stults, J.; Williams, L.; Williams, K.; Young, J.; Angeletti, R., Techniques in Protein Chemistry IV. *RH Angeletti, Editor* **1993**, 229-238.
140. Dai, X.; Su, Z.; Liu, J. O., An improved synthesis of a selective $[\alpha]_v[\beta]_3$ -integrin antagonist cyclo(-RGDFK-). *Tetrahedron Lett.* **2000**, *41* (33), 6295-6298.
141. Xiong, Z.; Cheng, Z.; Zhang, X.; Patel, M.; Wu, J. C.; Gambhir, S. S.; Chen, X., Imaging chemically modified adenovirus for targeting tumors expressing integrin $\alpha_v\beta_3$ in living mice with mutant herpes simplex virus type 1 thymidine kinase PET reporter gene. *J. Nucl. Med.* **2006**, *47* (1), 130-139.
142. Hermanson, G. T., *Bioconjugate techniques*. 2nd ed.; Academic press: Rockford, Illinois, USA, 2008; p 719.
143. Cauet, G.; Strub, J.-M.; Leize, E.; Wagner, E.; Dorsselaer, A. V.; Lusky, M., Identification of the Glycosylation Site of the Adenovirus Type 5 Fiber Protein. *Biochemistry* **2005**, *44* (14), 5453-5460.

144. Laughlin, S. T.; Agard, N. J.; Baskin, J. M.; Carrico, I. S.; Chang, P. V.; Ganguli, A. S.; Hangauer, M. J.; Lo, A.; Prescher, J. A.; Bertozzi, C. R., Metabolic Labeling of Glycans with Azido Sugars for Visualization and Glycoproteomics. In *Methods Enzymol.*, Minoru, F., Ed. Academic Press: 2006; Vol. Volume 415, pp 230-250.
145. Meldal, M.; Tornøe, C. W., Cu-Catalyzed Azide–Alkyne Cycloaddition. *Chem. Rev. (Washington, DC, U. S.)* **2008**, *108* (8), 2952-3015.
146. Wang, Q.; Chan, T. R.; Hilgraf, R.; Fokin, V. V.; Sharpless, K. B.; Finn, M., Bioconjugation by copper (I)-catalyzed azide-alkyne [3+ 2] cycloaddition. *J. Am. Chem. Soc.* **2003**, *125* (11), 3192-3193.
147. Gupta, S. S.; Kuzelka, J.; Singh, P.; Lewis, W. G.; Manchester, M.; Finn, M. G., Accelerated Bioorthogonal Conjugation: A Practical Method for the Ligation of Diverse Functional Molecules to a Polyvalent Virus Scaffold. *Bioconjugate Chem.* **2005**, *16* (6), 1572-1579.
148. Koizumi, N.; Mizuguchi, H.; Hosono, T.; Ishii-Watabe, A.; Uchida, E.; Utoguchi, N.; Watanabe, Y.; Hayakawa, T., Efficient gene transfer by fiber-mutant adenoviral vectors containing RGD peptide. *Biochim. Biophys. Acta, Gen. Subj.* **2001**, *1568* (1), 13-20.
149. Wu, E.; Pache, L.; Von Seggern, D. J.; Mullen, T.-M.; Mikyas, Y.; Stewart, P. L.; Nemerow, G. R., Flexibility of the Adenovirus Fiber Is Required for Efficient Receptor Interaction. *J. Virol.* **2003**, *77* (13), 7225-7235.
150. Wang, K.; Guan, T.; Cheresch, D. A.; Nemerow, G. R., Regulation of adenovirus membrane penetration by the cytoplasmic tail of integrin $\beta 5$. *J. Virol.* **2000**, *74* (6), 2731-2739.
151. Lyle, C.; McCormick, F., Integrin $\alpha_v\beta_5$ is a primary receptor for adenovirus in CAR-negative cells. *Virol. J.* **2010**, *7* (1), 148.
152. Gaertner, F.; Kessler, H.; Wester, H. J.; Schwaiger, M.; Beer, A., Radiolabelled RGD peptides for imaging and therapy. *Eur. J. Nucl. Med. Mol. Imaging* **2012**, 1-13.
153. Goodman, S. L.; Hölzemann, G.; Sulyok, G. A. G.; Kessler, H., Nanomolar small molecule inhibitors for $\alpha_v\beta_6$, $\alpha_v\beta_5$, and $\alpha_v\beta_3$ integrins. *J. Med. Chem.* **2002**, *45* (5), 1045-1051.
154. Hariharan, S.; Gustafson, D.; Holden, S.; McConkey, D.; Davis, D.; Morrow, M.; Basche, M.; Gore, L.; Zang, C.; O'Bryant, C., Assessment of the biological and pharmacological effects of the $\alpha_v\beta_3$ and $\alpha_v\beta_5$ integrin receptor antagonist, cilengitide (EMD 121974), in patients with advanced solid tumors. *Ann. Oncol.* **2007**, *18* (8), 1400-1407.

155. Schober, D.; Bayer, N.; Murphy, R. F.; Wagner, E.; Fuchs, R., Establishment of an assay to determine adenovirus-induced endosome rupture required for receptor-mediated gene delivery. *Gene Ther. Mol. Biol.* **1999**, *3*, 25-33.
156. Freimuth, P.; Springer, K.; Berard, C.; Hainfeld, J.; Bewley, M.; Flanagan, J., Coxsackievirus and Adenovirus Receptor Amino-Terminal Immunoglobulin V-Related Domain Binds Adenovirus Type 2 and Fiber Knob from Adenovirus Type 12. *J. Virol.* **1999**, *73* (2), 1392-1398.
157. Bai, M.; Campisi, L.; Freimuth, P., Vitronectin receptor antibodies inhibit infection of HeLa and A549 cells by adenovirus type 12 but not by adenovirus type 2. *J. Virol.* **1994**, *68* (9), 5925-5932.
158. Mattern, R. H.; Read, S. B.; Pierschbacher, M. D.; Sze, C. I.; Eliceiri, B. P.; Kruse, C. A., Glioma cell integrin expression and their interactions with integrin antagonists. *Cancer Ther.* **2005**, *3*, 325.
159. Asaoka, K.; Tada, M.; Sawamura, Y.; Ikeda, J.; Abe, H., Dependence of efficient adenoviral gene delivery in malignant glioma cells on the expression levels of the Coxsackievirus and adenovirus receptor. *J. Neurosurg.* **2000**, *92* (6), 1002-1008.
160. Van Houdt, W. J.; Wu, H.; Glasgow, J. N.; Lamfers, M. L.; Dirven, C. M.; Gillespie, G. Y.; Curiel, D. T.; Haviv, Y. S., Gene delivery into malignant glioma by infectivity-enhanced adenovirus: in vivo versus in vitro models. *Neuro-oncol.* **2007**, *9* (3), 280-290.
161. Huang, R.; Vider, J.; Kovar, J. L.; Olive, D. M.; Mellinghoff, I. K.; Mayer-Kuckuk, P.; Kircher, M. F.; Blasberg, R. G., Integrin $\alpha_v\beta_3$ -Targeted IRDye 800CW Near-Infrared Imaging of Glioblastoma. *Clin. Cancer Res.* **2012**, *18* (20), 5731-5740.
162. Monferran, S.; Nicolas, S.; Delmas, C.; Favre, G.; Bonnet, J.; E., C.-J.-M.; Toulas, C., $\alpha_v\beta_3$ and $\alpha_v\beta_5$ integrins control glioma cell response to ionising radiation through ILK and RhoB. *Int. J. Cancer* **2008**, *123*, 357-364.
163. McCoy, E.; Sontheimer, H., Expression and function of water channels (aquaporins) in migrating malignant astrocytes. *Glia* **2007**, *55* (10), 1034-1043.
164. Gutheil, J. C.; Campbell, T. N.; Pierce, P. R.; Watkins, J. D.; Huse, W. D.; Bodkin, D. J.; Cheresch, D. A., Targeted Antiangiogenic Therapy for Cancer Using Vitaxin: A Humanized Monoclonal Antibody to the Integrin $\alpha_v\beta_3$. *Clin. Cancer Res.* **2000**, *6* (8), 3056-3061.
165. Kowanetz, M.; Ferrara, N., Vascular Endothelial Growth Factor Signaling Pathways: Therapeutic Perspective. *Clin. Cancer Res.* **2006**, *12* (17), 5018-5022.
166. Villa, A.; Trachsel, E.; Kaspar, M.; Schliemann, C.; Somavilla, R.; Rybak, J.-N. L.; Borsi, C. R. I.; Neri, D., A high-affinity human monoclonal antibody specific to the

- alternatively spliced EDA domain of fibronectin efficiently targets tumor neo-vasculature *in vivo*. *Int. J. Cancer* **2008**, *122* (11), 2405-2413.
167. Hodivala-Dilke, K., $\alpha_v\beta_3$ integrin and angiogenesis: a moody integrin in a changing environment. *Curr. Opin. Cell Biol.* **2008**, *20*, 514–519.
 168. Ferrara, N.; Kerbel, R. S., Angiogenesis as a therapeutic target. *Nature* **2005**, *438* (7070), 967-974.
 169. Lewis, C. E.; De Palma, M.; Naldini, L., Tie2-expressing monocytes and tumor angiogenesis: regulation by hypoxia and angiopoietin-2. *Cancer Res.* **2007**, *67* (18), 8429-8432.
 170. Binetruy-Tournaire, R.; Demangel, C.; Malavaud, B.; Vassy, R.; Rouyre, S.; Kraemer, M.; Plouet, J.; Derbin, C.; Perret, G.; Mazie, J. C., Identification of a peptide blocking vascular endothelial growth factor (VEGF)-mediated angiogenesis. *EMBO J.* **2000**, *19* (7), 1525-1533.
 171. Sj, D.; Liu, W.; Simmons, C. A.; Moore, J. T.; Tian, G., Identifying substrates for endothelium-specific Tie-2 receptor tyrosine kinase from phage-displayed peptide libraries for high throughput screening. *Comb. Chem. High Throughput Screen.* **2001**, *4* (6), 525-533.
 172. Alghisi, G. C.; Ponsonnet, L.; Rüegg, C., The Integrin Antagonist Cilengitide Activates $\alpha_v\beta_3$, Disrupts VE-Cadherin Localization at Cell Junctions and Enhances Permeability in Endothelial Cells. *PLoS One* **2009**, *4* (2), e4449.
 173. Brooks, P. C.; Montgomery, A. M. P.; Rosenfeld, M.; Reisfeld, R. A.; Hu, T.; Klier, G.; Cheresch, D. A., Integrin $\alpha_v\beta_3$ antagonists promote tumor regression by inducing apoptosis of angiogenic blood vessels. *Cell* **1994**, *79* (7), 1157-1164.
 174. Murakami, P.; McCaman, M. T., Quantitation of Adenovirus DNA and Virus Particles with the PicoGreen Fluorescent Dye. *Anal. Biochem.* **1999**, *274* (2), 283-288.
 175. Magnusson, M. K. H., S.S.; Henning, P.; Boulanger, P.; Lindholm, L., Genetic retargeting of adenovirus vectors: functionality of targeting ligands and their influence on virus viability. *J. Gene Med.* **2002**, *4* (4), 356-370.
 176. Henning, P.; Lundgren, E.; Carlsson, M.; Frykholm, K.; Johannisson, J.; Magnusson, M. K.; Tang, E.; Franqueville, L.; Hong, S. S.; Lindholm, L.; Boulanger, P., Adenovirus type 5 fiber knob domain has a critical role in fiber protein synthesis and encapsidation. *J. Gen. Virol.* **2006**, *87* (11), 3151-3160.
 177. Matthews, Q. L.; Yang, P.; Wu, Q.; Belousova, N.; Rivera, A. A.; Stoff-Khalili, M. A.; Waehler, R.; Hsu, H. C.; Li, Z.; Li, J.; Mountz, J. D.; Wu, H. J.; Curiel, D. T.,

- Optimization of capsid-incorporated antigens for a novel adenovirus vaccine approach. *Viol. J.* **2008**, *5*.
178. Belousova, N.; Krendelchtchikova, V.; Curiel, D. T.; Krasnykh, V., Modulation of Adenovirus Vector Tropism via Incorporation of Polypeptide Ligands into the Fiber Protein. *J. Virol.* **2002**, *76* (17), 8621-8631.
 179. Xia, H.; Anderson, B.; Mao, Q.; Davidson, B. L., Recombinant human adenovirus: targeting to the human transferrin receptor improves gene transfer to brain microcapillary endothelium. *J. Virol.* **2000**, *74*, 11359-11366.
 180. Kreppel, F.; Gackowski, J.; Schmidt, E.; Stefan, K., Combined Genetic and Chemical Capsid Modifications Enable Flexible and Efficient De- and Retargeting of Adenovirus Vectors. *Mol. Ther.* **2005**, *12* (1), 107-117.
 181. Kreppel, F.; Kochanek, S., Modification of Adenovirus Gene Transfer Vectors With Synthetic Polymers: A Scientific Review and Technical Guide. *Mol. Ther.* **2007**, *16* (1), 16-29.
 182. Kreppel, F.; Kochanek, S., Modification of adenovirus gene transfer vectors with synthetic polymers: A scientific review and technical guide. *Molecular Therapy* **2008**, *16* (1), 16-29.
 183. Campos, S. K.; Parrott, M. B.; Barry, M. A., Avidin-based Targeting and Purification of a Protein IX-modified, Metabolically Biotinylated Adenoviral Vector. *Mol. Ther.* **2004**, *9* (6), 942-954.
 184. Pereboeva, L.; Komarova, S.; Roth, J.; Ponnazhagan, S.; Curiel, D. T., Targeting EGFR with metabolically biotinylated fiber-mosaic adenovirus. *Gene Ther* **2007**, *14* (8), 627-637.
 185. Vincenzi, B.; Schiavon, G.; Silletta, M.; Santini, D.; Tonini, G., The biological properties of cetuximab. *Crit Rev Oncol Hematol* **2008**, *68* (2), 14-14.
 186. Salomon, D. S.; Brandt, R.; Ciardiello, F.; Normanno, N., Epidermal growth factor-related peptides and their receptors in human malignancies. *Crit. Rev. Oncol. Hematol.* **1995**, *19* (3), 183-232.
 187. Engel, R. H.; Kaklamani, V. G., HER2-positive breast cancer: current and future treatment strategies. *Drugs* **2007**, *67* (9), 1329-1341.
 188. Nord, K.; Gunneriusson, E.; Ringdahl, J.; Ståhl, S.; Uhlén, M.; Nygren, P. Å., Binding proteins selected from combinatorial libraries of an α -helical bacterial receptor domain. *Nat. Biotechnol.* **1996**, *15* (8), 772-777.
 189. Nygren, P. Å., Alternative binding proteins: Affibody binding proteins developed from a small three-helix bundle scaffold. *FEBS J.* **2008**, *275* (11), 2668-2676.

190. Dreux, A. C.; Lamb, D. J.; Modjtahedi, H.; Ferns, G. A. A., The epidermal growth factor receptors and their family of ligands: Their putative role in atherogenesis. *Atherosclerosis* **2006**, *186* (1), 38-53.
191. Magnusson, M. K.; Henning, P.; Myhre, S.; Wikman, M.; Uil, T. G.; Friedman, M.; Andersson, K. M. E.; Hong, S. S.; Hoeben, R. C.; Habib, N. A.; Stahl, S.; Boulanger, P.; Lindholm, L., Adenovirus 5 vector genetically re-targeted by an affibody molecule with specificity for tumor antigen HER2/neu. *Cancer Gene Ther.* **2007**, *14* (5), 468-479.
192. Steffen, A. C.; Wikman, M.; Tolmachev, V.; Adams, G. P.; Nilsson, F. Y.; Stahl, S.; Carlsson, J., In vitro characterization of a bivalent anti-HER-2 affibody with potential for radionuclide-based diagnostics. *Cancer Biother. Radiopharm.* **2005**, *20* (3), 239-248.
193. Banerjee, P. S.; Ostapchuk, P.; Hearing, P.; Carrico, I., Chemoselective Attachment of Small Molecule Effector Functionality to Human Adenoviruses Facilitates Gene Delivery to Cancer Cells. *J. Am. Chem. Soc.* **2010**, *132* (39), 13615-13617.
194. Ning, X. H.; Guo, J.; Wolfert, M. A.; Boons, G. J., Visualizing metabolically labeled glycoconjugates of living cells by copper-free and fast Huisgen cycloadditions. *Angew. Chem. Int. Ed. Engl.* **2008**, *47* (12), 2253-2255.
195. Debets, M. F.; van Berkel, S. S.; Schoffelen, S.; Rutjes, F.; van Hest, J. C. M.; van Delft, F. L., Aza-dibenzocyclooctynes for fast and efficient enzyme PEGylation via copper-free (3+2) cycloaddition. *Chem. Commun.* **2010**, *46* (1), 97-99.
196. Dommerholt, J.; Schmidt, S.; Temming, R.; Hendriks, L. J. A.; Rutjes, F.; van Hest, J. C. M.; Lefeber, D. J.; Friedl, P.; van Delft, F. L., Readily Accessible Bicyclononynes for Bioorthogonal Labeling and Three-Dimensional Imaging of Living Cells. *Angew. Chem. Int. Ed. Engl.* **2010**, *49* (49), 9422-9425.
197. Agard, N. J.; Baskin, J. M.; Prescher, J. A.; Lo, A.; Bertozzi, C. R., A Comparative Study of Bioorthogonal Reactions with Azides. *ACS Chem. Biol.* **2006**, *1* (10), 644-648.
198. Hong, V.; Presolski, S.; Ma, C.; Finn, M., Analysis and Optimization of Copper-Catalyzed Azide-Alkyne Cycloaddition for Bioconjugation. *Angew. Chem. Int. Ed. Engl.* **2009**, *48* (52), 9879-9883.
199. Hong, V.; Steinmetz, N. F.; Manchester, M.; Finn, M. G., Labeling Live Cells by Copper-Catalyzed Alkyne-Azide Click Chemistry. *Bioconjugate Chem.* **2010**, *21* (10), 1912-1916.
200. Chen, H.; Bartlett, J.; Wilcher, R.; Samulski, R.; Berns, K.; Bohenzky, R.; Liu, S.; Chen, L.; Huang, J., Comparative observation of the recombinant adeno-associated virus 2 using transmission electron microscopy and atomic force microscopy. *Microsc. Microanal.* **2007**, *13* (5), 384-389.

201. Rexroad, J.; Wiethoff, C. M.; Green, A. P.; Kierstead, T. D.; Scott, M. O.; Middaugh, C. R., Structural stability of adenovirus type 5. *J. Pharm. Sci.* **2003**, *92* (3), 665-678.
202. Rexroad, J.; Martin, T. T.; McNeilly, D.; Godwin, S.; Middaugh, C. R., Thermal stability of adenovirus type 2 as a function of pH. *J. Pharm. Sci.* **2006**, *95* (7), 1469-1479.
203. Oh, I. K.; Mok, H.; Park, T. G., Folate immobilized and PEGylated adenovirus for retargeting to tumor cells. *Bioconjugate Chem.* **2006**, *17* (3), 721-727.
204. Awasthi, V.; Meinken, G.; Springer, K.; Srivastava, S. C.; Freimuth, P., Biodistribution of radioiodinated adenovirus fiber protein knob domain after intravenous injection in mice. *J. Virol.* **2004**, *78* (12), 6431-8.
205. Gaborit, N.; Larbouret, C.; Vallaghe, J.; Peyrusson, F.; Bascoul-Molleivi, C.; Crapez, E.; Azria, D.; Chardès, T.; Poul, M. A.; Mathis, G., Time-resolved Fluorescence Resonance Energy Transfer (TR-FRET) to Analyze the Disruption of EGFR/HER2 Dimers. *J. Biol. Chem.* **2011**, *286* (13), 11337-45.
206. Reynolds, P. N.; Zinn, K. R.; Gavriluk, V. D.; Balyasnikova, I. V.; Rogers, B. E.; Buchsbaum, D. J.; Wang, M. H.; Miletich, D. J.; Grizzle, W. E.; Douglas, J. T., A targetable, injectable adenoviral vector for selective gene delivery to pulmonary endothelium in vivo. *Mol. Ther.* **2000**, *2* (6), 562-578.
207. Shashkova, E. V.; Doronin, K.; Senac, J. S.; Barry, M. A., Macrophage depletion combined with anticoagulant therapy increases therapeutic window of systemic treatment with oncolytic adenovirus. *Cancer Res.* **2008**, *68* (14), 5896-5904.
208. Groot-Wassink, T.; Aboagye, E. O.; Wang, Y.; Lemoine, N. R.; Reader, A. J.; Vassaux, G., Quantitative Imaging of Na/I Symporter Transgene Expression Using Positron Emission Tomography in the Living Animal. *Mol. Ther.* **2004**, *9* (3), 436-442.
209. Gambhir, S. S.; Barrio, J. R.; Wu, L.; Iyer, M.; Namavari, M.; Satyamurthy, N.; Bauer, E.; Parrish, C.; MacLaren, D. C.; Borghei, A. R., Imaging of adenoviral-directed herpes simplex virus type 1 thymidine kinase reporter gene expression in mice with radiolabeled ganciclovir. *J. Nucl. Med.* **1998**, *39* (11), 2003.
210. Hofherr, S. E.; Adams, K. E.; Chen, C. Y.; May, S.; Weaver, E. A.; Barry, M. A., Real-Time Dynamic Imaging of Virus Distribution *In Vivo*. *PLoS One* **2011**, *6* (2), e17076.
211. Flexman, J. A.; Cross, D. J.; Lewellen, B. L.; Miyoshi, S.; Kim, Y.; Minoshima, S., Magnetically Targeted Viral Envelopes: A PET Investigation of Initial Biodistribution. *NanoBioscience, IEEE Transactions on* **2008**, *7* (3), 223-232.
212. Tang, G.; Zeng, W.; Yu, M.; Kabalka, G., Facile synthesis of *N*-succinimidyl 4-^[18F]fluorobenzoate (^[18F]SFB) for protein labeling. *J. Labelled Compd. Radiopharm.* **2008**, *51* (1), 68-71.

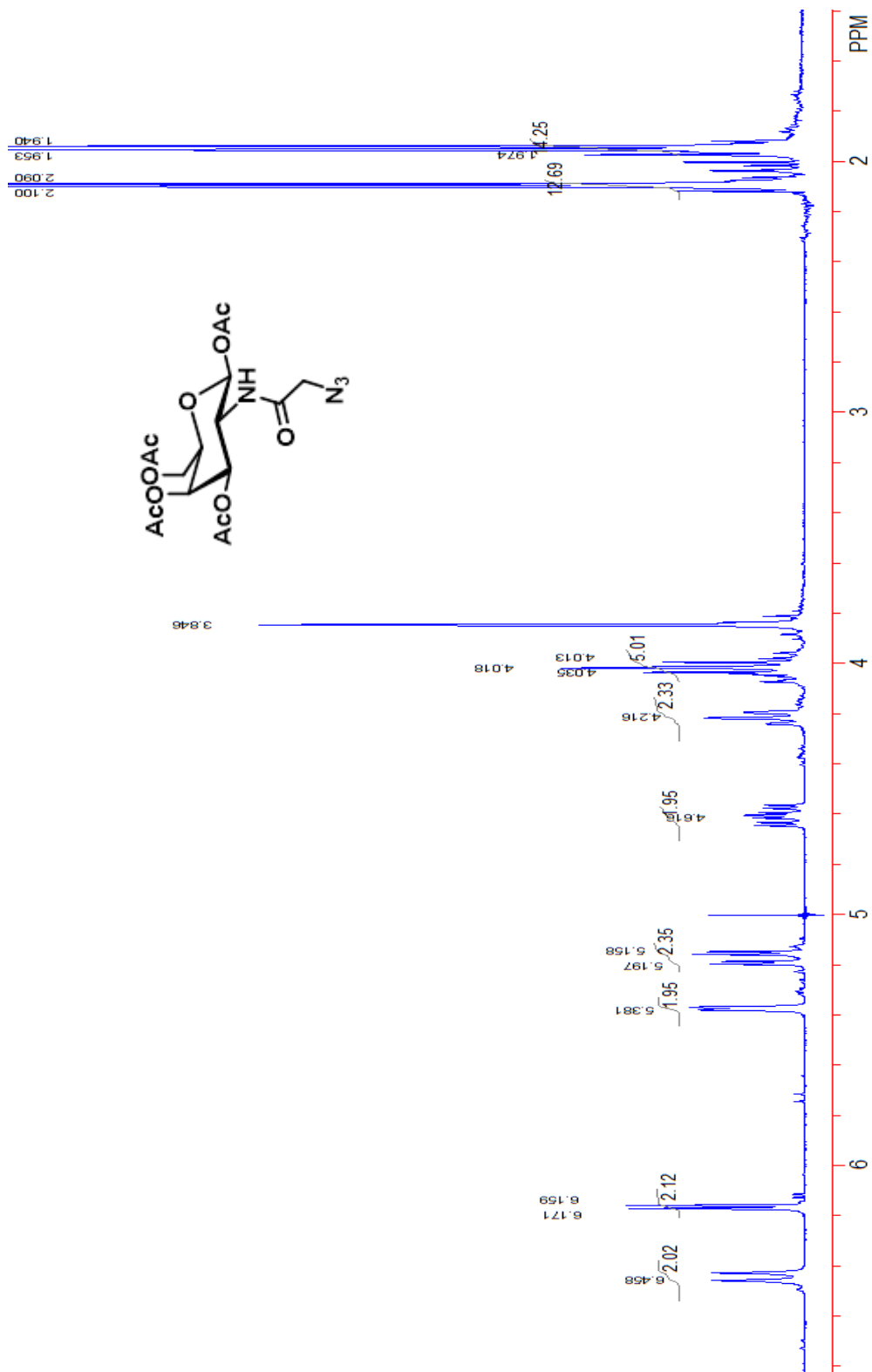
213. Glaser, M.; Årstad, E.; Luthra, S. K.; Robins, E. G., Two-step radiosynthesis of [¹⁸F]N-succinimidyl-4-fluorobenzoate ([¹⁸F]SFB). *J. Labelled Compd. Radiopharm.* **2009**, *52* (8), 327-330.
214. Scott, P. J. H.; Shao, X., Fully automated, high yielding production of N-succinimidyl 4-[¹⁸F]fluorobenzoate ([¹⁸F]SFB), and its use in microwave-enhanced radiochemical coupling reactions. *J. Labelled Compd. Radiopharm.* **2010**, *53* (9), 586-591.
215. Wester, H.-J.; Hamacher, K.; Stöcklin, G., A comparative study of N.C.A. Fluorine-18 labeling of proteins via acylation and photochemical conjugation. *Nucl. Med. Biol.* **1996**, *23* (3), 365-372.
216. Glaser, M.; Robins, E. G., 'Click labelling' in PET radiochemistry. *J. Labelled Compd. Radiopharm.* **2009**, *52* (10), 407-414.
217. Marik, J.; Sutcliffe, J. L., Click for PET: rapid preparation of [¹⁸F]fluoropeptides using CuI catalyzed 1,3-dipolar cycloaddition. *Tetrahedron Lett.* **2006**, *47* (37), 6681-6684.
218. Glaser, M.; Årstad, E., "Click Labeling" with 2-[¹⁸F]Fluoroethylazide for Positron Emission Tomography. *Bioconjugate Chem.* **2007**, *18* (3), 989-993.
219. Selvaraj, R.; Liu, S.; Hassink, M.; Huang, C.-w.; Yap, L.-p.; Park, R.; Fox, J. M.; Li, Z.; Conti, P. S., Tetrazine-trans-cyclooctene ligation for the rapid construction of integrin $\alpha_v\beta_3$ targeted PET tracer based on a cyclic RGD peptide. *Bioorg. Med. Chem. Lett.* **2011**, *21* (17), 5011-5014.
220. Reiner, T.; Keliher, E. J.; Earley, S.; Marinelli, B.; Weissleder, R., Synthesis and *In Vivo* Imaging of a ¹⁸F-Labeled PARP1 Inhibitor Using a Chemically Orthogonal Scavenger-Assisted High-Performance Method. *Angew. Chem., Int. Ed. Engl.* **2011**, *50* (8), 1922-1925.
221. Otsuka, F. L.; Welch, M. J.; Kilbourn, M. R.; Dence, C. S.; Dilley, W. G.; Wells, S. A., Antibody fragments labeled with fluorine-18 and gallium-68: *In vivo* comparison with indium-111 and iodine-125-labeled fragments. *Int. J. Rad. Appl. Instrum. B* **1991**, *18* (7), 813-816.
222. Garg, P. K.; Garg, S.; Bigner, D. D.; Zalutsky, M. R., Localization of fluorine-18-labeled Mel-14 monoclonal antibody F (ab')₂ fragment in a subcutaneous xenograft model. *Cancer Res.* **1992**, *52* (18), 5054-5060.
223. Nayak, T. K.; Brechbiel, M. W., Radioimmunoimaging with Longer-Lived Positron-Emitting Radionuclides: Potentials and Challenges. *Bioconjugate Chem.* **2009**, *20* (5), 825-841.
224. Anderson, C. J.; Welch, M. J., Radiometal-Labeled Agents (Non-Technetium) for Diagnostic Imaging. *Chem. Rev. (Washington, DC, U. S.)* **1999**, *99* (9), 2219-2234.

225. Cole, W. C.; DeNardo, S. J.; Meares, C. F.; McCall, M. J.; DeNardo, G. L.; Epstein, A. L.; O'Brien, H. A.; Moi, M. K., Serum stability of ^{67}Cu chelates: comparison with ^{111}In and ^{57}Co . *Int. J. Rad. Appl. Instrum. B* **1986**, *13* (4), 363.
226. Woodin, K. S.; Heroux, K. J.; Boswell, C. A.; Wong, E. H.; Weisman, G. R.; Niu, W.; Tomellini, S. A.; Anderson, C. J.; Zakharov, L. N.; Rheingold, A. L., Kinetic Inertness and Electrochemical Behavior of Copper(II) Tetraazamacrocyclic Complexes: Possible Implications for in Vivo Stability. *Eur. J. Inorg. Chem.* **2005**, *2005* (23), 4829-4833.
227. Di Bartolo, N. M.; Sargeson, A. M.; Donlevy, T. M.; Smith, S. V., Synthesis of a new cage ligand, SarAr, and its complexation with selected transition metal ions for potential use in radioimaging. *J. Chem. Soc., Dalton Trans.* **2001**, (15), 2303-2309.
228. Prasanphanich, A. F.; Nanda, P. K.; Rold, T. L.; Ma, L.; Lewis, M. R.; Garrison, J. C.; Hoffman, T. J.; Sieckman, G. L.; Figueroa, S. D.; Smith, C. J., [^{64}Cu -NOTA-8-Aoc-BBN (7-14) NH_2] Targeting Vector for Positron-Emission Tomography Imaging of Gastrin-Releasing Peptide Receptor-Expressing Tissues. *Proc. Natl. Acad. Sci. U. S. A.* **2007**, *104*, 12462-12467.
229. Lang, L.; Li, W.; Guo, N.; Ma, Y.; Zhu, L.; Kiesewetter, D. O.; Shen, B.; Niu, G.; Chen, X., Comparison study of [^{18}F] FAI-NOTA-PRGD2, [^{18}F] FPPRGD2, and [^{68}Ga] Ga-NOTA-PRGD2 for PET imaging of U87-MG tumors in mice. *Bioconjugate Chem.* **2011**, *22* (12), 2415-2422.
230. Alshoukr, F.; Prignon, A.; Brans, L.; Jallane, A.; Mendes, S.; Talbot, J. N.; Tourwé, D.; Barbet, J.; Gruaz-Guyon, A., Novel DOTA-neurotensin analogues for ^{111}In scintigraphy and ^{68}Ga PET imaging of neurotensin receptor-positive tumors. *Bioconjugate Chem.* **2011**, *22* (7), 1374-1385.
231. Jeong, J. M.; Hong, M. K.; Chang, Y. S.; Lee, Y.-S.; Kim, Y. J.; Cheon, G. J.; Lee, D. S.; Chung, J.-K.; Lee, M. C., Preparation of a Promising Angiogenesis PET Imaging Agent: ^{68}Ga -Labeled c(RGDyK)-Isothiocyanatobenzyl-1,4,7-Triazacyclononane-1,4,7-Triacetic Acid and Feasibility Studies in Mice. *J. Nucl. Med.* **2008**, *49* (5), 830-836.
232. Hatanaka, K.; Asai, T.; Koide, H.; Kenjo, E.; Tsuzuku, T.; Harada, N.; Tsukada, H.; Oku, N., Development of double-stranded siRNA labeling method using positron emitter and its in vivo trafficking analyzed by positron emission tomography. *Bioconjugate Chem.* **2010**, *21* (4), 756-763.
233. Chang, P. V.; Prescher, J. A.; Sletten, E. M.; Baskin, J. M.; Miller, I. A.; Agard, N. J.; Lo, A.; Bertozzi, C. R., Copper-free click chemistry in living animals. *Proc. Natl. Acad. Sci. U. S. A.* **2010**, *107* (5), 1821-1826.

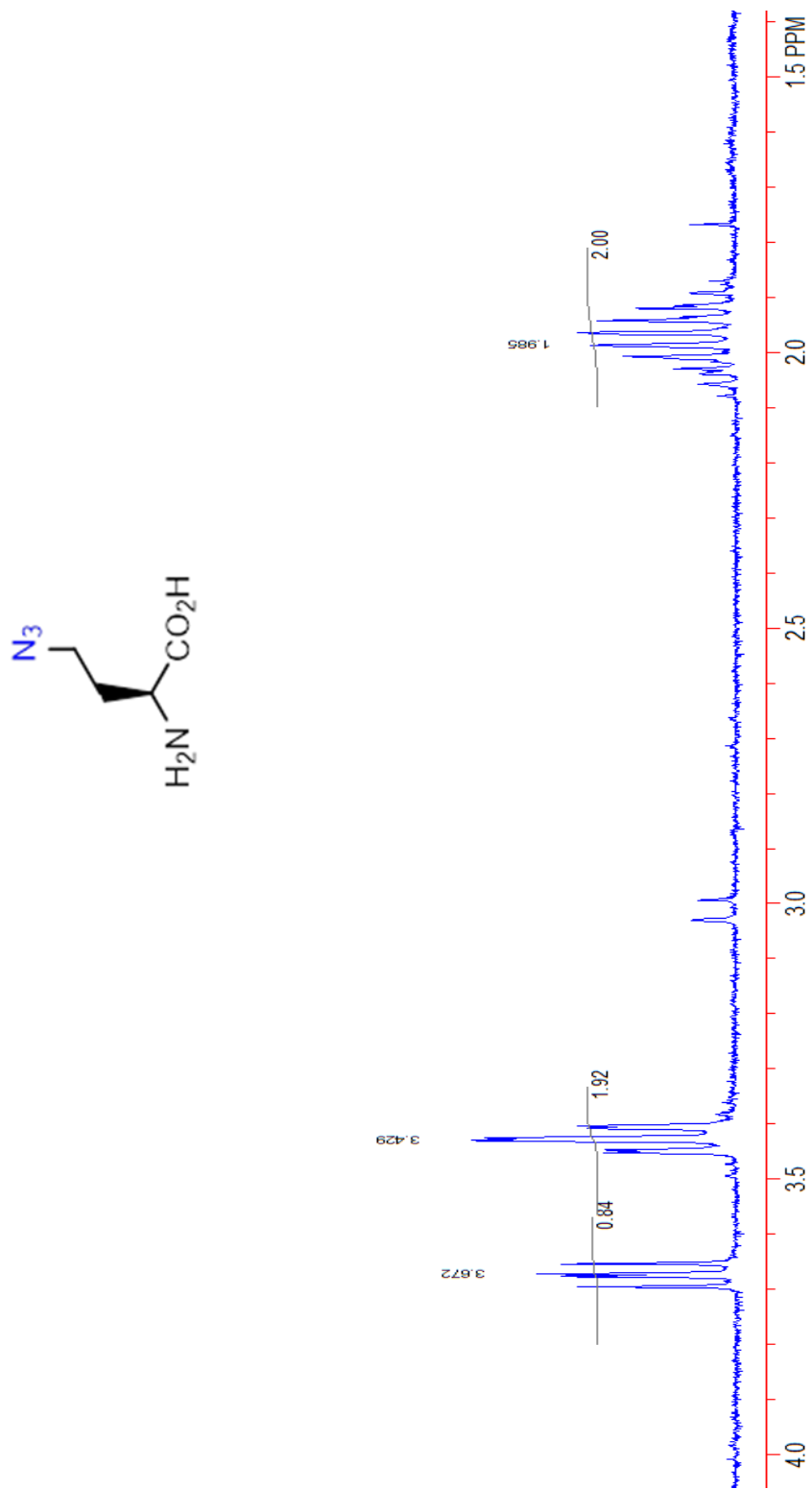
234. Li, Z. B.; Chen, K.; Chen, X., ⁶⁸Ga-labeled multimeric RGD peptides for microPET imaging of integrin $\alpha_v\beta_3$ expression. *Eur. J. Nucl. Med. Mol. Imaging* **2008**, *35* (6), 1100-1108.
235. Liu, Z.; Niu, G.; Shi, J.; Liu, S.; Wang, F.; Chen, X., ⁶⁸Ga-labeled cyclic RGD dimers with Gly3 and PEG4 linkers: promising agents for tumor integrin $\alpha_v\beta_3$ PET imaging. *Eur. J. Nucl. Med. Mol. Imaging* **2009**, *36* (6), 947-957.
236. Holland, J. P.; Sheh, Y.; Lewis, J. S., Standardized methods for the production of high specific-activity zirconium-89. *Nucl. Med. Biol.* **2009**, *36* (7), 729-739.
237. Verel, I.; Visser, G. W. M.; Boellaard, R.; Stigter-van Walsum, M.; Snow, G. B.; van Dongen, G. A. M. S., ⁸⁹Zr Immuno-PET: Comprehensive Procedures for the Production of ⁸⁹Zr-Labeled Monoclonal Antibodies. *J. Nucl. Med.* **2003**, *44* (8), 1271-1281.

Appendix

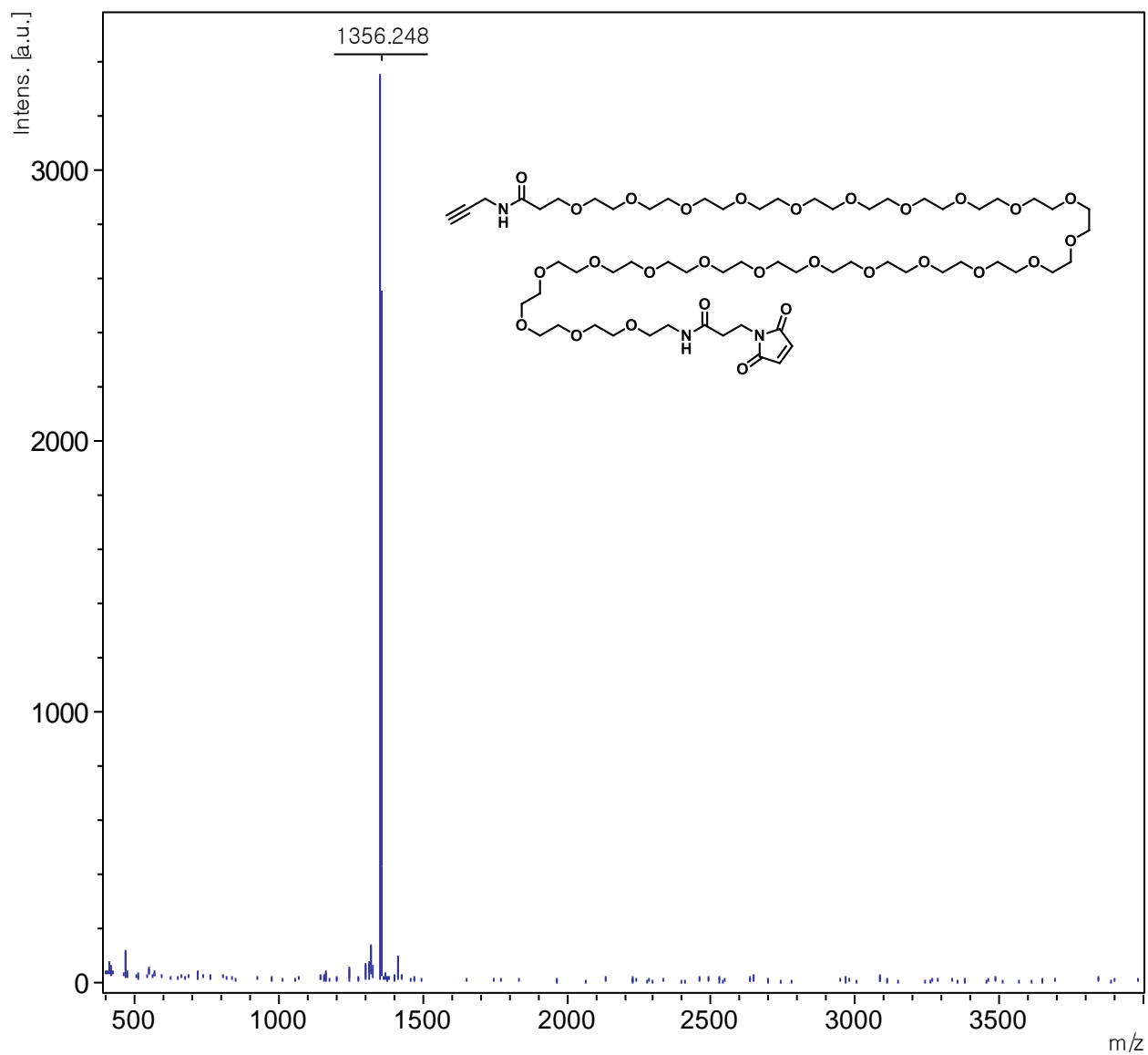
A 1. ¹ H NMR Spectrum of Ac ₄ GalNAz in D ₂ O (300 MHz)	203
A 2. ¹ H-NMR Spectrum of Azidohomoalanine (AHA) in D ₂ O (300 MHz).....	204
A 3. MALDI-TOF Spectrum of Alkyne-PEG ₂₄ -maleimide (3-2)	205
A 4. MALDI-TOF Spectrum of Alkyne-PEG ₂₄ -c(RGDfK) (3-3)	206
A 5. MALDI-TOF Spectrum of Alkyne-PEG ₂₄ -GGRGDS (3-3).....	207
A 6. MALDI-TOF Spectrum of affiEGFR-PEG ₂₄ -CCH	208
A 7. MALDI-TOF Spectrum of affiHer2-PEG ₂₄ -CCH.....	209
A 8. MALDI-TOF Spectrum of affiEGFR-PEG ₂₆ -BCN	210
A 9. ¹ H-NMR of Ethyl-(4-Trimethylammonium)benzoate Trifluoromethanesulfonate (5-2) in CD ₃ Cl (400MHz)	211
A 10. ¹³ C-NMR of Ethyl-(4-Trimethylammonium)benzoate Trifluoromethanesulfonate (5-2) in CD ₃ Cl (400 MHz)	212
A 11. ESI-Mass Spectrum of NOTA-PEG-BCN (5-5).....	213
A 12. MALDI-TOF Spectrum of Folate-PEG-Phosphine (5-6)	214
A 13. MALDI-TOF Spectrum of DFO-PEG-N ₃ (5-7).....	215
A 14. ¹ NMR Spectrum of DFO-PEG-N ₃ (5-7) in (CD ₃) ₂ SO (400 MHz)	216



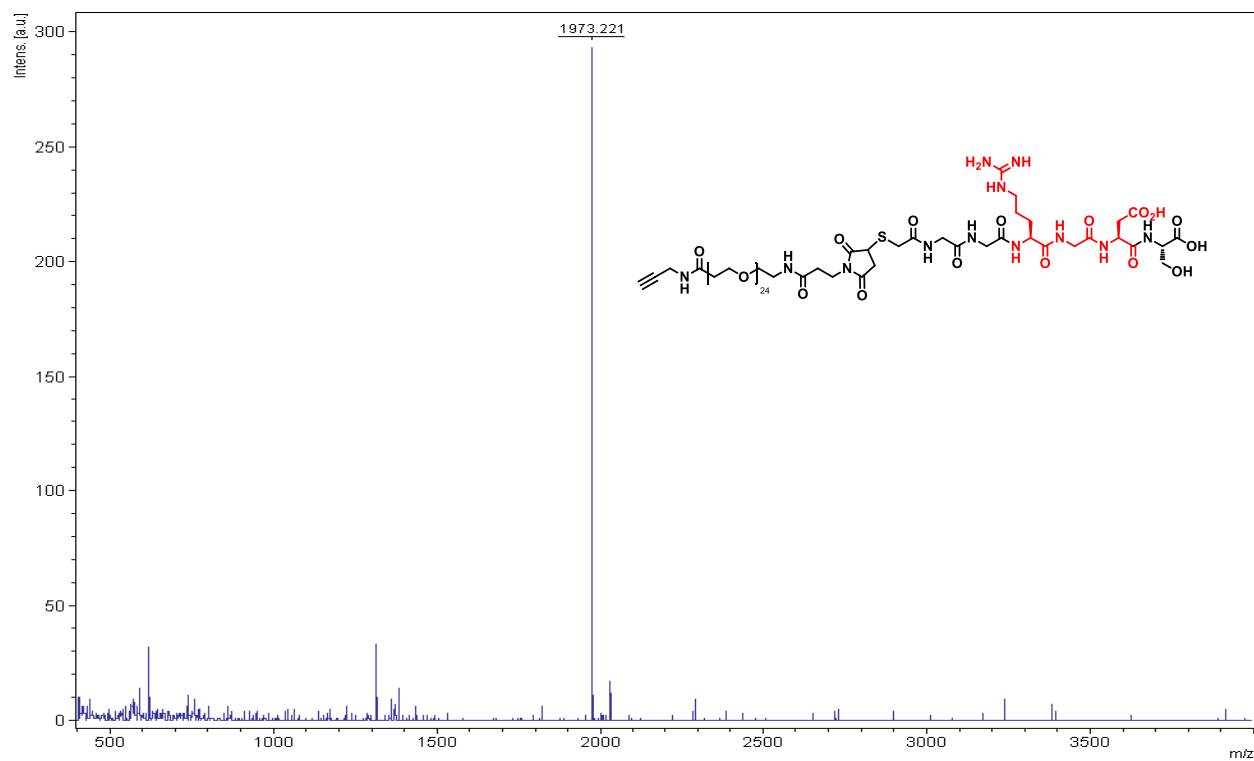
A 1. ¹H NMR Spectrum of Ac₄GalNAz in D₂O (300 MHz)



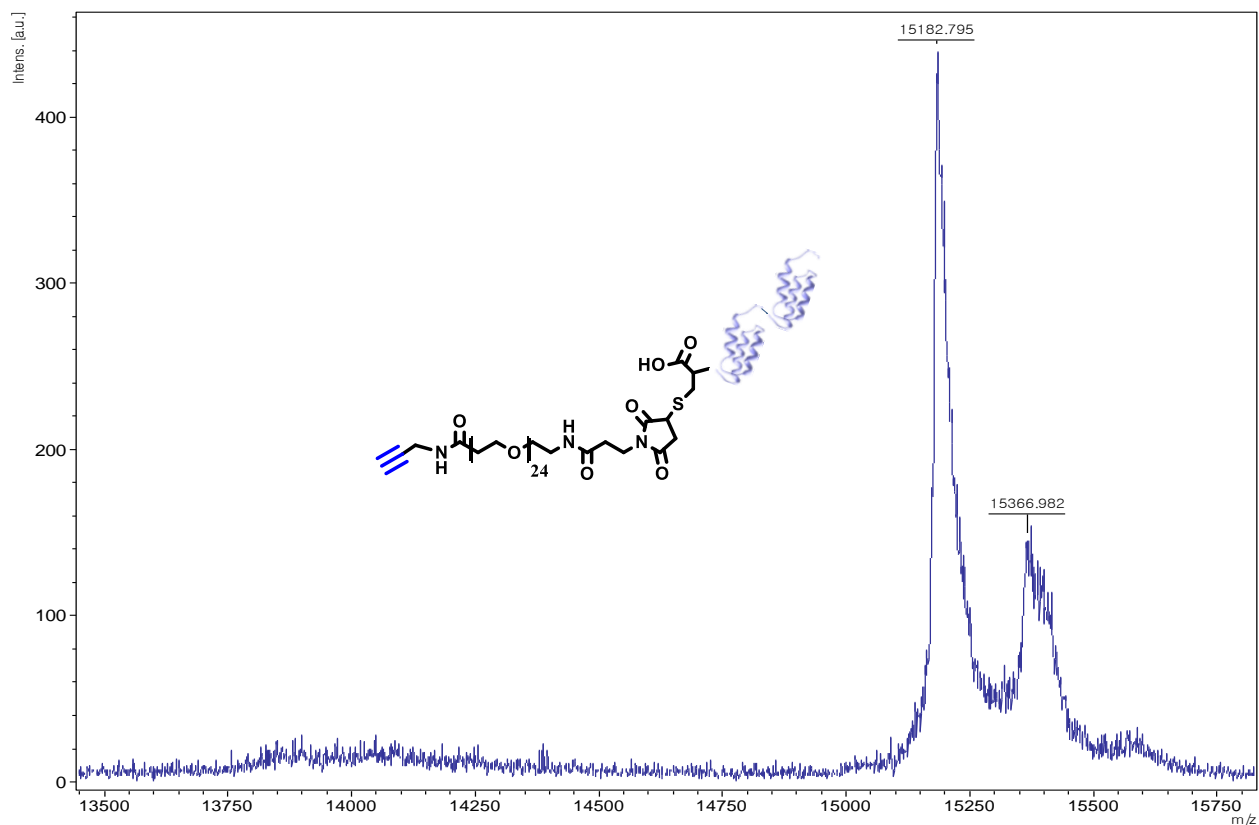
A 2. $^1\text{H-NMR}$ Spectrum of Azidohomoalanine (AHA) in D_2O (300 MHz)



A 3. MALDI-TOF Spectrum of Alkyne-PEG₂₄-maleimide (3-2)
m/z calcd. for [M] 1333.74, obsd. 1356.25 [M + Na]⁺



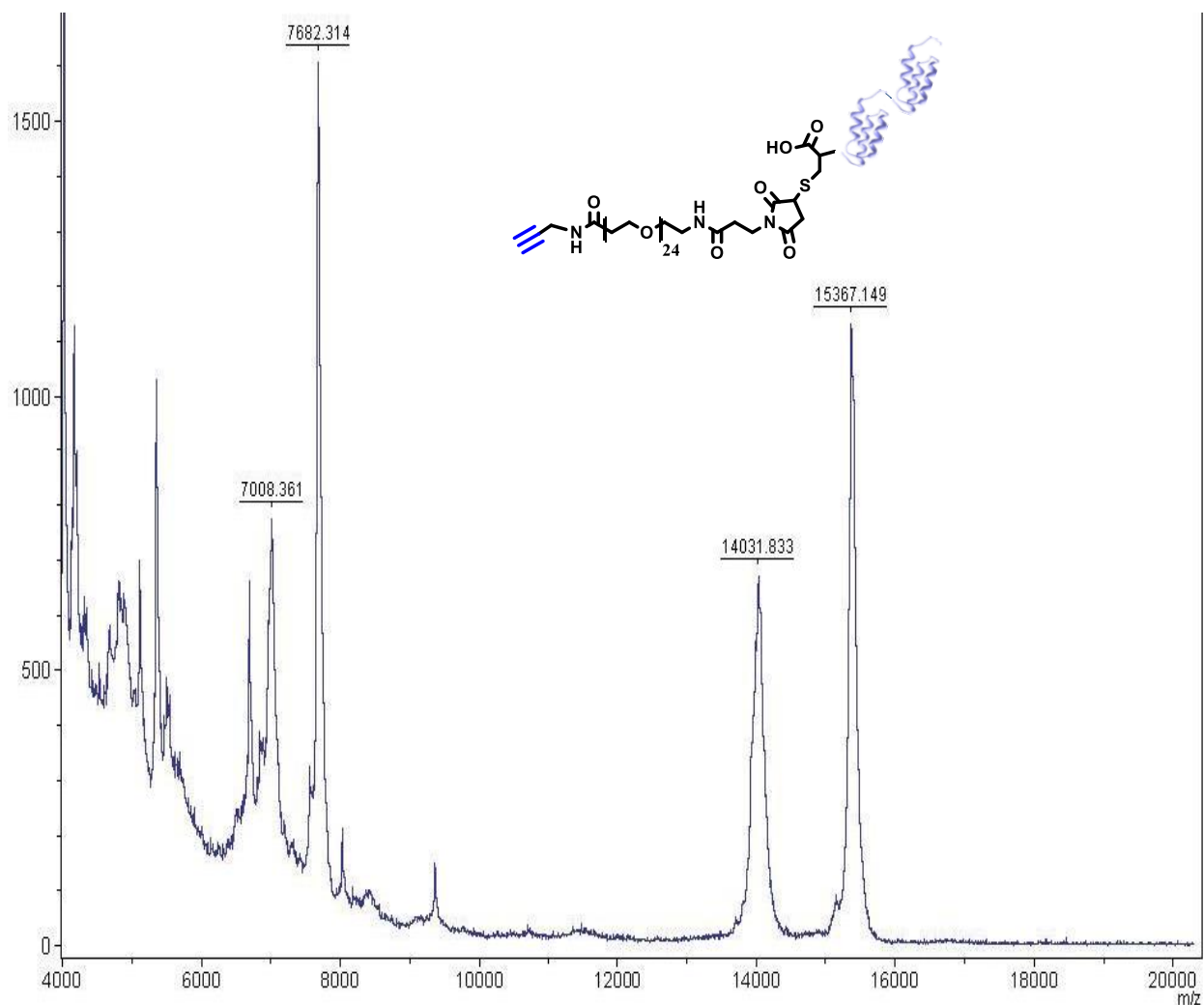
A 5. MALDI-TOF Spectrum of Alkyne-PEG₂₄-GGRGDS (3-3)
m/z calcd. [M] 1954.95, obsd. 1973.22 [M + NH₄]⁺



A 6. MALDI-TOF Spectrum of affiEGFR-PEG₂₄-CCH

m/z [M + H]⁺, calcd. 15186, obsd. 15183;

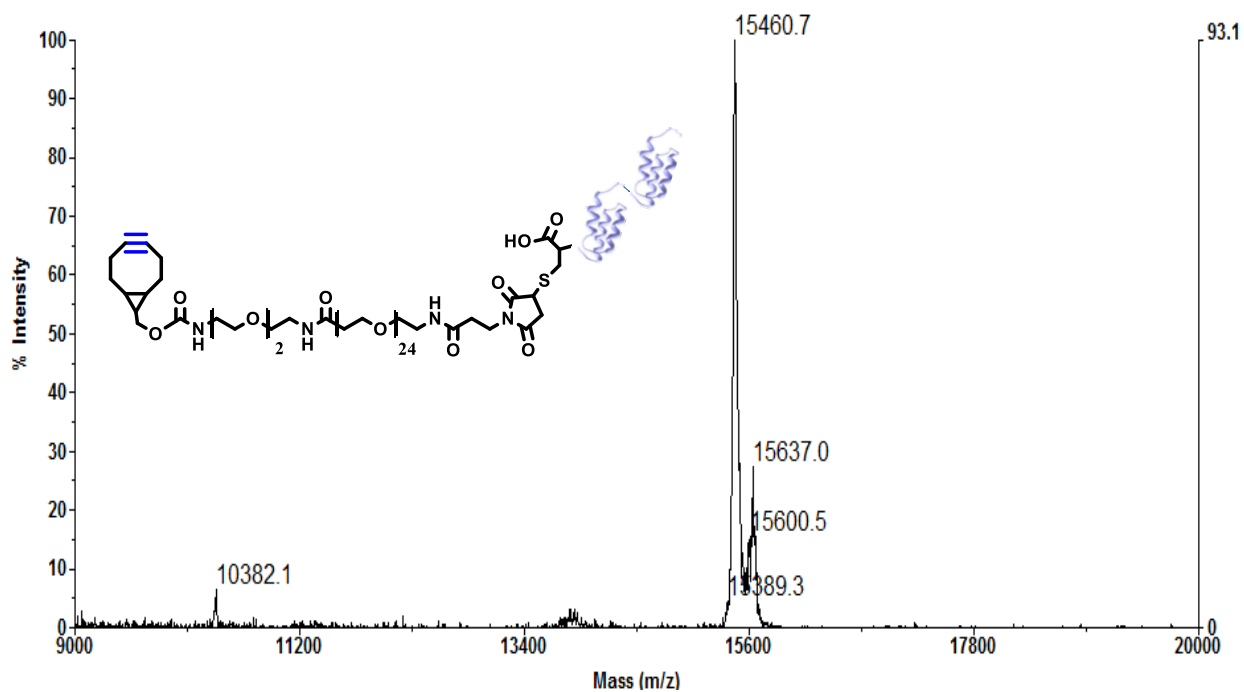
*The m/z calcd is monoisotopic mass based on the amino acid sequence of anti-EGFR affibody (GSSLQVDNKFNKEMWAAWEEIRNLPNLNGWQMTAFIASLVDDPSQSANLLAEAKKLN DAQAPKVDNKFNKEMWAAWEEIRNLPNLNGWQMTAFIASLVDDPSQSANLLAEAKKL NDAQAPKVDC).



A 7. MALDI-TOF Spectrum of affiHer2-PEG24-CCH

m/z [M + H]⁺, calcd. 15364, obsd. 15367;

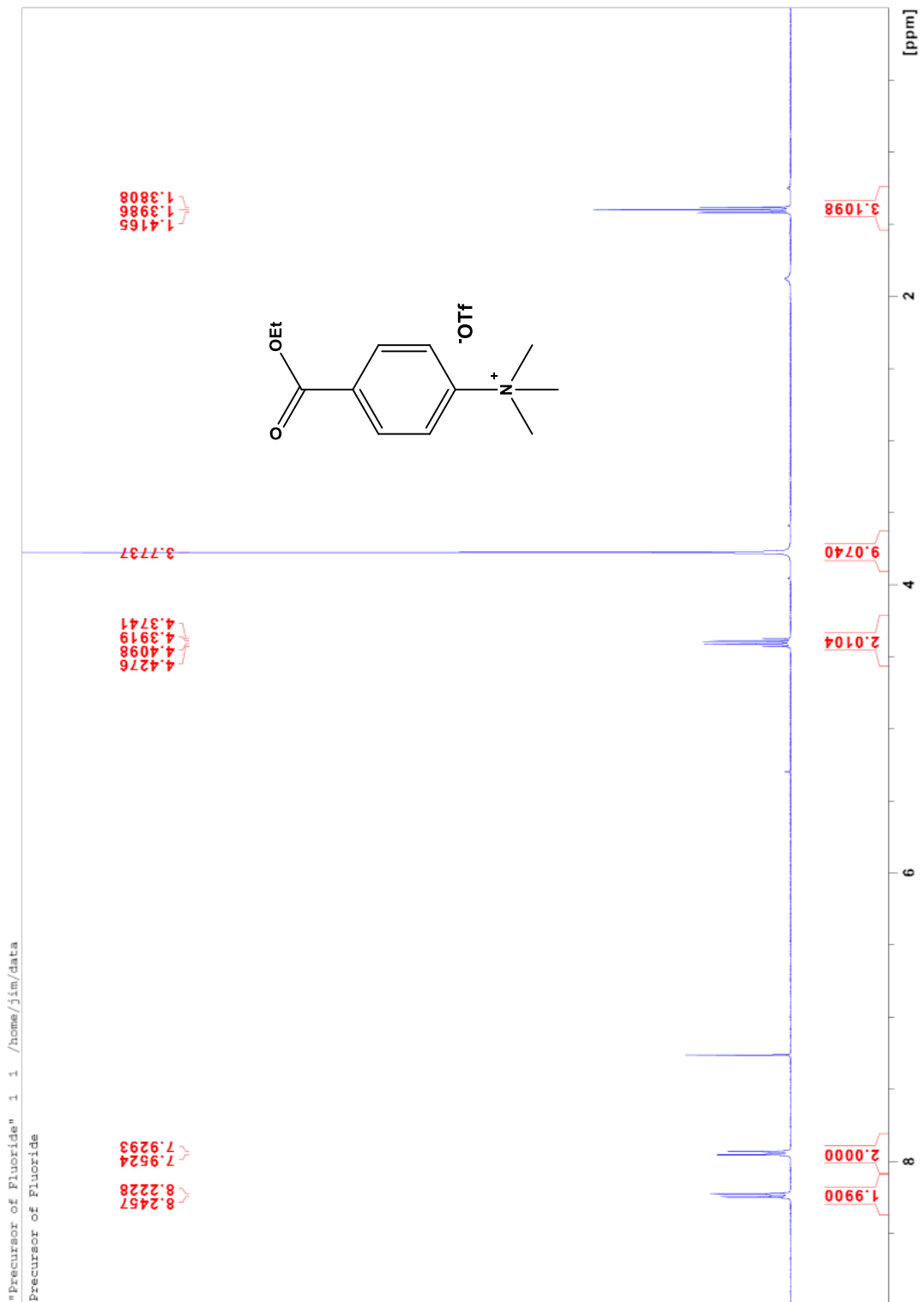
*The m/z calcd. is monoisotopic mass based on the amino acid sequence of anti-Her2 affibody (GSSLQVDNKFNKEMRNAYWEIALLPNLNVAQKRAFIRSLYDDPSQSANLLAEAKKLND AQAPKVDNKFNKEMRNAYWEIALLPNLNVAQKRAFIRSLYDDPSQSANLLAEAKKLND AQAPKVDC). Unconjugated affibody (m/z 14032) was removed by a size exclusion column (Mw cut-off: 100 KDa) after “click reaction” with virus.



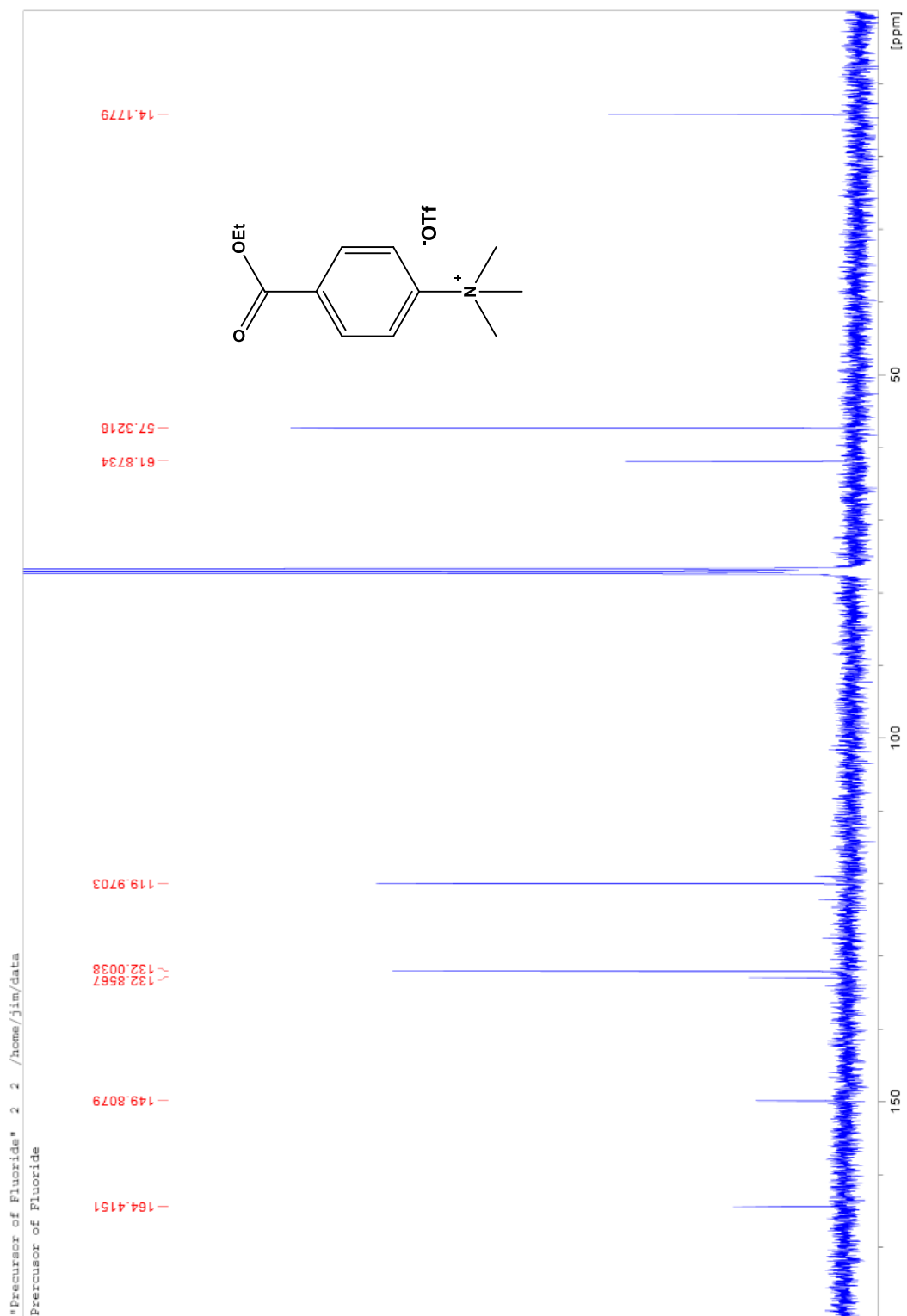
A 8. MALDI-TOF Spectrum of affiEGFR-PEG₂₆-BCN

m/z [M + H]⁺, , calcd 15456, obsd 15461;

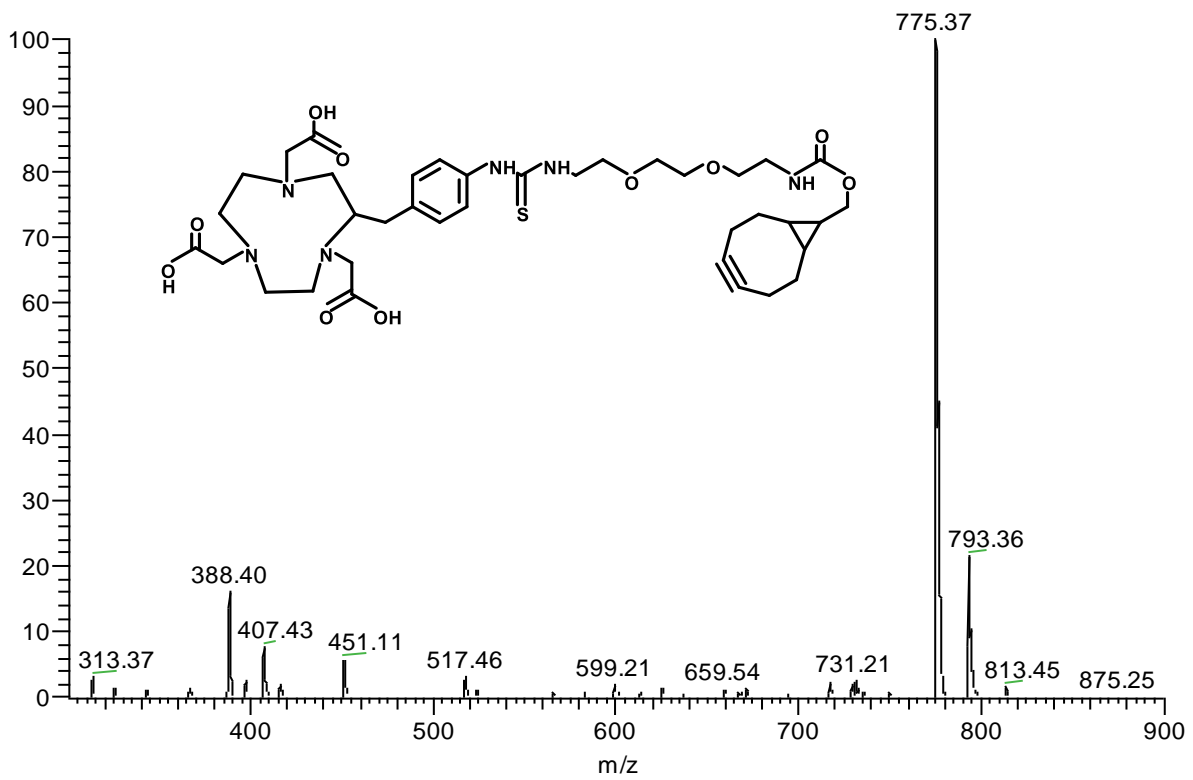
*The m/z calcd is monoisotopic mass based on the amino acid sequence of anti-EGFR affibody (GSSLQVDNKFNKEMWAAWEEIRNLPNLNGWQMTAFIASLVDDPSQSANLLAEAKKLN DAQAPKVDNKFNKEMWAAWEEIRNLPNLNGWQMTAFIASLVDDPSQSANLLAEAKKL NDAQAPKVDC).



A 9. $^1\text{H-NMR}$ of Ethyl-(4-Trimethylammonium)benzoate Trifluoromethanesulfonate (5-2) in CD_3Cl (400MHz)

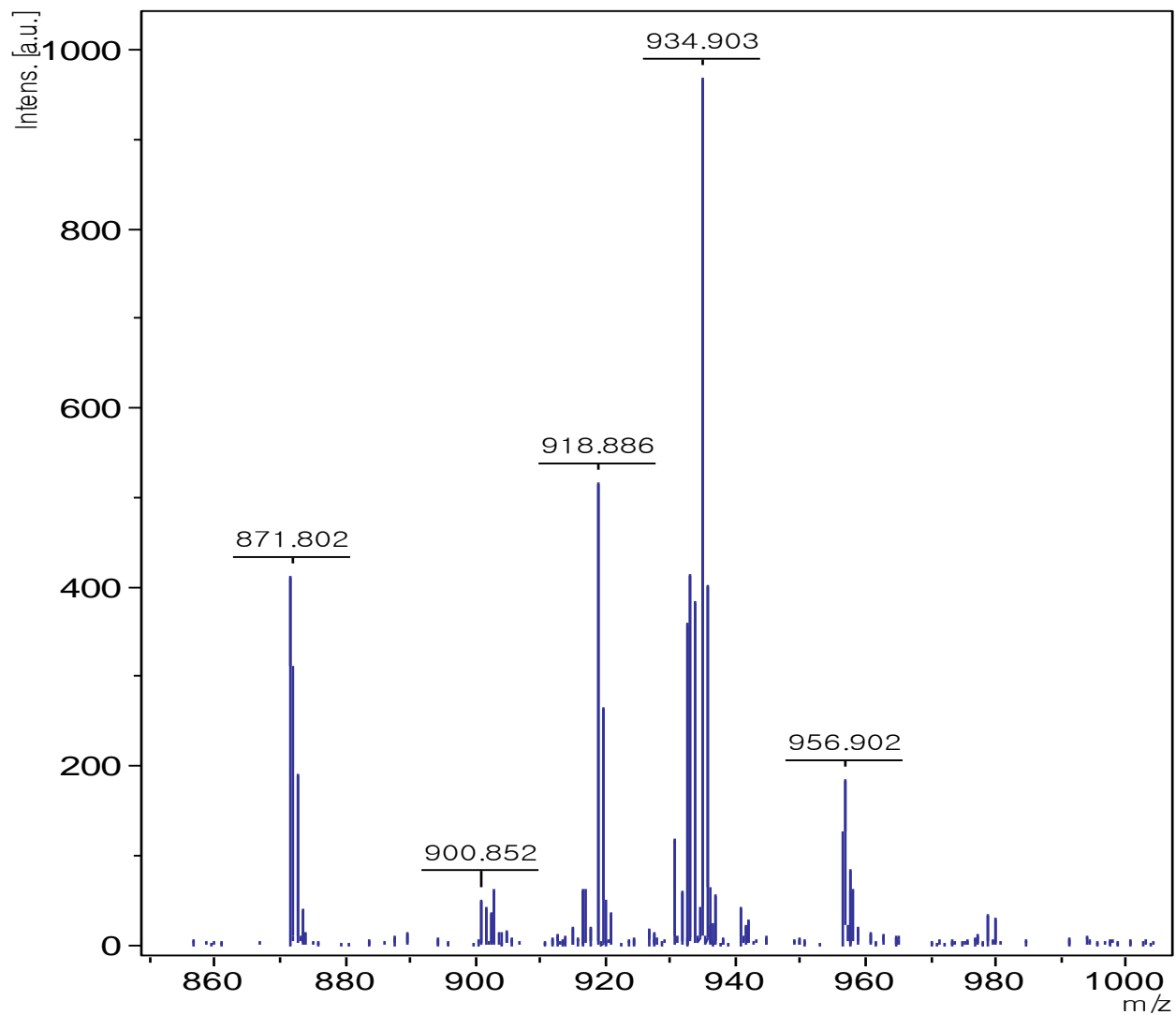


A 10. ^{13}C -NMR of Ethyl-(4-Trimethylammonium)benzoate Trifluoromethanesulfonate (5-2) in CD_3Cl (400 MHz)

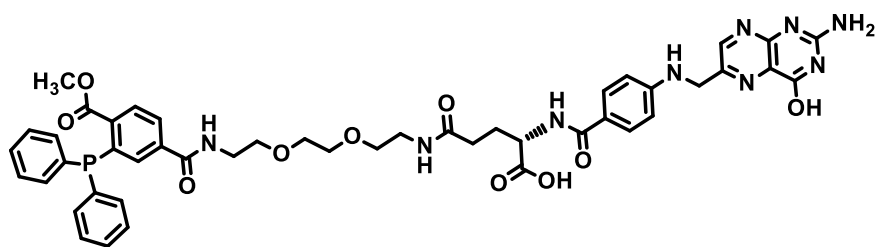


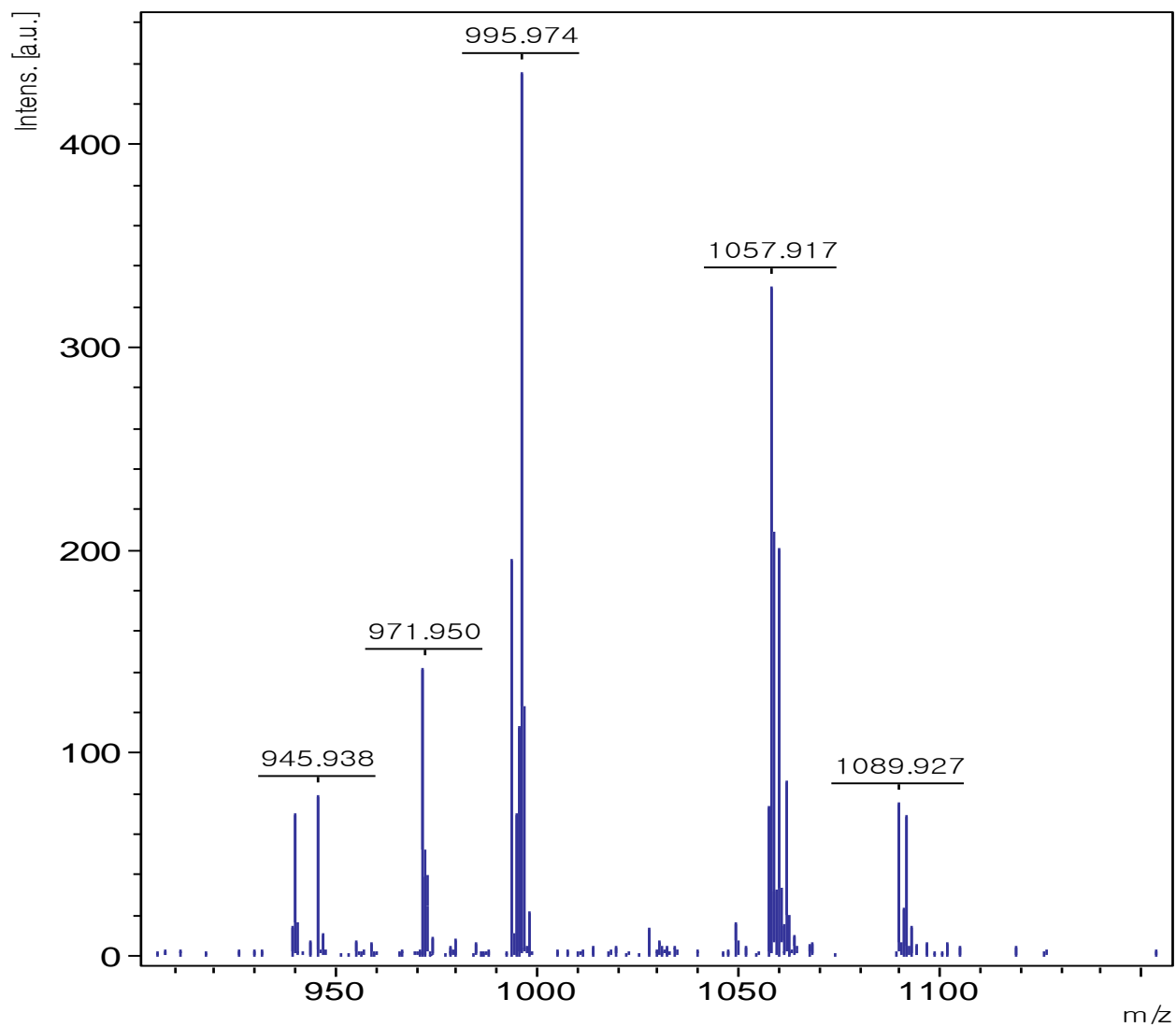
A 11. ESI-Mass Spectrum of NOTA-PEG-BCN (5-5)

ESI m/z calcd. for $[M + H]^+$ 775.36, obsd. 775.37 $[M + H]^+$.

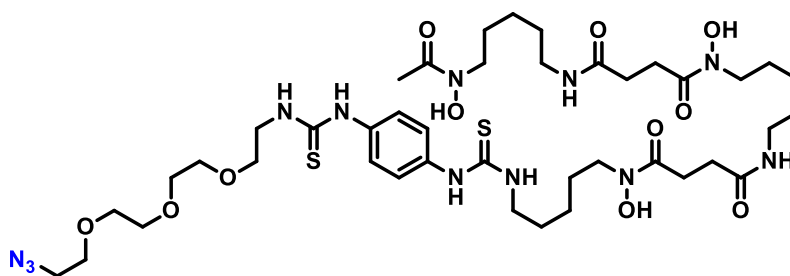


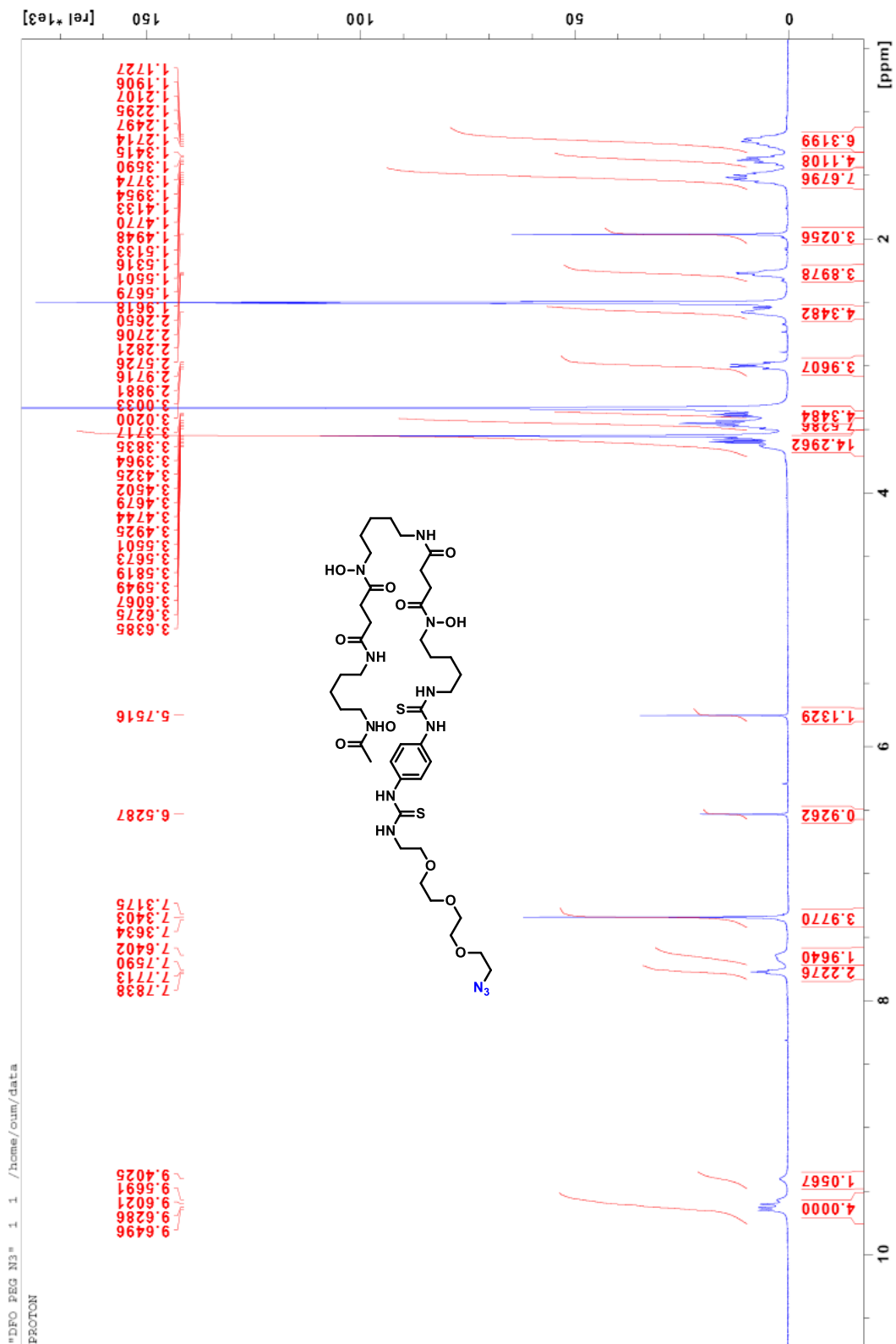
A 12. MALDI-TOF Spectrum of Folate-PEG-Phosphine (5-6)
 m/z calcd. for [M] = 917.33, obsd. for [M+H]⁺ = 918.86





A 13. MALDI-TOF Spectrum of DFO-PEG-N₃ (5-7)
 m/z calcd. for [M] = 970.47, obsd. for [M+H]⁺ = 971.95





A 14. ¹H NMR Spectrum of DFO-PEG-N₃ (5-7) in (CD₃)₂SO (400 MHz)